

# **Modal decomposition in the buckling analysis of thin-walled members**

**Dissertation**

**Sándor Ádány, PhD**

**Budapest**

**April, 2017**

## Table of Contents

1	Introduction .....	2
1.1	General.....	2
1.2	Investigated buckling types .....	4
1.3	Prediction of buckling capacity .....	5
1.4	G, D and L critical load calculation.....	6
1.5	Modal decomposition .....	8
1.6	Outline .....	9
2	Constrained Finite Strip Method for open cross-section members .....	10
2.1	Introduction .....	10
2.1.1	General .....	10
2.1.2	FSM essentials.....	10
2.1.3	Framework for constrained FSM .....	11
2.1.4	Definition of buckling classes .....	12
2.1.5	Further cFSM terminology .....	13
2.2	Derivation for $R_{GD}$ .....	14
2.2.1	Strategy.....	14
2.2.2	Impact of Criterion #1 – unbranched cross-sections .....	14
2.2.3	Impact of Criterion #1 – branched cross-sections .....	18
2.2.4	Impact of Criterion #2 .....	21
2.2.5	Assembling $R_{GD}$ .....	23
2.3	$R_G$ , $R_D$ , $R_L$ and $R_O$ matrices .....	24
2.3.1	Assembling $R_G$ .....	24
2.3.2	Assembling $R_D$ .....	25
2.3.3	Assembling $R_L$ .....	27
2.3.4	Defining $R_O$ .....	27
2.4	Application .....	28
2.4.1	Modal system .....	28
2.4.2	Pure buckling calculation .....	29
2.4.3	Mode identification .....	30
2.5	Summary and continuation of the work .....	31
3	Constrained Finite Strip Method for arbitrary flat-walled cross-section members.....	34

3.1	Introduction .....	34
3.1.1	General .....	34
3.1.2	FSM with generalized longitudinal shape functions .....	34
3.1.3	Basics of generalized cFSM .....	35
3.2	Role and decomposition of membrane shear .....	36
3.2.1	General .....	36
3.2.2	In-plane deformations in a single plate .....	37
3.2.3	Primary shear deformations in a member .....	38
3.3	Construction of the constraint matrices .....	44
3.3.1	Mode definition .....	44
3.3.2	Outline of mode construction .....	46
3.3.3	Global mode space .....	47
3.3.4	Other primary mode spaces .....	49
3.3.5	Exceptions: overlaps of primary mode spaces .....	52
3.3.6	Secondary mode spaces .....	52
3.4	Orthogonality within the mode spaces .....	54
3.4.1	General .....	54
3.4.2	Dependency on longitudinal shape functions .....	54
3.4.3	Orthogonality in cross-section .....	56
3.4.4	Ordering the cross-section orthogonal base vectors .....	57
3.5	Application .....	58
3.6	Summary and continuation of the work .....	62
4	Mode identification of deformations calculated by shell finite element analysis .....	64
4.1	Introduction .....	64
4.1.1	General .....	64
4.1.2	Problem statement .....	64
4.2	Approximation of FEM displacements .....	65
4.3	Proof-of-concept example .....	66
4.4	Approximation with reduced number of cFSM base functions .....	69
4.5	Summary and continuation of the work .....	71
5	Analytical formulae for global buckling .....	72
5.1	Introduction .....	72
5.1.1	General .....	72
5.1.2	Initial assumptions .....	72
5.2	Global buckling without in-plane shear .....	73

5.2.1	Definition for global buckling .....	73
5.2.2	Overview of derivations .....	74
5.2.3	Derivation options .....	75
5.2.4	Flexural buckling.....	78
5.2.5	Pure torsional buckling.....	80
5.2.6	Flexural-torsional buckling .....	82
5.2.7	Axial mode .....	85
5.2.8	Demonstrative examples .....	87
5.3	Flexural buckling with in-plane shear .....	89
5.3.1	Global buckling definition .....	89
5.3.2	Overview of derivations .....	89
5.3.3	Calculation options.....	91
5.3.4	The critical force .....	91
5.3.5	Demonstration of the buckling modes with shear .....	93
5.3.6	Demonstrative numerical examples .....	96
5.4	Summary and continuation of the work .....	98
6	Summary of the new scientific results .....	99
	References .....	101
	Appendix A: Orthogonality criteria .....	109
A1.	Orthogonality of $v$ .....	109
A2.	Orthogonality of $u$ .....	110
A3.	Orthogonality of $\partial v/\partial x$ .....	110
A4.	Orthogonality of $\varepsilon_x$ .....	111
A5.	Orthogonality of $\kappa_x$ .....	111
	Appendix B: Null criteria .....	113
B1.	Null transverse strain .....	113
B2.	Null longitudinal strain.....	114
B3.	Null shear strain.....	114
B4.	Null transverse curvature.....	116
B5.	Null longitudinal curvature.....	117
B6.	Null mixed curvature .....	118
B7.	Transverse equilibrium of the cross-section .....	120
	Appendix C: Derivation of the coefficient matrix for column buckling with neglecting in-plane shear.....	121
C1.	Global displacements of the member .....	121

C2.	Local displacements of a strip .....	121
C3.	Strains .....	124
C4.	Stresses .....	125
C5.	External potential.....	125
C6.	Internal potential.....	126
C7.	Total potential.....	126
C8.	Coefficient matrix.....	126
Appendix D: Derivation of the coefficient matrix for flexural buckling with considering in-plane shear.....		130
D1.	Global displacements of the member .....	130
D2.	Local displacements of a strip .....	130
D3.	Strains .....	132
D4.	Stresses .....	133
D5.	External potential.....	133
D6.	Internal potential.....	134
D7.	Total potential.....	134
D8.	Coefficient matrix.....	134

# List of Symbols

This dissertation includes a large number of equations with a large number symbols. Therefore, the strategy, in general, is to define the meaning of each symbol where (or: at least in the close vicinity where) it occurs. Hence it is not intended here to provide with a full list of all the symbols. However, it might be helpful to list those symbols which occur in various places, or which are thought to be the most important ones.

## Lowercase Latin italic letters

$a, b$	length and width of a strip, respectively
$a^{(k)}, b^{(k)}$	length and width of the $(k)$ -th strip, respectively
$b_i$	width of the $i$ -th flat plate of the cross-section (in Chapter 5 and in Appendices C and D)
$k_m$	$=m \times \pi / a$ (where $m$ is the number of half-waves along the length)
$m$	number of half-waves of the longitudinal shape function
$m$	number of nodes (in a cross-section) connecting to a certain node, in case of branched cross-sections (occurs only in Section 2.2.3)
$n$	number of nodes of the cross-section of the thin-walled member (i.e., number of nodal lines in the FSM model)
$n$	number of flat plates of the cross-section of the thin-walled member (in Chapter 5 and in Appendices C and D)
$n_m$	number of main nodes of the cross-section of the thin-walled member
$n_s$	number of sub-nodes of the cross-section of the thin-walled member
$n_e$	number of external nodes of the cross-section of the thin-walled member (i.e., those nodes to which only one single plate element is connected)
$n_{DOF}$	number of displacement degrees of freedom (DOF) in the FSM model
$n_M$	dimension of the deformation space, when deformations are constrained into a ‘M’ space
$p$	number of strips in the FSM model of a thin-walled member
$p_i$	participation (percentage) of the $i$ -th deformation mode (i.e., $i$ -th base vector) in a general deformation
$p_M$	participation (percentage) of the ‘M’ deformation space in a general deformation
$p_y$	loading in the longitudinal $y$ direction, uniformly distributed over the cross-section
$q$	number of trigonometric terms, when the longitudinal shape function is assumed in a trigonometric series form (i.e., it is the maximum number of the considered longitudinal half-waves)
$r_{0S}, r_{0S,r}$	polar radius or gyration of the thin-walled cross-section, calculated with and without considering the own plate inertias

$t$	thickness of a strip
$t^{(k)}$	thickness of the $(k)$ -th strip
$t_i$	thickness of the $i$ -th flat plate of the cross-section (in Chapter 5 and in Appendices C and D)
$u, v, w$	translational displacements (i.e., displacement functions) along the local $x$ , $y$ and $z$ axis, respectively
$u_1, u_2$	(local) translational displacement degrees of freedom for one strip in $x$
$v_1, v_2$	(local) translational displacement degrees of freedom for one strip in $y$
$w_1, w_2$	(local) translational displacement degrees of freedom for one strip in $z$
$u_1^{(j)}, u_2^{(j)}$	(local) translational displacement DOF for the $(j)$ -th strip in $x$
$v_1^{(j)}, v_2^{(j)}$	(local) translational displacement DOF for the $(j)$ -th strip in $y$
$w_1^{(j)}, w_2^{(j)}$	(local) translational displacement DOF for the $(j)$ -th strip in $z$
$u_{1[m]}, u_{2[m]}$	(local) translational displacement DOF for one strip for a specific $m$ value, i.e. for a specific number of longitudinal half-waves in $x$
$v_{1[m]}, v_{2[m]}$	(local) translational displacement DOF for one strip for a specific $m$ value, i.e. for a specific number of longitudinal half-waves in $y$
$w_{1[m]}, w_{2[m]}$	(local) translational displacement DOF for one strip for a specific $m$ value, i.e. for a specific number of longitudinal half-waves in $z$
$x, y, z$	local coordinate axes ( $y$ : longitudinal, $x$ : in the plane of the strip/plate, $z$ : perpendicular to the plane of the strip/plate)

### Uppercase Latin italic letters

$A$	cross-sectional area
$A_{s,Z}$	shear area along the $Z$ direction
$E$	modulus of elasticity of the material (in case of isotropic material)
$E_x, E_y$	modulus of elasticity in the $x$ and $y$ directions (in case of orthotropic material)
$F$	axial (compressive) force acting at the ends of the thin-walled member (i.e., the resultant of the $p_y$ distributed loading)
$G$	shear modulus of the material
$I_X, I_Z$	second moment of area calculated with regard to global $X$ - and $Z$ axis, respectively, with considering own plate inertias (i.e., the $b_i t_i^3/12$ terms)
$I_{X,r}, I_{Z,r}$	(reduced) second moment of area with regard to global $X$ - and $Z$ axis, respectively, with neglecting own plate inertias (i.e., the $b_i t_i^3/12$ terms),
$I_t$	torsion constant (of a thin-walled cross-section)
$I_w, I_{w,r}$	warping constant (of a thin-walled cross-section), with and without considering the through-thickness warping variation, respectively
$L$	length of the thin-walled column
$U, V, W$	translational displacements (i.e., displacement functions) along the global $X$ , $Y$ and $Z$ axis, respectively

$U_1, U_2, U_3 \dots$	global translational displacement degrees of freedom for the 1 <sup>st</sup> , 2 <sup>nd</sup> , 3 <sup>rd</sup> , etc. nodal lines in a finite strip model, in $x$ direction
$V_1, V_2, V_3 \dots$	global translational displacement degrees of freedom for the 1 <sup>st</sup> , 2 <sup>nd</sup> , 3 <sup>rd</sup> , etc. nodal lines in a finite strip model, in $y$ direction
$W_1, W_2, W_3 \dots$	global translational displacement degrees of freedom for the 1 <sup>st</sup> , 2 <sup>nd</sup> , 3 <sup>rd</sup> , etc. nodal lines in a finite strip model, in $z$ direction
$U_0, V_0, W_0$	amplitudes of the assumed global displacement functions for translational displacements along the global $X$ , $Y$ and $Z$ axis, respectively
$W$	work done by the loading on the displacements (in Chapter 5 and Appendices C and D)
$X, Y, Z$	global coordinate axes ( $Y$ : longitudinal)
$X_C, Z_C$	global coordinates of the mass centre of the cross-section
$X_S, Z_S$	global coordinates of the shear centre of the cross-section
$X_{SC}, Z_{SC}$	coordinates of shear centre with regard to mass centre

### Greek letters

$\alpha^{(k)}$	angle of the local $x$ axis of the $(k)$ -th strip, with respect to the global $X$ axis
$\varepsilon_x$	transverse normal strain (typically: function of $x$ , $y$ and $z$ )
$\varepsilon_y$	longitudinal normal strain (typically: function of $x$ , $y$ and $z$ )
$\varepsilon_y^{II}$	second-order part of the longitudinal normal strain (typically: function of $x$ , $y$ and $z$ )
$\gamma_{xy}$	in-plane shear strain (typically: function of $x$ , $y$ and $z$ )
$\kappa_x$	curvature in the transverse direction (i.e., along the local $x$ axis)
$\kappa_y$	curvature in the longitudinal direction (i.e., along the local $y$ axis)
$\kappa_{xy}$	mixed curvature (i.e., with respect to the local $x$ and $y$ axes)
$\lambda$ , or $\lambda_1, \lambda_2 \dots$	eigen-values, i.e., critical load factors
$\nu$	Poisson's ratio of the material (in case of isotropic material)
$\nu_x, \nu_y$	Poisson's ratio of in the $x$ and $y$ directions (in case of orthotropic material)
$\Pi$	potential energy function
$\Pi_{int}, \Pi_{ext}$	internal and external part of the potential energy function, respectively
$\theta$	rotation (i.e., rotation function) about the local $y$ longitudinal axis
$\Theta$	rotation (i.e., rotation function) about the global $Y$ longitudinal axis
$\theta_1, \theta_2$	(local) rotational degrees of freedom for one strip
$\theta_1^{(j)}, \theta_2^{(j)}$	(local) rotational DOF for the $(j)$ -th strip
$\theta_{1[m]}, \theta_{2[m]}$	(local) rotational DOF for one strip for a specific $m$ value, i.e. for a specific number of longitudinal half-waves



$\Theta_0$	amplitude of the assumed global displacement function for rotation about the global $Y$ longitudinal axis
$\sigma_y, \tau_{txy}$	longitudinal normal stress and in-plane shear stress from loading, respectively

**Bold letters (vectors, matrices)**

<b>d</b>	displacement vector (of the FSM problem), in general
<b>d<sub>M</sub></b>	displacement vector of the constrained FSM problem, when deformations are constrained into a ‘M’ space
<b>K<sub>e</sub>, K<sub>g</sub></b>	global elastic stiffness matrix and global geometric stiffness matrix, respectively
<b>K<sub>e,M</sub>, K<sub>g,M</sub></b>	global elastic and geometric stiffness matrix of the constrained FSM problem, when deformations are constrained into a ‘M’ space
<b>R</b>	constraint matrix for the constrained FSM, in general
<b>R<sub>M</sub></b>	constraint matrix for a specific ‘M’ deformation space
<b>Λ</b>	(diagonal) matrix with eigen-values (of an eigen-value problem) in its diagonal
<b>Λ<sub>M</sub></b>	(diagonal) matrix with eigen-values of a the constrained (generalized) eigen-value problem in its diagonal, when deformations are constrained into a ‘M’ space
<b>Φ</b>	matrix of eigen-vectors of a (generalized) eigen-value problem
<b>Φ<sub>M</sub></b>	matrix of eigen-vectors of a constrained (generalized) eigen-value problem, when deformations are constrained into a ‘M’ space

# 1 Introduction

## 1.1 General

In this dissertation buckling of thin-walled members is discussed. Thin-walled members appear in many engineering applications, but most frequently in the building industry, automotive industry and airplane industry. Thin-walled members can be made of various materials, including steel, aluminium, plastic, composites, or even reinforced concrete. Perhaps the most typical thin-walled mass products are the cold-formed steel products which are more and more widely used in structural engineering, either as secondary load-bearing elements (e.g., purlins, columns of partition walls, etc.) or as primary load-bearing elements (e.g., skeleton of low- and midrise buildings). Spreading of cold-formed steel is driven by the need of fast and economic construction, and supported by the development of the production technology as well as by the improvement in design methods, design standards, and computation techniques.

The work presented in this dissertation is essentially of theoretical nature, therefore, essentially independent of the application, and independent of the material of the member. Nevertheless, surely, the work has been initiated by the needs of cold-formed steel design, and the most evident and immediate application of the new results is in the design of cold-formed steel structures. That is why cold-formed steel will mostly be referenced as application (e.g., design recommendations, numerical examples, etc.). Though thin-walled members might have various topologies, here the focus is on the beam- or column-like members, built up from thin plates (like in cold-formed steel Z or C profiles). Examples are shown in **Figure 1.1**.

Moreover, it is assumed that the members are prismatic (like in case of almost any cold-rolled steel profile). Finally, it is assumed that the member is built up from flat plates that are connected with sharp corners (which is, in some cases, an approximation, e.g., cold-formed steel members never have exactly sharp corners).

Plate elements of thin-walled members (as defined above) are characterized by large width-to-thickness ratios, i.e., they are slender, consequently buckling is a potential (and in many cases: the governing) mode of failure. The term ‘buckling’ will be used here in two connected, but different senses. In a more general sense buckling is the phenomenon which takes place under the effect of compressive forces/stresses, which typically involves relatively large deformations/displacements, which typically takes place in the form of a sudden change in the displacement/deformation field, and in which the small disturbing effects, also known as imperfections, have prominent role. In the other, more special sense buckling has similar meaning, but the phenomenon is idealized, assuming perfectly elastic and homogeneous material, perfect initial geometry, perfectly proportional and aligned loading, etc.

Even in this more restricted sense buckling might be (and is) defined in various ways, here, it is fair to assume that buckling will take place as a bifurcation of equilibrium. This second, idealized buckling will also be referred here as *elastic buckling* or *linear buckling*. The load level at which bifurcation occurs is the *critical load*, also referred as buckling load. The state of the structure when bifurcation occurs is the critical state. The deformed shape that belongs to the secondary load path at the bifurcation point is the buckled shape, also referred as buckling mode. The process of determining the critical state (i.e., critical load, buckled shape) is the linear or elastic buckling analysis which in our cases will always mean the solution of a generalized eigen-value problem, in which the eigen-values are the critical load multipliers, and the eigen-vectors are the nodal representations of the buckled shapes.



(a) portal frames made of cold-formed steel members



(b) cold-formed steel Z-shaped purlins



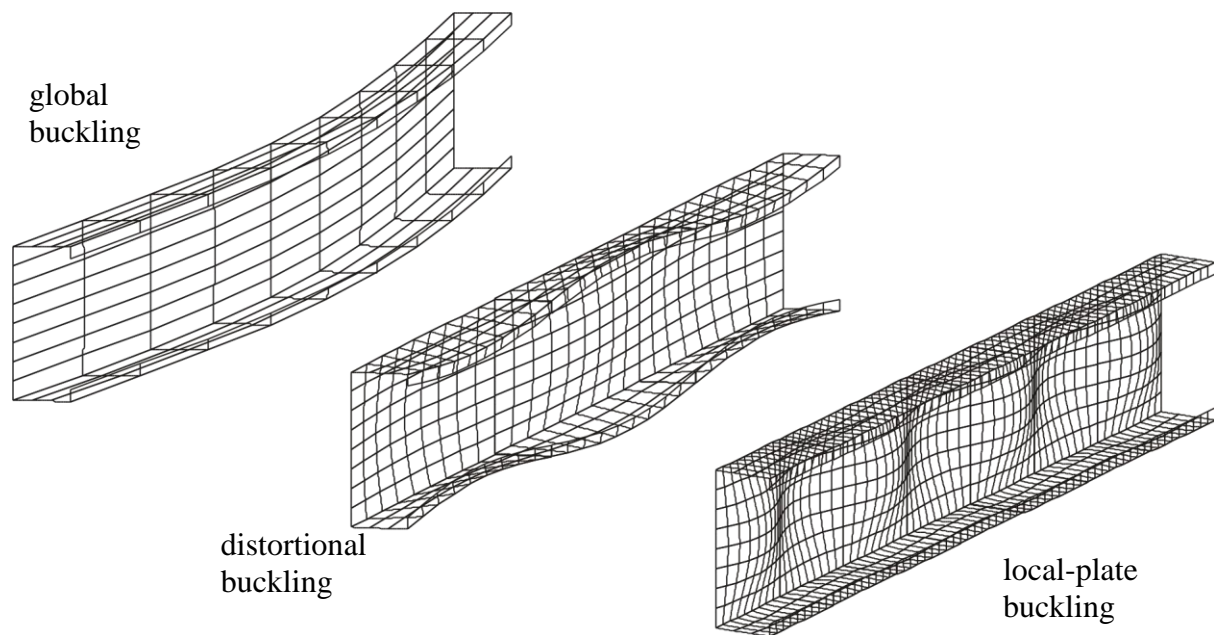
(c) trusses made of cold-formed steel profiles

**Figure 1.1:** Examples for thin-walled cold-formed steel members

The work summarized in this dissertation is focusing on this second interpretation of buckling, therefore, mostly the term ‘buckling’ will be used in the second, idealized sense. However, the application of the results is in the ‘buckling analysis’, with ‘buckling’ interpreted in the first, more general sense. In this sense buckling analysis is the whole process that tries to describe the buckling phenomenon in general, and which leads to the practically most important characteristics, namely: buckling capacity. Buckling capacity is the maximum load that the structure is able to sustain without failure induced by buckling. If safety margin is also added to the buckling capacity (e.g., according to some design specification), it is appropriate to use the term design (buckling) capacity.

## 1.2 Investigated buckling types

In typical applications the cold-formed steel members are subjected to compressive axial force and/or bending moment, from which longitudinal normal stresses develop. Under the effect of longitudinal compressive stresses usually three types (or: classes) of basic buckling phenomena are distinguished: local (L), distortional (D) and global (G) buckling. (Obviously, buckling might occur due to other-than-longitudinal stresses, e.g., shear buckling or web crippling, but these are out of the scope of this dissertation.) In a linear buckling analysis these buckling types most frequently take place in interaction with each other, i.e., the observed buckling pattern may have deformations combined from more than one buckling type. Buckling modes without this kind of interaction are referred to as *pure buckling modes*. Samples are shown in **Figure 1.2** for a member with C-shaped cross-section.



**Figure 1.2:** Illustration of global, distortional and local buckling modes

Although there seems to be a consensus among researchers and practitioners on the global-distortional-local classification of buckling modes, and although this classification directly appears in design specifications, too, formal definitions of the types has not existed for a long time, and even today there is no consensus on the exact meaning of the types.

Global buckling is a buckling mode where the member deforms with no or negligibly small deformation in its cross-sectional shape. Thus, the deformations can (primarily or solely) be characterized by the displacements of the system line of the member. Depending on the deformations and the type of loading, further sub-classes can be defined such as: flexural buckling, torsional buckling, flexural-torsional buckling and lateral-torsional buckling.

Local buckling (or local-plate buckling) is normally defined as the mode which involves plate-like deformations alone, without the translation of the intersection lines of the adjacent plate elements. Another important feature of local buckling is that the associated buckling length is the smallest among the three types, and typically less than the width of any plate that construct the cross-section.

Distortional buckling seems to be the most problematic mode. As far as the associated buckling length is concerned it is typically in between the lengths of local and global modes, while the transverse deformations involve both plate-like deformations and the translation of one or multiple intersection lines of adjacent plate elements.

### 1.3 Prediction of buckling capacity

The buckling capacity is (can be) quite different from the elastic critical load, due to two major effects: the capacity degrading effect of the always existing imperfections, and the capacity increasing effect of the ability of the structure to switch to another, more stable load bearing mechanism. These two major factors will determine the post-buckling behaviour.

Distinguishing between buckling types is important because each has its characteristic post-buckling behaviour. Local buckling typically has significant post-buckling reserve (at least for larger slendernesses where the behaviour is primarily elastic). Distortional buckling may have post-buckling reserve, too, but considerably less compared to local buckling. Global buckling has no post-buckling reserve at all: the capacity of the member is always less than its elastic critical load. Thus, (i) it is extremely important to clearly classify the various buckling modes in order to get realistic design capacity, and (ii) this explains why different design methods have been evolved for the various buckling types. The most widely applied design methods are briefly summarized as follows. As it becomes clear, design approaches require the correct calculation of the member critical load, since the design capacity is dependent on it. Not only the value of the critical load is crucial, but the type of the buckling, too, to be able to properly consider the effect of imperfections and the possible post-buckling reserves.

#### Global buckling

Global buckling is the most classical and most well-known among the buckling phenomena. The linear buckling problem for the flexural case was first formulated mathematically and solved by Euler more than two hundred years ago. Solutions for other cases of global buckling, such as torsional, flexural-torsional or lateral-torsional buckling, are also well-known. Also, there is a widely accepted and applied classic approach for the prediction of the corresponding design capacity, in which the capacity is the product of the cross-section capacity and a buckling reduction factor (i.e., ‘yield strength’ $\times$ ‘area’ $\times$ ‘reduction factor’). The reduction factor is dependent on the elastic critical load and some other (material and cross-section) parameters. It is to observe that the effect of restraints, as well as the effect of load distribution is considered in the linear buckling problem. In case of global buckling, all major design standards for (cold-formed) steel [1/1-6/1] use this approach, though there are differences in the actual formulae.

#### Local buckling

In our case local buckling means the buckling of one or multiple rectangular plates under the effect of a unilateral (longitudinal) normal stress. The solution for the linear buckling problem for a single plate is, again, a classic one, various cases are solved by Timoshenko at the beginning of 1900s. The most used technique for capacity prediction is based on the effective width approach, the idea of which is to calculate a reduced (so-called ‘effective’) width, then the capacity can be predicted as the reduced plate area times the yield strength (i.e., ‘reduced width’ $\times$ ‘thickness’ $\times$ ‘yield strength’). The effect of loading as well as the effect of edge restraints can be considered in the elastic buckling load. For the reduction factor to get the effective width, mostly the so-called Winter-formula is used [3/1], proposed in the middle of the 20<sup>th</sup> century, which calculates the reduction factor from the elastic critical stress.

When a thin-walled column/beam member is loaded by longitudinal stresses, there are multiple connected plate elements (partially or fully) in compression. The connected plate elements mean certain supports to each other (which is advantageous), and also their plate buckling is interaction with each other (which is disadvantageous). Codified design methods typically make a simplification and neglect the interaction of the connected plates, that is effective width is defined for each plate element separately from the others, and the so final

‘effective cross-section’ is then built up from the effective portions of the individual plate elements. Also, since plate buckling is associated with short buckling waves, the effect of loading (e.g., changing bending moment along the member axis) is practically negligible, hence, local buckling capacity is practically considered as characteristics of the cross-section.

### Distortional buckling

Distortional buckling is the newest form of buckling, first described approx. 50 years ago. In typical cases distortional buckling is the quasi-flexural buckling of a stiffener. General analytical solutions for the corresponding critical load are not known, though lately there are proposals for some cases, such as C- or Z-shaped columns, but the involved calculations and formulae can be considered to be too complicated for practical use. Even so, the capacity prediction is still based on the elastic critical load value.

There are two approaches. One approach calculates a reduction factor which is applied to reduce the thickness of the stiffener zone of the member [2/1]. The other approach uses a Winter-type formula (but with parameters different for those used for effective width calculation) to calculate a reduction factor which is applied for the whole cross-section of the member to reduce its cross-section capacity (similarly as in case of global buckling) [6/1]. Since distortional buckling is associated with relatively short buckling waves, the effect of loading (e.g., changing bending moment along the member axis) is typically assumed to be negligible, hence, distortional buckling capacity is practically considered as characteristics of the cross-section. It must be mentioned, however, that this assumption is just a rough approximation, more precise calculations clearly show that distortional buckling does depend on various parameters of the problem, not only on cross-section properties.

### The Direct Strength Method

Recently the so-called Direct Strength Method (DSM) has been proposed [7/1] and implemented in certain design standards. DSM integrates some of the existing approaches and extends them in order to have a uniform handling of all the three basic buckling phenomena. Essentially, DSM predicts a separate capacity for each of the G (global), D (distortional) and L (local) buckling, then the final capacity is simply the minimum of the three. Each individual capacity is predicted by using the same generic formula: ‘yield strength’ $\times$ ‘cross-section area’ $\times$ ‘reduction factor’. And in each of the G, D and L case the reduction factor is calculated from the corresponding G, D, or L elastic critical load by using a mode-specific formula. For the elastic critical load calculation FSM has been proposed, as shown in the next Section.

## **1.4 G, D and L critical load calculation**

In capacity prediction it is essential to calculate elastic critical load (where ‘load’ can be interpreted as ‘force’, ‘moment’, ‘stress’, or ‘load multiplier’) separately for G, D and L buckling. There are analytical or semi-analytical formulae for certain cases, but surely there are many practical cases where critical load formula are not available. Therefore, numerical methods should be applied. At the time when the work summarized in this dissertation started (circa 2003), there were three available numerical methods: shell finite element method (FEM), finite strip method (FSM), and generalized beam theory (GBT).

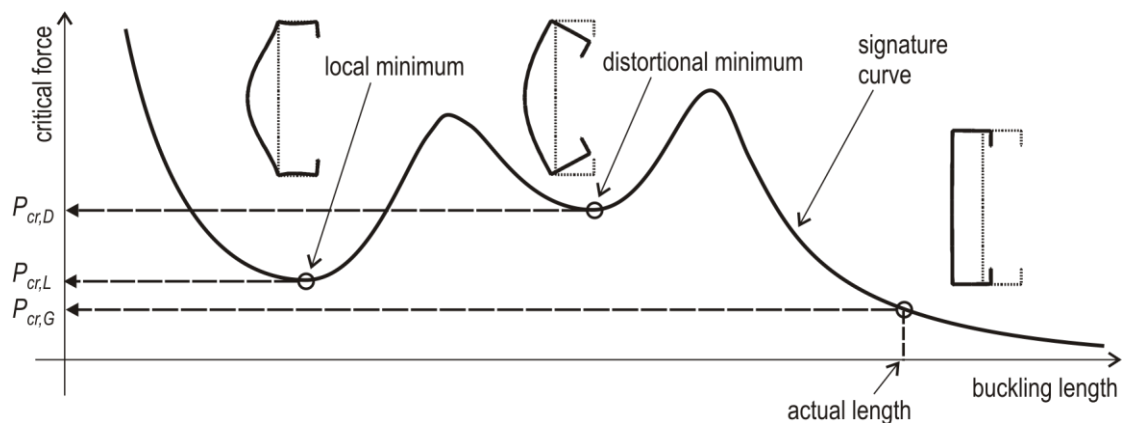
Among numerical methods, the finite element method (FEM) is by far the most popular and general. FEM is applicable to practically any structural member, loading, and boundary condition and a large number of FEM software packages are available, e.g., Ansys [8/1]. When applied for thin-walled members, a large number of shell elements, and consequently a large number of degrees of freedom (DOF), are required. If critical loads are to be determined separately for G, D and L, what practically necessary is first (i) to determine the first critical



loads (with the lowest critical values) and corresponding buckled shapes, then (ii) to systematically check the buckled shapes, and (iii) to select the ones that can be regarded as first L, first D and first G mode. The practical experience is that (i) at least several dozens, or sometimes a few hundred modes have to be calculated and judged, and (ii) in many cases it is not evident which mode should be considered as first mode, especially in case of distortional buckling, since most of the FEM-calculated buckling shapes show certain interaction of the modes. Furthermore, while for a single cross-section, browsing through hundreds of candidate buckling modes is inefficient, but for procedures which require multiple consecutive analyses (e.g., optimization) the method is essentially unusable.

For the buckling analysis of thin-walled prismatic members the finite strip method (FSM) has been found to be highly efficient, by using specific trigonometric base functions in the longitudinal direction of the member (while using classic polynomials in the transverse directions). The method has been proposed by Cheung [9/1-11/1], later popularized by Hancock [12/1] who formally implemented FSM into cold-formed steel member design, as well as developed a computer program THIN-WALL [13/1-15/1] available for the public. The method has further been popularized by Schafer [16/1], who developed the open source FSM software CUFSM [17/1-18/1], plus proposed a new design method, the so-called Direct Strength Method (DSM) [7/1], which is fully based on FSM elastic buckling analysis. (It is to note that other variants of FSM do exist, too, but in this dissertation FSM always refers to the one originated in [9/1-11/1], that can be regarded as specifically proposed for the stability analysis of thin-walled members.)

FSM employs significantly fewer DOF than FEM, therefore, FSM is computationally more efficient than FEM. The price of the reduced computational effort is limited applicability: classical FSM works only on prismatic members. From the point of view of determining critical loads for G, D or L buckling, FSM is similar to FEM. However, FSM software packages, like THIN-WALL and CUFSM tried to overcome this problem by the automatic determination of the critical stress as a function of the buckling half-wavelength, which plot is frequently referred as *signature curve*. In case of many practical cross-sections the signature curve has two minimum points at smaller wave-lengths, while after a certain wave-length it tends asymptotically to zero (or to a small non-zero value), see **Figure 1.3**. By using this signature curve the G, D and L critical loads can be determined as follows: the first minimum point can be regarded as critical load for L, the second minimum point as critical load for D, while the value at the global buckling length (based on the member length and end restraints) is the critical load for G. Unfortunately, the signature curve might have more or less than two minimum points; in such cases this procedure becomes uncertain, but even in these cases the signature curve can be useful in critical load determination.



**Figure 1.3:** Typical signature curve and buckled cross-section shapes of a C-section member

For many years the generalized beam theory (GBT) was the only method able to directly calculate critical loads separately for G, D or L buckling. Originally it was developed to analyse global and distortional modes, then extended to local (and other) modes, too [19/1-21/1]. First- and second-order (i.e., linear buckling) analyses are both possible, considering isotropic and various orthotropic materials [22/1-24/1]. Originally it handled simple cross-section members, then extended to very general cross-sections [25/1-28/1]. For a long time (including the time when the here-presented research has started, circa 2003) a major drawback of the method was that it lacked publicly available software implementation, which hole was later filled by the development of GBTUL software [29/1-30/1]. GBT shares most of the advantages and limitations of FSM: it elegantly handles straight prismatic members, with a relatively small number of DOF, but it is not easy (and in some cases, probably, impossible) to generalize it to more complicated cases (e.g., tapered members, members with holes, frames built up from thin-walled members, etc.). Nevertheless, GBT is probably the most researched area in thin-walled research during the last two decades, and here just a few important works are referred out of the many dozens of publications.

## 1.5 Modal decomposition

Two basic tasks can be identified and distinguished in the context of calculation of critical load for global-distortional-local buckling. One is the *calculation of pure critical load* when the aim is to calculate critical load specifically to G, D or L buckling. This could be done while forcing the member to deform in accordance with a buckling type (in other words: to *constrain* the deformation into a certain type). The lowest critical load from a constraint calculation could directly be used as critical load for the given buckling type.

The other task is *buckling mode identification*, when critical load is calculated without any preliminary restriction on the deformations (as in regular FEM or FSM calculations), but after the determination of the buckled shape it is identified, i.e., it is defined whether the given mode belongs to which class. Since general buckling modes rarely identical to any pure mode, in the practice the mode identification defines what the participations from global, distortional and local modes are in a general deformation mode. In real design situations, then, critical load for, say, distortional buckling can be estimated by the lowest critical load in which the participation of distortional deformations is dominant.

It is to note that modal identification can be applied to any deformations of a thin-walled member, however, in this dissertation it is applied only to buckled shapes obtained from a linear buckling analysis. Also, various calculations with enforced constraints can be performed (e.g., first- or second-order static analysis, dynamic analysis, etc.), however, in this dissertation only linear buckling problems are solved with constraints.

Evidently, both tasks require a clear definition of buckling classes, and require the ability of constructing deformations that satisfy the definition of a given class. When discussing these tasks in general, the whole problem will be referred here as *modal decomposition*. Modal decomposition has been a challenging task for a long time. The basic dilemma is that general methods, which can handle arbitrary cross-sections, boundary conditions, and loads, cannot do modal decomposition; while, specialized methods, which successfully solve buckling classification, cannot readily handle general cross-sections, boundary conditions, and loads. The general aim of the research summarized in this dissertation is to develop numerical procedures so that modal decomposition would become available for a relatively wide range of practical situations.



## 1.6 Outline

This dissertation summarizes the author's research activity on modal decomposition of thin-walled members. The dissertation focuses on those new results in which the author's contribution has been dominant. Other closely related works, some of them with the contribution from the author, will also be mentioned for the sake of completeness.

The dissertation covers results from approx. 10 years, i.e., from the period between 2003 and 2014. It starts with the presentation of the constrained Finite Strip Method (cFSM), where the fundamental buckling classes has been defined by mechanical criteria, and the criteria are systematically implemented into the semi-analytical finite strip method. cFSM was the first shell-model-based discretization method which was able to perform modal decomposition. The first version of cFSM was developed in 2004-05. This version handled members with pinned-pinned end restraints and open cross-section only. This original cFSM is presented in Section 2.

Later cFSM has been extended to handle other end restraints, and very recently, to handle closed cross-sections. This latter task – completed in 2012-14 – is summarized in Section 3 of this dissertation.

After development the original cFSM, modal system of base functions for the deformation-displacement field of a thin-walled member become available. The modal nature of the base system has been utilized in the (approximate) modal identification of buckling modes calculated by shell finite element analysis. The method, presented in Section 4, can be considered as the first method which provided an objective (i.e., mathematical) way to identify buckling modes calculated by shell FEM.

In validating numerical methods, comparison to analytical solution is always useful and important. Comparison of cFSM pure global results to classical analytical solutions revealed some differences. As it turned out, the differences are due to the differences between beam-model and shell-model. Therefore, shell-model-based analytical solutions for the critical loads have been worked out for a number of classical problems. In these works the thin-walled member is considered as a set of thin flat plates, constraints are introduced to enforce the member to deform in accordance to global mode (based on a certain global mode definition), from which alternative formulae for the critical loads are determined. In other words, the global modes are determined as in cFSM, but, unlike in cFSM, analytically. The analytical results are presented in Section 5.

## 2 Constrained Finite Strip Method for open cross-section members

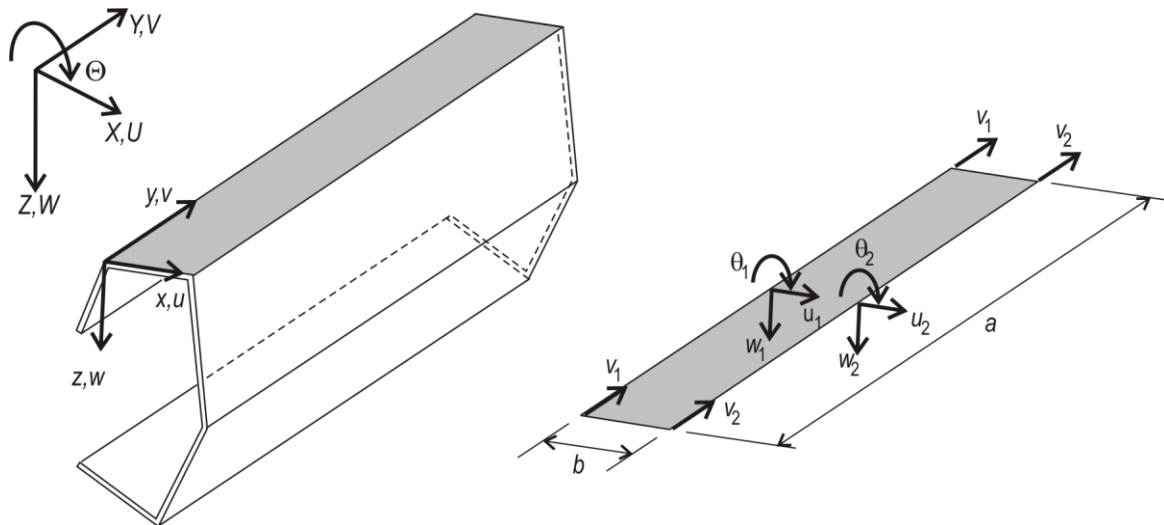
### 2.1 Introduction

#### 2.1.1 General

The constrained finite strip method (cFSM) is a special version of semi-analytical finite strip method (FSM), where mechanical constraints are applied to enforce the member to deform (e.g. buckle) in accordance with desired buckling modes: global, distortional, local, and other buckling. This Chapter summarizes the idea and most important derivations that are necessary for the method, following the publications [1/2-8/2]. First the FSM is briefly summarized (in Section 2.1.2). Then the constrained method is presented: the concept is outlined (Section 2.1.3), mode definitions are provided (Section 2.1.4), and some important cFSM terms are defined (Section 2.1.5). Then the constraints matrices are derived (in Sections 2.2 and 2.3). In Section 2.4 the application of the method is illustrated.

#### 2.1.2 FSM essentials

A typical open thin-walled member is given in **Figure 2.1**. The shaded portion is a strip (element) in an FSM mesh. Two left-handed coordinate systems are used throughout this Chapter: global and local, see **Figure 2.1**. The global coordinate system is denoted as:  $X$ - $Y$ - $Z$ , with the  $Y$  axis parallel with the longitudinal axis of the member. The local system is denoted as  $x$ - $y$ - $z$ , the  $y$  axis is parallel with  $Y$ ,  $x$  is the in-plane transverse direction, and the  $z$  axis is perpendicular to the  $x$ - $y$  plane. The displacement degrees of freedom (DOF) are assigned to nodal lines, that are longitudinal edge lines of the strips, and can be interpreted as amplitudes of the assumed longitudinal shape functions. Three translations ( $U$ - $V$ - $W$ ) and a rotation ( $\Theta$ ) are considered as global displacements. Similarly, there are three translations ( $u$ - $v$ - $w$ ) and a rotation ( $\theta$ ) in the local system. It is to mention that the positive sign of the rotational DOF throughout Section 2 is the opposite of the positive rotation of the coordinate system (as shown in **Figure 2.1**), since (slightly strangely) this sign rule was used in the original work of Cheung [9/1-11/1] which later was adopted by many other FSM work e.g. [16/1-18/1] including the first cFSM publications [1/2-8/2].



**Figure 2.1:** FSM discretization, coordinate systems, displacements

The displacements of each strip is comprised of small deflection plate bending ( $w, \theta$ ) and plane stress ( $u, v$ ) for the membrane behaviour. Standard linear and cubic shape function are used in the transverse direction, while trigonometric functions (or function series) in the longitudinal direction. In case of pinned-pinned end restraints and longitudinal end loading, simple sine and cosine functions are appropriate as follows [9/1-11/1]:

$$u(x, y) = \left[ \left( 1 - \frac{x}{b} \right) \left( \frac{x}{b} \right) \right] \begin{bmatrix} u_1 \\ u_2 \end{bmatrix} \sin \frac{m\pi y}{a} \quad (2.1)$$

$$v(x, y) = \left[ \left( 1 - \frac{x}{b} \right) \left( \frac{x}{b} \right) \right] \begin{bmatrix} v_1 \\ v_2 \end{bmatrix} \cos \frac{m\pi y}{a} \quad (2.2)$$

$$w(x, y) = \left[ \left( 1 - \frac{3x^2}{b^2} + \frac{2x^3}{b^3} \right) \left( x - \frac{2x^2}{b} + \frac{x^3}{b^2} \right) \left( \frac{3x^2}{b^2} - \frac{2x^3}{b^3} \right) \frac{x^3}{b^2} \left( -\frac{x^2}{b} \right) \right] \begin{bmatrix} w_1 \\ \vartheta_1 \\ w_2 \\ \vartheta_2 \end{bmatrix} \sin \frac{m\pi y}{a} \quad (2.3)$$

For an individual strip the plate bending and membrane behaviour are completely uncoupled; however, assembly of the strips into the global stiffness matrix causes coupling of membrane (in-plane) and bending (out-of-plane) behaviour any time the angle between two adjacent strips is nonzero.

It is to note that other boundary conditions may be treated but are not discussed here in Section 2. Moreover, at least two software implementations are available following these basic assumptions: THIN-WALL [13/1-15/1] and CUFSM [17/1-18/1]. The procedures presented here were implemented in CUFSM by using MatLab [9/2].

Both the elastic stiffness and geometric stiffness matrices can be assembled via the usual steps of finite element or finite strip method, see e.g. [16/1]. In case of  $\mathbf{K}_e$  linear elastic material is considered. In case of  $\mathbf{K}_g$  standard second-order strain terms are considered, assuming longitudinal end loads only (constant through the thickness and linearly changing with local  $x$  axis). Once the stiffness matrices are compiled, buckling modes of a thin-walled member can be determined by solving the generalized eigen-value problem as follows:

$$\mathbf{K}_e \Phi = \Lambda \mathbf{K}_g \Phi \quad (2.4)$$

where,  $\mathbf{K}_e$  is the global elastic stiffness matrix and is a function of the member length,  $a$ ,  $\Phi = [\Phi_1 \ \Phi_2 \ \dots \ \Phi_{n_{DOF}}]$ , is the matrix of eigen-vectors, where  $n_{DOF}$  is the number of DOF ( $n_{DOF}$  is equal to  $4 \times n$ , where  $n$  is the number of nodal lines),  $\Lambda = \text{diag}[\lambda_1 \ \lambda_2 \ \dots \ \lambda_{n_{DOF}}]$  is the diagonal matrix of eigen-values, and  $\mathbf{K}_g$  is the global geometric stiffness matrix. In a typical application of the FSM (for thin-walled members) Eq. (2.4) is solved for various member lengths for a given axial stress distribution, then the calculated  $\lambda$  values are plotted against the buckling length. Note, any deformation,  $\mathbf{d}$  (including a buckling mode,  $\Phi_i$ ) is described in terms of their global DOF, which include longitudinal ( $V$ ) translations, transverse ( $U$  and  $W$ ) translations, and rotations ( $\Theta$ ).

### 2.1.3 Framework for constrained FSM

The primary objective of cFSM is to define constraint matrices for each of the buckling mode classes. When applied, such a constraint matrix reduces the general deformation field, which is expressed by the  $n_{DOF}$  FSM DOF, to a smaller DOF deformation field that satisfies the criteria defined for the given class. In practice, relationship between the nodal displacements can be established in the form of:

$$\mathbf{d} = \mathbf{R}_M \mathbf{d}_M \quad (2.5)$$

where  $\mathbf{d}$  is a general  $n_{DOF}$ -element displacement vector,  $\mathbf{d}_M$  is a displacement vector in the reduced space, and  $\mathbf{R}_M$  is the constraint matrix related to a given mode. Note, the subscript  $M$  expresses the constraint to a mode or a group of modes, i.e.,  $M$  may be replaced by  $G$  (global),  $D$  (distortional),  $L$  (local),  $O$  (other) or any combination of them, e.g.  $GD$ ,  $GDL$ , etc. It should also be noted that the  $\mathbf{d}_M$  vector, being in a reduced DOF space, is not necessarily associated directly with the original FSM nodal displacement DOF, but rather should be interpreted as a vector of generalized coordinates.

Application of  $\mathbf{R}_M$ , via Eq. (2.5), defines a subspace of the original FSM DOF space that meets the criteria of mode  $M$ . Thus, the columns of  $\mathbf{R}_M$  may be considered as a set of base vectors in this space of mode  $M$ . Transformation inside the space of  $M$  is also possible, and thus the base vectors defined by  $\mathbf{R}_M$  are not unique. The vector space defined by the base vectors of a given mode (included in the relevant  $\mathbf{R}_M$ ) will also be referred to as the  $G$ ,  $D$ ,  $L$  or  $O$  space, as well as we may speak about the  $GD$  space (as a union of  $G$  and  $D$  spaces),  $GDL$  space (as a union of  $G$ ,  $D$  and  $L$  spaces), etc. Naturally, the  $GDLO$  space which includes all deformations is itself identical with the original FSM DOF space.

A buckling mode shape (eigen-vector,  $\Phi$ ) is itself a deformation field, and thus the constraint of Eq. (2.5) may be employed on  $\Phi$ . By introducing Eq. (2.5) into Eq. (2.4), then pre-multiplying by  $\mathbf{R}_M^T$ , we arrive at

$$\mathbf{R}_M^T \mathbf{K}_e \mathbf{R}_M \Phi_M = \Lambda_M \mathbf{R}_M^T \mathbf{K}_g \mathbf{R}_M \Phi_M \quad (2.6)$$

which can be re-written as

$$\mathbf{K}_{e,M} \Phi_M = \Lambda_M \mathbf{K}_{g,M} \Phi_M \quad (2.7)$$

which is recognizable as a new eigen-value problem, now in the constrained DOF space spanned by the given mode or modes ( $M$ ). Here,  $\mathbf{K}_{e,M}$  and  $\mathbf{K}_{g,M}$  are the elastic and geometric stiffness matrix of the constrained FSM problem, respectively, defined as

$$\mathbf{K}_{e,M} = \mathbf{R}_M^T \mathbf{K}_e \mathbf{R}_M \text{ and } \mathbf{K}_{g,M} = \mathbf{R}_M^T \mathbf{K}_g \mathbf{R}_M \quad (2.8)$$

Note,  $\mathbf{R}_M$  is an  $n_{DOF} \times n_M$  matrix, where  $n_M$  is the dimension of the reduced DOF space. Consequently,  $\mathbf{K}_{e,M}$  and  $\mathbf{K}_{g,M}$  are  $n_M \times n_M$  matrices unlike  $\mathbf{K}_e$  and  $\mathbf{K}_g$  which are much larger  $n_{DOF} \times n_{DOF}$  matrices. Thus, application of the constraint represents a form of model reduction. Finally,  $\Lambda_M$  is an  $n_M \times n_M$  diagonal matrix containing the eigen-values for the given mode or modes only, and  $\Phi_M$  is the matrix with the eigen-modes (or buckling modes) in its columns.

Derivation of each of the various  $\mathbf{R}_M$  matrices requires different methodologies. Some may be defined directly (e.g.,  $\mathbf{R}_L$  or  $\mathbf{R}_O$ ), while others require relatively long derivations (e.g.,  $\mathbf{R}_D$  or  $\mathbf{R}_G$ ). In some cases no other approach is known than the one used and presented below (e.g., for  $\mathbf{R}_D$ ), while in other cases more than one approach exist.

#### 2.1.4 Definition of buckling classes

The separation of *global* ( $G$ ), *distortional* ( $D$ ), *local* ( $L$ ) and *other* ( $O$ ) deformation modes are completed through implementation of the following three criteria.

Criterion #1: (a)  $\gamma_{xy} = 0$ , i.e., there is no in-plane shear, (b)  $\varepsilon_x = 0$ , i.e. there is no transverse strain, and (c)  $v$  is linear in  $x$  within a flat part (i.e. between two main nodes).

Criterion #2: (a)  $v \neq 0$ , i.e., the warping displacement is not constantly equal to zero along the whole cross-section, and (b) the cross-section is in transverse equilibrium.

Criterion #3:  $\kappa_x = 0$ , i.e., there is no transverse flexure.

Application of the criteria to the G, D, L, and O (global, distortional, local, and other) buckling mode classes is given in **Table 2.1**, defining whether the given criterion is fulfilled (Yes), not fulfilled (No), or irrelevant (–). It is to observe that Criterion 1 is essentially identical to the ones widely used in theories for open thin-walled beams, also referred to as Vlasov’s hypothesis.

**Table 2.1:** Mode classification

	<b>G</b> modes	<b>D</b> modes	<b>L</b> modes	<b>O</b> modes
Criterion #1 – Vlasov’s hypothesis	Yes	Yes	Yes	No
Criterion #2 – Longitudinal warping	Yes	Yes	No	–
Criterion #3 – Undistorted section	Yes	No	–	–

The above criteria are initiated by the generalized beam theory (GBT), which – before developing cFSM – was the only known method possessing the ability to produce and isolate solutions for all the global, distortional, and local buckling modes in a thin-walled members. It is to emphasize, however, that the complete set of these criteria never explicitly appeared in (early) GBT publications. Indeed, GBT does not require having such complete set of criteria, since in GBT there is no pre-defined displacement field which then is separated into some practically meaningful classes, but the displacement field is built up from the selected modes where the user – based on some intuition, or preliminary studies, or previous experiences – defines the modes to consider in the analysis.

Note, for cross-sections with less than or equal to one internal main node, the mode classes slightly overlap. In the original cFSM this problem has not been properly addressed, so, such cross-sections are assumed to be excluded in Section 2 (but will be handled in Section 3). Further, O mode space may be separated into *transverse extension* (T) and *shear* (S) mode spaces (see [1/2]). Since in the original cFSM publications this separation has not been used and/or utilized, therefore, will not be addressed in Section 2, but will be discussed in detail in Section 3. Finally, **Table 2.1** shows the mode classification as it is appeared and used in the original cFSM papers and software implementations; later the criteria are refined, as will be discussed in Section 3.

### 2.1.5 Further cFSM terminology

The line of intersection of two connecting plates will be called the *nodal line* (or simply: *node*), while the plates themselves are referred as *strips*. As will be shown, it is important to distinguish between *main nodes*, where the two connecting strips have a non-zero angle relative to one another, and *sub-nodes*, where the two connecting strips are parallel. Further, main nodes are categorized as *internal* main nodes (also referred as *corner* nodes) or *external* main nodes (also referred as *end* nodes), depending on whether at least two plates or only one single plate is connected to them. (Note, sub-nodes are always internal nodes). Thus, the total number of nodes (or nodal lines) is  $n$ , consisting of  $n_m$  main nodes and  $n_s$  sub-nodes ( $n_m + n_s = n$ ). Considering that the total number of nodal lines is  $n$ , and 4 displacements are assigned to each nodal line, the total number of displacement DOF is:  $n_{DOF} = 4 \times n$ .

In some cases (i.e., for global and distortional modes as will be shown) sub-nodes may be eliminated. The resulting strips, i.e. the flat plates between main nodes, are called *main strips*.

Thus, an open cross-section thin-walled member may be described as either the assemblage of  $(n-1)$  strips, or  $(n_m-1)$  main strips, whichever description is more appropriate. Note, all these terms are illustrated in **Figure 2.2**.

The order of the DOF in the displacement vector and in the global stiffness matrix has no theoretical importance. Nevertheless, a properly selected order makes the developed expressions simpler. For this reason we introduce here a special DOF order used throughout the sub-sequent derivations (in Chapter 2), as follows:

$$\mathbf{d} = [\mathbf{V}_m^T \quad \mathbf{V}_s^T \quad \mathbf{U}_m^T \quad \mathbf{W}_m^T \quad \mathbf{U}_s^T \quad \mathbf{W}_s^T \quad \mathbf{\Theta}^T]^T \quad (2.9)$$

where  $\mathbf{V}_m$  is an  $n_m$ -element partition for longitudinal translation ( $Y$ -dir.) of main nodes,  $\mathbf{V}_s$  is an  $n_s$ -element partition for longitudinal translation of sub-nodes,  $\mathbf{U}_m$  and  $\mathbf{W}_m$  are  $(n_m-2)$  element partitions for transverse translations of the internal main nodes,  $\mathbf{U}_s$  and  $\mathbf{W}_s$  are  $(n_s+2)$  element partitions for transverse translations of the external main nodes and sub-nodes,  $\mathbf{\Theta}$  is an  $(n_m+n_s)$  element partition with the rotational DOF.

## 2.2 Derivation for $\mathbf{R}_{GD}$

### 2.2.1 Strategy

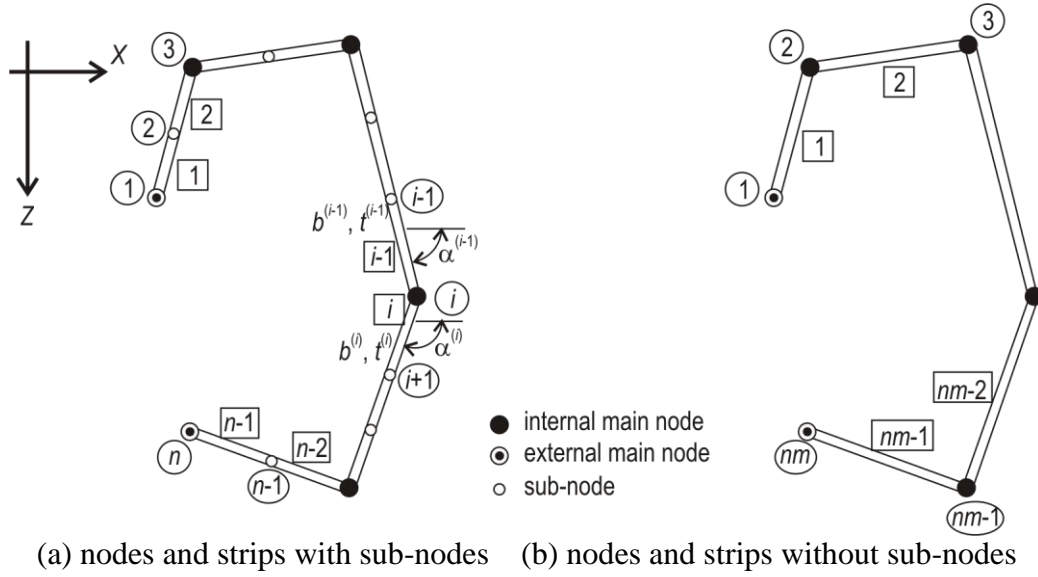
To have  $\mathbf{R}_G$  and  $\mathbf{R}_D$ , first  $\mathbf{R}_{GD}$  is derived, and then it is separated into  $\mathbf{R}_G$  and  $\mathbf{R}_D$ . What makes it possible and relatively convenient to follow this approach, is that as a direct consequence of the applied mode definitions, in the case of G and D modes, the member displacements ( $U$ ,  $W$ ,  $\Theta$ ) can be expressed as a function of the longitudinal displacements ( $V$ ), i.e., global and distortional modes are completely and uniquely defined by cross-section warping. Further, the warping displacements may themselves be used to separate the G and D spaces from one another. As a consequence, (i) it is possible to develop a mathematical relationship between longitudinal displacement DOF and all the other DOF, (ii) the number of GD base vectors is equal to the number of main nodes ( $n_m$ ), and (iii) any set of  $n_m$  independent warping distributions is applicable to serve as system of base vectors.

Thus, the main goal here is to establish the mathematical relationship between the longitudinal displacement DOF of the main nodes ( $\mathbf{V}_m$ ) and all other DOF. The relationship is set up in two steps: first the effect of Criterion #1 is considered, then, in the second step, the impact of Criterion #2 is taken into consideration.

### 2.2.2 Impact of Criterion #1 – unbranched cross-sections

Numbering of an open, unbranched cross-section can conveniently be handled by the system shown in **Figure 2.2**, where node and strip numbers appear in circles and squares, respectively.

When we consider Criterion #1, sub-nodes can (and should) be disregarded, as will become clear from the derivations. Linearity of warping within a flat element is automatically satisfied by the selection of FSM shape functions.



**Figure 2.2:** Description of an open, unbranched cross-section

The two null strain criteria can be written as:

$$\varepsilon_x = \frac{\partial u}{\partial x} = 0 \text{ and } \gamma_{xy} = \frac{\partial u}{\partial y} + \frac{\partial v}{\partial x} = 0 \quad (2.10)$$

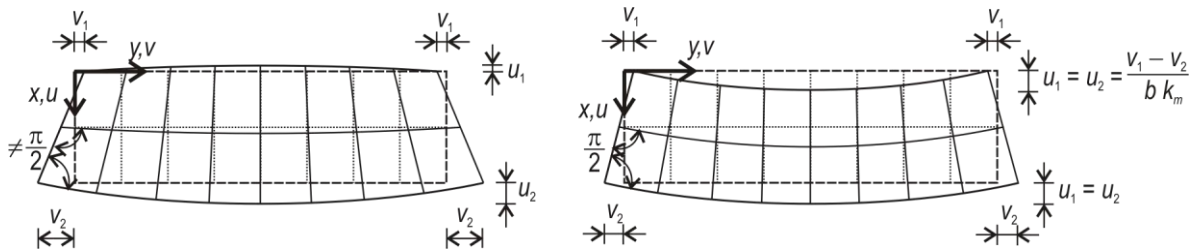
By substituting Eq. (2.1) into the null transverse strain criterion we get

$$u_1 = u_2 = u \quad (2.11)$$

Furthermore, by substituting Eq. (2.2) into the null shear strain criterion, we get:

$$u = (v_1 - v_2) \frac{1}{b k_m} \quad (2.12)$$

with  $k_m = m\pi/a$ . The physical meaning of Criterion #1 is illustrated in **Figure 2.3** where unconstrained (left) and constrained (right) deformations are shown.



**Figure 2.3:** Membrane deformations of a strip: general (left) and constrained (right)

Let us apply Eq. (2.12) for an open, unbranched cross-section. Let us consider the  $i$ -th main nodal line of with the connecting main strips:  $(i-1)$ -th and  $(i)$ -th. The angles of the main strips (with respect to the positive  $x$ -axis) are  $\alpha^{(i-1)}$  and  $\alpha^{(i)}$ , respectively.

$$u^{(i-1)} = \frac{1}{k_m} \left[ \frac{1}{b^{(i-1)}} \quad -\frac{1}{b^{(i-1)}} \right] \begin{bmatrix} v_1^{(i-1)} \\ v_2^{(i-1)} \end{bmatrix} \text{ and } u^{(i)} = \frac{1}{k_m} \left[ \frac{1}{b^{(i)}} \quad -\frac{1}{b^{(i)}} \right] \begin{bmatrix} v_1^{(i)} \\ v_2^{(i)} \end{bmatrix} \quad (2.13)$$

Considering connectivity and the equivalence between the local  $v$  and global  $V$  DOF, the above equation can be re-written as follows:

$$\begin{bmatrix} u^{(i-1)} \\ u^{(i)} \end{bmatrix} = \frac{1}{k_m} \begin{bmatrix} 1/b^{(i-1)} & -1/b^{(i-1)} & 0 \\ 0 & 1/b^{(i)} & -1/b^{(i)} \end{bmatrix} \begin{bmatrix} V_{i-1} \\ V_i \\ V_{i+1} \end{bmatrix} \quad (2.14)$$

The above equation provides relationship between the global longitudinal and local transverse displacements. In order to have the same relationship but expressed by the global transverse DOF, we need to make the appropriate coordinate transformation which leads to the relationship between the global nodal displacements ( $U, V$ ) and the local ( $u$ ) displacements of the  $(i-1)$ -th and  $(i)$ -th plate elements, as follows:

$$\begin{bmatrix} u^{(i-1)} \\ u^{(i)} \end{bmatrix} = \begin{bmatrix} \cos \alpha^{(i-1)} & \sin \alpha^{(i-1)} \\ \cos \alpha^{(i)} & \sin \alpha^{(i)} \end{bmatrix} \begin{bmatrix} U_i \\ W_i \end{bmatrix} \quad (2.15)$$

The equality of the left-hand sides of Eqs. (2.14) and (2.15) leads to the relationship between the longitudinal  $V$  displacements (warping) and the transverse  $U$  and  $W$  displacements, as follows:

$$\begin{bmatrix} \cos \alpha^{(i-1)} & \sin \alpha^{(i-1)} \\ \cos \alpha^{(i)} & \sin \alpha^{(i)} \end{bmatrix} \begin{bmatrix} U_i \\ W_i \end{bmatrix} = \frac{1}{k_m} \begin{bmatrix} 1/b^{(i-1)} & -1/b^{(i-1)} & 0 \\ 0 & 1/b^{(i)} & -1/b^{(i)} \end{bmatrix} \begin{bmatrix} V_{i-1} \\ V_i \\ V_{i+1} \end{bmatrix} \quad (2.16)$$

$$\begin{bmatrix} U_i \\ W_i \end{bmatrix} = \frac{1}{k_m D_i} \begin{bmatrix} \sin \alpha^{(i)} & -\sin \alpha^{(i-1)} \\ -\cos \alpha^{(i)} & \cos \alpha^{(i-1)} \end{bmatrix} \begin{bmatrix} 1/b^{(i-1)} & -1/b^{(i-1)} & 0 \\ 0 & 1/b^{(i)} & -1/b^{(i)} \end{bmatrix} \begin{bmatrix} V_{i-1} \\ V_i \\ V_{i+1} \end{bmatrix} \quad (2.17)$$

where  $D_i$  is the determinant of the matrix with the ‘sin’ and ‘cos’ terms, defined as:

$$D_i = \sin \alpha^{(i)} \cos \alpha^{(i-1)} - \sin \alpha^{(i-1)} \cos \alpha^{(i)} \quad (2.18)$$

Finally, based on Eq. (2.17), the relationship between the displacement vectors can be found:

$$\begin{bmatrix} U_2 \\ U_3 \\ \vdots \\ U_{nm-2} \\ U_{nm-1} \end{bmatrix} = \frac{1}{k_m} \begin{bmatrix} \left( \frac{\sin \alpha^{(2)}}{D_2 b^{(1)}} \right) & \left( -\frac{\sin \alpha^{(2)}}{D_2 b^{(1)}} - \frac{\sin \alpha^{(1)}}{D_2 b^{(2)}} \right) & \left( \frac{\sin \alpha^{(1)}}{D_2 b^{(2)}} \right) & 0 & 0 & 0 & 0 \\ 0 & \left( \frac{\sin \alpha^{(3)}}{D_3 b^{(2)}} \right) & \left( -\frac{\sin \alpha^{(3)}}{D_3 b^{(2)}} - \frac{\sin \alpha^{(2)}}{D_3 b^{(3)}} \right) & \left( \frac{\sin \alpha^{(2)}}{D_3 b^{(3)}} \right) & 0 & 0 & 0 \\ \vdots & \vdots & \vdots & \vdots & \vdots & \vdots & \vdots \\ 0 & 0 & 0 & 0 & \times & \times & \times \\ 0 & 0 & 0 & 0 & 0 & \times & \times \end{bmatrix} \begin{bmatrix} V_1 \\ V_2 \\ V_3 \\ \vdots \\ V_{nm-2} \\ V_{nm-1} \\ V_{nm} \end{bmatrix} \quad (2.19)$$



$$\begin{bmatrix} W_2 \\ W_3 \\ \vdots \\ W_{nm-2} \\ W_{nm-1} \end{bmatrix} = \frac{-1}{k_m} \begin{bmatrix} \left( \frac{\cos \alpha^{(2)}}{D_2 b^{(1)}} \right) & \left( -\frac{\cos \alpha^{(2)}}{D_2 b^{(1)}} - \frac{\cos \alpha^{(1)}}{D_2 b^{(2)}} \right) & \left( \frac{\cos \alpha^{(1)}}{D_2 b^{(2)}} \right) & 0 & 0 & 0 & 0 & 0 \\ 0 & \left( \frac{\cos \alpha^{(3)}}{D_3 b^{(2)}} \right) & \left( -\frac{\cos \alpha^{(3)}}{D_3 b^{(2)}} - \frac{\cos \alpha^{(2)}}{D_3 b^{(3)}} \right) & \left( \frac{\cos \alpha^{(2)}}{D_3 b^{(3)}} \right) & 0 & 0 & 0 & 0 \\ \vdots & \vdots & \vdots & \vdots & \vdots & \vdots & \vdots & \vdots \\ 0 & 0 & 0 & 0 & 0 & \times & \times & \times & 0 \\ 0 & 0 & 0 & 0 & 0 & 0 & \times & \times & \times \end{bmatrix} \begin{bmatrix} V_1 \\ V_2 \\ V_3 \\ \vdots \\ V_{nm-2} \\ V_{nm-1} \\ V_{nm} \end{bmatrix}$$

or, in a more compact form: (2.20)

$$\mathbf{U}_m = \frac{1}{k_m} \mathbf{S}_1 \mathbf{V}_m \text{ and } \mathbf{W}_m = -\frac{1}{k_m} \mathbf{C}_1 \mathbf{V}_m \quad (2.21)$$

where  $\mathbf{U}_m$  and  $\mathbf{W}_m$  are  $(n_m-2)$  element vectors with the  $U$  and  $W$  DOF for internal main nodes from 2 to  $(n_m-1)$ ,  $\mathbf{V}_m$  is an  $n_m$  element vector with the  $V$ -direction nodal displacements of the main nodes, while  $\mathbf{S}_1$  and  $\mathbf{C}_1$  are  $(n_m-2) \times n_m$  matrices, containing basic cross-section geometry data.

The above equations contain  $D_i$  in the denominator, thus, it can be valid only if the case of  $D_i = 0$  is excluded. Considering that Eq. (2.18) can conveniently be rewritten as:

$$D_i = \sin(\alpha^{(i)} - \alpha^{(i-1)}) \quad (2.22)$$

we may conclude that  $\alpha^{(i)}$  and  $\alpha^{(i-1)}$  must not be equal to each other, which is fulfilled for main nodes by definition, but certainly not for sub-nodes. This is why main nodes have special importance, and this is why sub-nodes must be disregarded when Eq. (2.21) is applied.

It is interesting to point out that the longitudinal (or: warping) displacement of the sub-nodes may easily be determined for GD modes. Eq. (2.21) provides a mathematical relationship between  $\mathbf{V}_m$  and the translational DOF for the main nodes. However, Criterion #1(c) has an important impact on the warping displacements of the sub-nodes, namely, for GD modes the warping distribution has to be linear between two main nodes (i.e., within a main strip). Thus, elements of  $\mathbf{V}_s$  can be calculated by linear interpolation, formally:

$$\mathbf{V}_s = \mathbf{B}_{vs} \mathbf{V}_m \quad (2.23)$$

where the elements of  $\mathbf{B}_{vs}$  can be calculated solely from strip widths. For example, the first two elements in the first row of  $\mathbf{B}_{vs}$  may be written as follows:

$$\mathbf{B}_{vs1,1} = 1 - \frac{b^{(1,1)}}{b^{(1)}} \text{ and } \mathbf{B}_{vs1,2} = \frac{b^{(1,1)}}{b^{(1)}} \quad (2.24)$$

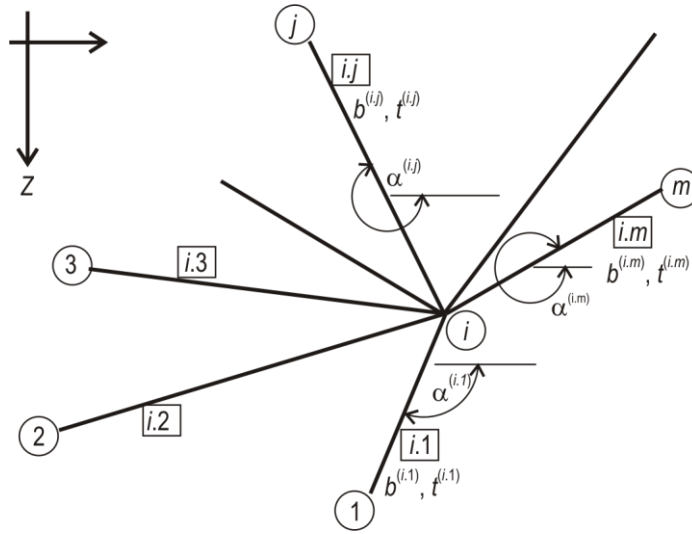
while other elements of the first row are zero. Here,  $b^{(1)}$  and  $b^{(1,1)}$  are the width of the first main strip and first strip, respectively. Construction of subsequent rows is similar.

Although Criterion #1 presents certain restriction for the external main nodes, (because no transverse extension is allowed in the first and last plate elements) the external main nodes are conveniently handled in the sub-sequent parts of the derivations, thus, they are not discussed further in this section.

### 2.2.3 Impact of Criterion #1 – branched cross-sections

In a branched cross-section there is at least one node to which more than two plates are connected. As it will be shown below, this kind of nodes make the main difference in deriving the relationships between the various DOFs, thus, we will first concentrate on a node like this.

Let us consider the  $i$ -th main node, with in adjoining plates, as it is presented in **Figure 2.4**. For the sake of simplicity, let us number the adjacent main nodes as 1, 2, 3, ...,  $j$ , ...  $m$ . The elements are denoted by their start and end nodes, like  $i.1$ ,  $i.2$ , ...,  $i.j$ , ...,  $i.m$ , the first and second index being the start and end node, respectively. It should be underlined here that there may be sub-nodes within any element, however, these sub-nodes will be handled later. For this reason the figure shows the main nodes only.



**Figure 2.4:** A general main node of a multi-branch cross-section with the adjacent elements and main nodes

Similarly to what has been done for unbranched cross-sections, let us apply Eq. (2.13) for all the plate elements that are connected to the  $i$ -th node. Doing so we get  $i_n$  equations of the following kind:

$$u^{(j)} = \frac{1}{k_m} \left[ \frac{1}{b^{(j)}} \quad -\frac{1}{b^{(j)}} \right] \begin{bmatrix} v_1^{(j)} \\ v_2^{(j)} \end{bmatrix} \quad j = 1 \dots m \quad (2.25)$$

Considering the relationship of local  $v$  and global  $V$  displacements, we can write that:

$$\begin{bmatrix} u^{(i.1)} \\ u^{(i.2)} \\ \vdots \\ u^{(i.j)} \\ \vdots \\ u^{(i.m)} \end{bmatrix} = \frac{1}{k_m} \begin{bmatrix} 1/b^{(i.1)} & -1/b^{(i.1)} & 0 & 0 & 0 & 0 & 0 \\ 1/b^{(i.2)} & 0 & -1/b^{(i.2)} & 0 & 0 & 0 & 0 \\ \vdots & \vdots & \vdots & \vdots & \vdots & \vdots & \vdots \\ 1/b^{(i.j)} & 0 & 0 & 0 & -1/b^{(i.j)} & 0 & 0 \\ \vdots & \vdots & \vdots & \vdots & \vdots & \vdots & \vdots \\ 1/b^{(i.m)} & 0 & 0 & 0 & 0 & 0 & -1/b^{(i.m)} \end{bmatrix} \begin{bmatrix} V_i \\ V_1 \\ V_2 \\ \vdots \\ V_j \\ \vdots \\ V_m \end{bmatrix} \quad (2.26)$$

Similarly to what has been done for unbranched cross-sections, the usual transformation matrix can be applied for the  $U_i$ ,  $W_i$  displacements, however, now, it should be applied  $i_n$  times, according to the number of connecting plate elements. Thus, we will arrive at an equation similar to Eq. (2.15), but with more rows:

$$\begin{bmatrix} u^{(i.1)} \\ u^{(i.2)} \\ \vdots \\ u^{(i.j)} \\ \vdots \\ u^{(i.m)} \end{bmatrix} = \begin{bmatrix} \cos \alpha^{(i.1)} & \sin \alpha^{(i.1)} \\ \cos \alpha^{(i.2)} & \sin \alpha^{(i.2)} \\ \vdots & \vdots \\ \cos \alpha^{(i.j)} & \sin \alpha^{(i.j)} \\ \vdots & \vdots \\ \cos \alpha^{(i.m)} & \sin \alpha^{(i.m)} \end{bmatrix} \begin{bmatrix} U_i \\ W_i \end{bmatrix} \quad (2.27)$$

which actually defines the relationship between the global  $U, W$  displacements of the given node and the local  $u$  displacements of the adjacent plate elements.

Looking at Eq. (2.27), it is easy to understand that the transverse displacement of a node with multiple connecting plates is over-determined, since there are only two unknowns (namely:  $U_i$  and  $W_i$ ) but  $i_n$  ( $i_n > 2$ ) equations. In other words, any two of the adjacent plate elements (with a distinct angle difference) would unambiguously determine the  $U_i$ ,  $W_i$  displacements, consequently, the rest of the equations are redundant. If we yet want to satisfy Eq. (2.27), we cannot have arbitrary  $u$ -s, therefore, we cannot have arbitrary  $V$  longitudinal displacements.

Mathematically, the problem can be handled as follows. Since the left-hand side of Eq. (2.26) and (2.27) are identical, their right-hand sides must be equal, too, which leads to the following equation:

$$\begin{bmatrix} \cos \alpha^{(i.1)} & \sin \alpha^{(i.1)} \\ \cos \alpha^{(i.2)} & \sin \alpha^{(i.2)} \\ \cos \alpha^{(i.3)} & \sin \alpha^{(i.3)} \\ \vdots & \vdots \\ \cos \alpha^{(i.j)} & \sin \alpha^{(i.j)} \\ \vdots & \vdots \\ \cos \alpha^{(i.m)} & \sin \alpha^{(i.m)} \end{bmatrix} \begin{bmatrix} U_i \\ W_i \end{bmatrix} = \frac{1}{k_m} \begin{bmatrix} \frac{1}{b^{(i.1)}} & -\frac{1}{b^{(i.1)}} & 0 & 0 & 0 & 0 & 0 & 0 \\ \frac{1}{b^{(i.2)}} & 0 & -\frac{1}{b^{(i.2)}} & 0 & 0 & 0 & 0 & 0 \\ \hline \frac{1}{b^{(i.3)}} & 0 & 0 & -\frac{1}{b^{(i.3)}} & 0 & 0 & 0 & 0 \\ \vdots & \vdots & \vdots & \vdots & \vdots & \vdots & \vdots & \vdots \\ \frac{1}{b^{(i.j)}} & 0 & 0 & 0 & 0 & -\frac{1}{b^{(i.j)}} & 0 & 0 \\ \vdots & \vdots & \vdots & \vdots & \vdots & \vdots & \vdots & \vdots \\ \frac{1}{b^{(i.m)}} & 0 & 0 & 0 & 0 & 0 & 0 & -\frac{1}{b^{(i.m)}} \end{bmatrix} \begin{bmatrix} V_{i.1} \\ V_{i.2} \\ V_{i.3} \\ V_{i.4} \\ \vdots \\ V_{i.j} \\ \vdots \\ V_{i.m} \end{bmatrix} \quad (2.28)$$

As it is discussed above, any two equations would determine the unknown  $U_i$ ,  $W_i$  displacements (provided the corresponding angles are different), thus, let us select the first two equations to calculate the  $U_i$ ,  $W_i$  transverse displacements, while the rest of the equations must be used to set up a restraint for the  $V$  longitudinal displacements. Thus, Eq. (2.28) can be partitioned as shown. By introducing some simplifying provisional notations:

$$\begin{bmatrix} \mathbf{A}_1 \\ \mathbf{A}_2 \end{bmatrix} \mathbf{D}_T = \frac{1}{k_m} \begin{bmatrix} \mathbf{B}_{11} & \mathbf{B}_{12} \\ \mathbf{B}_{21} & \mathbf{B}_{22} \end{bmatrix} \begin{bmatrix} \mathbf{D}_{L1} \\ \mathbf{D}_{L2} \end{bmatrix} \quad (2.29)$$

Considering that  $\mathbf{B}_{12}$  is a matrix with zero elements only, the  $\mathbf{D}_T$  transverse displacements can be expressed from the first row of Eq. (2.29), as follows:

$$\mathbf{D}_T = \frac{1}{k_m} \mathbf{A}_1^{-1} \mathbf{B}_{11} \mathbf{D}_{L1} \quad (2.30)$$

At the same time, the second row of Eq. (2.29) can be used to express the longitudinal displacements of the other nodes ( $\mathbf{D}_{L2}$ ):

$$\mathbf{D}_{L2} = \mathbf{B}_{22}^{-1} (k_m \mathbf{A}_2 \mathbf{D}_T - \mathbf{B}_{21} \mathbf{D}_{L1}) \quad (2.31)$$

where the matrix inversion can always be performed  $\mathbf{B}_{22}$  being a diagonal matrix with definitely non-zero diagonal elements. Furthermore, substituting Eq. (2.30) into Eq. (2.31) leads to the following formula:

$$\mathbf{D}_{L2} = (\mathbf{B}_{22}^{-1} \mathbf{A}_2 \mathbf{A}_1^{-1} \mathbf{B}_{11} - \mathbf{B}_{22}^{-1} \mathbf{B}_{21}) \mathbf{D}_{L1} \quad (2.32)$$

Thus, Eq. (2.32) defines the relationship between the longitudinal displacements of nodes associated with a given node. If there are multiple nodes with more than two adjacent plates, similar equations should be applied.

It is to be noted that the inverse matrix of  $\mathbf{A}_1$  can be easily calculated analytically. The inverse matrix exists only if the selected two plates are not parallel. However, in case of a node with more than two adjoining plates there are always two non-parallel ones, therefore, the above procedure can always be performed by the appropriate partitioning of the problem. It may also be interesting to mention that the term  $\mathbf{B}_{22}^{-1} \mathbf{B}_{21}$  is easy to calculate. In fact,  $\mathbf{B}_{22}^{-1} \mathbf{B}_{21}$  is a matrix with (-1)s in its first column and zeros elsewhere.

When considering the whole branched cross-sections, therefore, the main nodes can be grouped into determining and undetermining (redundant) groups. Obviously, determining main node group must be selected so that there would be (exactly) two neighbouring main nodes for each internal main nodes. Thus:

$$\mathbf{V}_m^T = [\mathbf{V}_{md}^T \quad \mathbf{V}_{mr}^T] \quad (2.33)$$

In the determination of the transverse displacements  $\mathbf{V}_{md}$  can be used similarly as  $\mathbf{V}_m$  of an unbranched cross-section, by equations similar to Eq. (2.21):

$$\mathbf{U}_m = \frac{1}{k_m} \mathbf{S}_1 \mathbf{V}_{md} \quad \text{and} \quad \mathbf{W}_m = -\frac{1}{k_m} \mathbf{C}_1 \mathbf{V}_{md} \quad (2.34)$$

The  $\mathbf{V}_{mr}$  redundant part of  $\mathbf{V}_m$  can be determined also from  $\mathbf{V}_{md}$ , by the consecutive application of Eq. (2.32) for each main node with more than two adjoining main strips. Alternatively, from the  $(\mathbf{B}_{22}^{-1} \mathbf{A}_2 \mathbf{A}_1^{-1} \mathbf{B}_{11} - \mathbf{B}_{22}^{-1} \mathbf{B}_{21})$  nodal matrices a cross-section matrix can be compiled, which leads to the following expression for the relationship of redundant and determining warping displacements:

$$\mathbf{V}_{mr} = \mathbf{B}_{vr} \mathbf{V}_{md} \quad (2.35)$$

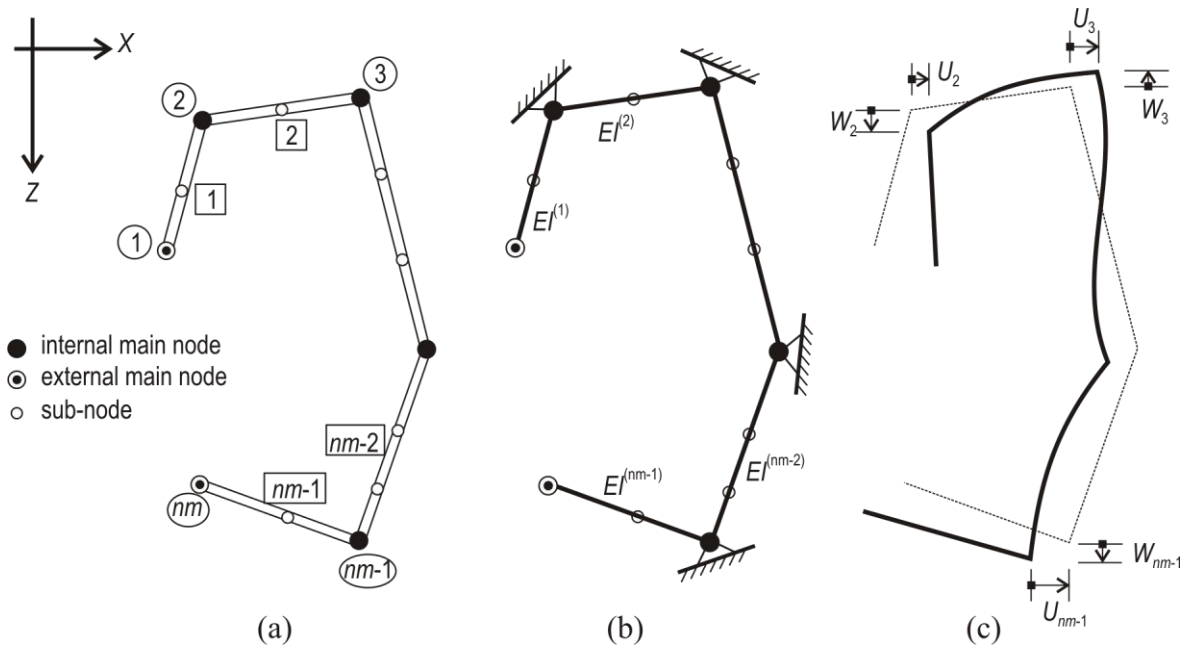
## 2.2.4 Impact of Criterion #2

The physical meaning of Criterion #2(a) is that the main nodal lines do not remain straight in G and D modes, since for non-uniform, non-zero  $\mathbf{V}_m$  non-zero  $\mathbf{U}_m$  and  $\mathbf{W}_m$  results, as can be seen from Eq. (2.21). (The only exception is when  $\mathbf{V}_m$  is constant, which leads to the so-called pure axial mode, as discussed later.)

Criterion #2(b) requires equilibrium of the transverse stress resultants of any cross-section. Thus, this criterion has a direct analogy to a multi-span beam bending problem, as detailed below. The analogy is illustrated in **Figure 2.5** where (a) the cross-section, (b) the equivalent beam model, and (c) the deformed geometry model are shown.

The equivalent beam's global geometry is identical with the cross-section geometry, which means that the nodes of the beam and those of the cross-section are identical. The bending rigidity of the equivalent beam is identical with the transverse plate rigidity of the member. The axial rigidity of the equivalent beam is assumed to be large, and the associated elongation/shortening negligible; therefore, only moments are considered in ensuring the cross-section equilibrium.

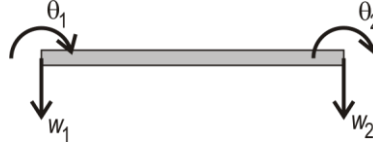
The assumed loading is a kinematic loading, expressed by the movement of the supports. These support displacements are exactly the transverse  $U$ ,  $W$  displacements in the  $\mathbf{U}_m$  and  $\mathbf{W}_m$  vectors of Eq. (2.21).



**Figure 2.5:** (a) cross-section, (b) the equivalent multi-span beam, (c) deformations due to imposed kinematic loading

The equivalent beam problem requires the solution of a statically indeterminate system. Basically, there are two solution alternatives: the flexibility method and the stiffness method. In [6/2], the flexibility method has been applied (for unbranched cross-sections), which follows more closely the developments in GBT [22/1]. However, the stiffness method is simpler to generalize, and better fits an FSM implementation. Further, the stiffness matrix which is necessary to solve the equivalent beam problem can easily be derived from the regular FSM element stiffness matrices, which has a great advantage in the practical implementation of cFSM. Thus, the stiffness method is summarized here, following [8/2].

Consider a single beam element, as shown in **Figure 2.6**. The assumed DOF is:  $w_1, \theta_1, w_2, \theta_2$ .



**Figure 2.6:** DOF of an equivalent beam element

The element stiffness matrix in the local coordinate system can be written as follows:

$$\mathbf{k}_{e,t} = \begin{bmatrix} \frac{12EI}{b^3} & & & \\ \frac{6EI}{b^2} & \frac{4EI}{b} & & \\ -\frac{12EI}{b^3} & -\frac{6EI}{b^2} & \frac{12EI}{b^3} & \\ \frac{6EI}{b^2} & \frac{2EI}{b} & -\frac{6EI}{b^2} & \frac{4EI}{b} \end{bmatrix} \quad \text{sym.} \quad (2.36)$$

where  $EI$  is the bending stiffness of the bar. (Note that the  $t$  subscript is applied to emphasize that the presented matrix is for *transverse* displacement components.)

Considering that the beam elements represent plate-like elements, bending rigidity should be taken as the plate bending rigidity, which can be formulated as follows, for isotropic and orthotropic material respectively:

$$EI = \frac{Ea^3t^3}{12(1-\nu^2)} \quad \text{or} \quad EI = \frac{E_x a^3 t^3}{12(1-\nu_x \nu_y)} \quad (2.37)$$

where  $\nu$  is the Poisson's ratio for isotropic material, while  $\nu_x$  and  $\nu_y$  are the Poisson's ratios in the two perpendicular directions for orthotropic material. The global stiffness matrix can be compiled from the  $\mathbf{k}_{e,t}$  element stiffness matrices via coordinate transformation and assembly.

Having the global transverse stiffness matrix compiled, the static equilibrium of the equivalent beam can be written as:

$$\mathbf{K}_{e,t} \mathbf{d}_t = \mathbf{q}_t \quad \text{or} \quad \begin{bmatrix} \mathbf{K}_{e,t,kk} & \mathbf{K}_{e,t,ku} \\ \mathbf{K}_{e,t,uk} & \mathbf{K}_{e,t,uu} \end{bmatrix} \begin{bmatrix} \mathbf{d}_{t,k} \\ \mathbf{d}_{t,u} \end{bmatrix} = \begin{bmatrix} \mathbf{q}_{t,k} \\ \mathbf{q}_{t,u} \end{bmatrix} \quad (2.38)$$

where  $\mathbf{K}_{e,t}$  is the transverse stiffness matrix (for the whole cross-section),  $\mathbf{d}_t$  is the displacement vector for the transverse DOF of the equivalent beam, and  $\mathbf{q}_t$  is the vector of nodal forces for the same DOF, and the  $\mathbf{k}$  and  $\mathbf{u}$  indexes correspond to the *known* and *unknown* sets of DOF. Thus,  $\mathbf{d}_{t,k}$  is that partition of the displacement vector which contains the known displacements, i.e., the  $U$  and  $W$  displacements of the internal main nodes, contained in the  $\mathbf{U}_m$  and  $\mathbf{W}_m$  vectors of Eq. (2.21) and  $\mathbf{d}_{t,u}$  contains the other (unknown) transverse displacements, including the translations of the external main nodes, the translations of the sub-nodes, and the rotations for all the nodes, collected in the  $[\mathbf{U}_s, \mathbf{W}_s, \mathbf{\Theta}]^T$  vector. Similarly,  $\mathbf{q}_{t,k}$  is the vector of nodal forces acting on the known DOF, while forces acting on the unknown DOF are the  $\mathbf{q}_{t,u}$  partition of the force vector. External loads are not applied on the equivalent beam, thus  $\mathbf{q}_{t,u}$  is zero. Thus, expanding and solving the lower partition of Eq. (2.38), the unknown displacements can formally be expressed as follows:

$$\mathbf{d}_{t,u} = -\mathbf{K}_{e,t,uu}^{-1} \mathbf{K}_{e,t,uk} \mathbf{d}_{t,k} \quad (2.39)$$

or, in a more explicit form:

$$\begin{bmatrix} \mathbf{U}_s \\ \mathbf{W}_s \\ \boldsymbol{\Theta} \end{bmatrix} = -\mathbf{K}_{e,t,uu}^{-1} \mathbf{K}_{e,t,uk} \begin{bmatrix} \mathbf{U}_m \\ \mathbf{W}_m \end{bmatrix} \quad (2.40)$$

It is worth mentioning that in the practice the matrix inversion need not be performed, since the  $-\mathbf{K}_{e,t,uu}^{-1} \mathbf{K}_{e,t,uk}$  product matrix can also be regarded as the formal solution of a linear equation system with multiple right-hand sides.

### 2.2.5 Assembling $\mathbf{R}_{GD}$

The calculation of  $\mathbf{R}_{GD}$  can be carried out by assembling its sub-matrices. Calculation of the sub-matrices can be completed on the basis of the preceding derivations, as summarized below.

The longitudinal displacements of the determining main nodes,  $\mathbf{R}_{GD,vmd}$ , can be arbitrarily selected. Each different  $\mathbf{R}_{GD,vmd}$  leads to a specific  $\mathbf{R}_{GD}$ , hence, to a specific base vector system, however, any  $\mathbf{R}_{GD,vmd}$  leads to the same GD space. Thus, the simplest natural solution is to set  $\mathbf{R}_{GD,vmd}$  equal to the identity matrix. Warping displacements of the redundant main nodes can be determined by using Eq. (2.35). Finally, the warping displacements of all the main nodes can be constructed as in Eq. (2.33).

$$\mathbf{R}_{GD,v_m} = \begin{bmatrix} \mathbf{I} \\ \mathbf{B}_{vr} \end{bmatrix} \quad (2.41)$$

(Obviously, if there are no redundant main nodes,  $\mathbf{B}_{vr}$  does not exist and  $\mathbf{R}_{GD,v_m}$  is simply equal to the identity matrix.) Warping displacements of sub-nodes  $\mathbf{R}_{GD,v_s}$  can be get by linear interpolation, by using Eq. (2.23):

$$\mathbf{R}_{GD,v_s} = \mathbf{B}_v \mathbf{R}_{GD,v_m} \quad (2.42)$$

Transverse translational DOF of internal main nodes  $\mathbf{R}_{GD,U_m}$  and  $\mathbf{R}_{GD,W_m}$  can be calculated by using Eq. (2.21):

$$\mathbf{R}_{GD,U_m} = \frac{1}{k_m} \mathbf{S}_1 \mathbf{R}_{GD,v_m} \text{ and } \mathbf{R}_{GD,W_m} = -\frac{1}{k_m} \mathbf{C}_1 \mathbf{R}_{GD,v_m} \quad (2.43)$$

Transverse translational DOF of other nodes, i.e.,  $\mathbf{R}_{GD,U_s}$ ,  $\mathbf{R}_{GD,W_s}$ , and  $\mathbf{R}_{GD,\boldsymbol{\Theta}}$  can be calculated by using Eq. (2.40):

$$\begin{bmatrix} \mathbf{R}_{GD,U_s} \\ \mathbf{R}_{GD,W_s} \\ \mathbf{R}_{GD,\boldsymbol{\Theta}} \end{bmatrix} = -\mathbf{K}_{t,uu}^{-1} \mathbf{K}_{t,uk} \begin{bmatrix} \mathbf{R}_{GD,U_m} \\ \mathbf{R}_{GD,W_m} \end{bmatrix} \quad (2.44)$$

Finally,  $\mathbf{R}_{GD}$  is composed from its partitions:

$$\mathbf{R}_{GD} = \begin{bmatrix} \mathbf{R}_{GD,v_m}^T & \mathbf{R}_{GD,v_s}^T & \mathbf{R}_{GD,U_m}^T & \mathbf{R}_{GD,W_m}^T & \mathbf{R}_{GD,U_s}^T & \mathbf{R}_{GD,W_s}^T & \mathbf{R}_{GD,\boldsymbol{\Theta}}^T \end{bmatrix}^T \quad (2.45)$$

## 2.3 $R_G$ , $R_D$ , $R_L$ and $R_O$ matrices

### 2.3.1 Assembling $R_G$

According to the basic FSM idea, member deformation is expressed as a function of cross-section deformations, since longitudinal deformation must take place in the assumed sine/cosine waves (i.e., the longitudinal shape functions). In addition, the definition of G modes ensures that all the cross-sectional deformations are excluded. These conditions lead to the conclusion that there are only 4 DOF for G modes, according to the 4 types of displacement of the rigid-body-like cross-section. Thus, this suggests that four global modes exist, characterized by (i) longitudinal translation, (ii) the two transverse translations and (iii) the rotation along the member longitudinal axis (i.e., the 4 basic DOF of the FSM model).

The mode, which exhibits longitudinal translation only, (and hence will be referred to as the *axial* mode) automatically defines a uniform warping distribution. The other three modes are also determined by rigid-body-like cross-section displacement; however, to derive the corresponding warping distribution requires further considerations. The idea employed is that application of unit displacements on the rigid cross-section defines the transverse DOF, including local  $u$  displacements, which are connected to the warping displacements by Criterion #1, which finally leads to the desired warping displacement distribution.

Applying unit  $U$ ,  $W$  or  $\Theta$  on the rigid cross-section determines all transverse displacement DOF. Note, this discussion focuses on the main nodes only, though all sub-nodes are determined as well. The nodal  $U$  and  $W$  displacements; however, can easily be transformed into local  $u$  and  $w$ . Considering that the global  $U$ - $W$ s are not arbitrary but correspond to a rigid-body cross-section displacement, and considering that rigid cross-section means no transverse strain, thus only one single  $u$  per (main) strip exists, and these  $u$ -s can be expressed (for example) as:

$$\mathbf{u} = \mathbf{C}_2 \begin{bmatrix} U_1 \\ \mathbf{U}_m \end{bmatrix} + \mathbf{S}_2 \begin{bmatrix} W_1 \\ \mathbf{W}_m \end{bmatrix} \quad (2.46)$$

where  $\mathbf{u}$  is a vector with the local  $u$ -s from 1 to  $(nm-1)$ ,  $U_1$  and  $W_1$  are displacements of the first (end) node, while  $\mathbf{S}_2$  and  $\mathbf{C}_2$  are  $(nm-1) \times (nm-1)$  diagonal matrices defined as  $\mathbf{S}_2 = \text{diag}(\sin\alpha^{(1)}, \sin\alpha^{(2)}, \dots)$  and  $\mathbf{C}_2 = \text{diag}(\cos\alpha^{(1)}, \cos\alpha^{(2)}, \dots)$ , with  $\alpha^{(i)}$  the angle of the main strips.

We can also consider the relationship between local  $u$ -s and the warping displacements, by applying Eq. (2.13):

$$\begin{bmatrix} u^{(1)} \\ u^{(2)} \\ \vdots \\ u^{(nm-1)} \end{bmatrix} = \frac{1}{k_m} \begin{bmatrix} 1/b^{(1)} & -1/b^{(1)} & 0 & \dots & 0 & 0 & 0 \\ 0 & 1/b^{(2)} & -1/b^{(2)} & \dots & 0 & 0 & 0 \\ \vdots & \vdots & \vdots & \ddots & \vdots & \vdots & \vdots \\ 0 & 0 & 0 & \dots & 0 & 1/b^{(nm-1)} & -1/b^{(nm-1)} \end{bmatrix} \begin{bmatrix} V_1 \\ V_2 \\ \vdots \\ V_{nm} \end{bmatrix} \quad (2.47)$$

or in short, with introducing a notation for the above matrix:

$$\mathbf{u} = \frac{1}{k_m} \mathbf{B}_2 \mathbf{V}_m \quad (2.48)$$



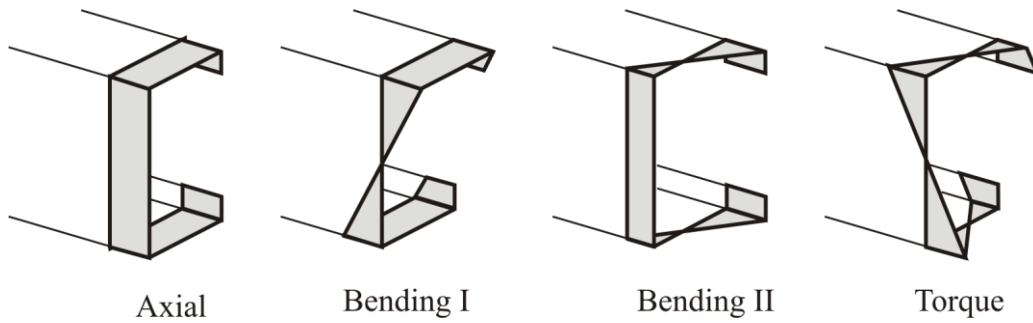
Considering Eqs. (2.46) and (2.48), we may write that:

$$\frac{1}{k_r} \mathbf{B}_2 \mathbf{V}_m = \mathbf{C}_2 \begin{bmatrix} U_1 \\ \mathbf{U}_m \end{bmatrix} + \mathbf{S}_2 \begin{bmatrix} W_1 \\ \mathbf{W}_m \end{bmatrix} \quad (2.49)$$

Now, if the transverse translations of the main nodes are determined by the rigid-body cross-section displacements, the corresponding  $\mathbf{V}_m$  warping distribution can be calculated from Eq. (2.49). The number of equations in Eq. (2.49) is  $(n_m-1)$ , while the number of unknowns is  $n_m$ , thus, one further condition must be introduced for the problem to become determinate. The selected condition is that the integral of the warping distribution over the whole cross-section should be zero. The resulting warping distributions are demonstrated in **Figure 2.7** for a symmetrical C-shaped cross-section. The presented warping functions can also be interpreted as warping associated with special loadings, namely pure axial force, pure bending about two non-parallel axes, and pure torque. The G modes will be referred to as the *axial* mode, *bending* modes and *torsional* mode.

By collecting the 4 characterizing (i.e., characterizing for the G mode space) warping distributions of the main nodes into a  $\mathbf{H}_G$  matrix, the  $\mathbf{R}_G$  global constraint matrix can be calculated as follows:

$$\mathbf{R}_G = \mathbf{R}_{GD} \mathbf{H}_G \quad (2.50)$$



**Figure 2.7:** Warping functions for global modes

As **Figure 2.7** suggests,  $\mathbf{H}_G$  can be determined directly from beam-model-based solutions. It may also be interesting to mention that though a direct relationship between transverse displacements and warping displacements exists, the magnitude can arbitrarily be set through the application of  $U$ ,  $W$  or  $\Theta$  of any magnitude on the rigid cross-section. From the viewpoint of the G space, the magnitude of the  $\mathbf{H}_G$  vectors is not relevant, therefore the  $\mathbf{H}_G$  vectors can be scaled arbitrarily.

Finally, it is useful to highlight here that the two bending modes can be defined an infinite number of ways, depending on the ratio of the applied  $U$  and  $W$ . In other words, transverse displacements in any two non-parallel directions can be applied to generate the two bending mode base vectors. In most cases the most convenient is to apply two perpendicular transverse displacements; moreover, it may have further advantage if the two directions coincide with the principal axes of the cross-section.

### 2.3.2 Assembling $\mathbf{R}_D$

Currently no direct definition for distortional modes is known, thus, the warping functions for the distortional modes are generated such that the space that they define together with the base vectors of the G space result in the GD space. In other words, the D space is the null space of the G space within GD. Any base vector in the G space must be *orthogonal* to any base vector

in the D space. More exactly, it is not the *vectors* themselves which have to be orthogonal, but rather the *warping functions*.

Though various orthogonality conditions are possible, we adopt the following condition:

$$\int v_r(x) v_s(x) t(x) dx = 0 \quad (2.51)$$

where the integral is over the whole cross-section,  $t(x)$  is the thickness, while  $v_r(x)$  and  $v_s(x)$  are two arbitrary warping functions of the G and D space, respectively. Note, that the above expression is nearly identical with the one used in GBT [22/1].

The integration can readily be performed strip by strip. Considering that the thickness is constant, then substituting the corresponding FSM shape functions:

$$\sum_{k=1}^p t^{(k)} \int_0^{b^{(k)}} \left[ \left( 1 - \frac{x}{b^{(k)}} \right) v_{r,1}^{(k)} + \frac{x}{b^{(k)}} v_{r,2}^{(k)} \right] \cos \frac{m\pi y}{a} \left[ \left( 1 - \frac{x}{b^{(k)}} \right) v_{s,1}^{(k)} + \frac{x}{b^{(k)}} v_{s,2}^{(k)} \right] \cos \frac{m\pi y}{a} dx = 0 \quad (2.52)$$

This finally leads to the following expression:

$$\sum_{k=1}^p A^{(k)} \left( 2v_{r,1}^{(k)} v_{s,1}^{(k)} + v_{r,1}^{(k)} v_{s,2}^{(k)} + v_{r,2}^{(k)} v_{s,1}^{(k)} + 2v_{r,2}^{(k)} v_{s,2}^{(k)} \right) = 0 \quad (2.53)$$

where  $A^{(k)}$  is the area of the  $k$ -th strip of the cross-section. Noting the equivalence of local  $v$  and global  $V$  nodal displacements the above expression can be re-written in terms of the global  $V$  displacements, and can be expressed by the following matrix equation:

$$\mathbf{V}_r^T \mathbf{O}_{vA} \mathbf{V}_s = 0 \quad (2.54)$$

where  $\mathbf{O}_{vA}$  is a  $n$  by  $n$  matrix, which is compiled from the  $A^{(k)}$  and  $2A^{(k)}$  terms (similarly as e.g., the stiffness matrix is compiled), while  $\mathbf{V}_r$  and  $\mathbf{V}_s$  denotes two (different) column vectors of  $\mathbf{V}$  which is constructed as  $\mathbf{V}^T = [\mathbf{V}_m^T \mathbf{V}_s^T]$ . (Note, more discussion on orthogonality is in Section 3, while derivation of  $\mathbf{O}$  orthogonality matrices can be found in Appendix A.)

The above condition can directly be applied for  $\mathbf{H}_G$  and  $\mathbf{H}_D$ , by taking into consideration the relationship of  $\mathbf{V}$  and  $\mathbf{V}_m$ , similarly as in Eq. (2.23):

$$\mathbf{H}_D^T [\mathbf{I} \ \mathbf{B}_v] \mathbf{O}_{vA} \begin{bmatrix} \mathbf{I} \\ \mathbf{B}_v^T \end{bmatrix} \mathbf{H}_G = 0 \quad (2.55)$$

where  $\mathbf{H}_D$  is the matrix the columns of which contains the warping DOF (of the main nodes) characterizing for the D mode space,  $\mathbf{0}$  is a matrix full with zeros,  $\mathbf{I}$  is the  $n_m$ -order identity matrix, and  $\mathbf{B}_v$  is the matrix defined at Eq. (2.23).

Since  $\mathbf{H}_G$  is known from the G mode space definition, the only unknown in the above equation is  $\mathbf{H}_D$ . Indeed,  $\mathbf{H}_D$  can be interpreted as the null-space of  $[\mathbf{I} \ \mathbf{B}_v] \mathbf{O}_{vA} \begin{bmatrix} \mathbf{I} \\ \mathbf{B}_v^T \end{bmatrix} \mathbf{H}_G$ .

Modern software tools, such as MatLab [9/2], provide a simple way to solve the problem numerically. Once  $\mathbf{H}_D$  is defined, the corresponding constraint matrix can be calculated as follows:

$$\mathbf{R}_D = \mathbf{R}_{GD} \mathbf{H}_D \quad (2.56)$$

### 2.3.3 Assembling $\mathbf{R}_L$

Definition of  $\mathbf{R}_L$  is a straightforward process and can be completed by the application of the defining criteria for L modes. First, L modes must meet the requirements given in Criterion #1, which results in the strict relationship between the longitudinal nodal displacements (warping) of the main nodes and the transverse nodal displacements of the internal main nodes, as formulated by Eq. (2.21) and /or (2.49). Moreover, Criterion #2 must not be fulfilled, which means that (i) all the warping displacements are zero, and (ii) transverse equilibrium may be violated. From the first condition, and considering Eq. (2.21), L modes have no translational displacements at any of the internal main nodes. Moreover, considering Criterion #1(a), local  $u$  displacements must be equal to zero for all the strips, that is no transverse strain is allowed. As a consequence, translation of other than internal main nodes is limited to the local  $w$  direction, i.e., perpendicular to the given plate element.

Since no other restriction is given for L modes, all the displacements that are not excluded by the above conditions are free to occur. Namely, the possible displacements include (i) the local  $w$ -direction translation of the external main nodes, (ii) the local  $w$ -direction translation of the sub-nodes, and (iii) the rotation  $\Theta$  of any nodes. All the other DOF are zero. A valid, and convenient way to have the  $\mathbf{R}_L$  matrix defined is to apply FEM-like (or FSM-like) base functions with unit displacement at one node while zeros at all the other nodes.

In practice,  $\mathbf{R}_L$  can be assembled from its partitions. Among the partitions of  $\mathbf{R}_L$ , the only ones with non-zero elements are  $\mathbf{R}_{L,Us}$ ,  $\mathbf{R}_{L,ws}$  and  $\mathbf{R}_{L,\Theta}$ , while all the other sub-matrices are zero by definition.

$$\mathbf{R}_{L,Vm} = \mathbf{0}, \mathbf{R}_{L,Vs} = \mathbf{0}, \mathbf{R}_{L,Um} = \mathbf{0} \text{ and } \mathbf{R}_{L,Wm} = \mathbf{0} \quad (2.57)$$

The non-zero partitions of  $\mathbf{R}_L$  may be written as follows:

$$\mathbf{R}_{L,Us} = [\mathbf{S}_3 \quad \mathbf{0}], \mathbf{R}_{L,ws} = [\mathbf{C}_3 \quad \mathbf{0}] \text{ and } \mathbf{R}_{L,\Theta} = [\mathbf{0} \quad \mathbf{I}] \quad (2.58)$$

where  $\mathbf{0}$  marks the partitions with zeros (of various sizes),  $\mathbf{I}$  marks the identity matrix (which in this case is an  $n \times n$  matrix), while  $\mathbf{S}_3$  and  $\mathbf{C}_3$  are diagonal matrices (both with  $(n_s+2) \times (n_s+2)$  size), and can be expressed as  $\mathbf{S}_3 = \text{diag}(-\sin\alpha_1, -\sin\alpha_2, \dots)$  and  $\mathbf{C}_3 = \text{diag}(\cos\alpha_1, \cos\alpha_2, \dots)$ , where  $\alpha_i$  is the angle of the strip at the location of the given  $i$ -th node. Finally,  $\mathbf{R}_L$  can be composed as follows:

$$\mathbf{R}_L = \begin{bmatrix} \mathbf{R}_{L,Vm}^T & \mathbf{R}_{L,Vs}^T & \mathbf{R}_{L,Um}^T & \mathbf{R}_{L,Wm}^T & \mathbf{R}_{L,Us}^T & \mathbf{R}_{L,ws}^T & \mathbf{R}_{L,\Theta}^T \end{bmatrix}^T \quad (2.59)$$

### 2.3.4 Defining $\mathbf{R}_O$

The characterizing feature of O modes is that they do not satisfy Criterion #1, that is transverse strains and/or in-plane shear are not zero, and a non-linear warping distribution between two main nodes is allowed. This latter criterion is strongly connected to the existence of in-plane shear deformations. Thus, deformations in the O space exhibit either transverse extension/shortening, or in-plane shear.

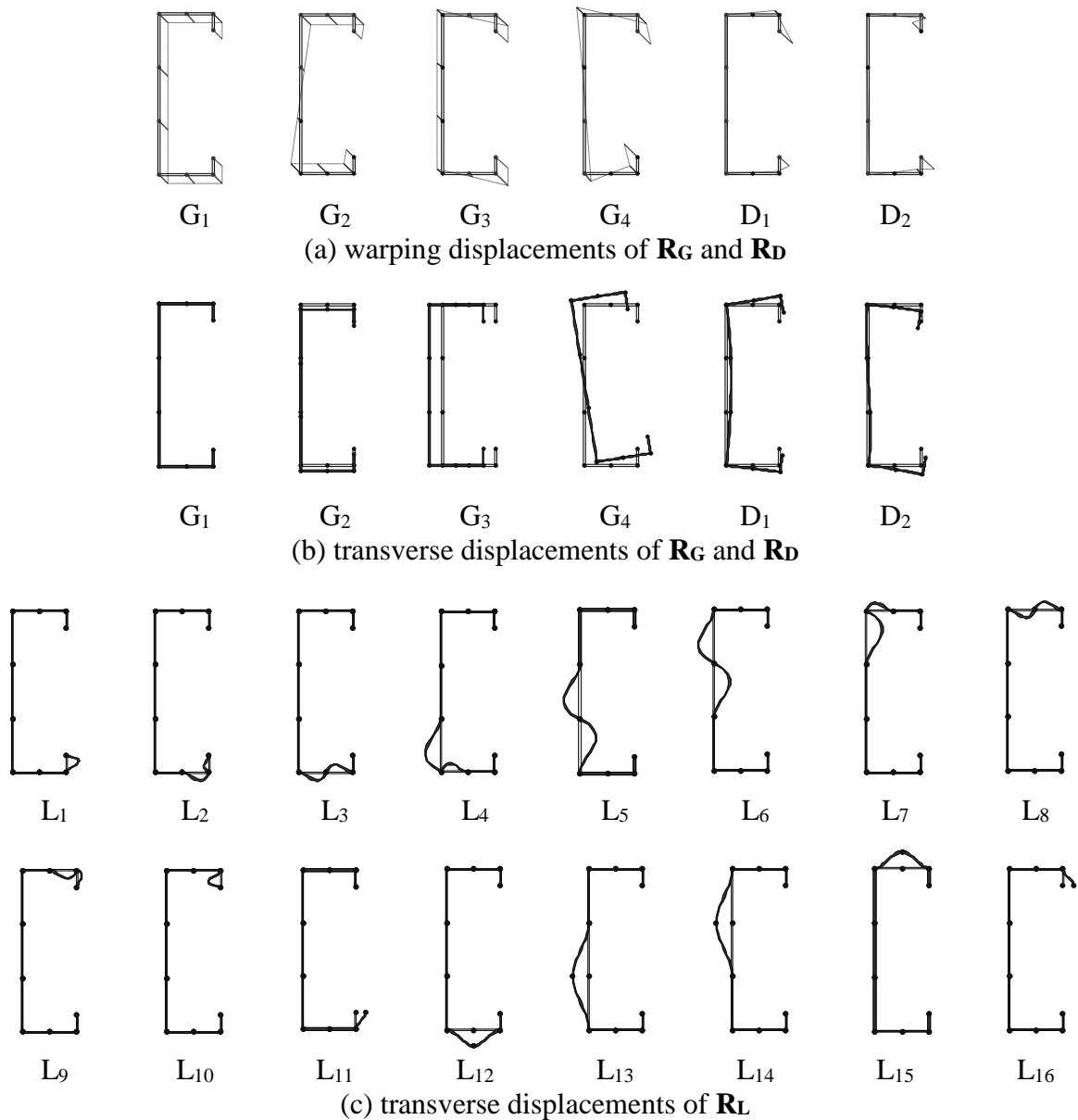
There are multiple ways to get  $\mathbf{R}_O$ . The simplest way is the direct application of the above considerations through a system of independent vectors with unit transverse extensions and unit shear deformations. Since both transverse strain and in-plane shear may occur in any strip, the number of transverse extension base vectors as well as the number of in-plane shear base vectors is equal to the number of strips (i.e.,  $n-1$ ). This approach is practical, and it is relatively easy to find the necessary  $2 \times (n-1)$  independent base functions, see, e.g. [1/2]. Other ways to generate  $\mathbf{R}_O$  are discussed e.g., in [8/2, 10/2].

## 2.4 Application

### 2.4.1 Modal system

The above-summarized procedures transform the *nodal* base system into a *modal* base system. The most important characteristics of the modal system is that the deformation classes are separated. (Further transformation within any class is still possible; this will be discussed in Section 3 of this dissertation.) **Figure 2.8** illustrates the modal system for a widely used lipped channel member. The cross-section is discretized by the main nodes and a few sub-nodes. Possible (typical) global (G), distortional (D) and local (L) deformations are shown.

The constraint matrices pave the way for two distinct applications. First, they provide means for stability solutions to be focused only on a given buckling class, which may be referred to as *modal solution* or *pure mode calculation*. The other important outcome of the constraint matrices is that they may be used to classify a conventional FSM stability solution into the different fundamental buckling classes, which may be referred to as *modal identification*.



**Figure 2.8:** Typical modal base system for a lipped channel member

## 2.4.2 Pure buckling calculation

As far as pure mode calculation is concerned, the essential step is the separation of the G, D, L and O mode spaces, which is completed by the **R** constraint matrices. The column vectors of the **R<sub>m</sub>** matrices can be regarded as base vectors of the given space.

Therefore, modal solution can directly be get, by solving the constrained generalized eigen-value problem of Eq. (2.6) or (2.7). The resulted eigen-vectors are the buckling modes that satisfy the criteria for a given class, and may conveniently be called as *pure buckling modes* (e.g., pure global modes, pure distortional modes, etc.). The corresponding eigen-values thus provide the critical load multipliers (or critical stresses, critical loads, etc.) for any pure modes, as required by most of the design codes for the prediction of design capacity of thin-walled members.

The number of eigen-vectors within a mode space (of G, D, L or O) is identical to the dimension of the given mode space, which provides a natural upper limit for the number of pure buckling modes. (Note, in some cases the number of practically relevant pure buckling modes is smaller than the space dimension.) Thus, the presented method clearly defines the (maximum) number of pure buckling modes for any mode class and for any open cross-section.

More importantly, solution of the eigen-value problem in the G, D, L or O mode space (hence determination of pure buckling modes) introduces a significant reduction of the problem to be solved: instead of searching the eigen-vectors and eigen-values in the  $n_{DOF}$ -dimensional space, much smaller spaces can be considered, which represents a significant computational advantage. The sizes of the sub-spaces are (generally) dependent on the cross-section, and can be expressed as follows: 4 for G space,  $(n_m-4)$  for the D space,  $(n_m+2n_s+2)$  for the L space, and  $(2 \times n_m + 2 \times n_s - 2)$  for the O space.

Concerning the space dimensions and pure modes the following remarks may be added.

The categorization of the so-called *pure axial mode* is uncertain. The mode definitions adopted here (see **Table 2.1**) suggest that this mode is a global mode. However, classical beam theory solutions normally do not consider this mode but discuss 3 global modes only (e.g., in case of a column with doubly-symmetrical cross-section two flexural and a torsional mode).

Though the number of D modes is usually equal to  $(n_m-4)$ , this formula is valid only if it yields to a non-negative number, i.e., when the number of main strips is at least 4. Otherwise, D modes do not exist. For example a standard channel section (without lips) has no D modes.

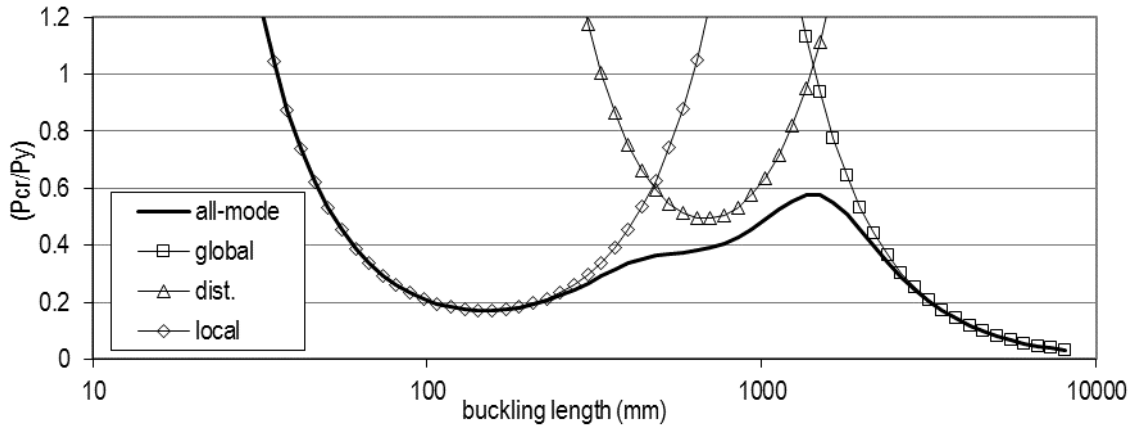
In case of a cross-section consisting of only 2 main strips (i.e., an angle), the global pure torsional mode coincides with one of the L modes. In this case, the number of either the G or the L modes is decreased by 1.

It may be interesting to mention that the constrained eigen-value problem can also be solved for sub-spaces within the G, D, L or O mode spaces. Practically this means that, instead of using the whole **R<sub>m</sub>** matrix, we may select any combination of its column vectors to solve the constrained eigen-value problem. If only one vector is selected, the problem reduces to a single-DOF problem, which yields to an *individual buckling mode* and corresponding critical load, which may have some practical advantage. Consider, as an example, the global buckling of a column: by the proper selection of base vectors, we may easily calculate *pure flexural* or *pure torsional* buckling.

Modal solution is demonstrated here by a numerical example from [1/2]. A column member with a C-shaped cross-section (which is widely applied in cold-formed steel industry) is analysed. The dimensions of the C sections are as follows: total depth is 200 mm, flange width is 50 mm, lip length is 20 mm, thickness is 1.5 mm. The material is isotropic with  $E=210$  GPa.

Critical forces are calculated for a wide range of buckling lengths in the following options: all-mode solution (i.e., classic FSM solution, also called ‘signature curve’), and pure global, pure distortional, and pure local buckling solutions. The results are plotted in **Figure 2.11**.

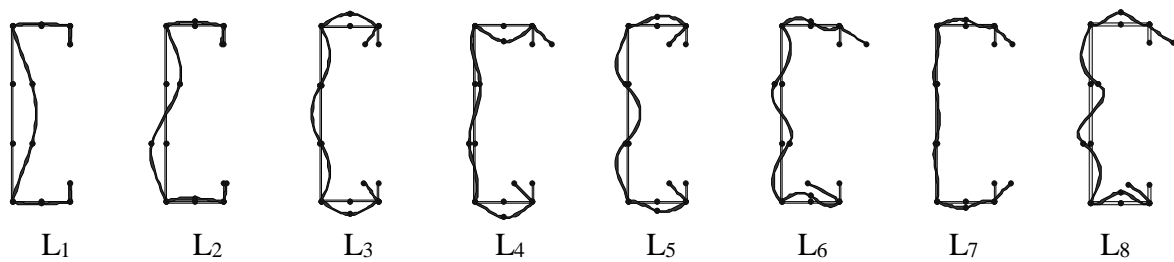
More examples can be found in [1/2, 5/2, 8/2].



**Figure 2.9:** Critical forces: unconstrained and constrained solutions

### 2.4.3 Mode identification

If the constrained eigen-value problem is solved within a certain (G, D, L or O) sub-space, it is evident that the resulting eigen-vectors span the same space as the column vectors of the given constraint matrix. Therefore, they can be regarded as another, *orthogonal* base system for the same space. The orthogonal L base system is illustrated in **Figure 2.10**, for the same section presented in **Figure 2.8**.



**Figure 2.10:** Possible orthogonal base vectors for L space

The columns of the solution of (2.7), i.e., columns of  $\Phi_M$  matrix will contain the orthogonal base vectors for the space. Since these vectors evidently span the given  $M$  space, they can be used to express any  $d_M$  vector of the space as a linear combination, as follows:

$$d_M = \Phi_M c_M \quad (2.60)$$

where  $\Phi_M$  is the  $n_M \times n_M$  matrix of the orthogonal modes, while elements of  $c_M$  vector defines the contribution of the modes.

The  $\Phi_M$  matrix can also be interpreted as a transformation matrix, which, if applied on  $\mathbf{R}_M$ , effectively transforms it to the orthogonal base system, but expressed in the original space of nodal DOF. To demonstrate this substitute Eq. (2.60) into Eq. (2.5):

$$\mathbf{d} = \mathbf{R}_M \mathbf{d}_M = \mathbf{R}_M \Phi_M \mathbf{c}_M = \mathbf{R}_M^0 \mathbf{c}_M \quad (2.61)$$

which proves that any  $\mathbf{d}$  nodal displacement vector that lies in a given  $M$  sub-space can be expressed as a linear combination of the column vectors of the  $\mathbf{R}_M^0$  matrix which latter is a transformed form of the corresponding constraint matrix having the orthogonal modes in its columns, but now expressed with the original FSM DOF (i.e., original FSM nodal displacements).

By determining the orthogonal modes for each of G, D, L and O, (i.e., solving the constrained eigen-value problem four times), the  $\Phi_G$ ,  $\Phi_D$ ,  $\Phi_L$ , and  $\Phi_O$  orthogonal base vectors become known, which can be expressed by the regular FSM nodal displacements, and finally can be assembled in a  $\mathbf{R}^0 = \mathbf{R}_{GDLO}^0 = [\mathbf{R}_G^0 \quad \mathbf{R}_D^0 \quad \mathbf{R}_L^0 \quad \mathbf{R}_O^0]$  matrix. Since G, D, L and O spaces together span the whole FSM DOF space, any  $\mathbf{d}$  displacement vector can be expressed as the linear combination of the column vectors (i.e., orthogonal axial base vectors) of  $\mathbf{R}^0$  matrix:

$$\mathbf{d} = [\mathbf{R}_G^0 \quad \mathbf{R}_D^0 \quad \mathbf{R}_L^0 \quad \mathbf{R}_O^0] [\mathbf{c}_G \quad \mathbf{c}_D \quad \mathbf{c}_L \quad \mathbf{c}_O]^T = \mathbf{R}_{GDLO}^0 \mathbf{c}_{GDLO} \quad (2.62)$$

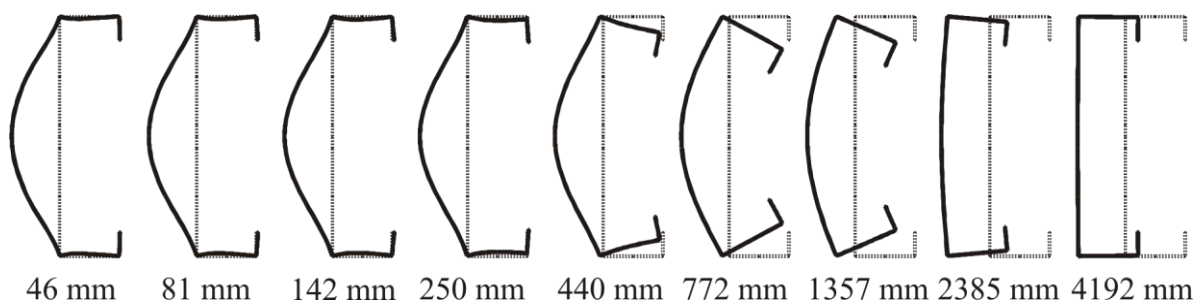
It should be pointed out that  $\mathbf{c}_{GDLO}$  vector, in fact, gives the contribution of any individual modes (or more generally: of the G, D, L and O modes) in the general  $\mathbf{d}$  displacement, thus, the task of *modal identification* is essentially solved. The participation of a given individual mode or a given  $M$  mode space can be calculated e.g., by the following equations:

$$p_i = |c_i| / \sum_{\text{all}} |c_i| \quad \text{and} \quad p_M = \sum_M |c_i| / \sum_{\text{all}} |c_i| \quad (2.63)$$

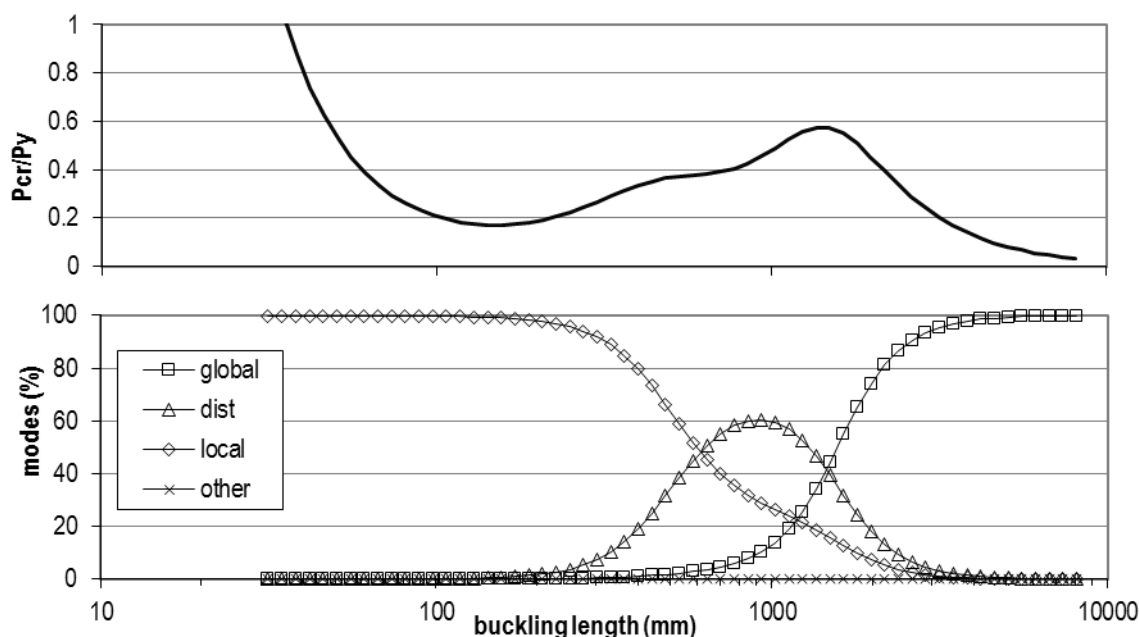
It is important to mention that the above procedure is not unique, and can be realized in multiple ways. One aspect is the orthogonalization. Since orthogonal base vectors are determined via a generalized eigen-value problem, they are dependent on the applied loading. The simplest loading is a uniformly distributed concentric compressive force, but other loading is possible, too. Another issue is the normalization of the orthogonal vectors. Various normalizations are possible, which may lead to slightly different  $\mathbf{c}_{GDLO}$  vector, hence, different mode identifications. The discussion of these questions is out of the scope of this dissertation (see e.g., [10/2]). The mode identification is illustrated here by a numerical example. The same C-section member is solved (i.e., all-mode solution), then the buckling modes are identified: participations from G, D, L and O modes are determined by the above process. Some deformed cross-section shapes are shown in **Figure 2.11**, while participations are presented in **Figure 2.12**.

## 2.5 Summary and continuation of the work

In the previous Sections the cFSM method has been presented. The cFSM can be considered as the first method which makes modal decomposition of a shell model (in this case: finite strip model) possible. The method is based on the proposed formal mechanical definition of G, D and L modes. The method can be applied to solve two basic problems: (i) to calculate critical loads for any pure (e.g., G, D or L) modes or any combination of individual modes (e.g., G+D, D+L, etc), and (ii) to perform modal identification of general deformation modes. The method has been implemented into the open source CUFSM software. (See Thesis #1 in Chapter 6 of this dissertation.)



**Figure 2.11:** Buckled cross-section shapes in unconstrained solution



**Figure 2.12:** Mode participation in unconstrained solution

The cFSM has been tested and validated by comparison to other methods, especially to analytical solutions (where available, that is mostly in case of global buckling) and to GBT [11/2-14/2]. The GBT-cFSM comparison covered extensive numerical studies as well as theoretical aspects. The comparison showed that cFSM, GBT and analytical formulae lead to very similar critical loads, however, small differences exist especially in case of global buckling. The existing differences can be traced back to the differences in initial assumptions, mostly in the mode definitions.

The immediate practical application of the cFSM method is the design of cold-formed steel members where critical loads for the various pure buckling modes are required by the design specifications. Obviously, practical design problems can be (and have been) solved without cFSM, but cFSM made the design more objective and fully automatic for a wide range of cross-sections. And, unlike GBT, cFSM was widely available for researchers and practitioners as being implemented in CUFSM.

However, beside the direct practical usefulness of cFSM, it initiated several new research results, too, as briefly summarized right below.

Though the working-out of (the first version of) cFSM was an important achievement in modal decomposition of thin-walled members, it did not solve all the problems. The most important questions remained to be answered are as follows.

- Numerical studies revealed some differences between critical forces for global buckling calculated by cFSM and other methods (including GBT and analytical solutions).



- Original cFSM works for open cross-sections only.
- cFSM requires that the member is highly regular in the longitudinal direction, due to the limitations of FSM itself.
- The available modal decomposition methods (including cFSM and GBT) are based on the assumption that the member is built up from *plane* elements. If the cross-section has curved parts, current mode decomposition methods lead to unsatisfactory results.

The first question is mainly theoretical one (since the differences are practically negligible in most cases). The others involve theoretical aspects, too, but with pronounced direct practical consequences.

Almost immediately after the birth of original cFSM its further development has started, trying to answering the above-mentioned challenges.

- The most direct development of the original cFSM is its extension to other end restraint conditions, by adding new longitudinal base functions, to be able to handle other than pinned-pinned end restraints. This work has been completed by Li and Schafer [15/2-18/2].
- Djafour and his colleagues, while developed their own version of cFSM, proposed alternative interpretation and definition for some cFSM constraint matrices, see [19/2-21/2]. Though he suggests that his version of cFSM works for closed cross-sections, he did not solve the real problem, i.e., torsional modes of closed cross-sections are not handled. Djafour and his colleagues have also presented a solution for constraining spline finite strip method [22/2].
- Casafont used the idea to constrain shell finite element models, see e.g. [23/2-25/2]. He developed pre- and post-processing routines to the Ansys commercial finite element software package which made it possible to calculate pure buckling modes of perforated thin-walled members. Though this work is practically useful, his method still involves limitations. For example, the necessary mechanical criteria are only approximately satisfied, therefore extreme cases (e.g. very short members, etc.) cannot be properly handled. Or, the method does not provide full decomposition, therefore, modal identification is not possible. Furthermore, the applied constraints increase the size of the problem, though theoretically the constraining should reduce the problem size (as in cFSM).
- cFSM initiated parametric studies on the effect of rounded corners, since cold-formed steel members are always produced with rounded corners. This research has been done partly under the guidance of the Author [26/2-31/2], partly of Schafer [32/2-33/2].
- Since cFSM can make design procedure clear and fully automatic, it is used in optimal shape search algorithms, too, see e.g. [34/2-39/2].
- The idea of modal decomposition of a general displacement field, as well as the cFSM base functions are also applied in identifying measured geometric imperfections of cold-formed steel members, see [40/2-41/2].
- cFSM has been extended to handle thin-walled members with arbitrary (flat-walled) cross-sections. This work has been completed by the Author, the results are presented in Chapter 3 of this dissertation.
- Another cFSM-initiated result is the application of cFSM base functions to identify FEM-calculated deformations. This idea has been proposed by the Author, then later developed by others, too. This will be discussed in Chapter 4 of this dissertation.
- cFSM induced new analytical results, too, achieved primarily by the Author. New analytical formulae for some global buckling modes are derived on the basis of modelling the member as a set of connected plate elements. This work is the topic of Chapter 5 of this dissertation.

### 3 Constrained Finite Strip Method for arbitrary flat-walled cross-section members

#### 3.1 Introduction

##### 3.1.1 General

In Chapter 2 the constrained Finite Strip Method (cFSM) is presented as originally developed and published. In this Chapter it will be generalized. The generalization, first of all, involves the extension of the method to cover arbitrary flat-walled cross-sections, including closed cross sections and more generally shaped cross-sections. The new, generalized cFSM is based on an improved FSM version where various end restraints are handled by employing various trigonometric series as longitudinal base functions. That is why the FSM is revisited here and the general BC FSM version is very briefly summarized (in Section 3.1.2). Then, the generalized cFSM is presented. Since in case of closed cross-sections or any cross-section with one or multiple closed parts the in-plane (membrane) shear deformations have pronounced role, first these shear deformations are discussed and a modal system is proposed for the description of the shear deformations (in Section 3.2). In Section 3.3 the construction of the constraint matrices is summarized. Though some of the constraint matrices have already been derived in Chapter 2 (e.g.,  $\mathbf{R}_G$ ,  $\mathbf{R}_D$ ,  $\mathbf{R}_L$ ), in Section 3.3 a novel approach is used: (i) practically meaningful sub-spaces are introduced, and (ii) a unified approach is used for the construction of all the constraint matrices. In Section 3.4 possible, practically useful transformation of the base systems (i.e., constraint matrices) are discussed. Finally, some illustrative examples are presented (in Section 3.5).

##### 3.1.2 FSM with generalized longitudinal shape functions

In Section 2 FSM is summarized by assuming the simplest longitudinal shape functions which corresponds to pinned-pinned (or: simple-simple) end restraints. However, other end restraints can also be handled, by using more complicated longitudinal shape functions, namely: trigonometric series, see [11/1, 15/2-18/2]. The  $u$ ,  $v$  and  $w$  displacements in this case are approximated (within a strip) as follows:

$$u(x, y) = \sum_{m=1}^q \left[ \left( 1 - \frac{x}{b} \right) \left( \frac{x}{b} \right) \right] \begin{bmatrix} u_{1[m]} \\ u_{2[m]} \end{bmatrix} Y_{[m]} \quad (3.1)$$

$$v(x, y) = \sum_{m=1}^q \left[ \left( 1 - \frac{x}{b} \right) \left( \frac{x}{b} \right) \right] \begin{bmatrix} v_{1[m]} \\ v_{2[m]} \end{bmatrix} Y'_{[m]} \frac{a}{m\pi} \quad (3.2)$$

$$w(x, y) = \sum_{m=1}^q \left[ \left( 1 - \frac{3x^2}{b^2} + \frac{2x^3}{b^3} \right) \left( -x + \frac{2x^2}{b} - \frac{x^3}{b^2} \right) \left( \frac{3x^2}{b^2} - \frac{2x^3}{b^3} \right) \left( \frac{x^2}{b} - \frac{x^3}{b^2} \right) \right] \begin{bmatrix} w_{1[m]} \\ \vartheta_{1[m]} \\ w_{2[m]} \\ \vartheta_{2[m]} \end{bmatrix} Y_{[m]} \quad (3.3)$$

where  $a$  is the member length and  $b$  is the width of the given strip, while  $Y_{[m]}$  is the longitudinal base function. The  $Y_{[m]}$  functions are dependent on the end restraints, as follows:

$$\text{pinned-pinned: } Y_{[m]} = \sin \frac{m\pi y}{a} \quad (3.4)$$

$$\text{clamped-clamped: } Y_{[m]} = \sin \frac{m\pi y}{a} \sin \frac{\pi y}{a} \quad (3.5)$$

$$\text{pinned-clamped: } Y_{[m]} = \sin \frac{(m+1)\pi y}{a} + \frac{m+1}{m} \sin \frac{m\pi y}{a} \quad (3.6)$$

$$\text{clamped-free: } Y_{[m]} = 1 - \cos \frac{(m-1/2)\pi y}{a} \quad (3.7)$$

$$\text{clamped-guided: } Y_{[m]} = \sin \frac{(m-1/2)\pi y}{a} \sin \frac{\pi y}{2a} \quad (3.8)$$

Note, the assumed coordinate systems and displacement DOF are identical to those shown in **Figure 2.1**, with one important difference: throughout Chapter 3 the positive rotational DOF is in accordance with the positive rotation of the coordinate system (i.e., it is just opposite the sign rule used in Chapter 2).

While in the pinned-pinned case the solution can be found for any  $m$  term independently of the other  $m$  terms, i.e., the  $m$  terms are uncoupled, in case of other end restraints (e.g. clamped-clamped) the  $m$  terms are coupled. This also means that it is not enough to consider one single  $m$  term, but multiple  $m$  terms are necessary in the solution. This does not essentially modify the FSM procedure, but increases the size of the problem, i.e., the size of the stiffness matrices. While the size of the local matrices for a specific  $m$  term is 8 by 8, for the series solution it is:  $(8 \times q)$  by  $(8 \times q)$ .

From the local stiffness matrices the whole member's (global) stiffness matrices (elastic and geometric,  $\mathbf{K}_e$  and  $\mathbf{K}_g$ ) can be compiled as usual, by transformation to global coordinates and assembly. The size of the global matrices is  $(4 \times p \times q)$  by  $(4 \times p \times q)$ , where  $p$  is the number of strips and  $q$  is the number of considered terms in the longitudinal shape functions.

For a given distribution of edge tractions on a member the geometric stiffness matrix scales linearly, resulting in the classic eigen-buckling problem, formally the same as in Eq. (2.4), however, the size of the matrices are different. From the equation the eigen-values (i.e., critical load multipliers) and eigen-modes (i.e., buckling modes) can be determined.

### 3.1.3 Basics of generalized cFSM

The new, generalized cFSM has a number of novel features. First, it is developed for the general BC (series) FSM version.

Then, a simple, but practically useful novelty is the organization of mode spaces into *primary* and *secondary* mode spaces. Primary modes are those deformation modes which exist even if a minimal discretization is used, that is if one strip per one flat plate is applied. In other words: degrees of freedom (DOF) are assumed at the *main nodes* only. Secondary modes, on the other hand, are those modes which exist only if flat plates are discretized into multiple strips, i.e., when *sub-nodes* are applied which are located within a flat plate. Even more precisely, in fact, any discretization can be applied to the member, but primary modes will use only DOF at main nodes, while secondary modes will use DOF at sub-nodes only.

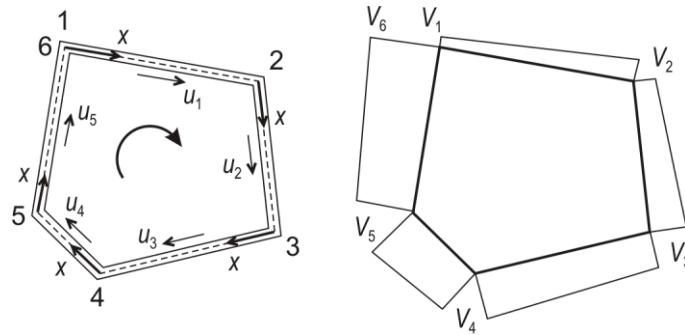
An essential novelty is the application of new (in-plane) shear modes. These shear modes will be presented in Section 3.2 here. Along with the introduction of new shear modes the global and shear mode spaces are further subdivided into smaller sub-spaces. This is reflected by the new, more refined mode description table, which summarizes the most important mechanical features of the mode spaces and sub-spaces.

## 3.2 Role and decomposition of membrane shear

### 3.2.1 General

Though in **Table 2.1** it is not detailed, S/T space can be subdivided into two characteristic sub-spaces: shear (S) space in which the null-transverse-strain criterion is still satisfied but the null-shear-strain criterion not, and transverse extension (T) space in which none of the strains are zero. Here, we are concentrating on the S sub-space, therefore, on in-plane shear deformations. In-plane shear deformations are essential to handle closed cross-sections and general cross-sections with closed part(s), and also to include shear-deformable beam theories in global buckling modes in cFSM. The presentation of the result is based on [1/3-2/3]

If twisting rotation is applied for a cross-section geometry as shown in **Figure 3.1**,  $\partial u / \partial y > 0$  for each strip (by properly selecting local coordinate systems). If the in-plane shear strain is zero, however,  $\partial v / \partial x < 0$  for each strip. Therefore,  $V_1 > V_2 > V_3 > V_4 > V_5 > V_6$ . If the cross-section is open (i.e. node 1 and 6 are two different nodes), such warping distribution is physically possible. If the cross-section is closed, however, (i.e., there is physical continuity at node 1=6,)  $V_1 = V_6$  should be satisfied, which is clearly incompatible with the null-shear-strain criterion. The conclusion is that torsion of closed cross-sections (or any cross-section with one or multiple closed parts) requires in-plane shear.



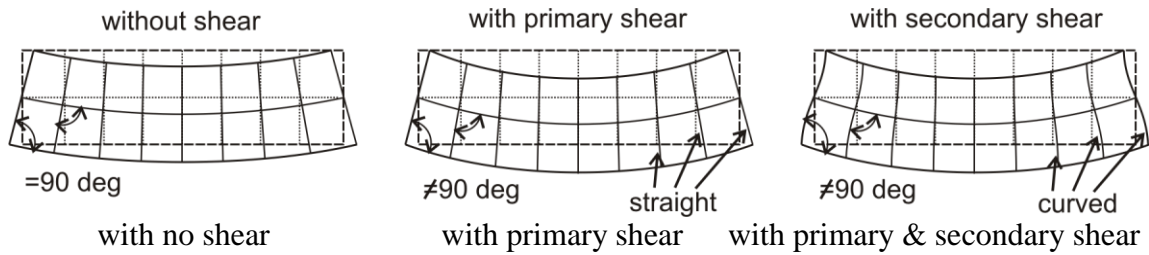
**Figure 3.1:** Null-shear-strain and closed cross-sections

Classical buckling solutions (e.g., presented by Euler) exclude shear deformations of the beam/column by adopting Euler-Bernoulli beam theory, assuming that: (i) the cross-section planes remain planes during axial and flexural deformations, and (ii) that normals to the undeformed middle line remain normal during the deformations. This also means that the plate elements of a thin-walled member cannot exhibit in-plane shear deformations. In case of shear-deformable beam theory the first criterion can be still valid, but normals to the undeformed middle line do not remain normal during deformation. This also means that the plate elements of a thin-walled member can have in-plane shear deformations.

Depending on the shear deformations, three basic categories are defined here. If shear deformations are excluded, it is referred as beam model with *no shear*. If (in-plane) shear (in the plate elements) is allowed, and if the shear deformations are resulted in linear warping distribution, the model will be referred here as beam model with *primary shear*. If the shear deformations are more general and resulted in nonlinear warping distribution, the model will be referred here as model with *secondary shear*. It is to note that the linearity or nonlinearity of the warping deformations is interpreted at the middle planes of the strips.

### 3.2.2 In-plane deformations in a single plate

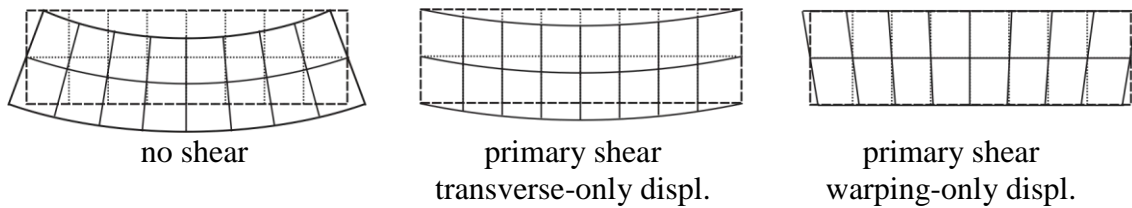
Let us first analyse the deformations of a flat plate element of a member. In accordance with the mode definition table (**Table 2.1**) in most of the deformation modes the transverse extension is forced to be zero, i.e.,  $\varepsilon_x = \partial u / \partial x = 0$ . Transverse strain is zero if the transverse displacement is constant (in  $x$ ). Practically it means that the longitudinal fibres are parallel with each other, which furthermore means that the in-plane deformations are similar to that of a beam member in flexure. The in-plane deformation field of a flat plate thus can be illustrated as in **Figure 3.2**, for various possible shear deformations.



**Figure 3.2:** Null-transverse-extension in-plane deformations in a strip

If the shear is non-zero and the warping is linear (in  $x$ ), the deformation field can readily be considered as the superposition of two basic deformation components. The two basic components can be any two out of three (see **Figure 3.3**): a) a *no shear* component, b) a *primary shear* component with *transverse-only* displacements, and c) a *primary shear* component with *warping-only* displacements. Evidently, only two out of the three are linearly independent, i.e., each of the three basic components can be expressed by the linear combination of the other two.

The most general deformation field is the one with non-linear warping. This field can be considered as the superposition of three basic components, for example: no shear + primary shear + secondary shear. For the primary shear component either warping-only or transverse-only components can be used.



**Figure 3.3:** Deformation components for linear warping

(It is to note that, alternatively, the general deformation field could be composed as: warping-only primary shear + transverse-only primary shear + secondary shear. From practical point of view it is more convenient to have a shear-free component, so we will use the first way to compose the general deformation field.)

When applied in FSM, the above deformation components need to be described with strips. In case of no-shear component one strip per one flat plate element is appropriate to use. Applying null-transverse-strain and null-shear-strain criteria to a single strip for a specific  $m$  term, linearity of  $v$  in  $x$  is automatically satisfied (by the selected transverse shape functions). The effect of null-transverse-strain criterion can easily be obtained by substituting  $\varepsilon_x = \partial u / \partial x = 0$  into the  $u(x,y)$  function, which is satisfied if

(3.9)

$$u_{1[m]} = u_{2[m]}$$

for any  $m$ . (Thus, transverse translation can conveniently be denoted by  $u_{[m]}$ , or simply  $u$ .)

The effect of null-shear-strain criterion (together with null-transverse-strain) can be obtained similarly. It leads to:

$$u_{[m]} = \frac{v_{1[m]} - v_{2[m]}}{b} \frac{a}{m\pi} \quad (3.10)$$

It is to observe that the above equations are essentially identical to Eq. (2.11) and Eq. (2.12), even though the here-assumed longitudinal function is different. Moreover, in the above formula  $(v_{1[m]} - v_{2[m]})/b$  is nothing else than the rate of change of the warping, i.e., the rotation of the plate edge around the local  $z$ -axis, which is therefore linearly proportional to the transverse displacement. As it can be seen, the no-shear component is characterized by non-zero transverse and non-zero warping displacements.

As far as primary shear component is concerned, again, one strip per one flat plate element is appropriate to use. Null-transverse-strain criterion is still satisfied, therefore,  $u_{1[m]} = u_{2[m]} = u_{[m]}$ , but the in-plane shear strain is non-zero. In fact, in-plane shear strain is constant in the local  $x$  direction.

In case of warping-only displacements  $u = 0$  and, consequently  $\partial u / \partial y = 0$  and  $\partial v / \partial x = \text{const}(x)$ , which leads to  $\gamma_{xy} = \text{const}(x)$ . (The notation ‘const( $x$ )’ means ‘constant in  $x$ ’.)

In case of transverse-only displacements  $v(x) = \text{const}(x)$  and  $u(x) = \text{const}(x)$ , consequently  $\partial u / \partial y = \text{const}(x)$  and  $\partial v / \partial x = 0$ , which leads to  $\gamma_{xy} = \text{const}(x)$ .

In case of secondary shear, let us first assume that we have only one strip per one flat plate. Null-transverse-strain criterion is still satisfied, which means that  $\partial u / \partial y = \text{const}(x)$ . At the same time, the warping varies linearly, that is  $v(x) = \text{lin}(x)$  within one strip due to the selection of shape functions. This means that  $\partial v / \partial x = \text{const}(x)$ . Thus, within one strip  $\gamma_{xy} = \text{const}(x)$ , and nonlinear warping is not possible. However, if multiple strips are applied within a flat plate element of a member, nonlinear warping might be achieved. In fact, any nonlinear warping functions can be approximated by any required accuracy by applying a fine enough discretization (i.e., large enough number of strips).

A basic conclusion is thus, that no-shear and primary shear components can readily be described by using one strip per one flat plate in a member. Secondary shear requires multiple strips per flat plates. Hence, it will be assumed here that in case of no-shear and primary shear modes the simplest one strip per one plate discretization is used, while in case of secondary shear modes multiple strips are assumed within one flat plate element.

### 3.2.3 Primary shear deformations in a member

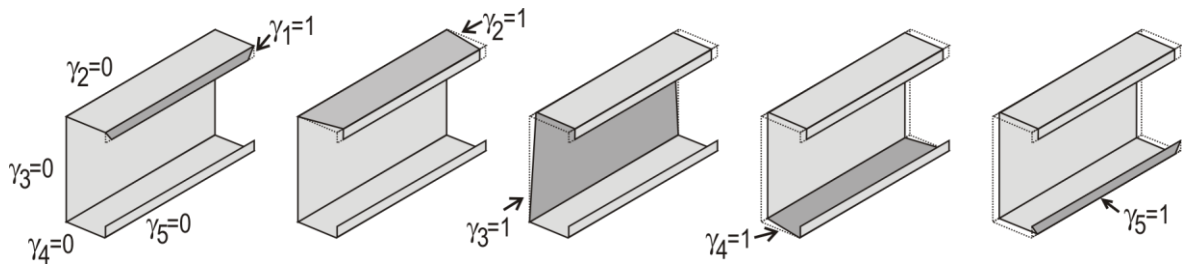
#### 3.2.3.1 Unit and zero shear strains

Primary shear in a member can typically be described by various base systems. Since the most characterizing mechanical feature of primary shear is that in-plane shear strain is constant in  $x$  within a flat plate element, a natural base system is to use 1-s and 0-s for the *shear strain* in

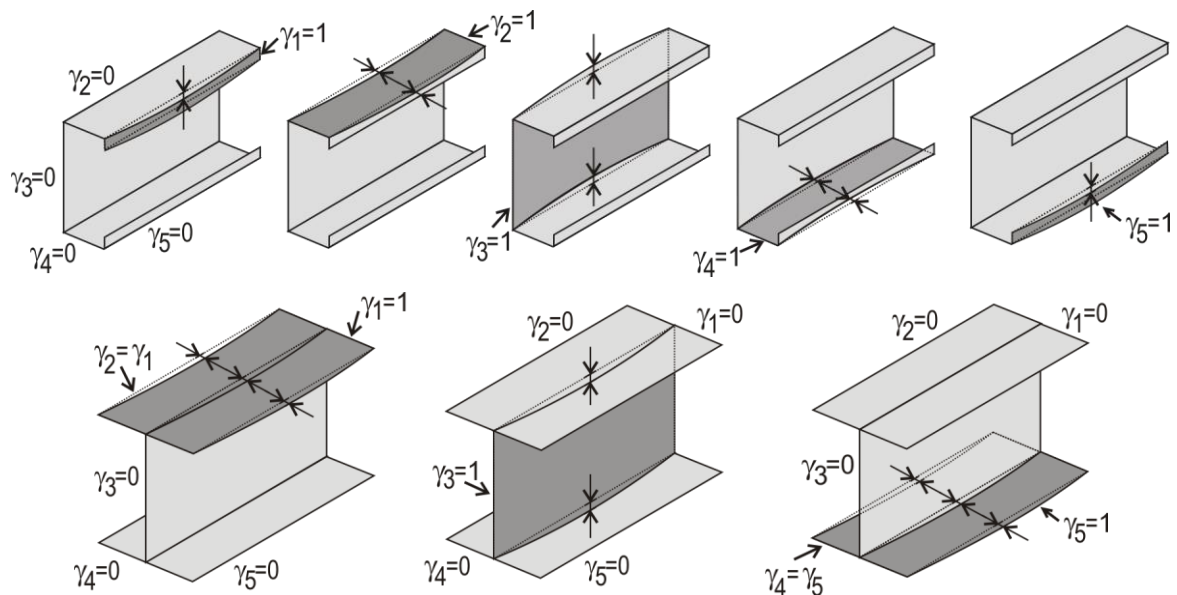
the various plates (i.e. main strips). The important conclusion is that the *number of independent primary shear modes is equal to the number of flat plate elements* of the member.

The base system with unit and zero shear strain might be realized by either having warping-only or transverse-only displacements. Warping-only base system with unit and zero shear strains is illustrated in **Figure 3.4** for an open unbranched cross-section. The illustrated longitudinal distribution of warping displacements corresponds to a cosine function, that is simple-simple end restraints. (Note, those plates are highlighted in the figures, where the shear strain is non-zero). As it can be seen, such base system is physically possible for any open cross-section member, but it can also be easily understood that such base system is physically impossible (i.e., geometrically incompatible) for any closed cross-section or cross-section with closed part(s).

In **Figure 3.5** similar base systems are shown, however, with transverse-only displacements. The illustrated longitudinal distribution of transverse displacements corresponds to a sine function, that is simple-simple end restraints. If the cross-section is open and unbranched, such base system is always possible. However, if the cross-section is branched, not all the deformed shapes with unit and zero shear strains are physically possible. This is illustrated in **Figure 3.5** (bottom) for an I-section, where only 3 linearly independent deformations are geometrically compatible out of the 5.



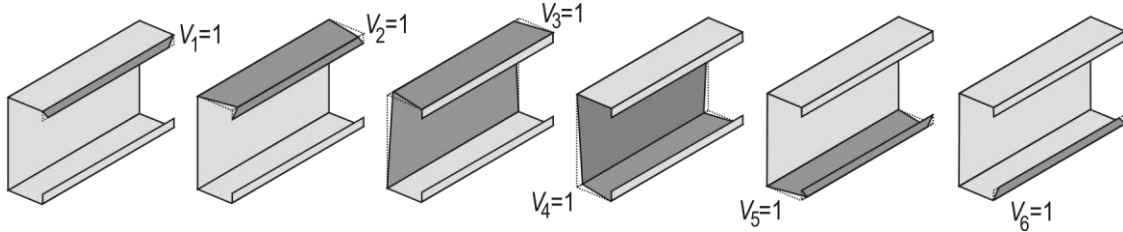
**Figure 3.4:** Unit and zero shear strains, warping-only displacements



**Figure 3.5:** Zero and non-zero shear strains, transverse-only displacements

### 3.2.3.2 Unit and zero warping displacements

Warping-only displacements can be described by applying 1-s and 0-s as (nodal) *warping displacements*, as illustrated in **Figure 3.6**. Obviously, such base system is existing for any cross-section shape, and the number of base vectors is equal to the number of nodal lines. The vectors are linearly independent and involves in-plane shear, therefore, it can serve as a base system. However, the space spanned by these base vectors is not identical to the space of primary shear modes. There are (might be) two differences.



**Figure 3.6:** Unit and zero warping displacements

One difference is that the space spanned by the base vectors (with 1-s and 0-s as warping displacements) is always larger than the space of primary shear. By simply summarizing the base vectors, we arrive at a deformation mode with uniform warping, i.e. the *axial mode*, which does not involve shear, so, it is clearly out of the space of primary shear.

The other potential difference is discussed as follows. In case of open (unbranched or branched) cross-section, for the number of nodal lines ( $n$ ) and number of plate elements ( $p$ ):  $p = n - 1$ . As we have seen, the dimension of primary shear mode space is  $p$ . We have  $n$  base vectors with unit and zero warping, therefore,  $n - 1$  base vectors with non-zero shear strain can be defined, which is just the number of independent primary shear modes. Thus, in case of open cross-sections the base system with unit and zero warping displacements properly spans the whole space of primary shear (plus, includes the axial mode).

In case of a closed cross-section:  $p = n$ . The dimension of primary shear mode space is  $p$ , while there are only  $n - 1 = p - 1$  base vectors with non-zero shear. This means that the base system with unit and zero warping displacements does not span the whole space of primary shear modes; in fact, one primary shear mode is missing.

If the cross-section is more general, but with closed part(s),  $p \geq n$ . Obviously, the base system with unit and zero warping displacements does not span the whole space of primary shear modes, but some shear modes are missing.

The conclusion is that the base system with unit and zero warping displacements might span the whole or only a part of the primary shear modes space, depending on the cross-section topology.

### 3.2.3.3 Unit and zero transverse displacements

It is also possible to define a base system with unit and zero *transverse displacements* (i.e., by forcing unit translation in  $U$  or  $W$  direction in one node, while forcing zero translation elsewhere). If the number of nodal lines is  $n$ ,  $2n$  such base vectors exist. Obviously, the so-constructed base system spans a much larger space than the space of primary shear. This base system contains deformations which are out of the desired space, but still, it does not necessarily includes the whole space of primary shear.

If the unit transverse displacements are arbitrary, the null-transverse-strain criterion is not necessarily satisfied. Thus, only those combinations of the transverse displacements are appropriate which satisfy the null-transverse-strain criterion. In a member with  $p$  strips the



null-transverse-strain means  $p$  criteria, given by  $p$  equations. If  $\tilde{p}$  denotes the linearly independent equations out of these  $p$  equations, the number of modes with zero transverse strain determined by the base system with unit and zero transverse displacements will be:  $2n - \tilde{p}$ . In many cases (i.e., many cross-section shapes)  $\tilde{p} = p$ , but in case of a general cross-sections  $\tilde{p} \leq p$ . (Note, there is no simple and generally applicable way to decide the number of linearly independent equations. The problem is analogous to deciding kinematic determinacy of a 2D truss. If truss-bars are assigned to each walls of the cross-section and hinges are assumed in the wall junctions, the cross-section is transformed into a 2D truss. If the so-constructed equivalent truss is kinematically determinate or indeterminate,  $\tilde{p} = p$ . If the equivalent truss is kinematically overdeterminate,  $\tilde{p} < p$ . In case of simpler truss geometries the determinacy can be decided by visual inspection, while for a complicated geometry the determinacy can be determined by numerical analysis.)

If the cross-section has outstand elements with end-nodes (i.e., nodes to which only one single plate/strip is connected), the space must further be reduced. In case of an end-node, the  $U+W$  displacement cannot be arbitrary, since if  $U+W$  is transformed into local  $w$ -directional displacement (with  $u = 0$ ), the resulting deformation is shear-free (for the outstand plate). Therefore, the number of independent deformations with primary shear is finally:  $2n - \tilde{p} - n_e$ , where  $n_e$  is the number of end-nodes in the cross-section.

For example, in case of open unbranched cross-sections  $p = n - 1$ ,  $\tilde{p} = p$  and  $n_e = 2$ , therefore the number of compatible independent base vectors with non-zero shear is:  $2n - \tilde{p} - n_e = p$ . Thus, in this case the base system with unit and zero transverse displacements properly spans the whole space of primary shear modes.

If the cross-section is open and branched,  $p = n - 1$ ,  $\tilde{p} = p$  and  $n_e > 2$ . The number of compatible independent base vectors with non-zero shear is smaller than  $p$  (in fact,  $p + 2 - n_e$ ). It means that some modes are missing, as can also be seen in **Figure 3.5** (bottom).

In case of closed cross-sections:  $p = n$ ,  $\tilde{p} = p$  and  $n_e = 0$ , therefore the number of compatible independent base vectors with non-zero shear is:  $2n - \tilde{p} - n_e = p$ . Thus, there are no missing shear modes.

If the cross-section is general, but with closed part(s), the number of compatible modes that can be described by unit and zero transverse displacements can be equal to or smaller than  $p$ . Some shear modes, thus, might be missing.

The conclusion here is that the base system with unit and zero transverse displacements can be used to construct deformations with primary shear. During the construction one must exclude the modes with non-zero transverse strains and the modes with zero shear strains (due to outstand elements). The number of compatible modes can be equal to or smaller than the number of theoretically existing independent shear modes, the potential deficiency being dependent on the cross-section.

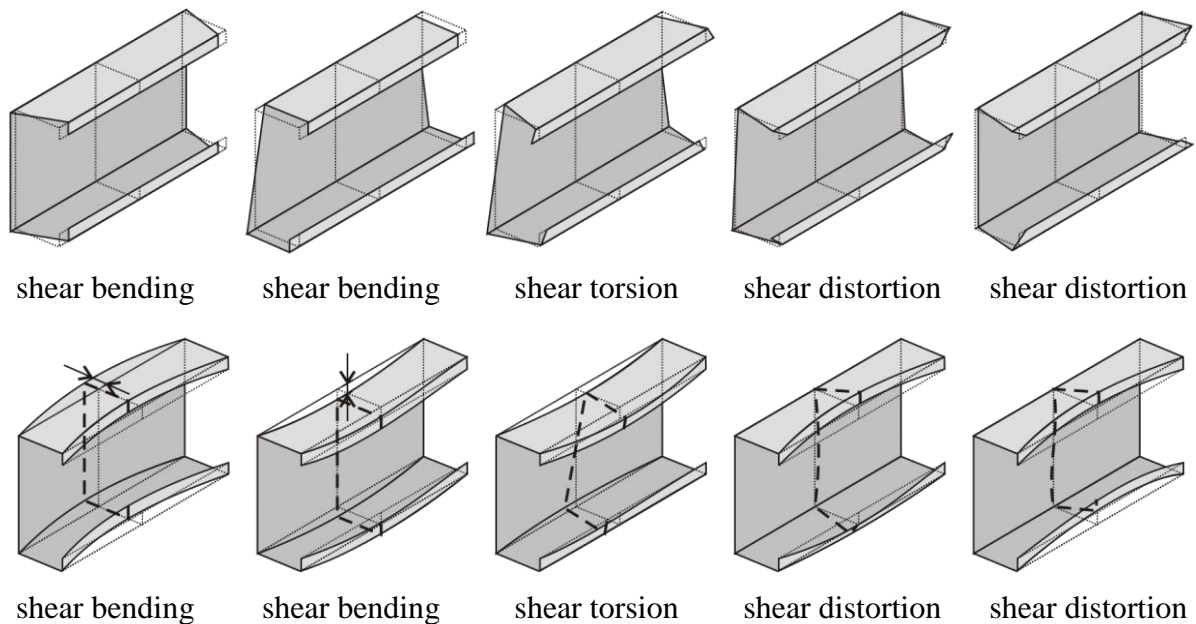
#### 3.2.3.4 Modal shear

A common feature of primary shear ( $S_P$ ), global (G) and distortional (D) modes is that they involve warping and/or transverse displacements. In G and D the non-zero warping displacements are associated with non-zero transverse displacements, unlike in case of primary shear modes, where either the warping or transverse displacements are (or can be) zero. Another common feature of G, D and  $S_P$  modes is that one strip per one flat plate element is enough to use (i.e., no sub-nodes are necessary).

Based on these common features, it is possible to define shear modes by taking the warping displacements of G and D modes only, while forcing zeros for all the other displacements. The so-constructed modes will obviously linearly independent, and involve shear strains in one or multiple flat plates (i.e., main strips). Moreover, these modes are characterized by constant shear strain within any flat plate element (i.e., any main strip). All these characteristics are identical to those of the modes defined by unit and zero warping displacements as shown in Section 3.2.3.2. It means that the mode space defined by the warping displacements of the G and D modes is a sub-space of the primary warping-only shear modes.

Similarly, it is possible to take the transverse displacements of G and D modes only, while forcing zero warping displacements. The so-constructed modes will obviously linearly independent, and involve shear strains in one or multiple flat plates/strips. Moreover, these modes are characterized by constant shear strain within any flat plate, and also characterized by transverse-only displacements. All these characteristics are identical to those of the modes defined by unit and zero transverse displacements as shown in Section 3.2.3.3. It means that the mode space defined by the transverse displacements of the G and D modes is a sub-space of the primary transverse-only shear modes.

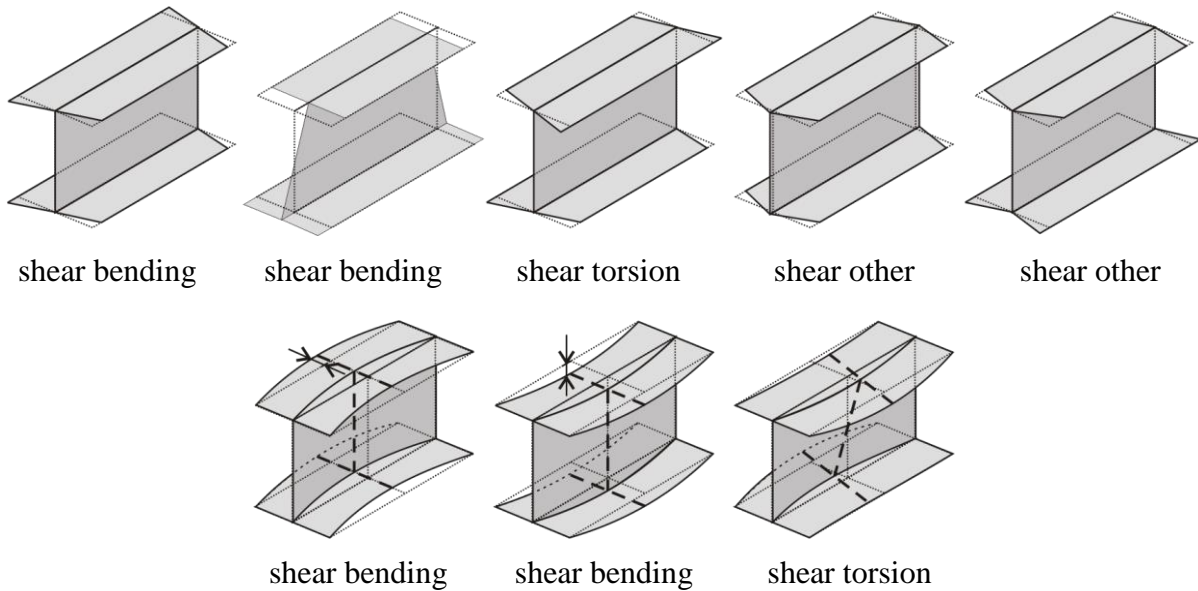
In **Figure 3.7** the warping-only and transverse-only primary shear modes of a C-section member are presented. There are two shear bending modes, one shear torsion mode, two shear distortional modes, and both warping-only and transverse-only set of shear modes are found (top and bottom row, respectively).



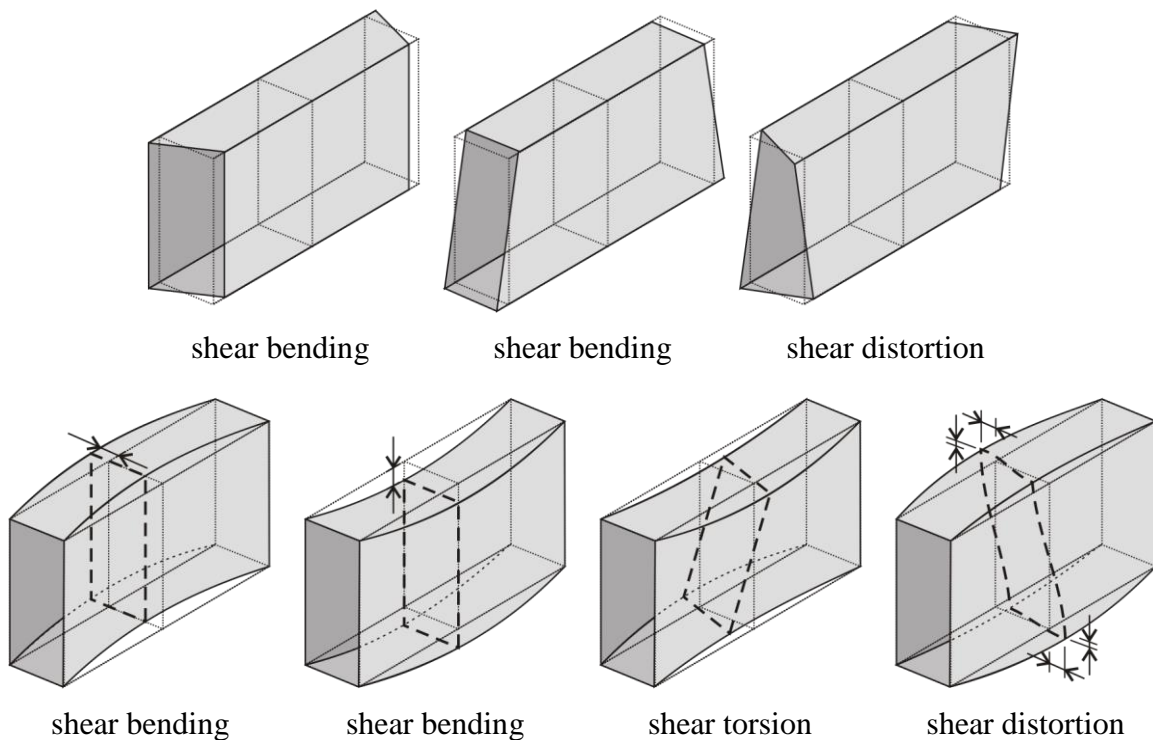
**Figure 3.7:** Primary shear modes of a C section (top: warping-only, bottom: transverse-only)

In case of an I section (**Figure 3.8**), there are no distortional modes. There are 5 plate elements, therefore, 5 primary shear modes. The primary shear modes therefore are consisted of: two shear bending modes (either warping-only or transverse-only), one shear torsion mode (either warping-only or transverse-only), and two other primary shear modes (which exist only among warping-only modes).

Primary shear modes of a rectangular hollow section (RHS) are shown **Figure 3.9**. Since the cross-section is closed, global torsion does not exist, but there is one distortional mode. The number of warping-only shear modes is 3, while the number of transverse-only shear modes is 4 (in accordance with the previous considerations and figures). Thus, two shear bending and one shear distortional modes exist with both warping-only and transverse-only displacements, but there is an additional transverse-only shear mode too, which is nothing else than a shear torsional mode. (Note, a more general cross-section is illustrated in **Figure 3.11**.)



**Figure 3.8:** Primary shear modes of an I section



**Figure 3.9:** Primary shear modes of a rectangular hollow section

### 3.3 Construction of the constraint matrices

As the original derivation of cFSM [1/2-8/2] assumed open cross-sections, therefore, many of the formulae cannot directly be applied for closed cross-sections. Therefore, the derivations need to be generalized by removing the possible most restrictions with regard to cross-section topology. This generalization is another important (and necessary) feature of the generalized cFSM. In fact, the generalization of the derivations is the topic of the following Section of this dissertation, based on [3/3-8/3].

#### 3.3.1 Mode definition

Mechanical characteristics of the mode spaces and sub-spaces are given in **Table 3.1**. Three in-plane strains and three out-of-plane curvatures are given, as follows:  $\varepsilon_x = \partial u / \partial x$ ,  $\varepsilon_y = \partial v / \partial y$ ,  $\gamma_{xy} = \partial u / \partial y + \partial v / \partial x$ ,  $\kappa_x = \partial^2 w / \partial x^2$ ,  $\kappa_y = \partial^2 w / \partial y^2$  and  $\kappa_{xy} = \partial^2 w / \partial x \partial y$ , where all the  $u$ ,  $v$  and  $w$  functions are interpreted at the middle surface of the plates (i.e., at  $z = 0$ ). Moreover, ‘C’, ‘L’ and ‘NL’ mean piece-wise constant, piece-wise linear and non-linear in local  $x$  direction, where the ‘piece’ is a flat plate between two main nodes. It is to note that  $\varepsilon_y$  could be substituted by  $v$ , while  $\kappa_y$  could be substituted by  $w$ . In row ‘eq.’ it is given whether the cross-section equilibrium is satisfied or not (Y or N, respectively). Finally, in the last row it is also given (for informative purpose) whether the deformation mode is associated with rigid-body-type cross-section displacements or not (Y or N, respectively). It is to observe that between the various warping-only  $S$  modes there is no mechanical difference, they are separated only for practical purpose. A final important comment is that although **Table 3.1** is virtually different from **Table 2.1**, there is no conflict between the two tables: the new mode definition table does not modify the original mode definitions, it only gives more details.

**Table 3.1:** Mechanical criteria for mode classes in the generalized cFSM

	primary modes														secondary m.		
	$G_A$	$G_B$	$G_T$	$D$	$L_P$	$S_{Bw}$	$S_{Tw}$	$S_{Dw}$	$S_{Cw}$	$S_{Bt}$	$S_{Tt}$	$S_{Dt}$	$S_{Ct}$	$T_P$	$L_S$	$S_S$	$T_S$
$\varepsilon_x$	0	0	0	0	0	0	0	0	0	0	0	0	0	C	0	0	NL
$\varepsilon_y$	C	L	L	L	0	L	L	L	L	0	0	0	0	0	0	NL	0
$\gamma_{xy}$	0	0	0	0	0	C	C	C	C	C	C	C	C	C	0	NL	NL
$\kappa_x$	0	0	0	L	L	0	0	0	0	0	0	L	L	L	NL	0	0
$\kappa_y$	0	C	L	NL	NL	0	0	0	0	C	L	NL	NL	NL	NL	0	0
$\kappa_{xy}$	0	0	C	NL	NL	0	0	0	0	0	C	NL	NL	NL	NL	0	0
eq.	Y	Y	Y	Y	N	Y	Y	Y	Y	Y	Y	Y	N	N	N	Y	N
rigid	Y	Y	Y	N	N	Y	Y	Y	Y	Y	Y	N	N	N	N	Y	Y

The terminology and short description of the subspaces are given here as follows.

- $G_A$  is the *axial* mode space, which involves uniform warping displacement only (and which is typically considered as part of the  $G$  space).
- $G_B$  is *global bending* sub-space of  $G$  space, consisted of two bending modes.
- $G_T$  is the *global torsion* sub-space that involves the rigid-body torsion of the cross-section, and since it is part of the  $G$  space, it is shear free (therefore typically

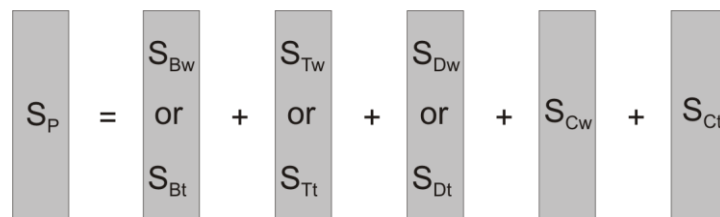
associated with warping displacements, too).  $G_T$  exists only if the cross-section is open, since if the cross-section is closed or has closed part(s), shear-free torsion is physically impossible.

- $D$  is the space of *distortional* mode space.
- $L_P$  is the mode space for *primary local(-plate)* modes.
- $S_{Bw}$  is the *primary (warping-only) shear bending* mode space, characterized by warping displacements identical to those of  $G_B$ .
- $S_{Tw}$  is the *primary (warping-only) shear torsion* mode space, characterized by warping displacements identical to those of  $G_T$ . If  $G_T$  does not exist,  $S_{Tw}$  does not exist, neither.
- $S_{Dw}$  is the *primary (warping-only) shear distortional* mode space, characterized by warping displacements identical to those of  $D$ .
- $S_{Cw}$  is the *primary (warping-only) other shear* mode space, that is the subspace of primary warping-only shear mode (i.e., with constant shear strain along  $x$ ) which is not part of any of  $S_{Bw}$ ,  $S_{Tw}$ , and  $S_{Dw}$ .
- $S_{Bt}$  is the *primary (transverse-only) shear bending* mode space, characterized by transverse displacements identical to those of  $G_B$ .
- $S_{Tt}$  is the *primary (transverse-only) shear torsion* mode space, characterized by transverse displacements identical to those of  $G_T$ . If  $G_T$  does not exist,  $S_{Tt}$  does still exist, since rigid-body-type torsional displacements for the cross-section can always be applied.
- $S_{Dt}$  is the *primary (transverse-only) shear distortional* mode space, characterized by transverse displacements identical to those of  $D$ .
- $S_{Ct}$  is the *primary (transverse-only) other shear* mode space, that is the subspace of primary transverse-only shear mode (i.e., with constant shear strain along  $x$ ) which is not part of any of  $S_{Bt}$ ,  $S_{Tt}$ , and  $S_{Dt}$ .
- $T_P$  is the mode space for *primary transverse extension* modes.
- $L_S$  is the mode space for *secondary local(-plate)* modes.
- $S_S$  is the mode space for *secondary shear* modes (with warping-only displacements).
- $T_S$  is the mode space for *secondary transverse extension* modes.

Detailed information on shear sub-spaces is given in Section 3.2, while the practical way of constructing the various spaces and sub-spaces is summarized in Sections 3.3 and 3.4.

As far as  $G_B$ ,  $S_{Bw}$  and  $S_{Bt}$  are concerned, any two of them are linearly independent of each other. However, all the three are linearly dependent, therefore, any of them can be expressed by the linear combination of the other two. Similar linear dependency exists for  $D$ ,  $S_{Dw}$  and  $S_{Dt}$ . Finally, the same is true for  $G_T$ ,  $S_{Tw}$  and  $S_{Tt}$ , at least if  $G_T$  exists. (If  $G_T$  does not exist,  $S_{Tw}$  does not exist, neither, therefore, linear dependency is not an issue.) It is also to note that  $S_{Cw}$  and  $S_{Ct}$  are linearly independent sub-spaces and obviously independent of  $G$  and  $D$ , too.

Thus, the primary shear mode space can be composed as illustrated in **Figure 3.10**.



**Figure 3.10:** Decomposition of primary shear modes

### 3.3.2 Outline of mode construction

In the following Sections of the dissertation the generalized derivations for the deformation modes are presented. The derivations closely follow **Table 3.1**. The construction of the modes is presented in accordance of the order of **Table 3.1**, starting with the  $G_A$  axial mode and ending with the secondary modes. It is to note that the order of primary mode spaces is not arbitrary, since the construction of certain modes requires the knowledge of other modes.

For the construction of the base system of any mode space, three kinds of information will be used. One is directly included in **Table 3.1**, namely: for any mode space or sub-space certain strain components are equal to zero. These *null criteria*, found in the first 6 rows of **Table 3.1**, are practically useful, since these are the ones that can easily be enforced. In row #7 it is given whether transverse equilibrium of the cross-section is satisfied or not. Since transverse equilibrium can also be interpreted as nullity of the unbalanced nodal forces/moments, transverse equilibrium is also treated as a null criterion, which, again, can easily be enforced.

The two other types of information are similar, namely: the various spaces must be *linearly independent* of each other, while the sub-spaces must be *orthogonal* to each other (in a certain sense). Linear independency is enforced by *independency criteria*, orthogonality can be enforced by *orthogonality criteria*.

Both null criteria and orthogonality criteria are (mostly) expressed by matrix equations, where the matrices are applied to the displacement vectors in order to enforce the embedded criterion. Matrices for null criteria are denoted by  $\mathbf{Z}$  and an appropriate subscript (where the subscript comes from the first column of **Table 3.1**). The orthogonality matrices are denoted by  $\mathbf{O}$  and an appropriate subscript. The subscripts determine which displacement or strain component distribution is orthogonal, e.g.,  $\mathbf{O}_v$  expresses orthogonality of  $v$  functions, i.e., warping distributions. All the orthogonality criteria are interpreted for the cross-section middle line. (Note, independency criteria do not require any special constraint matrix.)

The derivation of  $\mathbf{Z}$  and  $\mathbf{O}$  matrices are summarized in Appendix A and B. Note, all the  $\mathbf{Z}$  matrices are compiled so that the column number would be equal to the DOF number (i.e., the length of the displacement vector), therefore, enforcement of a null criterion requires  $\mathbf{Z}\mathbf{d} = \mathbf{0}$ . (Note, in some cases further conditions are needed to be satisfied, which conditions, however, can also be expressed by simple matrices.) The orthogonality matrices are square matrices, row and column number being equal to the DOF number. Therefore, enforcement of an orthogonality criterion for two non-identical displacement vectors requires  $\mathbf{d}_r^T \mathbf{O} \mathbf{d}_s = \mathbf{0}$ . Finally, independency criterion is enforced by requiring the scalar product of two displacement vectors to be zero, i.e.,  $\mathbf{d}_r^T \mathbf{d}_s = \mathbf{0}$ .

Comments on the size of the spaces and sub-spaces are provided. In some cases simple rule can be given for the sub-space dimension, in other cases such simple rule does not exist. It is to emphasize, however, that the preliminary knowledge of the space dimensions is not required, in fact, the dimension is ultimately determined by the process of constructing the given space or sub-space. Some other comments are also given, e.g., on the distribution of some displacements or strains. These comments are generally valid, but exceptions might exist. The exceptions are limited to very simple cross-section topologies, which are discussed separately at the end of Section 3.

The modes are illustrated in **Figure 3.11**. The presented deformed shapes correspond to simple-simple end restraints with one longitudinal single half-wave. It is to emphasize that **Table 3.1** defines mode spaces, but does not specifically define a base system for any (multi-dimensional) mode space. It means that various base systems are possible, as discussed later. **Figure 3.11** shows possible base vectors.

### 3.3.3 Global mode space

#### 3.3.3.1 Axial mode space

Axial mode is a mode where  $\varepsilon_x = \gamma_{xy} = \kappa_x = \kappa_y = \kappa_{xy} = 0$ , plus transverse equilibrium is satisfied. All these criteria are summarized by the following mathematical expression:

$$\begin{bmatrix} \mathbf{Z}_{ex} \\ \mathbf{Z}_{gxy} \\ \mathbf{Z}_{kx} \\ \mathbf{Z}_{ky} \\ \mathbf{Z}_{kxy} \\ \mathbf{Z}_{eq} \end{bmatrix} \mathbf{d}_{GA} = \mathbf{0} \text{ and } \Theta_i = \Theta_j \text{ for any } i \text{ and } j \text{ and } \Theta_i = 0 \text{ for any } i \quad (3.11)$$

Transverse equilibrium is automatically satisfied for any rigid-body cross-sectional displacements (e.g., if  $\kappa_x = 0$ ), therefore, it can be eliminated. Null longitudinal curvature and null mixed curvature (i.e.,  $\kappa_{xy} = 0$ ) require that  $\Theta_i = 0$ , while null transverse curvature requires that  $\Theta_i = \Theta_j$  for any  $i$  and  $j$ . However, if  $\Theta_i = 0$ ,  $\Theta_i = \Theta_j$  is automatically satisfied. Moreover,  $\mathbf{Z}_{kx}$  becomes identical to  $\mathbf{Z}_{kxy}$  if  $\Theta_i = 0$ . Consequently, if null mixed curvature is enforced, null transverse curvature criterion is automatically satisfied. Thus, the above criterion can be written in a simplified form as follows:

$$\begin{bmatrix} \mathbf{Z}_{ex} \\ \mathbf{Z}_{gxy} \\ \mathbf{Z}_{ky} \\ \mathbf{Z}_{kxy} \end{bmatrix} \mathbf{d}_{GA} = \mathbf{Z}_{GA} \mathbf{d}_{GA} = \mathbf{0} \text{ and } \Theta_i = 0 \text{ for any } i \quad (3.12)$$

Mathematically, the above criteria can be handled as follows. The  $\mathbf{d}_{GA}$  vector must satisfy (i) the  $\mathbf{Z}_{GA} \mathbf{d}_{GA} = \mathbf{0}$  equation, (ii) and the  $\Theta_i = 0$  equations. This latter condition can also be expressed in matrix form as follows:

$$\mathbf{d}_{GA} = \begin{bmatrix} \mathbf{I} \\ \mathbf{0} \end{bmatrix} \bar{\mathbf{d}}_{GA} = \mathbf{Z}_0 \bar{\mathbf{d}}_{GA} \quad (3.13)$$

where  $\bar{\mathbf{d}}_{GA}$  contains the non-zero elements of the  $\mathbf{d}_{GA}$  displacement vector,  $\mathbf{I}$  is an identity matrix the size of which is equal to total number of DOF which are (might be) non-zero, while  $\mathbf{0}$  is a matrix full of zeros, with column number equal to the size of  $\mathbf{I}$ , while row number equal to the number of DOF which are zero. In the actual case, therefore, if there are  $n$  nodal lines in the finite strip model,  $\mathbf{I}$  is a  $3n$  by  $3n$  square matrix, while  $\mathbf{0}$  is an  $n$  by  $3n$  matrix.

Eq (3.12) can be written as follows:

$$\begin{bmatrix} \mathbf{Z}_{ex} \\ \mathbf{Z}_{gxy} \\ \mathbf{Z}_{ky} \\ \mathbf{Z}_{kxy} \end{bmatrix} \begin{bmatrix} \mathbf{I} \\ \mathbf{0} \end{bmatrix} \bar{\mathbf{d}}_{GA} = (\mathbf{Z}_{GA} \mathbf{Z}_0) \bar{\mathbf{d}}_{GA} = \mathbf{0} \quad (3.14)$$

from which  $\bar{\mathbf{d}}_{GA}$  can formally be expressed as the null-space of the  $\mathbf{Z}_{GA} \mathbf{Z}_0$  matrix:

$$\bar{\mathbf{d}}_{GA} = \text{null}(\mathbf{Z}_{GA} \mathbf{Z}_0) \quad (3.15)$$

Finally the  $\mathbf{d}_{GA}$  displacement vector(s) can be achieved by solving the following equation:

$$\mathbf{d}_{GA} = \mathbf{Z}_0 \bar{\mathbf{d}}_{GA} = \mathbf{Z}_0 \cdot \text{null}(\mathbf{Z}_{GA} \mathbf{Z}_0) \quad (3.16)$$

Since the *null* function determines a base system for all the vectors that satisfy the given criteria, the resulted displacement vectors are nothing else than the constraint matrix, in this actual case, the  $\mathbf{R}_{GA}$  constraint matrix for the axial mode space. Therefore:

$$\mathbf{R}_{GA} = \mathbf{Z}_0 \cdot \text{null}(\mathbf{Z}_{GA} \mathbf{Z}_0) \quad (3.17)$$

By looking at the structure and physical meaning of the various  $\mathbf{Z}$  matrices, one might conclude that: (i) null transverse curvature enforces rigid-body type cross-section displacements, (ii) null mixed curvature enforces zero rotation, (iii) null longitudinal curvature enforces zero transverse translations, (iv) null transverse normal strain and null membrane shear strain criteria define a relationship between transverse and longitudinal translational displacements, however, if there are no translations, the warping must be zero or constant. Thus, in case of a general cross-section the above equation defines one single displacement field characterized by uniform warping along the cross-section. Therefore there is no need to formally solve Eq. (3.17), since uniform warping can be defined directly.

### 3.3.3.2 Global bending mode space

Bending mode is a mode where  $\epsilon_x = \gamma_{xy} = \kappa_x = \kappa_{xy} = 0$ , plus transverse equilibrium is satisfied. As mentioned at the axial mode space, null mixed curvature criterion includes null transverse curvature criterion, therefore, can be disregarded. Also, null transverse curvature criterion includes transverse equilibrium. Therefore, the displacement vectors of the bending mode class, i.e., the  $\mathbf{R}_{GB}$  constraint matrix must satisfy the following criteria:

$$\begin{bmatrix} \mathbf{Z}_{ex} \\ \mathbf{Z}_{gxy} \\ \mathbf{Z}_{kxy} \end{bmatrix} \mathbf{R}_{GB} = \mathbf{0} \text{ and } \Theta_i = 0 \text{ for any } i \quad (3.18)$$

Similarly, as presented for the axial mode space, the  $\Theta_i = 0$  criteria can be incorporated into the matrix equation.

By looking at the structure and physical meaning of the various  $\mathbf{Z}$  matrices, one might conclude that: (i) null transverse curvature enforces rigid-body type cross-section displacements, (ii) null mixed curvature enforces zero rotation, (iii) null transverse normal strain and null membrane shear strain criteria define a relationship between transverse and longitudinal translational displacements, therefore, if transverse translations are determined, the warping translations are determined, too. Thus, in case of a general cross-section the above equation defines a 3-dimensional mode space, characterized by rigid-body cross-section displacements with zero rotation. Obviously, this 3-dimensional space includes the already defined and discussed axial mode, too. Therefore, one must subtract the axial mode from the 3-dimensional space defined by Eq. (3.18). The simplest way to complete the subtraction is to add an orthogonality criterion to Eq. (3.18). Bending modes are characterized by linear warping distribution over the whole cross-section, therefore, warping distribution of  $G_A$  and  $G_B$  modes are orthogonal. Namely:

$$\sum_{(k)=1}^{n_{strip}} \int_0^{b^{(k)}} v_{GA}^{(k)} v_{GB}^{(k)} dx = 0 \quad \text{or} \quad \mathbf{R}_{GA}^T \mathbf{O}_v \mathbf{R}_{GB} = 0 \quad (3.19)$$



Eq. (3.18) thus can be extended as follows:

$$\begin{bmatrix} \mathbf{Z}_{\text{ex}} \\ \mathbf{Z}_{\text{gxy}} \\ \mathbf{Z}_{\text{kxy}} \\ \mathbf{R}_{\text{GA}}^T \mathbf{O}_v \end{bmatrix} \mathbf{R}_{\text{GB}} = \mathbf{0} \quad \text{and} \quad \Theta_i = 0 \text{ for any } i \quad (3.20)$$

from which  $\mathbf{R}_{\text{GB}}$  can be expressed.

This equation leads to two independent mode vectors, i.e., two bending modes. Both bending modes are characterized by piecewise linear warping distribution and transverse rigid-body-type cross-section displacements in two non-coinciding directions. The above equation does not specifically determine two base vectors, only the mode space. Practically it means that transverse displacements in any two non-coinciding directions can be used as base vectors for the  $G_B$  space. Typically, it is convenient to select two perpendicular directions. Moreover, further orthogonalization within the  $G_B$  space is possible (which is equivalent to select two principal axes for the base vectors), which question is further discussed in Section 3.4.

### 3.3.3.3 Global torsion mode space

Global torsion mode is a mode where  $\varepsilon_x = \gamma_{xy} = \kappa_x = 0$ , plus transverse equilibrium is satisfied. Moreover, the (primary) warping distribution of torsion mode is orthogonal to those of axial and bending modes. Therefore,  $\mathbf{R}_{\text{GT}}$  can be calculated from the following equation:

$$\begin{bmatrix} \mathbf{Z}_{\text{ex}} \\ \mathbf{Z}_{\text{gxy}} \\ \mathbf{Z}_{\text{kx}} \\ \mathbf{R}_{\text{GA}}^T \mathbf{O}_v \\ \mathbf{R}_{\text{GB}}^T \mathbf{O}_v \end{bmatrix} \mathbf{R}_{\text{GT}} = \mathbf{0} \quad \text{and} \quad \Theta_i = \Theta_j \text{ for any } i \text{ and } j \quad (3.21)$$

This equation leads to either one or zero mode vector. If global torsion mode exists, typically the resulted displacements include piecewise linear warping distribution.

### 3.3.4 Other primary mode spaces

Constraint matrices for the other primary mode spaces can be constructed similarly, by applying the null criteria according to **Table 3.1**, and by applying orthogonality and independency criteria where necessary. The order of the construction is not arbitrary. The necessary matrix equations are summarized as follows.

$$\begin{bmatrix} \mathbf{Z}_{\text{ex}} \\ \mathbf{Z}_{\text{gxy}} \\ \mathbf{Z}_{\text{eq}} \\ \mathbf{R}_{\text{GA}}^T \mathbf{O}_v \\ \mathbf{R}_{\text{GB}}^T \mathbf{O}_v \\ \mathbf{R}_{\text{GT}}^T \mathbf{O}_v \end{bmatrix} \mathbf{R}_{\text{D}} = \mathbf{0} \quad (3.22)$$

$$\begin{bmatrix} \mathbf{Z}_{\text{ex}} \\ \mathbf{Z}_{\text{gxy}} \end{bmatrix} \mathbf{R}_{\text{LP}} = \mathbf{0} \quad \text{and} \quad V_i = 0 \quad \text{for all the nodes} \quad (3.23)$$

$$\begin{bmatrix} \mathbf{Z}_{\text{ex}} \\ \mathbf{Z}_{\text{ky}} \\ \mathbf{Z}_{\text{kxy}} \\ \mathbf{R}_{\text{GA}}^T \mathbf{O}_{\text{v}} \end{bmatrix} \mathbf{R}_{\text{SPw}} = \mathbf{0} \text{ and } \Theta_i = 0 \text{ for any } i \quad (3.24)$$

$$\begin{bmatrix} \mathbf{Z}_{\text{ex}} \\ \mathbf{Z}_{\text{ky}} \\ \mathbf{Z}_{\text{kxy}} \\ \mathbf{R}_{\text{GA}}^T \\ \mathbf{R}_{\text{SBw}}^T \mathbf{O}_{\text{dvx}} \\ \mathbf{R}_{\text{STw}}^T \mathbf{O}_{\text{dvx}} \\ \mathbf{R}_{\text{SDw}}^T \mathbf{O}_{\text{dvx}} \end{bmatrix} \mathbf{R}_{\text{SCw}} = \mathbf{0} \quad (3.25)$$

$$\begin{bmatrix} \mathbf{Z}_{\text{ex}} \\ \mathbf{Z}_{\text{kxy}} \end{bmatrix} \mathbf{d}_{\text{SBt}} = \mathbf{0} \text{ and } \Theta_i = 0 \text{ and } V_i = 0 \text{ for any } i \quad (3.26)$$

$$\begin{bmatrix} \mathbf{Z}_{\text{ex}} \\ \mathbf{Z}_{\text{kx}} \\ \mathbf{R}_{\text{SBt}}^T \mathbf{O}_{\text{u}} \end{bmatrix} \mathbf{R}_{\text{STt}} = \mathbf{0} \text{ and } \Theta_i = \Theta_j \text{ for any } i \text{ and } j, \text{ and } V_i = 0 \text{ for any } i \quad (3.27)$$

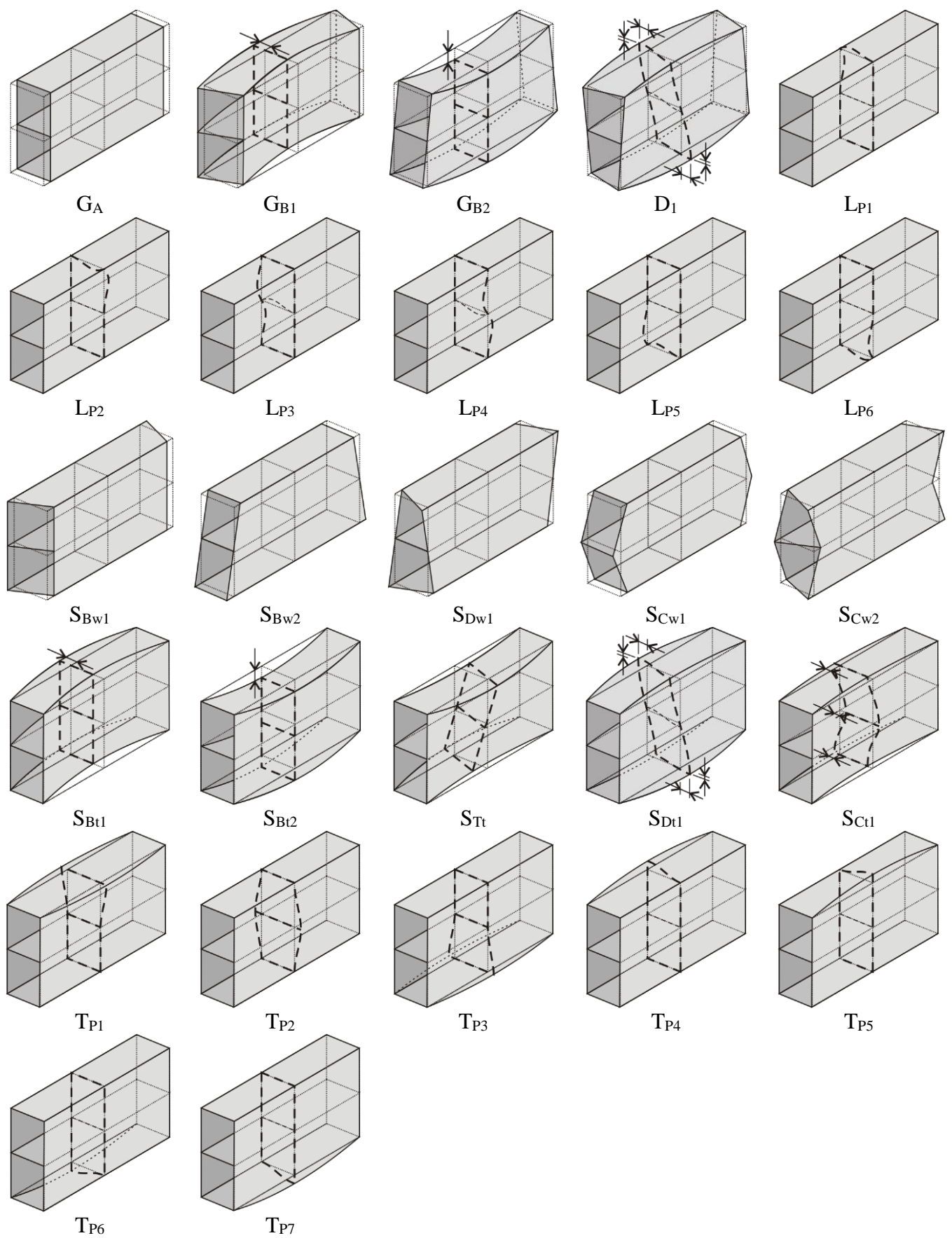
$$\begin{bmatrix} \mathbf{Z}_{\text{ex}} \\ \mathbf{Z}_{\text{eq}} \\ \mathbf{R}_{\text{SBt}}^T \mathbf{O}_{\text{u}} \\ \mathbf{R}_{\text{STt}}^T \mathbf{O}_{\text{u}} \end{bmatrix} \mathbf{R}_{\text{SDt}} = \mathbf{0} \text{ and, and } V_i = 0 \text{ for any } i \quad (3.28)$$

$$\begin{bmatrix} \mathbf{Z}_{\text{ex}} \\ \mathbf{R}_{\text{LP}}^T \\ \mathbf{R}_{\text{SBt}}^T \mathbf{O}_{\text{u}} \\ \mathbf{R}_{\text{STt}}^T \mathbf{O}_{\text{u}} \\ \mathbf{R}_{\text{SDt}}^T \mathbf{O}_{\text{u}} \end{bmatrix} \mathbf{R}_{\text{SCt}} = \mathbf{0} \text{ and } V_i = 0 \text{ for any } i \quad (3.29)$$

$$\begin{bmatrix} \mathbf{R}_{\text{LP}}^T \\ \mathbf{R}_{\text{SBt}}^T \\ \mathbf{R}_{\text{STt}}^T \\ \mathbf{R}_{\text{SDt}}^T \\ \mathbf{R}_{\text{Sot}}^T \end{bmatrix} \mathbf{R}_{\text{TP}} = \mathbf{0} \text{ and } V_i = 0 \text{ for any } i \quad (3.30)$$

It is to note that primary warping-only shear space can be determined, but cannot be separated into  $\mathbf{S}_{\text{Bw}}$ ,  $\mathbf{S}_{\text{Tw}}$  and  $\mathbf{S}_{\text{Dw}}$  purely from the mechanical criteria of **Table 3.1**. However, since they possess warping distribution identical to that of  $\mathbf{G}_{\text{B}}$ ,  $\mathbf{G}_{\text{T}}$  and  $\mathbf{D}$ , respectively, the constraint matrices can easily be constructed from the constraint matrices of the corresponding global sub-spaces. The same is true for  $\mathbf{S}_{\text{Bt}}$  and  $\mathbf{S}_{\text{Dt}}$ .

All the resulted mode spaces are illustrated in **Figure 3.11** for a two-cell cross-section.



**Figure 3.11: Modal decomposition of a 2-cell cross-section**

### 3.3.5 Exceptions: overlaps of primary mode spaces

The above presented procedures for the calculation of various modes lead to distinct mode spaces for almost all the cases. Overlap occurs between shear and global modes, independently of the cross-section shape or topology, as already mentioned above. This question is discussed in full detail in [1/3-2/3]. Moreover, overlap of the spaces occurs in case of some very specific cross-section topologies, namely, if the cross-section has zero corner node (i.e., the cross-section is consisted of a single plate), or one corner node (i.e., the cross-section has an L, T or X shape). These overlaps are discussed in detail in [5/3].

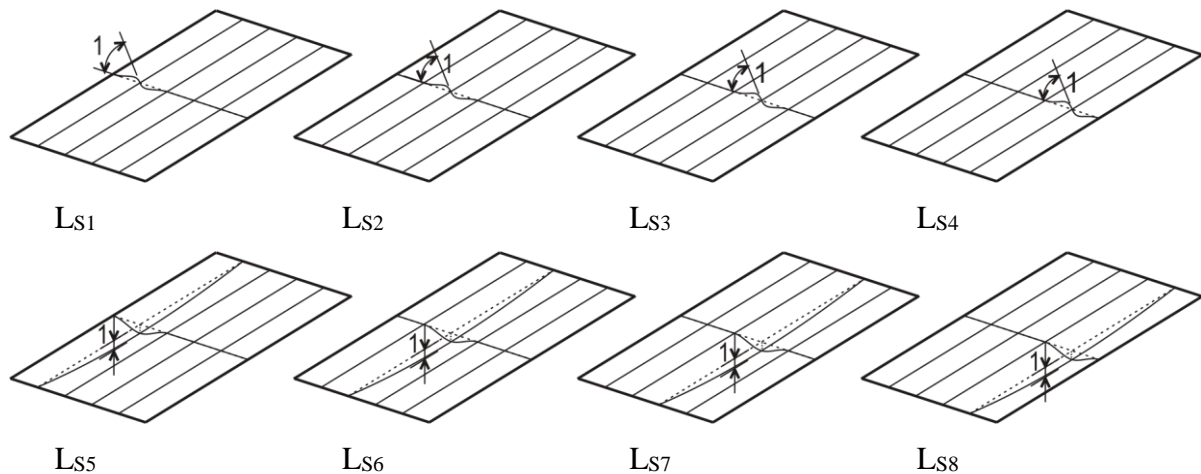
### 3.3.6 Secondary mode spaces

#### 3.3.6.1 Secondary local mode space

In case of primary local mode space the transverse curvature function is piece-wise linear (i.e., linear within a flat plate element in between two main nodes), while secondary local modes are characterized by non-linear transverse curvature function even within a flat plate element. Otherwise the primary and secondary local mode vectors share the same mechanical features.

Therefore, similarly to the primary L modes, secondary L modes have zero warping, zero transverse extension and in-plane shear strain. The simplest construction of the base vectors is to apply 1-s and 0-s for the rotational and  $w$ -directional translational DOF of the sub-nodes. (Note, all the DOF of all the main nodes are zero, since main nodes are fully handled by the primary local modes.) This means that the number of linearly independent secondary local base vectors is twice the number of sub-nodes.

The enforcement of 1-s and 0-s can be completed plate by plate. For one plate the resulted base system is illustrated in **Figure 3.12**.



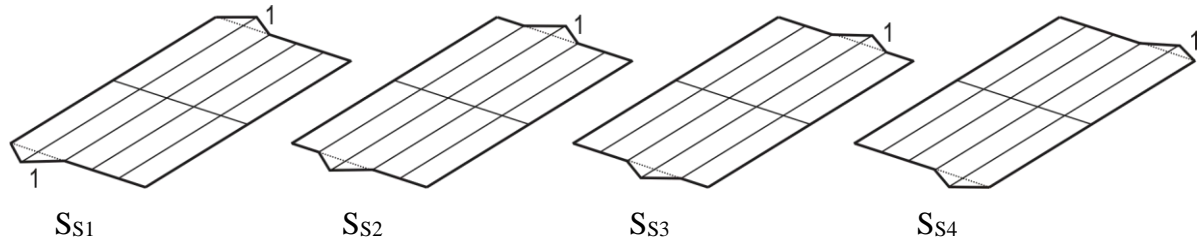
**Figure 3.12:** Base system for secondary local mode space of a single plate

### 3.3.6.2 Secondary shear mode space

In case of primary shear mode space it is the in-plane shear strain function which is piece-wise linear along the local  $x$ -axis (i.e., linear within a flat plate element in between two main nodes), while secondary shear modes are characterized by non-linear shear strain function even within a flat plate element. Otherwise the primary and secondary shear mode vectors share the same mechanical features.

In case of primary shear modes two sets are generated: warping-only and transverse-only mode spaces. It is easy to understand that transverse-only secondary modes are physically impossible. Let us consider a flat element and assume multiple strips. If local  $u$  is enforced in any strip, the same local  $u$  must occur in all the strips in order to maintain geometric compatibility. This means, furthermore, that the shear strain in each strip will be the same (in any cross-section, i.e., for any value of  $y=Y$ ).

Thus, secondary shear modes can be constructed solely by the warping-only way. The simplest construction of the base vectors is to apply 1-s and 0-s for the warping DOF of the sub-nodes, see **Figure 3.13**. (Note, all the DOF of all the main nodes are zero, since main nodes are fully handled by the primary shear modes.) This means that the number of linearly independent secondary shear base vectors is equal to the number of sub-nodes.

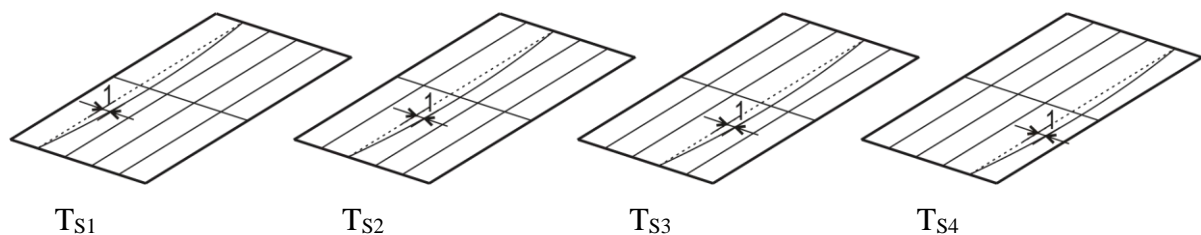


**Figure 3.13:** Base system for secondary shear mode space of a single plate

### 3.3.6.3 Secondary transverse extension mode space

In case of primary transverse extension mode space it is the local  $u$  displacement function which is piece-wise linear along the local  $x$ -axis (i.e., linear within a flat plate element in between two main nodes), while secondary transverse extension modes are characterized by non-linear local  $u$  function even within a flat plate element. Otherwise the primary and secondary transverse extension mode vectors share the same mechanical features.

Therefore, similarly the primary T modes, secondary T modes have zero warping. The simplest construction of the base vectors is to apply 1-s and 0-s for the local  $u$ -directional translational DOF of the sub-nodes, see **Figure 3.14**. (Note, all the DOF of all the main nodes are zero, since main nodes are fully handled by the primary transverse extension modes.) This means that the number of linearly independent secondary transverse extension base vectors is equal to the number of sub-nodes.



**Figure 3.14:** Base system for secondary transverse extension mode space of a single plate

## 3.4 Orthogonality within the mode spaces

### 3.4.1 General

The construction of the various mode spaces are presented previously in Section 3.3. The presented procedures fully and unambiguously determine the mode spaces. The spaces are determined by their base vectors (or: base functions). The presented procedures lead to a *native* (or: natural) set of base vectors for any mode space. However, transformation within any (multi-dimensional) space is possible, i.e., base vectors can be defined in infinite number of ways. From practical aspects it might be useful to apply other than the native base vectors.

If the mode space is one-dimensional (such as A, or G<sub>T</sub>), obviously there is no need or possibility for various base systems.

In certain cases more than one way exists to create a native base system. For example, in case of L<sub>P</sub> space, the mode vectors can be determined by solving Eq. (3.23), or by setting 1-s and 0-s for rotations and *w*-directional translations of end-nodes.

In case of multi-dimensional spaces there is infinite number of base systems. Here, orthogonal base systems will be presented. However, orthogonality can be interpreted in various ways even within the same mode space. Two basic interpretations can be considered: (i) orthogonality in cross-section sense, and (ii) orthogonality in member sense.

The orthogonality in member sense is essentially the same kind of orthogonality which is included in CUFSM and discussed in detail in [10/2]. Therefore, member orthogonality is not discussed here.

The most important feature of cross-section orthogonality is that the base vectors are intended to be determined independently of the longitudinal shape functions (which also means that independently of the length of the member, and independently of the end restraints) and independently of the loading. Since the construction of the native base vectors involve the effect of member length (and ultimately that of the longitudinal shape functions), first dependency on longitudinal shape functions are discussed.

### 3.4.2 Dependency on longitudinal shape functions

Though longitudinal shape functions are appearing in multiple places in the derivations, mostly they can be eliminated during the derivations and finally most of the mode spaces are independent of the longitudinal base functions, consequently, independent of member length and of end restraints.

Basically there is one matrix in which the effect of longitudinal base functions is directly included, this is  $\mathbf{Z}_{\text{gxy}}$ . The effect is visible by the existence of the  $\frac{a}{m\pi}$  or  $\frac{m\pi}{a}$  term in Eq. (B20) or Eq. (B21). This term comes from the first derivative of the internal function of  $Y_{[m]}$ , where  $Y_{[m]}$  is the longitudinal shape function for the (local) displacements  $u$  and  $w$ . In the semi-analytical FSM the  $Y_{[m]}$  functions are selected so that this first derivative of internal functions would be identical for any end restraint condition. In this sense, thus, for the given set of longitudinal base functions  $\mathbf{Z}_{\text{gxy}}$  is independent of the end restraints, while the effect of longitudinal base function appears only in the  $m\pi/a$  term.

The  $m\pi/a$  term is dependent on the  $m$  parameter (which can roughly be interpreted as the number of half-waves along the length), and the member length  $a$ . It can be understood that this term makes the relationship between local  $u$  and local  $v$  displacements if null-shear-strain criterion is enforced: the smaller this  $m\pi/a$  ratio is, the smaller the warping displacements are that belong to a certain transverse displacement.

Which mode spaces are affected by the  $m\pi/a$  ratio? By looking at the construction of the mode spaces it turns out that only  $G_B$ ,  $G_T$  and  $D$  modes are affected. In all the other mode spaces either local  $v$  or local  $u$  is zero. A common feature of these mode spaces is that there is a one-to-one relationship between the warping and transverse displacements of the member cross-section. (This is more evident from the original cFSM derivations where this relationship is expressed by closed-formed formulae, see [4/2].) Therefore, either the warping displacements, or the transverse displacements unambiguously define these mode spaces. The warping or transverse displacements alone are independent of the length, thus, it is possible to have the interpretation that the  $G_B$ ,  $G_T$  and  $D$  mode spaces are essentially determined by either the warping displacements or transverse displacements, though when constructing the mode vectors one must consider both warping and transverse displacements, therefore, must consider dependence on  $m$  and  $a$ .

Even so, it must be decided whether warping displacements or transverse displacements are taken as the determining part of the displacements. In most cross-sections this decision has no any theoretical or practical importance. However, if the cross-section is too simple, i.e., it has zero or one corner node only,  $G_B$  and  $G_T$  space overlaps with other spaces. If the overlapping modes are assigned to global spaces, these modes will have transverse displacements but no warping displacements (since just this is the feature of these modes that causes the overlapping). Therefore, it seems to be somewhat more general to consider the transverse displacements as the determining part of the displacements for the  $G_B$ ,  $G_T$  and  $D$  mode spaces. (It is to note, however, that in GBT and original cFSM the construction of  $G_B$ ,  $G_T$  and  $D$  modes are based on rather the warping displacements than transverse displacements.)

Thus, there are mode spaces which are de facto independent of  $m$  and  $a$ , while for  $G_B$ ,  $G_T$  and  $D$  mode spaces it is possible to select a part of the displacements which characterizes the whole displacement field and which is independent of  $m$  and  $a$ .

There are at least two advantages of having quasi length-independent version of base vectors. One is a computational advantage. In a typical cFSM analysis either multiple lengths or multiple  $m$  terms are considered (or both), which means that nearly identical calculations are repeated multiple times. It is computationally efficient to construct an initial base vector first for a specific value of  $a$  and  $m$ , say,  $a_0$  and  $m_0$ , while the effect of changing  $m\pi/a$  ratio can easily be considered by multiplying, say, the warping displacements by  $m/m_0$  and  $a_0/a$  ratios.

Another important consequence of applying an initial set of base vectors is that the order of the individual base vectors can be kept constant during a cFSM analysis, even if the length, or the considered  $m$  terms are changing. Thus, if cFSM analysis aims to calculate a specific buckling mode for various lengths and/or various end restraints, the necessary individual mode vector or vectors will be found in the same position within the full set of base vectors. Indeed, these length-independent base vectors can be constructed solely based on the geometry of the cross-section middle-line, and in this way this length-independent base vector set can be considered as a “property” of the cross-section geometry.

### 3.4.3 Orthogonality in cross-section

Cross-section orthogonal base vectors (functions) are interpreted as follows: (i) some displacement functions (or derivatives of displacement function) are orthogonal to each other, (ii) the orthogonality is satisfied by base vectors within the same mode space, and (iii) the orthogonality is interpreted in cross-sections (rather than in the member).

The orthogonality is interpreted here as:

$$\int f_r f_s ds = 0 \text{ if } r \neq s \text{ and } \int f_r f_s ds \neq 0 \text{ if } r = s \quad (3.31)$$

where  $f$  function is a displacement function (or derivative of displacement function), which can be determined from a displacement vector. Since orthogonality is intended to be interpreted for a cross-section (rather than for the whole member),  $f$  function must be selected so that it would be characteristic for the cross-section. Similar orthogonality condition has already been applied during the construction of the mode spaces. The most evident one of such orthogonality conditions is the orthogonality of warping functions within the  $G_D$  space. These functions are characteristic for  $G$  and  $D$  spaces, thus, can readily be used to create orthogonal mode vectors. For other mode spaces other functions might be advantageous. It is to emphasize that the orthogonalization process, though practically useful and based on mechanical considerations, has no unambiguous mechanical background, which means that there is no one-and-single good solution but there are (or might be) multiple reasonable solutions. In the following a possible “best” approach is followed where the orthogonalization is based on that geometric property which is considered to be the most characterizing for the given space. Namely: warping for  $G$ , transverse curvature for  $L$ , in-plane shear strain for  $S$ , and in-plane transverse strain for  $T$ . As far as  $D$  is concerned, it can be orthogonalized in two meaningful ways, either by using the warping functions or by using the transverse curvature functions. The two orthogonalization schemes lead to visually similar, but mathematically not always exactly identical orthogonal mode vectors. It is experienced that for the most typical sections (such as lipped channel) there is no practical difference between the two approaches, however, for more complicated sections the orthogonalization with regard to transverse curvature is practically better.

For the potentially multi-dimensional primary mode spaces the following equations apply:

$$\mathbf{R}_{GB}^T \mathbf{O}_v \mathbf{R}_{GB} = \mathbf{D} \quad (3.32)$$

$$\mathbf{R}_D^T \mathbf{O}_v \mathbf{R}_D = \mathbf{D} \text{ or } \mathbf{R}_D^T \mathbf{O}_{kx} \mathbf{R}_D = \mathbf{D} \quad (3.33)$$

$$\mathbf{R}_{LP}^T \mathbf{O}_{kx} \mathbf{R}_{LP} = \mathbf{D} \quad (3.34)$$

$$\mathbf{R}_{SCw}^T \mathbf{O}_{dvx} \mathbf{R}_{SCw} = \mathbf{D} \quad (3.35)$$

$$\mathbf{R}_{SCt}^T \mathbf{O}_u \mathbf{R}_{SCt} = \mathbf{D} \quad (3.36)$$

$$\mathbf{R}_{TP}^T \mathbf{O}_{ex} \mathbf{R}_{TP} = \mathbf{D} \quad (3.37)$$

where  $\mathbf{D}$  is a diagonal matrix (of various size) with non-zero elements in the main diagonal, while  $\mathbf{O}$  matrices represent the orthogonality criteria. The derivation of the  $\mathbf{O}$  matrices can be found in the Appendix A.



Similarly, for the (typically multi-dimensional) secondary mode spaces:

$$\mathbf{R}_{\text{LS}}^T \mathbf{O}_{\text{kx}} \mathbf{R}_{\text{LS}} = \mathbf{D} \quad (3.38)$$

$$\mathbf{R}_{\text{SS}}^T \mathbf{O}_{\text{dxx}} \mathbf{R}_{\text{SS}} = \mathbf{D} \quad (3.39)$$

$$\mathbf{R}_{\text{TS}}^T \mathbf{O}_{\text{ex}} \mathbf{R}_{\text{TS}} = \mathbf{D} \quad (3.40)$$

It is to note that  $S_B$  and  $S_D$  spaces are (or can be) multi-dimensional, too. However, these spaces should be tied to  $G_B$  and  $D$ , therefore, if  $G_B$  and  $D$  are orthogonalized,  $S_B$  and  $S_D$  are automatically orthogonalized in the same way.

The native base vectors for a given  $M$  mode space,  $\mathbf{R}_M^n$ , do not usually satisfy the above equations, instead,  $\mathbf{R}_M^n^T \mathbf{O} \mathbf{R}_M^n$  is a fully populated matrix. In order to have the orthogonal version the base vectors,  $\mathbf{R}_M^n^T \mathbf{O} \mathbf{R}_M^n$  must be diagonalized, which requires the solution of a simple eigen-value problem.

It is also to note that in case of  $S$  mode space orthogonality is interpreted for the in-plane shear strain  $\gamma_{xy} = \partial u / \partial y + \partial v / \partial x$ . However, if  $u = 0$ , (as in case of warping-only shear modes,) the shear strain is simplified to  $\gamma_{xy} = \partial v / \partial x$ , hence orthogonality of  $\gamma_{xy}$  is equivalent to that of  $\partial v / \partial x$  (which can be enforced by  $\mathbf{O}_{\text{dxx}}$ ). Similarly, if  $v = 0$ , (as in case of transverse-only shear modes,) the shear strain is simplified to  $\gamma_{xy} = \partial u / \partial y$ , hence orthogonality of  $\gamma_{xy}$  is equivalent to that of  $\partial u / \partial y$ . However, the distribution of  $\partial u / \partial y$  along the cross-section middle line is identical to that of the  $u$  function, therefore the orthogonality can be enforced by  $\mathbf{O}_u$ .

### 3.4.4 Ordering the cross-section orthogonal base vectors

The importance of ordering the individual base vectors (within a mode space) is a practical one. A reasonable base vector order might help in selecting the mode vectors if a specific buckling mode is aimed to calculate. Moreover, if a mode space is large enough, and the practically more important base vectors are somehow identified, it is reasonable to run the analysis in a reduced DOF space, by selecting the practically more important base vectors only, which leads to a reduced problem size (and therefore, to a faster process).

The here proposed procedure involves two major steps: (i) scaling the base vectors and (ii) ordering the base vectors.

As far as scaling is concerned a simple but straightforward way is to set the maximum value of a characteristic displacement component to 1. The characteristic displacement component can be the local  $w$  for  $G_B$ ,  $G_T$ ,  $D$ ,  $L$  (including both primary and secondary  $L$ ) and transverse-only  $S$  modes, the local  $v$  for  $G_A$  and warping-only  $S$  modes (including secondary shear modes), while the local  $u$  for  $T$  modes (both primary and secondary).

The ordering is not a theoretically well-established process, i.e., various ordering strategies are possible and can be reasonable. The here-followed procedure aims to define the order so that the order would follow the practical importance of the vectors of a given sub-space (i.e., the most important vector should come first, etc.). The ‘practical importance’ of a base vector is measured by the likeliness of its contribution in the first (or: first few) elastic buckling modes of a thin-walled member with the actual cross-section geometry if the member is subjected to some typical longitudinal loading. This aim can be achieved if the ordering is based on a measure which is closely related to the strain energy content of the deformation

mode represented by the base vector. However, since here both the orthogonalization and the ordering are intended to be independent of the longitudinal distribution of the displacements (i.e., independent of the member length, of end restraints, of applied longitudinal shape functions), this energy-related measure must be interpreted to the cross-section.

As an example, L modes are characterized by zero warping, zero transverse membrane strains, zero shear membrane strains, but non-zero transverse curvature (i.e., non-zero transverse strains for  $z \neq 0$ ). It is possible and reasonable, therefore, to define the measure of strain energy content by the following expression:

$$\int \kappa_x \kappa_x ds \quad \text{or} \quad \sum_{(k)=1}^p \int_0^{b^{(k)}} \kappa_x^{(k)} \kappa_x^{(k)} dx \quad (3.41)$$

where  $p$  is the number of strips. As it is shown in the derivation of  $\mathbf{O}_{\mathbf{kx}}$  (in Appendix B), the above expression can be written as  $\mathbf{R}_L^T \mathbf{O}_{\mathbf{kx}} \mathbf{R}_L$ , which is essentially similar to the one that appears in Eq. (3.34) or (3.38).

For all the sub-spaces the measure of strain energy content can be determined similarly, by using that strain component which is the most characterizing for the given cross-section deformation. Namely: longitudinal in-plane strain  $\varepsilon_y$  for G, transverse curvature  $\kappa_x$  for D and L, in-plane shear strain  $\gamma_{xy}$  for S, and in-plane transverse strain  $\varepsilon_x$  for T. (Note the distribution of  $\varepsilon_y$  is identical to that of the  $v$  warping function, therefore,  $\mathbf{O}_v$  can be used for the G space.)

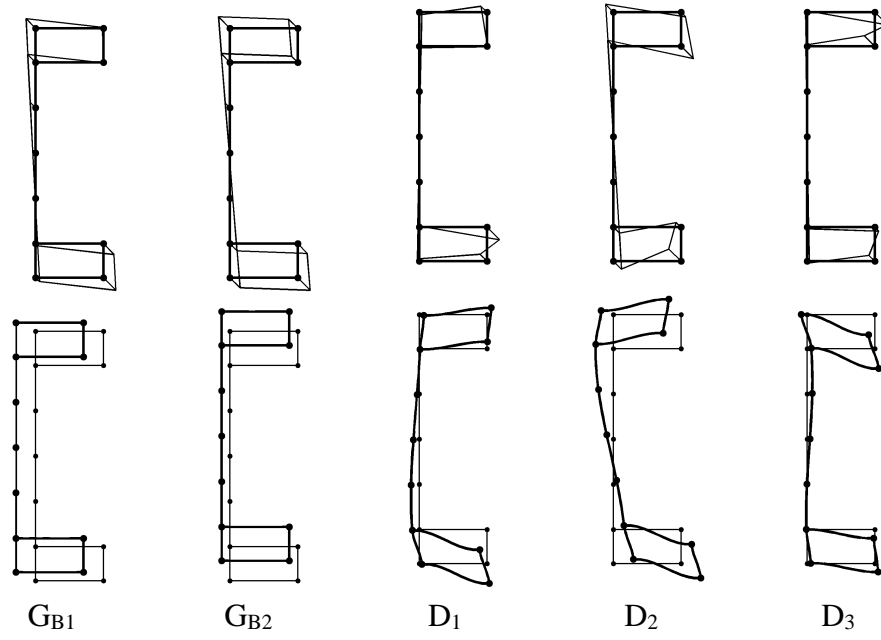
It is to note that  $S_B$  and  $S_D$  spaces are tied to  $G_B$  and D, therefore, if base vectors of  $G_B$  and D are ordered,  $S_B$  and  $S_D$  are automatically ordered in the same way.

### 3.5 Application

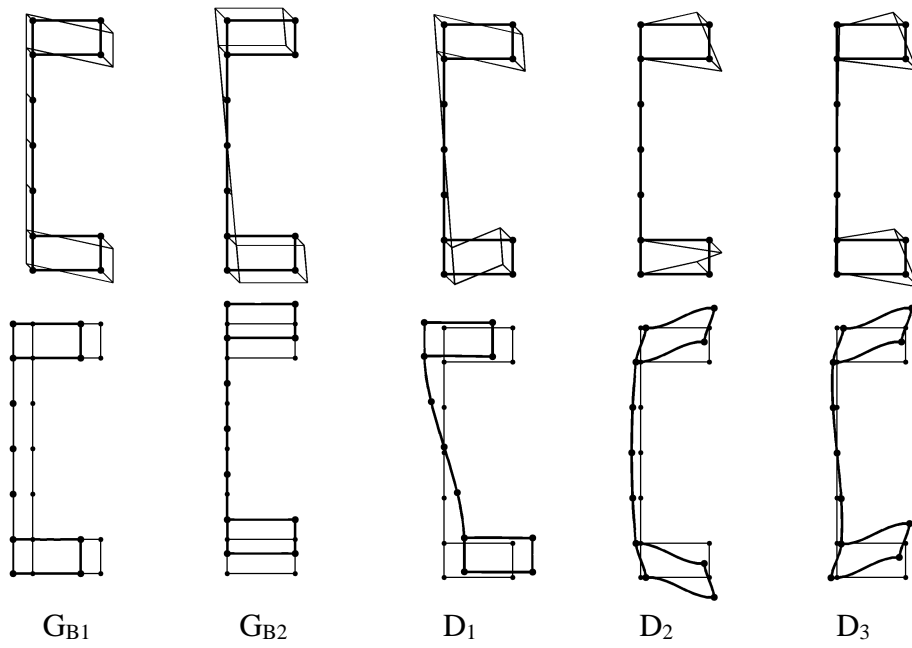
To illustrate the extended features of the generalized cFSM, the above described procedures are applied for a hollow-flange U-section member. More examples can be found e.g., in [5/3].

**Figures 3.15 to 3.26** show the ‘native’ and ‘orthogonal’ base systems for the actual cross-section. (To reduce the sizes of secondary spaces, a rough discretization is used, having a few sub-nodes in the web only.)

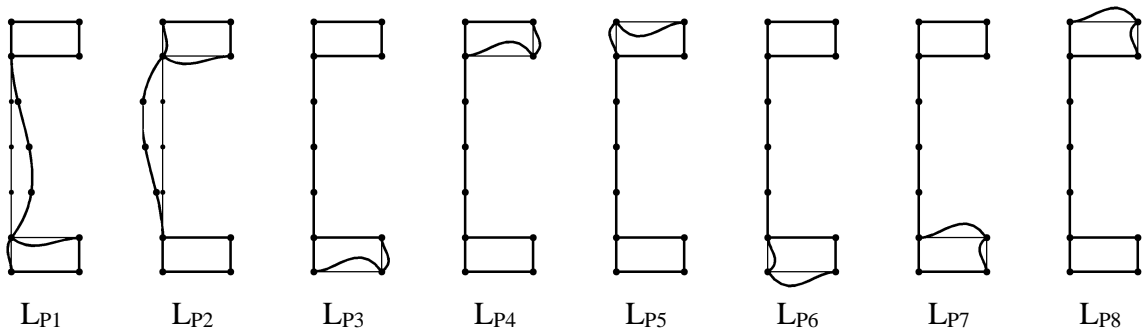
In **Figure 3.27** critical load values are plotted in the function of buckling length, for a beam member in uniform bending. The cross-section is a hollow-flange U, with total depth of 440 mm, flange width of 120 mm, flange depth of 60 mm, thickness of 2 mm. The material is isotropic (steel), with  $E=210$  GPa. The critical stresses are calculated employing several options (and with using a proper discretization): all-mode solution (i.e., classic FSM solution, also called ‘signature curve’), and pure “global”, distortional, and local buckling solutions. For the “global” mode, it is essential to consider G and  $S_T$  modes, since lateral-torsional buckling is associated with torsional deformations, and rigid-body torsional deformation for closed sections is found in the  $S_T$  space. The modal identification of the all-mode curve (i.e., so-called signature curve) is shown in **Figure 3.28**, where G, D, L, S and T participations are given in percentages as a function of length. Selected buckled mode shapes and modal participations are provided in **Figure 3.29**. More discussion of the results, as well as additional examples can be found in [5/3].



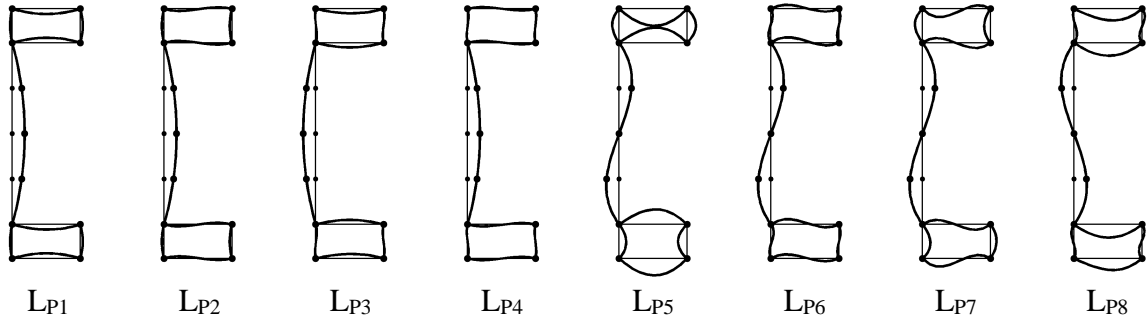
**Figure 3.15:** Native base system for the  $G_B$  and  $D$  spaces



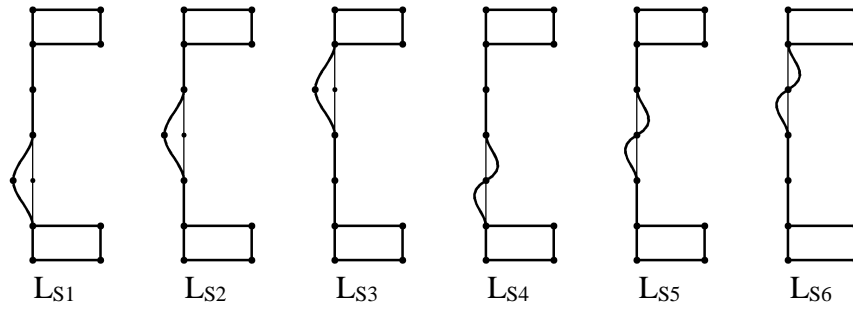
**Figure 3.16:** Cross-section orthogonal base system for the  $G_B$  and  $D$  spaces



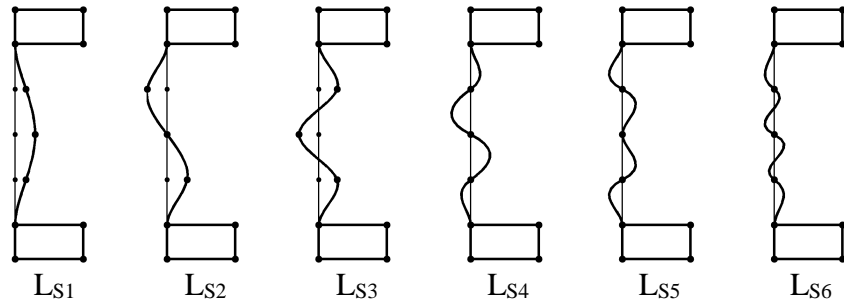
**Figure 3.17:** Native base system for the  $L_P$  space



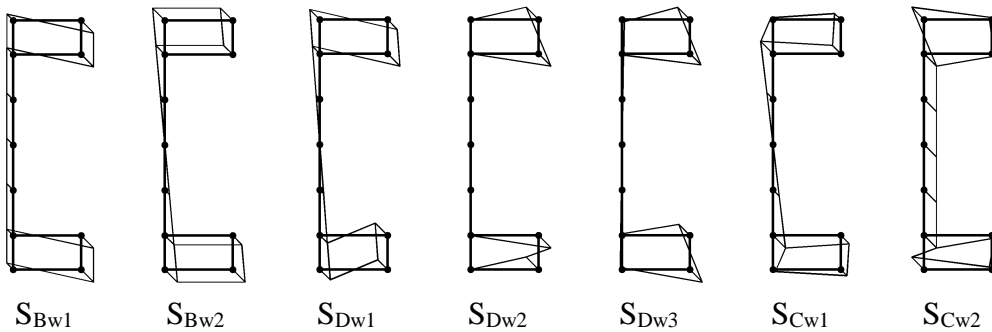
**Figure 3.18:** Cross-section orthogonal base system for the  $L_P$  space



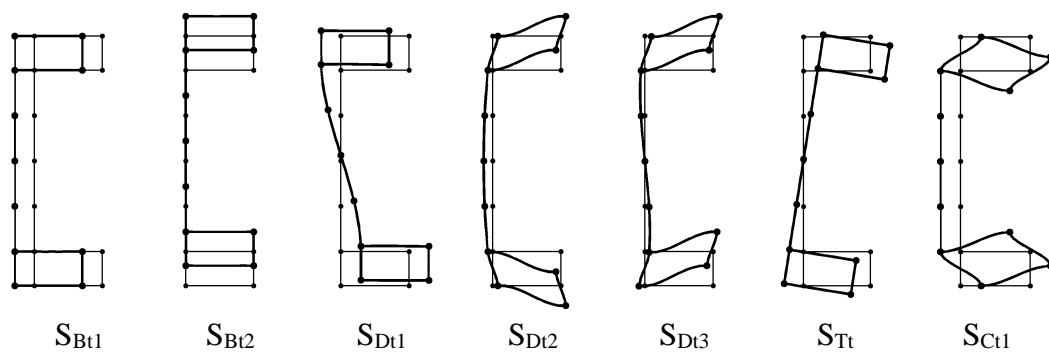
**Figure 3.19:** Native base system for the  $L_S$  space



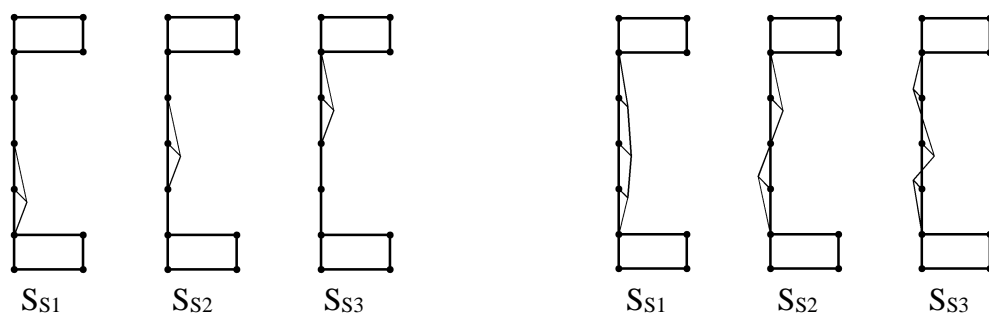
**Figure 3.20:** Cross-section orthogonal base system for the  $L_S$  space



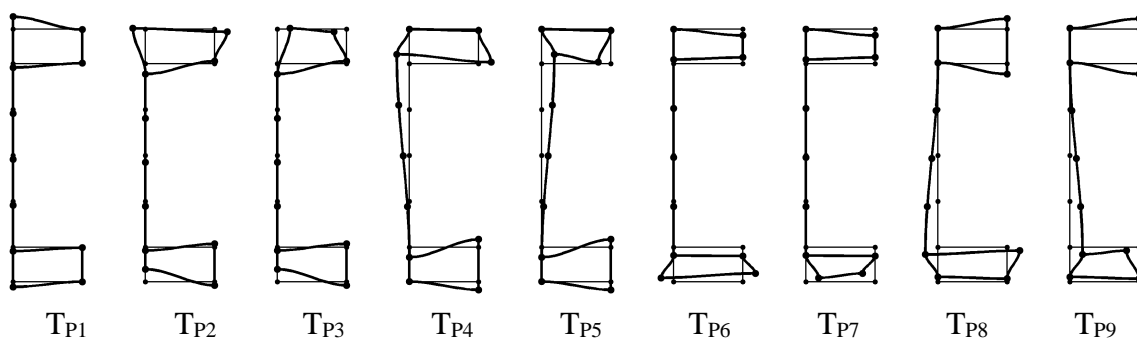
**Figure 3.21:** Cross-section orthogonal base system for the  $S_{Pw}$  space



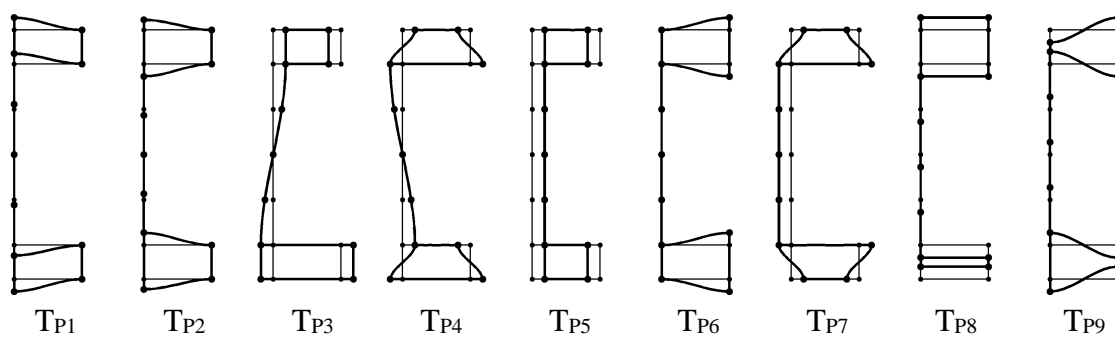
**Figure 3.22:** Cross-section orthogonal base system for the  $S_{Pt}$  space



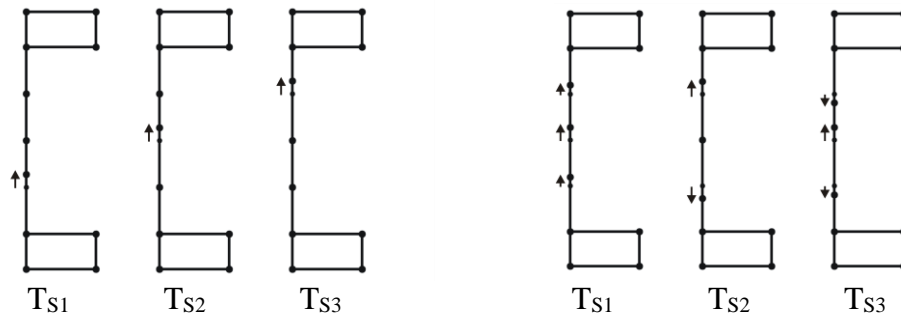
**Figure 3.23:** Native (left) and cross-section orthogonal (right) base system for the  $S_s$  space



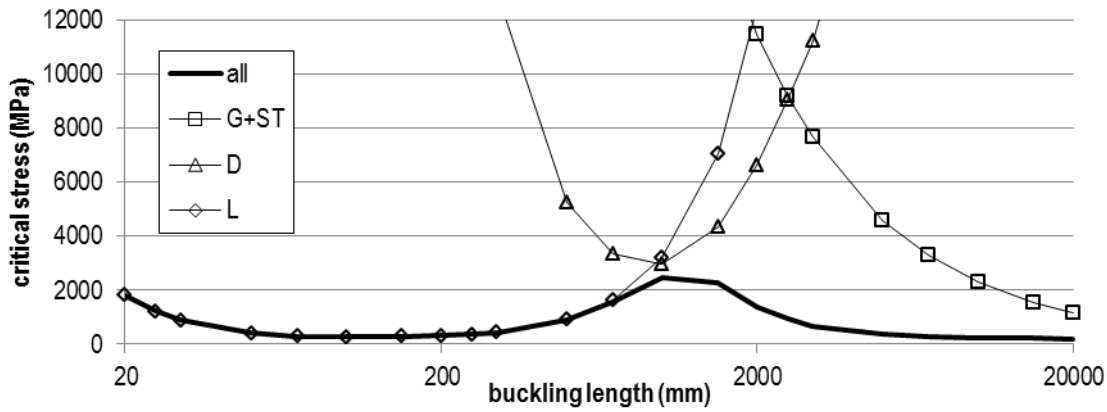
**Figure 3.24:** Native base system for the  $T_P$  space



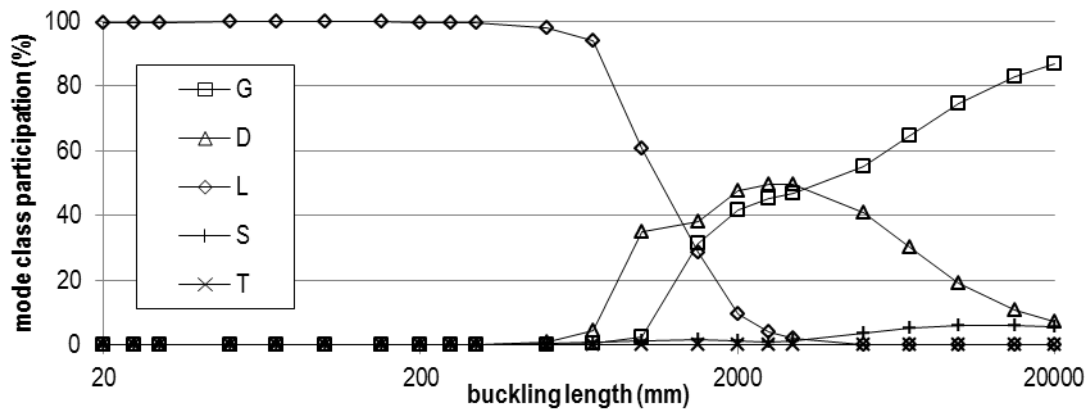
**Figure 3.25:** Cross-section orthogonal base system for the  $T_P$  space



**Figure 3.26:** Native (left) and cross-section orthogonal (right) base system for the  $T_s$  space



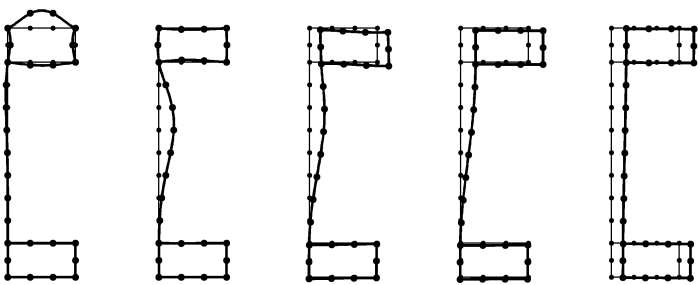
**Figure 3.27:** All-mode and pure-mode critical stresses for the hollow-flange U-beam



**Figure 3.28:** Mode participations in all-mode solution for the hollow-flange U-beam

### 3.6 Summary and continuation of the work

In this Chapter a generalized cFSM has been presented. The generalized cFSM has extended capabilities, the most important one is that it handles arbitrary flat-walled cross-sections. Moreover, various (series) longitudinal functions are considered, new, practically meaningful subspaces are introduced, and cross-section orthogonal base systems are proposed. (See Thesis #2 in Chapter 6.)

buckled shape					
length (mm)	100	300	1500	2500	15000
G %	0.0	0.0	31.4	45.2	82.8
D %	0.1	0.2	38.2	49.8	11.0
L %	99.7	99.4	28.7	4.1	0.0
S %	0.2	0.4	1.6	1.0	6.2
T %	0.0	0.0	0.0	0.0	0.0

**Figure 3.29:** Buckled shape samples and mode participations in all-mode solution of the hollow-flange U-beam

The generalized cFSM method has been implemented into a new version of CUFSM software. (Unfortunately, at the moment, the new version of CUFSM is not publicly available.)

The practical usefulness of the generalized cFSM is obvious: not only cold-rolled members, but members with closed part(s) can be handled, such as aluminium or plastic extrusions, welded steel members, etc. Moreover, the “too” simple cross-sections (like L, T or X) are properly handled (unlike in the original cFSM).

There are still two basic limitations of the method. One is the set of limitations caused by the FSM itself. In order to remove these limitations, the constraining technique should be applied within the context of finite element method. This would further (significantly) generalize the method, by allowing the analysis of thin-walled members with intermediate supports, members with (certain) cross-section changes, members with holes/perforations, etc. In fact, this work has already started by the Author, the first results have already been published [9/3-17/3].

The other basic limitation of the cFSM method is that it requires flat-walled member (model). This limitation is caused by the currently used definition of local and distortional modes, therefore, this limitation is shared by GBT, too. Though the handling of members with small curved parts (e.g., cold-formed members with rounded corners) is solved as far as practical design is concerned (see e.g. [26/2-33/2], it remains an interesting topic for further (theoretical) research how the modal decomposition methods can be extended for members with curved cross-sections.

It is also to mention that generalization is possible even within the context of semi-analytical FSM, by considering more general loading and more second-order terms in the stability analysis. Such version of cFSM has very lately been developed by Rendall and colleagues [18/3-21/3].

## 4 Mode identification of deformations calculated by shell finite element analysis

### 4.1 Introduction

#### 4.1.1 General

The cFSM method (as presented in the previous Chapters) successfully solves two basic tasks: pure buckling mode calculation and modal identification. Since the method is based on the finite strip method, it can handle only those problems which are within the realm of FSM. Since there is practical need to analyse more general cases, there has been research effort to push the limits of cFSM and to analyse members that cannot directly be handled by cFSM.

Based on cFSM, Casafont (and his colleagues) showed how the mechanical constraints used in cFSM can partially be implemented into a commercial finite element software package (see [23/2-25/2]) and how the member can be enforced to deform in accordance with the mechanical criteria of a given mode space. Incidentally, they have analysed perforated members, and successfully calculated arbitrary pure or coupled buckling modes to such members (which otherwise cannot be analysed by FSM). However, since in their method the mechanical criteria are satisfied only approximately (i.e., not for the whole displacement field but only at sufficiently large number of locations), their method is not able to make a base transformation, therefore, modal identification is not possible.

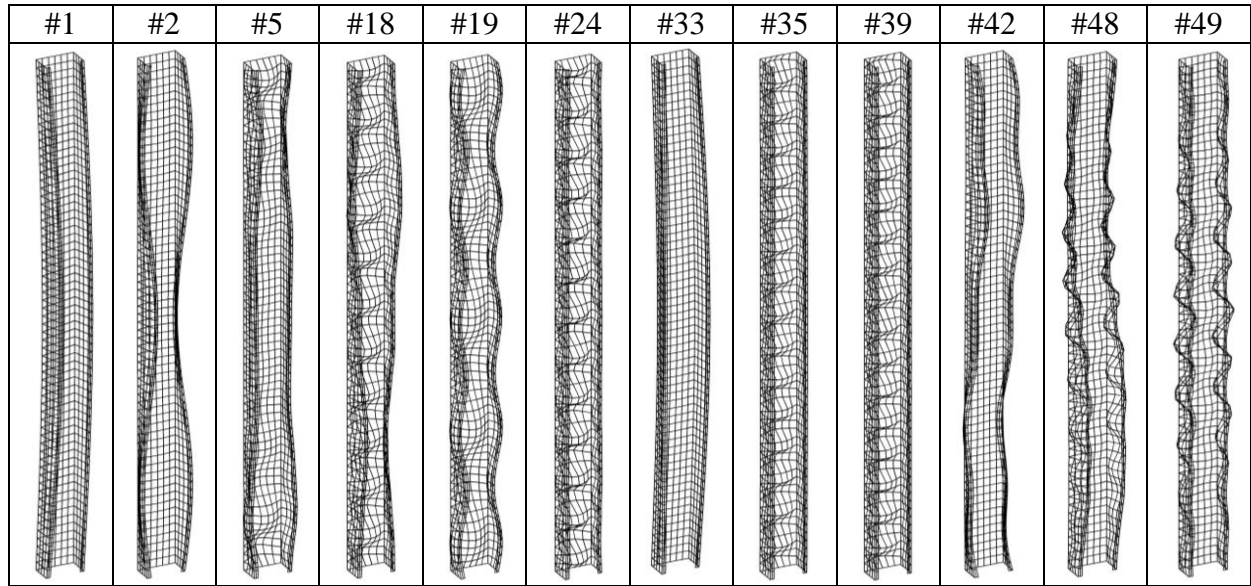
At the same time approximate modal identification of deformations calculated by FEM analysis has also been proposed by the Author (later applied and extended by others). The method, originally presented in [1/4-2/4], employs the base functions of cFSM to approximate the FEM-calculated deformations. The derivations are presented in Section 4.2. In Section 4.3 the concept is proved by numerical studies. Since the proposed method is relatively time-consuming, enhancement of the method has also been proposed, see Section 4.4.

#### 4.1.2 Problem statement

Design specifications – in many cases – require the knowledge of critical load for the characteristic buckling types. If a problem does not fit to CUFSM or GBTUL, calculation of pure buckling mode is problematic or impossible. In such cases (e.g., a cold-formed purlin elastically supported at certain intervals and subjected to some transverse distributed loading) it is still possible to perform a shell FEM analysis, but the calculated buckling shapes must somehow be identified so that critical load factors associated with the desired modes could be (at least approximately) determined.

Since a typical shell FEM model requires thousands of degrees of freedom, thousands of candidate buckling shapes can be calculated. Even if only those with the lowest critical load factors are considered, it is not unusual that a couple of dozens of shapes must be identified. Without some mathematical method, the identification is fairly subjective, since the practical experience is that FEM-calculated buckled shapes rarely look like pure buckled shapes. This is illustrated in **Figure 4.1**, where some buckled shapes are shown, calculated by shell FEM analysis for a C section column member. Some of the modes can easily be identified (e.g., #1, #2, #24, #33), while other modes are problematic (e.g., #5, #18, #42, #48). However, by using the cFSM base functions, a simple mathematical (i.e., objective) identification method can be established.





**Figure 4.1:** FEM-calculated buckling modes

## 4.2 Approximation of FEM displacements

A FEM displacement function is intended to be approximated by the linear combination of cFSM base functions. The base functions are expressed by base vectors and thus the minimization precedes on the error vector (instead of error *function*). The solution is presented in [1/4-2/4], and can be summarized as follows.

To have the best approximation, the norm of the  $\mathbf{d}_{\text{err}}$  error vector is minimized:

$$\min(\mathbf{d}_{\text{err}}^T \mathbf{d}_{\text{err}}) \quad (4.1)$$

Considering that the error can be expressed as the difference between the finite element displacement vector ( $\mathbf{d}_{\text{FE}}$ ) and its approximation, i.e., the  $\Phi \mathbf{c}$  linear combination of the cFSM base vectors, Eq. (4.1) can be written as:

$$\min((\mathbf{d}_{\text{FE}} - \Phi \mathbf{c})^T (\mathbf{d}_{\text{FE}} - \Phi \mathbf{c})) \quad (4.2)$$

where  $\Phi$  is the matrix with the FSM base vectors and  $\mathbf{c}$  is the vector of unknown combination factors (i.e.,  $\mathbf{c}$  is the modal identification answer that we seek). Expanding Eq. (4.2), then simplifying, the function to be minimized can be expressed as:

$$\min(\mathbf{d}_{\text{FE}}^T \mathbf{d}_{\text{FE}} - 2\Phi^T \mathbf{d}_{\text{FE}} \mathbf{c} + \mathbf{c}^T \Phi^T \Phi \mathbf{c}) = \min(f(\mathbf{c})) \quad (4.3)$$

Minimization finally leads to a linear system of equations to be solved for  $\mathbf{c}$ :

$$\frac{\partial f(\mathbf{c})}{\partial \mathbf{c}} = 0 \quad \rightarrow \quad \Phi^T \Phi \mathbf{c} = \Phi^T \mathbf{d}_{\text{FE}} \quad (4.4)$$

After calculating the combination factors,  $p_i$  participation of an individual buckling mode (or base function) can be calculated as follows:

$$p_i = |c_i| / \sum_{\text{all}} |c_i| \quad (4.5)$$

where  $c_i$  is an element of the  $\mathbf{c}$  vector.

The  $p_M$  participation of a class  $M$  can be calculated as follows:

$$p_M = \frac{\sum_M |c_i|}{\sum_{\text{all}} |c_i|} \quad (4.6)$$

where  $M$  denotes that summation should be over all elements of a given mode class.

Once the FEM displacement function is expressed by the cFSM base functions, the error of the approximation can conveniently be measured as the norm of the error vector relative to the norm of the displacement vector:

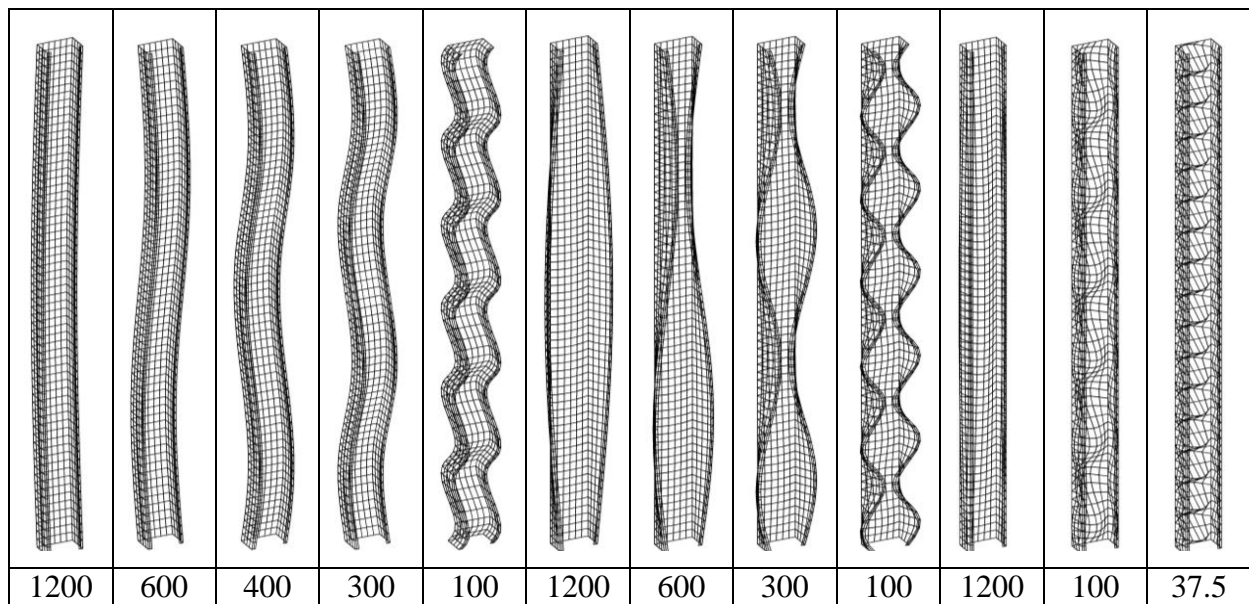
$$\text{error} = \sqrt{\mathbf{d}_{\text{err}}^T \mathbf{d}_{\text{err}}} / \sqrt{\mathbf{d}_{\text{FE}}^T \mathbf{d}_{\text{FE}}} \quad (4.7)$$

### 4.3 Proof-of-concept example

To illustrate the application and capabilities of the proposed identification method, a parametric study is completed on a symmetric lipped channel (C-shape) column. The column length is 1200 mm, with a web height of 100 mm, flange width of 60 mm, lip lengths of 10 mm, and thickness of 2 mm. Note, the dimensions are for the mid-line, and sharp corners are employed. Steel material is assumed with a Young's modulus of 210 000 MPa and Poisson's ratio of 0.3. Various model parameters are examined, including FEM mesh density, number of cFSM base functions, support conditions, and type of loading (i.e., column or beam).

The FEM calculations are conducted in ANSYS [8/1], using 4-node, 24-DOF shell elements (SHELL63 in ANSYS terminology) in a highly regular rectangular mesh. Both the cross-section discretization and longitudinal element dimension is constant along the member length, and is defined so that the aspect ratio of all the shell elements is close to unity.

The cFSM base functions are characterized by the deformed cross-section shape and by the longitudinal wave-length. Samples of the cFSM base functions are presented in **Figure 4.2**, where the base functions for one global mode (namely: flexural) are shown for various half-wave lengths (namely: for  $m = 1, 2, 3, 4$  and 12), as well as some distortional (for  $m = 1, 2, 4$  and 5) and local (for  $m = 1, 12$  and 32) deformation modes are shown.



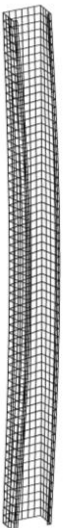
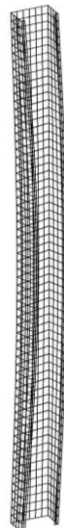
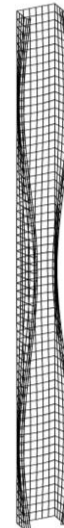
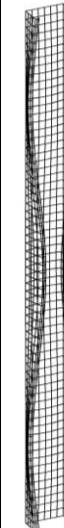



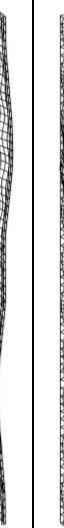




**Figure 4.2:** Selected modes with various wave-lengths (wave-lengths are in mm)

To illustrate the proposed modal identification method, first a simple column problem is solved for the geometric and material data given above. The column is simply supported (i.e., pinned at both ends). The first 50 buckling modes are calculated in ANSYS. This covers those modes where the buckling load is smaller than (approximately) 3 times the minimum (first) buckling load. For each buckling mode the cFSM modal identification approximation as described herein is performed. The accuracy of the cFSM approximation is measured by the error, as defined in Eq. (4.7).

A relatively fine cross-section discretization is used, with 3, 5 and 1 sub-nodes in the flanges, web and flange lips, respectively. Thus, the total number of nodes within a cross-section is 19. In the finite element analysis the member is divided into 64 elements in the longitudinal direction, therefore the total number of FE nodes is 1235, while the total number of displacement degrees of freedom (DOF) is 7410.

The cross-section discretization of the cFSM base functions is identical to that of the FE model, while the  $m$  number of longitudinal half-waves is from 1 to 32, thus, a maximum of 32 half-waves are considered along the member length. Note, even though the cross-section discretizations in cFSM and FEM are identical, this does not mean identical DOF, since FSM nodal lines have only 4 displacement DOF. In the actual example 19 FSM nodal lines implies 76 FSM DOF for a given  $m$  half-wave number, thus, the total number of the considered cFSM base functions is  $76 \times 32 = 2432$  FSM DOF.

Participation results are presented in **Table 4.1** where the G, D, L and O participations, as well as the calculated error are given for the first 50 buckling modes of a pinned-pinned column problem. Deformed shapes for selected cases are presented in **Figure 4.3**: both FEM solutions ( $\mathbf{d}_{FE}$ ) and their cFSM approximations ( $\Phi_{\mathbf{c}}$ ) are shown.

mode 1		mode 2		mode 24		mode 18		mode 48		mode 5	
											
$\Phi_{\mathbf{c}}$	$\mathbf{d}_{FE}$	$\Phi_{\mathbf{c}}$	$\mathbf{d}_{FE}$	$\Phi_{\mathbf{c}}$	$\mathbf{d}_{FE}$	$\Phi_{\mathbf{c}}$	$\mathbf{d}_{FE}$	$\Phi_{\mathbf{c}}$	$\mathbf{d}_{FE}$	$\Phi_{\mathbf{c}}$	$\mathbf{d}_{FE}$

**Figure 4.3:** cFSM approximation ( $\Phi_{\mathbf{c}}$ ) of FE eigen-modes ( $\mathbf{d}_{FE}$ ) for columns with FSM-like end restraints

**Table 4.1:** GDLO participations for the first 50 buckling modes of the illustrative example

mode	G	D	L	O	error	mode	G	D	L	O	error
nr	%	%	%	%	%	nr	%	%	%	%	%
1	85.9	5.5	0.2	8.4	0.0	26	8.0	81.3	5.2	5.5	0.1
2	1.0	91.3	4.7	3.0	0.0	27	0.3	11.2	86.7	1.8	0.9
3	0.9	83.7	11.0	4.4	0.0	28	10.8	83.2	2.5	3.5	0.0
4	0.5	37.6	58.2	3.8	0.1	29	1.5	5.1	91.6	1.8	1.4
5	0.5	37.7	58.9	2.9	0.1	30	0.2	8.5	89.6	1.7	1.4
6	0.5	72.3	21.3	5.9	0.0	31	3.8	4.3	89.9	2.0	2.5
7	0.6	30.3	66.4	2.7	0.1	32	0.2	13.9	84.1	1.9	2.5
8	0.3	24.0	72.5	3.1	0.1	33	70.8	19.3	1.3	8.6	0.0
9	0.3	13.5	83.8	2.4	0.1	34	10.1	75.3	8.3	6.3	0.1
10	0.5	23.5	73.2	2.8	0.1	35	13.7	5.6	77.8	2.9	5.2
11	0.6	29.0	67.8	2.6	0.1	36	0.5	69.8	25.1	4.6	0.2
12	0.4	15.5	81.2	2.9	0.1	37	3.1	74.2	14.6	8.0	0.0
13	0.2	8.5	88.8	2.5	0.1	38	0.2	28.2	68.9	2.7	5.0
14	0.3	18.4	79.0	2.3	0.2	39	15.8	9.6	69.7	4.9	99.6
15	0.8	41.6	53.7	3.9	0.1	40	0.3	23.9	71.7	4.1	99.6
16	0.4	11.1	86.1	2.3	0.3	41	15.2	9.4	70.3	5.1	99.9
17	1.3	82.0	13.1	3.5	0.0	42	15.3	69.6	9.1	6.0	0.1
18	0.7	39.4	57.5	2.4	0.3	43	0.7	21.7	71.9	5.6	99.9
19	0.6	26.3	68.6	4.5	0.0	44	14.5	10.8	70.2	4.5	99.9
20	0.6	19.4	76.9	3.2	0.5	45	1.5	34.6	57.1	6.8	1.7
21	1.2	68.9	26.3	3.5	0.0	46	4.2	26.8	63.9	5.2	2.4
22	0.7	50.2	42.8	6.3	0.0	47	1.9	42.3	48.4	7.5	0.7
23	0.2	14.7	82.9	2.2	0.5	48	9.8	46.0	39.2	5.0	0.3
24	0.8	7.6	89.6	2.0	0.8	49	0.6	14.5	79.6	5.3	0.6
25	4.4	83.9	5.8	5.8	0.0	50	7.9	39.8	47.3	5.1	0.4

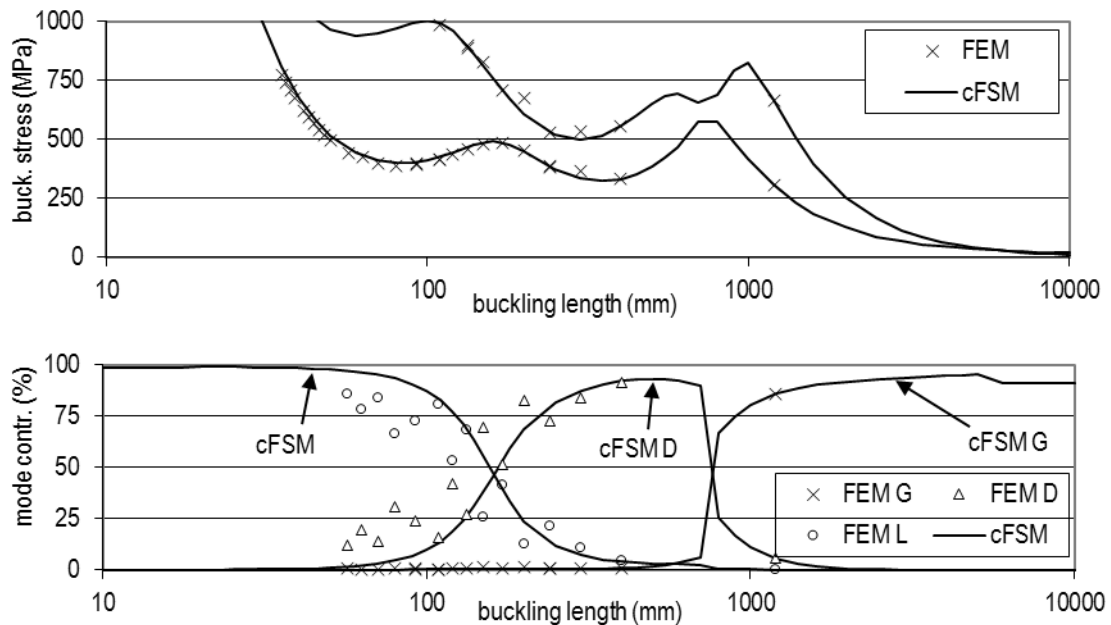
For most of the modes the cFSM approximation is excellent, as both the deformed shapes of **Figure 4.3** and small error in **Table 4.1** indicates. More exactly, in 45 buckling modes out of the considered 50 the cFSM approximation of the FEM buckling modes are practically accurate, and there are only 5 buckling modes where the method failed to yield realistic approximations. Careful examination of the 5 buckling modes with significant identification error shows that all involve more than 32 small buckling half-waves, which fully explains the failure of the cFSM approximation, since the maximum number of half-waves applied is 32. (Obviously, by increasing the number of half-waves in the cFSM functions the erroneous cases could be reduced.)

The GDLO participations of **Table 4.1** are in accordance with engineering expectations. For example, mode #1 is clearly global (flexural-torsional), #2 is dominantly distortional, #24 is local. In most of the cases various modes are coupled, sometimes with similar wave-lengths (e.g., D+L #19, G+D #33), but just as often with different wave-lengths (see e.g., G+D #42, G+L #35, D+L #18, G+D+L #48). The proposed mode identification method successfully handles cases where deformations are more-or-less localized, see e.g., #5.

Furthermore, a reasonable agreement is experienced when comparing the provided GDLO participations to those calculated by the cFSM solution itself (as implemented in CUFSM

[17/1]). This is demonstrated in **Figure 4.4** where the proposed approximate identification of the FE solutions are compared with the cFSM solutions. A buckling half-wavelength is manually assigned to most of the 50 modes: for some modes e.g., #1, #2, #19, #24 o #33 this is readily apparent, for other modes, e.g., #5, more judgment is required and in some cases no single half-wavelength can be assigned, see e.g. #18, #35, #42, #48. Buckling stresses and dominant half-wavelengths predicted by the FE and the FSM models are nearly identical, see **Figure 4.4** (top). Modal participation (**Figure 4.4**, bottom) highlights some of the additional information contained in the FE models. In the FSM model only one buckling mode can exist at a given half-wavelength, but FE models may have different half-wavelengths superposed, thus the modal participation shows some scatter about the traditional cFSM predictions.

Based on the presented calculations it may be concluded that the proposed modal identification method is a viable identification technique for the considered pinned-pinned column problem if the minimal half-wave length of the cFSM base functions is selected so that it would be smaller than the minimal buckling length of the buckling mode desired to identify.



**Figure 4.4:** Comparison of (a) buckling stress and (b) mode participation as a function of half-wavelength

## 4.4 Approximation with reduced number of cFSM base functions

The numerical studies presented above prove the applicability of the proposed buckling mode identification method. It is also suggested, however, that a relatively fine FEM discretization is necessary if various buckling modes are to be identified, including ones with small buckling lengths. Since the number of cFSM base functions is tied to the FEM mesh, a fine mesh requires a significant number of cFSM base functions, which ultimately results in fairly significant computational effort. This is clearly unfavourable. At the same time, by looking at the details of the participation calculations, one can immediately observe that many of the applied cFSM base functions have negligible contribution in any buckling mode of practical interest, which suggests that by carefully applying a selected subset of cFSM base functions the computational effort might be significantly reduced without deteriorating the results.

Two options for reducing the number of cFSM base functions have been tested: (i) ‘manual’ or user selection of a subset of the cFSM base functions, and (ii) ‘automatic’ selection of the base functions based on the eigen-value associated with Eq. (2.7). In the ‘manual’ method those cFSM functions that likely have minor importance are disregarded. Namely: higher cross-sectional L modes are disregarded, since these L modes involve smaller transverse waves, which are practically irrelevant in normal conditions. O modes rarely have high participations and therefore all O modes are disregarded. In the example this reduces the number of cross-section deformation modes to 10 (in case of a C section), independent of the cross-section discretization, thus, the total number of cFSM base functions is equal to  $10m_{max}$  where  $m_{max}$  is the number of various longitudinal half-waves.

The ‘automatic’ method utilizes the fact that cFSM base functions themselves are eigen-functions, i.e., buckling modes of a column problem. Those base functions corresponding to eigen-values larger than  $r$  times the minimal eigen-value are disregarded. Thus, the only necessary parameter is  $r$ . Note, this option influences both the cross-section deformation modes and the longitudinal wave-lengths, by filtering out base functions with important cross-section deformations but with unrealistic longitudinal wave-lengths (e.g., G modes with many small longitudinal waves, or L modes with very long half-waves, etc.).

**Table 4.2:** Change of GDLO participations and errors for the first 30 buckling modes of the beam problem with reduced number of cFSM functions:  
‘manual’ reduction on the left, ‘automatic’ reduction on the right

mode	$\Delta G$	$\Delta D$	$\Delta L$	$\Delta O$	$\Delta$ -error	mode	$\Delta G$	$\Delta D$	$\Delta L$	$\Delta O$	$\Delta$ -error
nr	%	%	%	%	%	nr	%	%	%	%	%
min	0.4	0.0	-0.7	-8.2	0.1	min	-4.1	-3.4	-1.6	-5.0	0.3
max	7.6	7.9	0.1	-3.3	1.4	max	5.5	3.9	4.1	4.5	3.4
average	0.9	4.9	-0.3	-5.5	0.7	average	-0.5	1.7	0.4	-1.6	1.1

The GDLO participations have been calculated for the column problem of the previous Section with a reduced number of cFSM base functions. For the ‘manual’ reduction all G and D modes and the first 4 L modes have been considered (remaining L and O modes are disregarded). This reduces the number of cFSM base functions to 320 (instead of the original 2432), with  $m_{max}=32$ . In case of the ‘automatic’ reduction  $r=30$  has been used, which yields to similar (but slightly smaller) number of base functions, namely: 283, while keeping some or all of the cross-section modes from all four buckling classes (thus, some O modes, too). The results are summarized in **Table 4.2** (for the first 30 FE buckling modes), where the *change* of the participations and errors are given with respect to the results obtained with all the cFSM base functions, see **Table 4.1**. The minimum, maximum and average changes are given.

Both reduction methods work reasonably. There are no significant changes in the results: the increased error is typically negligible, and the GDLO participations are essentially unchanged. The most important change is that in case of the ‘manual’ option the O contributions disappear and they are added primarily to G or D contributions (whichever is more dominant). A properly selected subset of cFSM base functions can significantly decrease the problem size and therefore significantly decrease computation time. It might be interesting to mention that in case of the specific example the computation time on an ordinary PC (circa 2009) could be as long as 1 hour if all 2432 cFSM base functions are considered, but dropped to less than a minute if a reduced subset with 300 functions are used (using MatLab).

As far as the difference between the ‘manual’ or ‘automatic’ reduction is concerned, both options are effective and applicable. Still, the ‘automatic’ option seems to be advantageous since (i) it requires less judgment and input from the user, (ii) it might lead to more accurate participation results, (iii) it is easy to control the size of the problem and/or the accuracy of the results, and (iv) it yields a smaller number of cFSM base functions (compared to the ‘manual’ option and assuming approx. the same accuracy of the results, which should become more evident for longer members.)

## 4.5 Summary and continuation of the work

In this Chapter the method developed for the identification of FEM-calculated deformation modes has been presented. The method employs the cFSM base functions, the linear combination of which is used to approximate the deformations. Since in the cFSM base functions the various mode classes are separated, the separation can readily be done for the linear combination, too, which directly leads to the contribution of each mode class to the analysed displacement field. The method is illustrated for the identification of buckling modes of pinned-pinned columns. A way to reduce the number of employed cFSM base functions is also proposed and illustrated. (Thesis #3 is based on these results, see Chapter 6.)

The proposed identification method induced some further research work. First, the method has been tested for other end restraints [3/4-4/4], and it was concluded that the simple sinusoidal cFSM base functions can be applied to other-than-pinned end restraints, too, provided the transverse translational displacements are restrained.

Furthermore, Joó (with the contribution of the Author) applied the method for beam problems, including Z-shaped members with intermediate elastic restraints (as in case of e.g., purlins with trapezoidal sheeting). It was also demonstrated how the identification method can be used in design calculations, see [5/4].

Li and Schafer further extended the method. First, they investigated how other FSM longitudinal shape functions can be utilized to handle various end restraints. Finally, they proposed a so-called generalized set of cFSM base functions which was proved to be applicable to members with arbitrary end restraints. Later they also applied the identification method for deformations obtained from (geometrically and materially) nonlinear finite element analysis [6/4-8/4]. This work has been continued till lately by Li [9/4]

It is also to mention that Nedelcu has been proposed a similar mode identification method, but with using base functions distilled from GBT, see [10/4-12/4].

## 5 Analytical formulae for global buckling

### 5.1 Introduction

#### 5.1.1 General

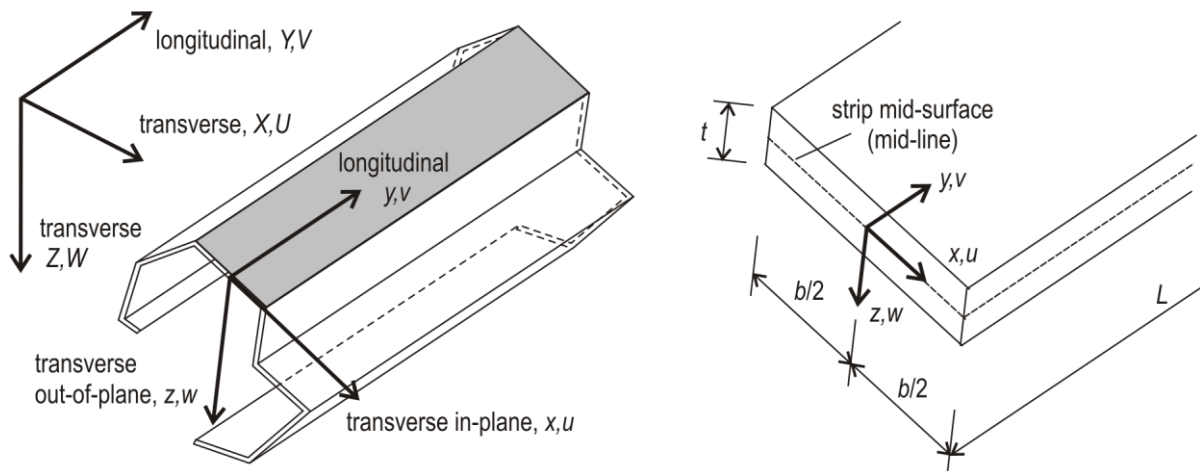
The birth of cFSM made it possible, and CUFSM software made it very easy to calculate critical loads for classical global buckling (e.g., flexural buckling) and compare the results to classical analytical solutions (e.g., Euler formula in case of flexural buckling). The comparison revealed some differences, the two most important ones being that (i) cFSM global buckling critical forces were a few percent higher than those from classical analytical solutions, and (ii) cFSM global buckling critical forces typically (but not always) were found to tend to a finite value as the member length approaches zero while analytical solutions predict infinitely large critical values for extremely small length.

In order to provide explanation for the experienced differences, research work started aiming to derive alternative analytical formulae for global buckling. The alternative derivations imitate the cFSM assumptions and will be referred as formulae based on *shell model*, while the classical analytical formulae will be referred here as ones based on *beam model*. Note, the term *beam* is used to describe a model where the beam or column member is modelled by a one-dimensional element, that is line, to which cross-section properties are assigned. On the other hand, the term *shell* is used to describe a model where two-dimensional elements are used, in this specific case flat strips, and both in-plane (membrane) strains/stresses and out-of-plane displacements (i.e., bending strains/stresses) are considered.

First, in Section 5.1.2, the initial assumptions are summarized, while Sections 5.2 and 5.3 presents the main steps and most important results of the derivations with neglecting or considering in-plane shear deformations, respectively, based on [1/5-5/5]. Demonstrative numerical examples are also provided.

#### 5.1.2 Initial assumptions

An illustration of the member as well as the applied global ( $X,Y,Z$ ) and local ( $x,y,z$ ) coordinate systems are presented in **Figure 5.1**.



**Figure 5.1:** Coordinate-systems, basic terminology



The applied basic mechanical assumptions intend to imitate those of a FSM or shell FEM solution. More exactly, the assumption system closely follows that of the semi-analytical FSM, as implemented in CUFSM, see [16/1-18/1].

For the analysed member it is assumed that: (i) the analysed member is a column, (ii) the column is prismatic, (iii) the column is supported by two hinges at its ends, (iv) the column is loaded by a compressive force (uniformly distributed along the cross-section), (v) its material is linearly elastic, and (vi) it is free from imperfections (residual stresses, initial deformations, material inhomogeneities, etc.).

As far as boundary support conditions are concerned, the applied longitudinal shape functions correspond to ‘globally and locally pinned’ and ‘free to warp’ support conditions. More precisely, for both column ends: (i) local transverse translations (i.e., in the  $x$  and  $z$  direction) are restrained, which also means that global transverse translations (i.e., in the  $X$  and  $Z$  direction) are restrained, (ii) translations in the  $y$  or  $Y$  direction can freely occur, i.e., the cross-section warping is allowed, (iii) local twisting rotations of the strips are restrained, which also means that global twisting of the cross-section is restrained, (iv) and finally local rotations about the strips’ local  $x$ -axis can freely occur, as well as global rotations about global  $X$  and  $Z$  axis can freely take place.

For the member deformation and displacements we assume that (i) the member is modelled by 2D surface elements, i.e., *strips*, (ii) in-plane (membrane) and out-of-plane (plate bending) deformations are allowed, (iii) for the in-plane behaviour a classical 2D stress state is considered, (iv) for the out-of-plane behaviour a classical Kirchhoff plate is considered, and (v) displacements are constrained to global buckling mode.

For the derivations the energy method is used. The total potential of the member is expressed, and critical force is searched by utilizing that in equilibrium the total potential is stationary.

## 5.2 Global buckling without in-plane shear

### 5.2.1 Definition for global buckling

Classical solutions for stability problems of beams or columns are based on beam models. This means that the assumed displacements are assigned to cross-sections along the axis of the member. It is to highlight that this does not mean rigid cross-sections with zero deformations, but it does mean that cross-sectional deformations are assumed to be small, therefore, a priori assumed to be negligible. (Note, longitudinal stresses are necessarily associated with transverse strains due to Poisson effect, and transverse strains lead to cross-section deformations: first of all width-change of the strips, but, if multiple strips are connected to each other, width changes usually induce flexural deformations, too.)

When the member is handled as a set of connecting plate elements (such as strips in FSM or shell elements in FEM applications), exact imitation of beam theory assumptions is generally not possible, since in case of an arbitrary cross-section shape, it is practically impossible to find boundary conditions which enforce the reference line (i.e., line defined by cross-section mass centres) to deform (i.e., buckle) exactly as in beam theory solutions, but otherwise allow all the other DOF free.

The conclusion is that the global buckling definition embedded in beam model solutions cannot be directly applied in shell model solutions, therefore an appropriate definition for

global buckling is necessary. Here, probably the simplest practically applicable definition is proposed and will be used, namely: *global buckling is a buckling mode when all the possible cross-section deformations are excluded*. In other words, cross-section deformations are restricted to such an extent which is *possible* with the assumed DOF, while all the other cross-section deformations are assumed to be negligibly small. In case of shell model, this means that a buckling mode is global if the relative positions of any cross-section nodes do not change during the deformations.

Classical solutions for buckling of columns (or beams) are based on Euler-Bernoulli-Navier beam model theory. There are two important assumptions: (i) the *cross-section planes remain planes* and (ii) *normals to the undeformed middle line remain normal during the deformations*. When it is intended to apply for thin-walled members, this definition can directly be applied if the member has axial and/or flexural deformations. However, if the member has torsional deformations, too, the above definitions need to be generalized. The following generalization is applied here: the two basic assumptions must be satisfied by each plate element of the thin-walled member. (For the sake of mathematical precision, in this case there is an almost trivial further assumption, namely: the axial displacements must be continuous along the cross-section line.) In Section 5.2 these assumptions of the Euler-Bernoulli-Navier hypotheses are assumed to be valid (whilst the effect of the elimination of the second part of the hypothesis is discussed in Section 5.3).

It is to mention that this global buckling definition is exactly identical to that used in the derivations of the constrained finite strip method (cFSM), see Chapter 2 and 3.

## 5.2.2 Overview of derivations

In classical column buckling solutions that are based on beam model, three displacement degrees of freedom are considered (transverse translations and rotation about the longitudinal axis), as a direct consequence of (i) not considering cross-section deformations and (ii) assuming longitudinal displacement distribution in a predefined form (e.g., sinusoidal form in case of flexural buckling of a pinned-pinned column).

To define global DOF for a shell model, the same logic is followed. The applied assumptions are as follows: (i) there is no deformation of the cross-section mid-line in accordance with the applied definition for global buckling, (ii) through-thickness deformations are disregarded, (again, in accordance with global buckling definition), (iii) longitudinal shape functions are assumed in a pre-defined form, which form is defined by the boundary conditions and the differential equations of the flat plate elements.

These assumptions finally exclude all but 4 modes of displacements: transverse translations ( $U$  and  $W$ ), longitudinal translation ( $V$ ), and rotation about the longitudinal axis ( $\Theta$ ). All these displacements requires a certain reference point to which they are assigned: the *mass centre* for the translational DOF, while the *shear centre* of the cross-section for the rotation.

The global displacement functions can be expressed as follows:

$$U = U_0 \sin \frac{m\pi y}{L} = U_0 \sin(k_m y) \quad (5.1)$$

$$W = W_0 \sin \frac{m\pi y}{L} = W_0 \sin(k_m y) \quad (5.2)$$

$$\Theta = \Theta_0 \sin \frac{m\pi y}{L} = \Theta_0 \sin(k_m y) \quad (5.3)$$

$$V = V_0 \cos \frac{m\pi y}{L} = V_0 \cos(k_m y) \quad (5.4)$$

where  $L$  is the member length,  $m$  is the number of considered half-waves, and the subscript '0' denotes the amplitude of the displacement component. The details of the derivations are given in Appendix C. The main steps are summarized here.

- Starting from the above global displacement functions, first the displacement amplitudes of the mid-points of each strip are expressed ( $u_{m0,i}$ ,  $v_{m0,i}$ ,  $w_{m0,i}$  and  $\theta_{m0,i}$ ).
- From the strips' mid-point displacements the whole displacement field of the strips can be constructed, i.e.,  $u(x,y,z)$ ,  $v(x,y,z)$ ,  $w(x,y,z)$ .
- By derivations, first and second-order strains can be determined.
- From the first-order strains stresses can be calculated by applying generalized Hooke's law.
- The internal potential, i.e., strain energy can be determined by using (first-order) stresses and strains and by integrating the elementary strain energy for the whole volume of each strip.
- The external potential, i.e. the negative of the work done by the external loading can be determined by using the second-order strains and by integrating the elementary work for the whole volume of each strip.

As soon as the total potential is expressed by the four displacement parameters ( $U_0$ ,  $V_0$ ,  $W_0$  and  $\Theta_0$ ) the critical forces can be determined, utilizing that in equilibrium the total potential energy is stationary. A set of 4 (linear) equations can be established for the 4 displacement parameters of the problem as follows:

$$\frac{\partial \Pi}{\partial V_0} = 0 \quad \frac{\partial \Pi}{\partial U_0} = 0 \quad \frac{\partial \Pi}{\partial W_0} = 0 \quad \frac{\partial \Pi}{\partial \Theta_0} = 0 \quad \rightarrow \quad \begin{bmatrix} C_{11} & 0 & 0 & 0 \\ 0 & C_{22} & C_{23} & C_{24} \\ 0 & C_{32} & C_{33} & C_{34} \\ 0 & C_{42} & C_{43} & C_{44} \end{bmatrix} \begin{bmatrix} V_0 \\ U_0 \\ W_0 \\ \Theta_0 \end{bmatrix} = \begin{bmatrix} 0 \\ 0 \\ 0 \\ 0 \end{bmatrix} \quad (5.5)$$

Note, the coefficient matrix is symmetric,  $C_{12} = C_{13} = C_{14} = 0$  for any option, while the other elements of the coefficient matrix are given in Appendix C.

To have non-trivial solution, the coefficient matrix has to be singular:

$$\det(\mathbf{C}) = 0 \quad (5.6)$$

which leads to the critical values of loads. Since in the first row/column of the  $\mathbf{C}$  matrix non-zero element is only in the main diagonal, the above equation leads to a 3<sup>rd</sup>-order polynomial, plus a 1<sup>st</sup> order equation. In a general case the solution for the 3<sup>rd</sup>-order equation cannot be easily expressed, therefore, general closed-formed solution cannot be given here. Specific cases, however, are discussed in detail in the subsequent Sections.

### 5.2.3 Derivation options

As can be seen above, the total energy of the structure is expressed in the function of the displacements. This total potential energy is the sum of (i) accumulated elastic strain energy, (i.e. internal energy) and (ii) potential energy of the external loads (i.e., external energy).

As far as the potential energy of the external loading is concerned, for conservative loads, it is the negative of the work done by the loads as the structure deforms. When calculating this work, in order to have stability solution, the nonlinearity of the strain-displacement relationship must be considered. As usual, second-order approximation is used. Moreover,

considering that (i) the load is applied in the longitudinal direction only, (ii) the transverse strain is excluded by the global buckling definition, and (iii) through-thickness strain is disregarded, it is enough to deal with the  $\varepsilon_y$  longitudinal strain.

Looking at the relevant textbooks, one might conclude that two options are normally used. In classical beam-model-based column buckling solutions the following expression is used for the strain:

$$\varepsilon_y = \frac{\partial v}{\partial y} + \frac{1}{2} \left[ \left( \frac{\partial u}{\partial y} \right)^2 + \left( \frac{\partial w}{\partial y} \right)^2 \right] \quad (5.7)$$

Practically it means that the shortening of the beam due to transverse flexure (in either local  $x$  or  $z$  direction) is considered as second-order effect.

At the other hand, classic textbooks on theory of elasticity or on shell finite elements usually define the  $\varepsilon_y$  strain component as follows (see e.g. [6/5]):

$$\varepsilon_y = \frac{\partial v}{\partial y} + \frac{1}{2} \left[ \left( \frac{\partial u}{\partial y} \right)^2 + \left( \frac{\partial v}{\partial y} \right)^2 + \left( \frac{\partial w}{\partial y} \right)^2 \right] \quad (5.8)$$

Between the two options the  $(\partial v / \partial y)^2$  term makes the difference. It is interesting to note that semi-analytical FSM solutions include this additional term, see e.g., [10/1-11/1, 16/1-18/1]. It would be hard to give any definite statement about shell finite element applications due to their large variety, still, it seems to be fair to assume that mostly if not exclusively they are based on the second, more general formula. It might be interesting to mention that consideration of the  $(\partial v / \partial y)^2$  term is possible in beam finite element applications, too, if geometrically non-linear frame analysis is intended to perform, see e.g., Chapter 9 of [7/5].

For an elementary volume (with  $dA$  area any  $dy$  length) the (second-order) elementary work done by the external loading  $p_y$  (which is a uniformly distributed loading over the cross-section for the investigated case) can be calculated as:

$$dW = p_y dA \cdot \varepsilon_y^{II} dy \quad (5.9)$$

with

$$\varepsilon_y^{II} = \frac{1}{2} \left[ \left( \frac{\partial u}{\partial y} \right)^2 + \left( \frac{\partial w}{\partial y} \right)^2 \right] \text{ or } \varepsilon_y^{II} = \frac{1}{2} \left[ \left( \frac{\partial u}{\partial y} \right)^2 + \left( \frac{\partial v}{\partial y} \right)^2 + \left( \frac{\partial w}{\partial y} \right)^2 \right] \quad (5.10)$$

The total work is simply the integral of the  $dW$  elementary work along the length and over the whole cross-section, which latter integration can conveniently be done strip by strip. However, there are still two further options. In case of integrations over a cross-section (which is a quite frequent engineering task, consider e.g., calculation of practically any cross-section property,) the mathematically precise formula is:

$$W = p_y \sum_{i=1}^n \left[ \int_{-\frac{t_i}{2}}^{+\frac{t_i}{2}} \int_0^L \int_{-\frac{b_i}{2}}^{+\frac{b_i}{2}} (\varepsilon_y^{II}) dx dy dz \right] \quad (5.11)$$

where  $L$  is the member length,  $b_i$  and  $t_i$  is the width and thickness of the  $i$ -th strip, respectively, while  $n$  is the number of strips. In case of thin-walled cross-sections the integration over the thickness is frequently simplified, by neglecting the effect of through-thickness variation of the strain, which yields to a simplified formula:

$$W = p_y \sum_{i=1}^n \left[ t_i \int_0^L \int_{-\frac{b_i}{2}}^{+\frac{b_i}{2}} (\varepsilon_y^{II}) dx dy \right] \quad (5.12)$$

(For example, when second moment of area is calculated, the application of the second expression is equivalent with neglecting the  $b_i t_i^3/12$  terms, which is commonly used for thin-walled cross-sections, see e.g., Annex C of [2/1].

The accumulated elastic strain energy as the member is deformed can be expressed by well-known integral formulae. For the investigated problem, utilizing that  $\varepsilon_x = \kappa_x = \gamma_{xy} = 0$ , the expression is:

$$\Pi_{int} = \frac{1}{2} \sum_{i=1}^n \left[ \int_0^L \int_{-\frac{b_i}{2}}^{+\frac{b_i}{2}} (\sigma_y \varepsilon_y) dx dy \right] + \frac{1}{2} \sum_{i=1}^n \left[ \int_0^L \int_{-\frac{b_i}{2}}^{+\frac{b_i}{2}} (m_y \kappa_y) dx dy \right] + \frac{1}{2} \sum_{i=1}^n \left[ \int_0^L \int_{-\frac{b_i}{2}}^{+\frac{b_i}{2}} (m_{xy} \kappa_{xy}) dx dy \right] \quad (5.13)$$

where  $m_y$  and  $m_{xy}$  are moments for a unit-width strip portion, while  $\kappa_y$  and  $\kappa_{xy}$  are corresponding curvatures, and  $\sigma_y$  is the longitudinal membrane stress (in our case:  $\sigma_y = p_y$ ). It is to be observed that the first term of the above expression corresponds to the membrane strain energy while the second and third terms to the bending strain energy.

However, similarly to the external potential, it is possible to consider a simplifying option, by neglecting the effect of strain-stress variation through the thickness. It can also be understood that this simplification is equivalent with neglecting the bending strain energy, which leads to the following simplified expression for the strain energy:

$$\Pi_{int} = \frac{1}{2} \sum_{i=1}^n \left[ \int_0^L \int_{-\frac{b_i}{2}}^{+\frac{b_i}{2}} (\sigma_y \varepsilon_y) dx dy \right] \quad (5.14)$$

Since the external potential can be calculated by 4 different ways, while internal potential by 2 different ways, 8 different options are considered here for the total potential energy, as summarized in **Table 5.1**.

**Table 5.1:** Definition of calculation options

option	<i>nnn</i>	<i>nny</i>	<i>nyn</i>	<i>nyy</i>	<i>ynn</i>	<i>yny</i>	<i>yyn</i>	<i>yyy</i>
$(\partial v / \partial y)^2$ term considered?	no	no	no	no	yes	yes	yes	yes
through-thickness stress-strain variation in external potential?	no	no	yes	yes	no	no	yes	yes
through-thickness stress-strain variation in internal potential?	no	yes	no	yes	no	yes	no	yes

### 5.2.4 Flexural buckling

Let us consider the case of flexural buckling, by assuming that the analysed cross-section is mono-symmetrical (or: double-symmetrical), and also assuming that the axis of symmetry is the (global) X-axis. In this case the  $C_{23}=C_{32}$  elements and the  $C_{24}=C_{42}$  elements are zero, which simplifies the second equation of Eq. (5.5) as follows:

$$C_{22}U_0 = 0 \quad (5.15)$$

The non-trivial solution exist if  $C_{22} = 0$ , from which the critical force can easily be expressed for the various options. The formulae are summarized in **Table 5.2**

In the table the following notations are used:

$$F_Z = \frac{\pi^2 EI_Z}{(1-\nu^2)L^2} \text{ and } F_{Z,r} = \frac{\pi^2 EI_{Z,r}}{(1-\nu^2)L^2} \text{ and } F_a = \frac{EA}{1-\nu^2} \quad (5.16)$$

in which  $E$  is the modulus of elasticity,  $\nu$  is the Poisson's ratio,  $L$  is the member length, while the applied cross-sectional properties are as follows:  $A$  is the cross-sectional area,  $I_Z$  is the second moment of area calculated with regard to global Z-axis, with considering own plate inertias (i.e., the  $b_i t_i^3/12$  terms),  $I_{Z,r}$  is the (reduced) second moment of area with regard to global Z-axis, with neglecting own plate inertias (i.e., the  $b_i t_i^3/12$  terms).

If the longitudinal second-order strain term  $(\partial v/\partial y)^2$  is neglected, i.e., for  $n \times \times$  options, the solution for the critical force is very similar to the well-known Euler-formula  $\pi^2 EI/L^2$ . The moment of inertia can be  $I_Z$  or  $I_{Z,r}$ , depending on whether the through-thickness strain/stress variation is considered or not in the strain energy calculation, which is equivalent to consider or not the  $b_i t_i^3/12$  own plate inertia terms. Both  $I_Z$  and  $I_{Z,r}$  are widely accepted and used in the practice, moreover, in most of thin-walled cross-sections the difference between them is negligible.

However, there is another important difference between the presented solutions and the Euler-formula: the  $(1-\nu^2)$  term in the denominator. This is clearly the consequence of the applied 2D model and the global buckling definition which does not allow transverse extension/shortening of the strips ( $\varepsilon_x = 0$ ), therefore introduces an increase of the bending stiffness. The increased stiffness is directly reflected in the increase of the critical force with regard to Euler-formula. The magnitude of this increase is dependent on the value of Poisson's ratio. For usual steel, for example,  $\nu = 0.3$ , which means approx. 10% rigidity increase, since  $1/(1-\nu^2) = 1.10$ .

If the longitudinal second-order strain term  $(\partial v/\partial y)^2$  is considered, i.e., for  $y \times \times$  options, the solution for the critical force for flexural buckling takes a slightly more complex form. As far as tendencies are concerned, it is easy to understand that the effect of the  $(\partial v/\partial y)^2$  term vanishes as  $L \rightarrow \infty$ . For example, let us consider the  $nnn$  and  $ynn$  cases:

$$\lim_{L \rightarrow \infty} \frac{F_{cr,Z}^{ynn}}{F_{cr,Z}^{nnn}} = \lim_{L \rightarrow \infty} \frac{\frac{1}{1-\nu^2} \frac{\pi^2 E A I_{Z,r}}{L^2 A + \pi^2 I_{Z,r}}}{\frac{1}{1-\nu^2} \frac{\pi^2 E I_{Z,r}}{L^2}} = \lim_{L \rightarrow \infty} \frac{L^2 A}{L^2 A + \pi^2 I_{Z,r}} = \lim_{L \rightarrow \infty} \frac{1}{1 + \frac{\pi^2 I_{Z,r}}{L^2 A}} = 1 \quad (5.17)$$

**Table 5.2:** Critical force formulae for flexural buckling

option	critical force for flexural buckling (about Z)	$L \rightarrow 0$
$nnn$	$F_{cr,Z}^{nnn} = F_{Z,r} = \frac{\pi^2 EI_{Z,r}}{(1-\nu^2)L^2}$	$\rightarrow \infty$
$nn y$	$F_{cr,Z}^{nn y} = F_Z = \frac{\pi^2 EI_Z}{(1-\nu^2)L^2}$	$\rightarrow \infty$
$n y n$	$F_{cr,Z}^{n y n} = F_{Z,r} = \frac{\pi^2 EI_{Z,r}}{(1-\nu^2)L^2}$	$\rightarrow \infty$
$n y y$	$F_{cr,Z}^{n y y} = F_Z = \frac{\pi^2 EI_Z}{(1-\nu^2)L^2}$	$\rightarrow \infty$
$y n n$	$F_{cr,Z}^{y n n} = \frac{1}{1-\nu^2} \frac{\pi^2 E A I_{Z,r}}{L^2 A + \pi^2 I_{Z,r}} = \frac{1}{\frac{1}{F_{Z,r}} + \frac{1}{F_a}}$	$\frac{EA}{1-\nu^2}$
$y n y$	$F_{cr,Z}^{y n y} = \frac{1}{1-\nu^2} \frac{\pi^2 E A I_Z}{L^2 A + \pi^2 I_{Z,r}} = \frac{1}{\frac{1}{F_Z} + \frac{1}{F_a} \frac{F_{Z,r}}{F_Z}}$	$\frac{EA}{1-\nu^2} \frac{I_Z}{I_{Z,r}}$
$y y n$	$F_{cr,Z}^{y y n} = \frac{1}{1-\nu^2} \frac{\pi^2 E A I_{Z,r}}{L^2 A + \pi^2 I_Z} = \frac{1}{\frac{1}{F_{Z,r}} + \frac{1}{F_a} \frac{F_Z}{F_{Z,r}}}$	$\frac{EA}{1-\nu^2} \frac{I_{Z,r}}{I_Z}$
$y y y$	$F_{cr,Z}^{y y y} = \frac{1}{1-\nu^2} \frac{\pi^2 E A I_Z}{L^2 A + \pi^2 I_Z} = \frac{1}{\frac{1}{F_Z} + \frac{1}{F_a}}$	$\frac{EA}{1-\nu^2}$

On the other hand, for very short columns the difference between the corresponding  $n \times \times$  and  $y \times \times$  cases is significant, which can be well illustrated with  $L \rightarrow 0$ . It is evident that for any  $n \times \times$  option the critical force tends to infinity, while for the  $y \times \times$  cases it tends to a finite value, see **Table 5.2**.

As far as the various options are concerned, it may be fair to say that  $\times n y$  and  $\times y n$  options are slightly inconsistent, since it does not seem to be logical to consider through-thickness strain/stress variation in one component of the potential energy but neglect it in another component. In spite of this inconsistency,  $y n y$  is still an existing option: it is included e.g., in [10/1-11/1] and in the CUFSM software [17/1-18/1] since option  $y n y$  is exactly identical to what is implemented in CUFSM (when mode decomposition is enforced). Moreover, the same inconsistency is possible to find in well-known and widely accepted finite element software applications, as demonstrated by numerical examples, see below and in [4/5]. This inconsistency causes negligible error in the majority of practical cases, but it is possible to find applications when its effect is not negligible.

### 5.2.5 Pure torsional buckling

Pure torsional buckling might occur if the analysed cross-section is double-symmetrical or point-symmetrical, therefore  $X_{SC} = Z_{SC} = 0$ . This means that  $C_{42}=C_{43}=C_{24}=C_{34}=0$  in the coefficient matrix, therefore, the 4<sup>th</sup> equation of Eq. (5.5) is simplified to:

$$C_{44}\Theta_0 = 0 \quad (5.18)$$

The non-trivial solution exist if  $C_{44} = 0$ , from which the critical force can be expressed for the various options, as summarized in **Table 5.3**

**Table 5.3:** Critical force formulae for pure torsional buckling

option	critical force for pure torsional buckling	$L \rightarrow \infty$	$L \rightarrow 0$
<i>nnn</i>	$F_{cr,Y}^{nnn} = \frac{F_{w,r}}{r_{0S,r}^2} = \frac{1}{ir_{0S,r}^2} \left( \frac{\pi^2 EI_{w,r}}{(1-\nu^2)L^2} \right)$	0	$\rightarrow \infty$
<i>nnY</i>	$F_{cr,Y}^{nnY} = \frac{F_w + F_t}{r_{0S,r}^2} = \frac{1}{r_{0S,r}^2} \left( \frac{\pi^2 EI_w}{(1-\nu^2)L^2} + GI_t \right)$	$\frac{GI_t}{r_{0S,r}^2}$	$\rightarrow \infty$
<i>nyn</i>	$F_{cr,Y}^{nyn} = \frac{F_{w,r}}{r_{0S}^2} = \frac{1}{r_{0S}^2} \left( \frac{\pi^2 EI_{w,r}}{(1-\nu^2)L^2} \right)$	0	$\rightarrow \infty$
<i>nyY</i>	$F_{cr,Y}^{nyY} = \frac{F_w + F_t}{r_{0S}^2} = \frac{1}{r_{0S}^2} \left( \frac{\pi^2 EI_w}{(1-\nu^2)L^2} + GI_t \right)$	$\frac{GI_t}{r_{0S}^2}$	$\rightarrow \infty$
<i>ynn</i>	$F_{cr,Y}^{ynn} = \frac{F_{wr}F_a}{r_{0S,r}^2 F_a + F_{wr}} = \frac{1}{\frac{1}{F_{cr,Y}^{nnn}} + \frac{1}{F_a}}$	0	$\frac{EA}{1-\nu^2}$
<i>yny</i>	$F_{cr,Y}^{yny} = \frac{(F_w + F_t)F_a}{r_{0S,r}^2 F_a + F_{wr}} = \frac{1}{\frac{1}{F_{cr,Y}^{nnY}} + \frac{1}{F_a} \frac{F_{w,r}}{F_w + F_t}}$	$\frac{GI_t}{r_{0S,r}^2}$	$\frac{EA}{1-\nu^2} \frac{I_{w,r}}{I_{w,r}}$
<i>yyN</i>	$F_{cr,Y}^{yyN} = \frac{F_{wr}F_a}{r_{0S}^2 F_a + F_w} = \frac{1}{\frac{1}{F_{cr,Y}^{nyn}} + \frac{1}{F_a} \frac{F_w}{F_{w,r}}}$	0	$\frac{EA}{1-\nu^2} \frac{I_{w,r}}{I_w}$
<i>yyy</i>	$F_{cr,Y}^{yyy} = \frac{(F_w + F_t)F_a}{r_{0S}^2 F_a + F_w} = \frac{1}{\frac{1}{F_{cr,Y}^{nyY}} + \frac{1}{F_a} \frac{F_w}{F_w + F_t}}$	$\frac{GI_t}{r_{0S}^2}$	$\frac{EA}{1-\nu^2}$



In the above table the symbols are as follows.

$$F_w = \frac{\pi^2 EI_w}{(1-\nu^2)L^2} \text{ and } F_{w,r} = \frac{\pi^2 EI_{w,r}}{(1-\nu^2)L^2} \text{ and } F_t = GI_t \quad (5.19)$$

$$r_{0S}^2 = \frac{I_X + I_Z}{A} + X_{SC}^2 + Z_{SC}^2 \text{ and } r_{0S,r}^2 = \frac{I_{X,r} + I_{Z,r}}{A} + X_{SC}^2 + Z_{SC}^2 \quad (5.20)$$

in which  $G$  is the shear modulus,  $I_w$  and  $I_{w,r}$  are warping constant, with and without considering the through-thickness warping variation, respectively,  $I_t$  is the torsion constant,  $I_X$  is the second moment of area calculated with regard to global  $X$ -axis, with considering own plate inertias (i.e., the  $bit_i^3/12$  terms),  $I_{X,r}$  is the (reduced) second moment of area with regard to global  $X$ -axis, with neglecting own plate inertias (i.e., the  $bit_i^3/12$  terms), finally,  $X_{SC}$  and  $Z_{SC}$  are the coordinates of shear centre with regard to mass centre, i.e.,  $X_{SC} = X_S - X_C$  and  $Z_{SC} = Z_S - Z_C$ , where  $X_C$  and  $Z_C$  are the global coordinates of the mass centre of the cross-section, while  $X_S$  and  $Z_S$  are the global coordinates of the shear centre of the cross-section. The other symbols are defined previously.

If the longitudinal second-order strain term  $(\partial v / \partial y)^2$  is neglected, i.e., for  $n \times \times$  options, the solutions for the critical force are similar to the classical beam-model-based solution, which is usually given as follows, see e.g., [8/5]:

$$F_{cr,Y} = \frac{1}{r_{0S}^2} \left( \frac{\pi^2 EI_w}{L^2} + GI_t \right) \quad (5.21)$$

The above (beam-model-based) classical solution is most similar to the solutions for  $nny$  and  $nyy$  options (between which the only difference is how the polar radius of gyration is calculated: without or with considering the warping variation through the thickness).

The most trivial difference is the  $(1-\nu^2)$  term in the denominator of the warping term (i.e.,  $\pi^2 EI_w / L^2$ ). Similarly to what has already been mentioned for flexural buckling, this  $1/(1-\nu^2)$  term is clearly the consequence of the applied 2D model and global buckling definition which prevents transverse extension/shortening of the strips. Unlike in flexural buckling, however, the difference is not constant (for a given value of  $\nu$ ), but depends on the beam length. As  $L \rightarrow \infty$ , the effect of  $1/(1-\nu^2)$  term vanishes, while for  $L \rightarrow 0$  the effect of restrained transverse contraction tends to  $1/(1-\nu^2)$ .

Another potential difference is how the warping constant is calculated. Though in classical solutions usually ' $I_w$ ' symbol is used, its meaning is most likely  $I_{w,r}$  (according to the notations used here), since the  $I_w$  warping constant with considering through-thickness warping variation is hardly used in the practice. Most textbooks concentrate on  $I_{w,r}$  only (see e.g. Annex C of [2/1]), while formulae for  $I_w$  are limited to single plates, T and L sections, see e.g., [6/5]. Since the increment of  $I_w$  with regard to  $I_{w,r}$ , which sometimes referred as *secondary warping*, is usually neglected in the engineering practice, whilst the torsion constant  $I_t$  is normally taken into account, the critical force for pure torsional buckling in the practice is slightly different from any of the shell-model based solutions.

If the longitudinal second-order strain term  $(\partial v / \partial y)^2$  is considered, i.e., for  $y \times \times$  options, the solution for the critical force for pure torsional buckling takes a slightly more complex form. As far as tendencies are concerned, it is easy to prove that the effect of the  $(\partial v / \partial y)^2$  term vanishes as  $L \rightarrow \infty$ . For example, in case if  $nny$  and  $yyy$  cases:

$$\begin{aligned}
\lim_{L \rightarrow \infty} \frac{F_{cr,Y}^{nyy}}{F_{cr,Y}^{yyy}} &= \lim_{L \rightarrow \infty} \frac{F_{cr,Y}^{nyy}}{\frac{1}{\frac{1}{F_{cr,Y}^{nyy}} + \frac{1}{F_a} \frac{F_w}{F_w + F_t}}} = \lim_{L \rightarrow \infty} \left( 1 + \frac{F_{cr,Y}^{nyy}}{F_a} \frac{F_w}{F_w + F_t} \right) = \\
&= \lim_{L \rightarrow \infty} \left( 1 + \frac{\frac{F_w + F_t}{r_{0S}^2}}{F_a} \frac{F_w}{F_w + F_t} \right) = \lim_{L \rightarrow \infty} \left( 1 + \frac{F_w}{r_{0S}^2 F_a} \right) = \lim_{L \rightarrow \infty} \left( 1 + \frac{\pi^2 EI_w}{r_{0S}^2 EAL^2} \right) = 1
\end{aligned} \tag{5.22}$$

Similarly to flexural buckling, for any regular double-symmetrical (or point-symmetrical) cross section in case of all the  $n \times \times$  options (i.e., when longitudinal second-order strain term is not considered) the critical forces tend to infinity as  $L$  approaches zero, while in case of all the  $y \times \times$  options (i.e., when longitudinal second-order strain term is not considered) the critical forces tend to a finite value as  $L$  approaches zero, see **Table 5.3**.

Moreover, in case of all the  $\times \times n$  options (i.e., when through-thickness strain variation is not considered in calculating strain energy) the critical forces tend to zero as  $L$  tends to infinity, while in case of all the  $\times \times y$  options (i.e., when through-thickness strain variation is considered in calculating strain energy) the critical forces tend to  $GI_t$  as  $L$  tends to infinity (see **Table 5.3**).

## 5.2.6 Flexural-torsional buckling

Let us consider the case of flexural-torsional buckling, by assuming that the analysed cross-section is mono-symmetrical, and also assuming that the axis of symmetry is the (global)  $Z$ -axis. In this case the  $C_{32}=C_{23}$  and  $C_{34}=C_{43}$  elements of coefficient matrix of Eq. (5.5) are zero. Therefore the 2<sup>nd</sup> and 4<sup>th</sup> rows of the equation can be written as follows:

$$\begin{bmatrix} C_{22} & C_{24} \\ C_{42} & C_{44} \end{bmatrix} \begin{bmatrix} U_0 \\ \Theta_0 \end{bmatrix} = \begin{bmatrix} 0 \\ 0 \end{bmatrix} \tag{5.23}$$

which leads to a 2<sup>nd</sup>-order equation:

$$C_{22}C_{44} - C_{24}^2 = 0 \tag{5.24}$$

The equation can be solved analytically for any option. The critical force can be expressed in the general form as follows:

$$F_{FT} = \frac{F_F \alpha_T + F_T \alpha_F - 2\alpha \alpha_\omega F_\omega}{2(\alpha_F \alpha_T + \alpha \alpha_\omega^2)} - \sqrt{\left( \frac{F_F \alpha_T + F_T \alpha_F - 2\alpha \alpha_\omega F_\omega}{2(\alpha_F \alpha_T + \alpha \alpha_\omega^2)} \right)^2 - \frac{F_F F_T - \alpha F_\omega^2}{\alpha_F \alpha_T + \alpha \alpha_\omega^2}} \tag{5.25}$$

with symbols defined in **Table 5.4** Note,  $0 < \alpha < 1$ , while  $\alpha_F$ ,  $\alpha_T$  and  $\alpha_\omega$  are equal to or greater than 1.

The formula of Eq. (5.25) is similar to the classical analytical solution, which becomes more evident if the critical force for the simplest  $nnn$  (or  $nyn$ ) option is expressed, as follows:

$$F_{FT}^{nnn} = \frac{1}{2 \left( 1 + \frac{Z_{SC}^2}{r_{0S}^2} \right)} \left[ F_F + F_T - \sqrt{(F_F + F_T)^2 - 4 \left( 1 + \frac{Z_{SC}^2}{r_{0S}^2} \right) F_F F_T} \right] \quad (5.26)$$

The formula of Eq (5.26) is seemingly identical with that of the classical solution, see e.g., [8/5] or [2/1]. Even so, the classical beam-model-based critical force is not identical to any of the shell-model-based solutions, since the  $F_F$  and  $F_T$  terms (i.e., the critical forces for flexural and for pure torsional buckling) are slightly different from how they are usually calculated in the engineering practice. (E.g., the effect of secondary warping, or the effect of restrained transverse contraction, as discussed in the previous Sections.) Ultimately this leads to the conclusion that the presented shell-model-based critical force for FT buckling will never perfectly coincide with the classical solution most likely used in the practice.

**Table 5.4:** Definition of symbols in critical force formula for flexural-torsional buckling

opt.	$F_F$	$F_T$	$F_\omega$	$\alpha$	$\alpha_F$	$\alpha_T$	$\alpha_\omega$
<i>nnn</i>	$F_{cr,Z}^{nnn}$	$F_{cr,Y}^{nnn}$	0	$\frac{Z_{SC}^2}{r_{0S,r}^2}$	1	1	1
<i>nnY</i>	$F_{cr,Z}^{nnY}$	$F_{cr,Y}^{nnY}$	$\frac{\pi^2 EI_{\omega Z}}{(1-\nu^2)L^2}$	$\frac{Z_{SC}^2}{r_{0S,r}^2}$	1	1	1
<i>nyn</i>	$F_{cr,Z}^{nyn}$	$F_{cr,Y}^{nyn}$	0	$\frac{Z_{SC}^2}{r_{0S}^2}$	1	1	1
<i>nyy</i>	$F_{cr,Z}^{nyy}$	$F_{cr,Y}^{nyy}$	$\frac{\pi^2 EI_{\omega Z}}{(1-\nu^2)L^2}$	$\frac{Z_{SC}^2}{r_{0S}^2}$	1	1	1
<i>ynn</i>	$F_{cr,Z}^{ynn}$	$F_{cr,Y}^{ynn}$	0	$\frac{Z_{SC}^2}{r_{0S,r}^2}$	$1 + \frac{\pi^2 I_{Z,r}}{L^2 A}$	$1 + \frac{\pi^2 I_{w,r}}{L^2 A r_{0S,r}^2}$	1
<i>yny</i>	$F_{cr,Z}^{yny}$	$F_{cr,Y}^{yny}$	$\frac{\pi^2 EI_{\omega Z}}{(1-\nu^2)L^2}$	$\frac{Z_{SC}^2}{r_{0S,r}^2}$	$1 + \frac{\pi^2 I_{Z,r}}{L^2 A}$	$1 + \frac{\pi^2 I_{w,r}}{L^2 A r_{0S,r}^2}$	1
<i>yyn</i>	$F_{cr,Z}^{yyn}$	$F_{cr,Y}^{yyn}$	0	$\frac{Z_{SC}^2}{r_{0S}^2}$	$1 + \frac{\pi^2 I_Z}{L^2 A}$	$1 + \frac{\pi^2 I_w}{L^2 A r_{0S}^2}$	$1 + \frac{\pi^2 I_{\omega Z}}{L^2 A}$
<i>yyy</i>	$F_{cr,Z}^{yyy}$	$F_{cr,Y}^{yyy}$	$\frac{\pi^2 EI_{\omega Z}}{(1-\nu^2)L^2}$	$\frac{Z_{SC}^2}{r_{0S}^2}$	$1 + \frac{\pi^2 I_Z}{L^2 A}$	$1 + \frac{\pi^2 I_w}{L^2 A r_{0S}^2}$	$1 + \frac{\pi^2 I_{\omega Z}}{L^2 A}$

In the above table the new symbols are as follows.

$$F_{\omega X} = \frac{\pi^2 EI_{\omega X}}{(1-\nu^2)L^2} \text{ and } F_{\omega Z} = \frac{\pi^2 EI_{\omega Z}}{(1-\nu^2)L^2} \quad (5.27)$$

in which the cross-sectional properties are:

$$I_{\omega X} = \begin{cases} \frac{1}{X_{SC}} \int_A \omega \cdot (Z - Z_C) dA & \text{if } X_{SC} \neq 0 \\ 0 & \text{if } X_{SC} = 0 \end{cases} \quad (5.28)$$

$$I_{\omega Z} = \begin{cases} -\frac{1}{Z_{SC}} \int_A \omega \cdot (X - X_C) dA & \text{if } Z_{SC} \neq 0 \\ 0 & \text{if } Z_{SC} = 0 \end{cases} \quad (5.29)$$

It might be interesting to highlight that unlike in case of flexural or torsional buckling, the formulae of some of the  $n \times \times$  options are different from classical solutions. More specifically, if we consider  $nn$  or  $ny$  option, the critical force formula can be expressed as follows.

$$F_{FT} = \frac{1}{2 \left( 1 + \frac{Z_{SC}^2}{r_{0S}^2} \right)} \left[ F_F + F_T - 2 \frac{Z_{SC}^2}{r_{0S}^2} F_{\omega} \right] - \sqrt{\left( F_F + F_T - 2 \frac{Z_{SC}^2}{r_{0S}^2} F_{\omega} \right)^2 - 4 \left( 1 + \frac{Z_{SC}^2}{r_{0S}^2} \right) \left( F_F F_T - \frac{Z_{SC}^2}{r_{0S}^2} F_{\omega}^2 \right)} \quad (5.30)$$

The most evident difference between Eq. (5.26) and Eq. (5.30) is the  $F_{\omega}$  term. It might be interesting to mention that  $F_{\omega}$  is dependent on a cross-section property denoted by  $I_{\omega Z}$ , which has a magnitude comparable to  $I_t$ , therefore, the  $F_{\omega}$  term is negligibly small with regard to  $F_{cr,X}$  or  $F_{cr,Z}$  in many practical cases. It is possible to find cross-sections and column lengths, however, where the influence of the  $F_{\omega}$  term is not negligible, therefore, the differences between the various  $n \times \times$  options are not negligible.

Finally, it is to mention that solutions for  $y \times \times$  options are more complicated formulae than those for  $n \times \times$  options. If the member length is long, the difference between any  $n \times \times$  and its  $y \times \times$  counterpart is negligible. However, as  $L \rightarrow 0$ ,  $n \times \times$  solutions tend to infinity, while  $y \times \times$  solutions approach a finite value. For the sake of completeness, let us mention here that in case of  $ynn$  and  $yyy$  options this finite value is  $F_a$ , while in case of  $yny$  and  $yyn$  options these finite values can be expressed by the following formulae:

$$\lim_{L \rightarrow 0} F_{FT}^{yny} = \frac{F_a}{2} \left[ \frac{I_Z I_{w,r} + I_w I_{Z,r}}{I_{Z,r} I_{w,r}} - \sqrt{\left( \frac{I_Z I_{w,r} + I_w I_{Z,r}}{I_{Z,r} I_{w,r}} \right)^2 - 4 \frac{I_Z I_w - Z_{SC}^2 I_{\omega Z}^2}{I_{Z,r} I_{w,r}}} \right] \quad (5.31)$$

$$\lim_{L \rightarrow 0} F_{FT}^{yyn} = \frac{F_a}{2} \left[ \frac{I_Z I_{w,r} + I_w I_{Z,r}}{I_Z I_w - Z_{SC}^2 I_{\omega Z}^2} - \sqrt{\left( \frac{I_Z I_{w,r} + I_w I_{Z,r}}{I_Z I_w - Z_{SC}^2 I_{\omega Z}^2} \right)^2 - 4 \frac{I_{Z,r} I_{w,r}}{I_Z I_w - Z_{SC}^2 I_{\omega Z}^2}} \right] \quad (5.32)$$

### 5.2.7 Axial mode

The first three equations of Eq. (5.5) have been discussed in detail in the previous Sections. Finally, let us consider the last equation which always independent of the other three.

In case of  $n \times \times$  options, i.e., when the longitudinal second-order strain term  $(\partial v / \partial y)^2$  is neglected, the last equation of Eq. (5.5) is:

$$-F_a V_0 = 0 \quad (5.33)$$

which does not yield to a critical force. However, if the  $(\partial v / \partial y)^2$  term is considered, as in  $y \times \times$  options, the last equation of Eq. (5.5) takes the following form:

$$(F - F_a) V_0 = 0 \quad (5.34)$$

from which a critical force can be expressed as:

$$F_{cr,A} = F_a = \frac{EA}{1 - \nu^2} \quad (5.35)$$

Thus, if transverse displacements of the column are restrained, i.e.,  $U_0 = W_0 = \Theta_0 = 0$ , but longitudinal displacement is allowed, a critical force can still be calculated which is the  $F_{cr,A}$  value. This unusual buckling mode is referred here as *axial mode*. It should be emphasized that even though the column axis remains straight in axial mode, the displacement field of the column is not identical to that of a pre-buckling state, since in this latter case  $V$  varies *linearly* along the column longitudinal axis, see Eq. (5.36), while in the axial mode  $V$  is a *cosine* function, see Eq. (5.4).

$$V = V_0 \left( 1 - \frac{2y}{L} \right) \quad (5.36)$$

The difference between the first-order deformations and axial mode is illustrated in **Figure 5.2**

It might be interesting to mention that buckling in axial mode can be regarded as a bifurcation of equilibrium. To demonstrate this, it is convenient to show a load-displacement plot, where ‘load’ is the applied force, while ‘displacement’ is selected to be the *rate of change of the engineering strain* (i.e.,  $\varepsilon_y' = \partial \varepsilon_y / \partial y$ ) at the column ends. In case of first-order solution this displacement parameter is zero, while in case of axial mode buckling it is calculated as follows:

$$\varepsilon_y' = \frac{\partial \varepsilon_y}{\partial y} = \frac{\partial^2 V}{\partial y^2} = -V_0 \frac{m^2 \pi^2}{L^2} \cos \frac{m\pi y}{L} \quad (5.37)$$

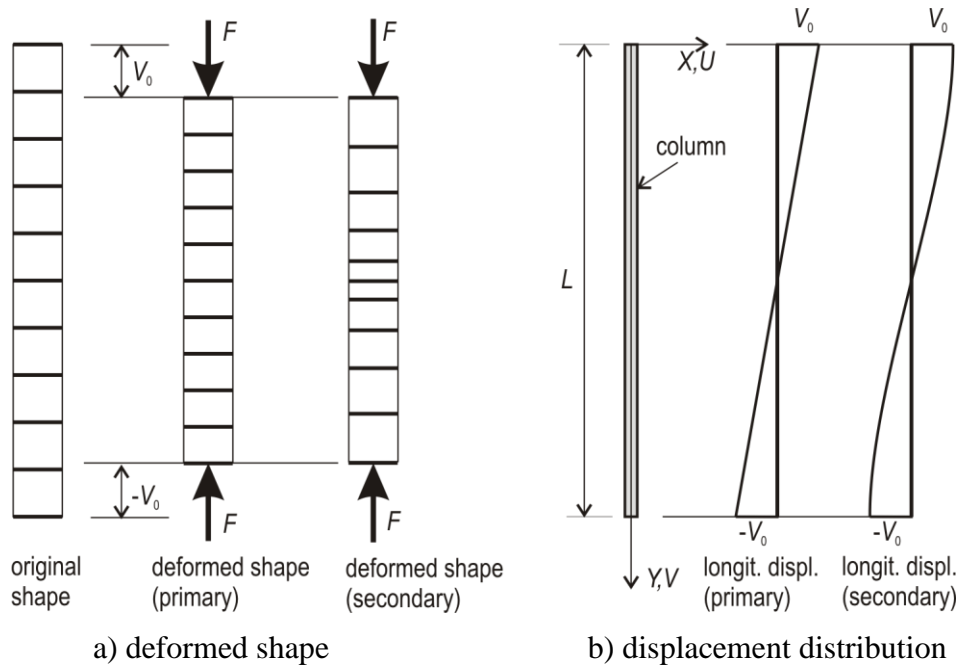
$$\varepsilon_{y0}' = \pm V_0 \frac{m^2 \pi^2}{L^2} \quad (5.38)$$

which can be zero or an arbitrary (small) non-zero value. Therefore, the load-displacement plot looks like the one in **Figure 5.3**.

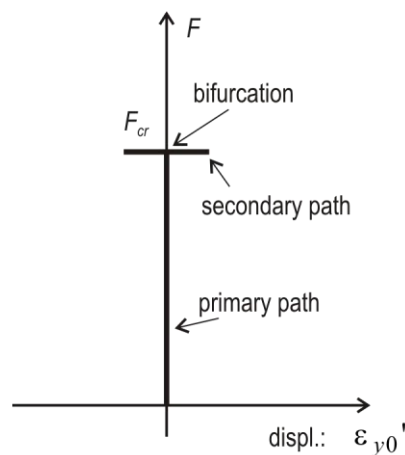
Even though the axial mode is a mathematically possible solution of Eq. (5.5), the value of the associated critical force is extremely high, therefore, it is surely impossible to experience buckling in axial mode for a real column. Still, this buckling mode has some influence on all the other modes (i.e., flexural, torsional or flexural-torsional), as soon as the  $(\partial v / \partial y)^2$  term is considered in the potential energy of the external loading. By looking at the critical force

formulae for  $y \times x$  options, (see e.g., **Table 5.2** or Table 5.3,) the formulae can be interpreted as Dunkerley-type interaction formulae, where the interaction takes place between the axial mode and flexural or torsional mode. More precisely, the formulae are essentially in accordance with Föppl-Papkovich theorem see e.g., [9/5]. The existence of Dunkerley-type interaction for flexural-torsional buckling is less evident from the formulae of **Table 5.4**, but it is found by numerical results, see [4/5].

Finally, it is to mention that the effect of axial deformations on the critical force is reported by some textbooks, too. For example, it is mentioned in [10/5] in connection with flexural buckling.



**Figure 5.2:** Longitudinal displacements in axial mode

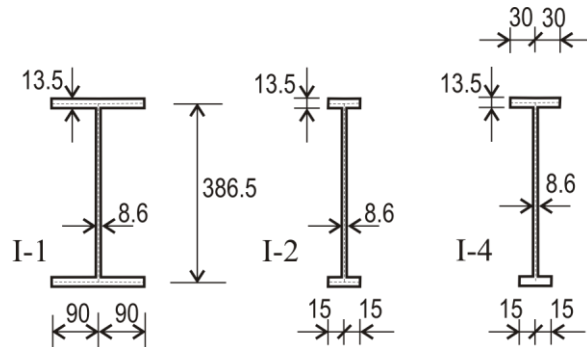


**Figure 5.3:** Bifurcation of equilibrium in case of axial mode buckling

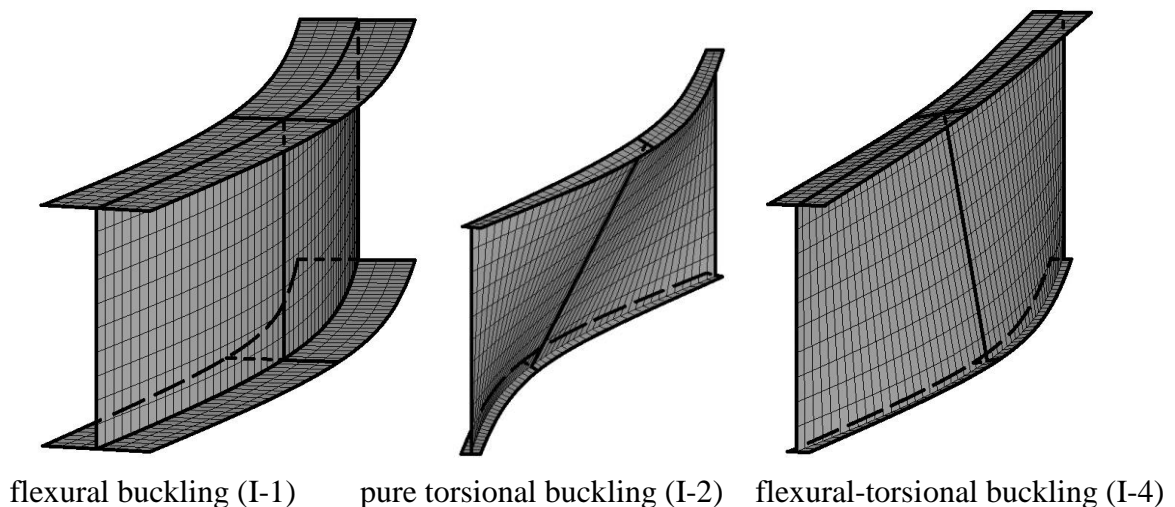
### 5.2.8 Demonstrative examples

In the previous Sections the shell-model-based analytical formulae for various global column buckling types have been derived and briefly discussed from theoretical aspects. In this Section numerical studies are shown, based on [4/5]: flexural, pure torsional and flexural-torsional buckling of simply supported columns are considered and critical forces are calculated by using various methods, namely: shell-model-based formulae in 8 options (as detailed above), cFSM, shell FEM, GBT (as implemented in GBTUL), and the analytical formulae as in Annex C of [2/1]. In case of shell FEM Ansys is used with carefully selected restraints so that the shell model would approximate the cFSM assumptions as much as possible. (For details about the shell model, see [4/5].) Various cross-sections are considered in the studies, three of them presented here, see **Figure 5.4**. The members are assumed to be made of steel ( $E=210000$  MPa), however, with assuming  $\nu=0$  in order to eliminate the differences caused by the restrained or unrestrained transverse strains. The critical forces are calculated a fairly wide range of column lengths in order to be able to compare the tendencies at extreme lengths, too.

Some typical deformed shapes are shown in **Figure 5.5** (from the shell FEM analysis), while numerical results are summarized in tables (**Table 5.5** to **Table 5.8**). As it can be observed, in case of flexural buckling of a usual cross-section (I-1) the differences between the various methods are negligible at least for practical member lengths (i.e., if the column is not too short). In other cases, however, e.g., in the cross-section has unusual dimensions, or, if buckling involves torsion, or, especially if the member length is extremely short, the differences between the results from the various methods are more significant.



**Figure 5.4:** Sample cross-sections



flexural buckling (I-1)      pure torsional buckling (I-2)      flexural-torsional buckling (I-4)

**Figure 5.5:** Some typical FEM buckling modes

**Table 5.5:** Critical forces for flexural buckling of I-1 section

length		mm	→ 0	10	100	1000	10000	→ inf
calculation option	nnn	kN	inf	2.72E+08	2 719 688	27 197	271.97	0
	nny	kN	inf	2.72E+08	2 723 934	27 239	272.39	0
	nyn	kN	inf	2.72E+08	2 719 688	27 197	271.97	0
	nyy	kN	inf	2.72E+08	2 723 934	27 239	272.39	0
	ynn	kN	1 718 619	1 707 827	1 053 128	26 773	271.93	0
	yny	kN	1 721 302	1 710 493	1 054 773	26 815	272.35	0
	yyn	kN	1 715 940	1 705 181	1 052 122	26 773	271.93	0
	yyy	kN	1 718 619	1 707 844	1 053 765	26 814	272.35	0
	GBT	kN	-	-	2 723 934	27 239	272.39	-
	cFSM	kN	-	1 710 509	1 054 782	26 815	272.35	-
	FEM	kN	-	1 710 564	1 054 804	26 825	272.49	-
	EC3	kN	inf	2.72E+08	2 719 688	27 197	271.97	0

**Table 5.6:** Critical forces for flexural buckling of I-2 section

length		mm	→ 0	10	100	1000	10000	→ inf
calculation option	nnn	kN	inf	1 259 115	12 591	125.91	1.2591	0
	nny	kN	inf	1 683 717	16 837	168.37	1.6837	0
	nyn	kN	inf	1 259 115	12 591	125.91	1.2591	0
	nyy	kN	inf	1 683 717	16 837	168.37	1.6837	0
	ynn	kN	868 119	513 842	12 411	125.89	1.2591	0
	yny	kN	1 160 869	687 121	16 596	168.35	1.6837	0
	yyn	kN	649 195	428 343	12 352	125.89	1.2591	0
	yyy	kN	868 119	572 790	16 517	168.34	1.6837	0
	GBT	kN	-	1 683 717	16 837	168.37	1.6830	-
	cFSM	kN	-	687 122	16 596	168.35	1.6837	-
	FEM	kN	-	686 056	16 594	168.36	1.6871	-
	EC3	kN	inf	1 259 115	12 591	125.91	1.2591	0

**Table 5.7:** Critical forces for pure torsional buckling of I-2 section

length		mm	→ 0	10	100	1000	10000	→ inf
calculation option	nnn	kN	inf	2 711 540	27 115	271.2	2.71	0
	nny	kN	inf	3 018 235	30 969	1 095.8	797.12	794.11
	nyn	kN	inf	2 710 301	27 103	271.0	2.71	0
	nyy	kN	inf	3 016 855	30 954	1 095.3	796.76	793.74
	ynn	kN	868 119	657 588	26 294	271.1	2.71	0
	yny	kN	966 055	731 966	30 031	1 095.5	797.12	794.11
	yyn	kN	780 111	605 755	26 193	270.9	2.71	0
	yyy	kN	868 119	674 271	29 915	1 095.0	796.76	793.74
	GBT	kN	-	3 018 235	30 969	1 095.9	797.12	-
	cFSM	kN	-	731 967	30 031	1 095.5	797.12	-
	FEM	kN	-	732 396	30 043	1 095.5	797.12	-
	EC3	kN	inf	2 712 334	27 910	1 065.3	796.82	794.11



**Table 5.8:** Critical forces for flexural-torsional buckling of I-4 section

length		mm	→ 0	10	100	1000	10000	→ inf
calculation option	nnn	kN	inf	2 039 103	20 391	203.91	2.039	0
	nny	kN	inf	2 507 555	25 469	592.52	17.700	0
	nyn	kN	inf	2 038 713	20 387	203.87	2.039	0
	nyy	kN	inf	2 507 075	25 464	592.44	17.700	0
	ynn	kN	1 038 219	687 947	19 998	203.87	2.039	0
	yny	kN	1 044 887	845 916	24 978	592.37	17.700	0
	yyn	kN	844 306	597 072	19 906	203.82	2.039	0
	yyy	kN	1 038 219	734 265	24 864	592.26	17.700	0
	GBT	kN	-	2 507 556	25 469	592.52	17.700	-
	cFSM	kN	-	845 913	24 978	592.37	17.700	-
	FEM	kN	-	846 542	24 988	592.28	17.698	-
	EC3	kN	inf	2 039 500	20 787	544.97	17.272	0

## 5.3 Flexural buckling with in-plane shear

### 5.3.1 Global buckling definition

The applied global buckling definition here is essentially identical to that of Section 5.2, with one important difference. In Section 5.2 in-plane (membrane) shear deformations have been excluded by adopting Euler-Bernoulli-Navier beam theory. Here, the first assumption of the Euler-Bernoulli-Navier hypothesis is still kept, but the second one is not, i.e., *normals to the undeformed middle line do not remain normal during deformation*. It is still assumed, however, that the shear deformations are resulted in linear warping distribution. According to the terminology of Section 3, thus, *primary shear* is considered only (together with global deformation modes).

As it has been discussed in Section 3.2.2, deformations with primary shear can be realized in a few ways as a superposition of two basic deformation modes. Here the selected two basic components are (i) the shear-free global deformation mode and (ii) the transverse-only deformation mode. Since here the focus is on flexural buckling, global-bending and shear-bending modes are considered.

### 5.3.2 Overview of derivations

In classical flexural buckling solutions that are based on beam model, one single displacement degree of freedom is considered i.e., (transverse translation), as a direct consequence of (i) not considering cross-section deformations and (ii) assuming longitudinal displacement distribution in a predefined form (in the case of two-hinged column: sinusoidal form).

To define global DOF for a shell model, the same logic is followed. The applied assumptions are as follows: (i) there is no transverse deformation of the cross-section mid-line, (ii) through-thickness deformations are disregarded, and (iii) longitudinal shape functions are assumed in a pre-defined form, which form is defined by the boundary conditions and the differential equations of the flat plate elements. Moreover, (iv) linear warping is assumed.

These assumptions finally exclude all but 7 modes of displacements: transverse translations ( $U$  and  $W$ ), longitudinal translation ( $V$ ), rotation about the longitudinal axis ( $\Theta$ ), two pure

shear modes with  $U$  and  $W$  translations, and a shear mode with twisting. (In cFSM terminology: 4 G modes, 2  $S_B$  modes and 1  $S_T$  mode.) However, if we aim flexural buckling here, it is enough to consider fewer modes, namely: axial mode, one global bending mode and the corresponding shear bending mode. The reference line is the line going through the cross-sections' mass centres.

The investigated column is assumed globally and locally pinned at both ends, therefore the global displacement function can be written as follows:

$$W = W_0 \sin \frac{m\pi y}{L} = W_0 \sin(k_m y) = (W_0^n + W_0^s) \sin(k_m y) \quad (5.39)$$

$$V = V_0 \cos \frac{m\pi y}{L} = V_0 \cos(k_m y) \quad (5.40)$$

where  $L$  is the member length,  $m$  is the number of considered half-waves, and the subscript '0' denotes the amplitude of the displacement component. It is to highlight that the transverse displacement is superposed from two components, the 'no shear' component is denoted by a superscript 'n', while the (pure) 'shear' component is marked by a superscript 's'.

The derivations follow the same logic as summarized in Section 5.2.2. The details of the derivations can be found in [5/5], and are also given in Appendix D. The main steps are summarized here as follows.

- Starting from the above global displacement functions, first the displacement amplitudes of the mid-points of each strip are expressed ( $u_{m0,i}$ ,  $v_{m0,i}$  and  $w_{m0,i}$ ).
- From the strips' mid-point displacements the whole displacement field of the strips can be constructed, i.e.,  $u(x,y,z)$ ,  $v(x,y,z)$ ,  $w(x,y,z)$ .
- First and second-order strains can be determined.
- From the first-order strains stresses can be calculated by applying Hooke's law.
- The internal potential, i.e., strain energy can be determined by using (first-order) stresses and strains and by integrating the elementary strain energy for the whole volume of each strip.
- The external potential, i.e. the negative of the work done by the external loading can be determined by using the second-order strains and by integrating the elementary work for the whole volume of each strip.

As soon as the total potential is expressed by the three displacement parameters ( $V_0$ ,  $W_0^n$  and  $W_0^s$ ) the critical forces can be determined, utilizing that in equilibrium the total potential energy is stationary. A set of 3 (linear) equations can be established as follows:

$$\frac{\partial \Pi}{\partial V_0} = 0 \quad \frac{\partial \Pi}{\partial W_0^n} = 0 \quad \frac{\partial \Pi}{\partial W_0^s} = 0 \quad \rightarrow \quad \begin{bmatrix} C_{11} & 0 & 0 \\ 0 & C_{22} & C_{23} \\ 0 & C_{32} & C_{33} \end{bmatrix} \begin{bmatrix} V_0 \\ W_0^n \\ W_0^s \end{bmatrix} = \begin{bmatrix} 0 \\ 0 \\ 0 \end{bmatrix} \quad (5.41)$$

Note, the coefficient matrix is symmetric, and the non-zero elements of the coefficient matrix are given in Appendix D.

The critical forces can be calculated by utilizing that the coefficient matrix has to be singular. Obviously, the 1<sup>st</sup> equation is independent of the others, therefore, singularity of the coefficient matrix lead to first- and second-order equations.

### 5.3.3 Calculation options

The external potential can be determined in the 4 options as detailed in Section 5.2.3. The expressions for the external work are identical to those in Eqs. (5.10) to (5.12).

The accumulated elastic strain energy can be expressed in two options. For the investigated problem, utilizing that  $\varepsilon_{x,i} = \kappa_{x,i} = \kappa_{xy,i} = 0$ , the exact expression is:

$$\Pi_{int} = \frac{1}{2} \sum_{i=1}^n \left[ t_i \int_0^{L+\frac{b_i}{2}} \int_{-\frac{b_i}{2}}^{\frac{b_i}{2}} (\sigma_{y,i} \varepsilon_{y,i}) dx dy \right] + \frac{1}{2} \sum_{i=1}^n \left[ t_i \int_0^{L+\frac{b_i}{2}} \int_{-\frac{b_i}{2}}^{\frac{b_i}{2}} (\tau_{xy,i} \gamma_{xy,i}) dx dy \right] + \frac{1}{2} \sum_{i=1}^n \left[ \int_0^{L+\frac{b_i}{2}} \int_{-\frac{b_i}{2}}^{\frac{b_i}{2}} (m_{y,i} \kappa_{y,i}) dx dy \right] \quad (5.42)$$

where  $\sigma_y$  and  $\varepsilon_y$  is the longitudinal membrane stress and strain, respectively (in this case:  $\sigma_y = p_y$ ),  $\tau_{xy}$  and  $\gamma_{xy}$  is the shear membrane stress and strain, respectively, and other symbols are defined above. It is to be observed that the first and second term of the above expression correspond to the membrane strain energy while the third term to the bending strain energy.

The above expression can be simplified by neglecting the effect of strain-stress variation through the thickness. This simplification is equivalent with neglecting the bending strain energy, which leads to:

$$\Pi_{int} = \frac{1}{2} \sum_{i=1}^n \left[ t_i \int_0^{L+\frac{b_i}{2}} \int_{-\frac{b_i}{2}}^{\frac{b_i}{2}} (\sigma_{y,i} \varepsilon_{y,i}) dx dy \right] + \frac{1}{2} \sum_{i=1}^n \left[ t_i \int_0^{L+\frac{b_i}{2}} \int_{-\frac{b_i}{2}}^{\frac{b_i}{2}} (\tau_{xy,i} \gamma_{xy,i}) dx dy \right] \quad (5.43)$$

Finally, the total potential energy can be expressed in 8 different options, as summarized in **Table 5.1**. Out of the 8 options, 4 can be considered as consistent: *nnn*, *nny*, *ynn*, and *yyy*. These consistent options will mostly be discussed here. However, as it is proved in [3/5-4/5], *yny* option is the one mostly used in numerical shell implementations, therefore, this *yny* option will also be presented here.

### 5.3.4 The critical force

The first equation in Eq. (5.41) is always independent of the others, therefore can be handled separately. In case of  $n \times \times$  options this first equation does not lead to any critical force, while in case of  $y \times \times$  options it leads to a critical force equal to  $F_a$ .

The second and third rows form an equation system. The critical forces can be found by utilizing that the coefficient matrix has to be singular, which leads to a linear or quadratic equation as follows:

$$F^2 \frac{F_{X,r}}{F_a} \alpha_1 - F(F_{X,r} \alpha_2 + F_{s,Z} \alpha_3) + F_{X,r} F_{s,Z} + \Delta F_X (F_{X,r} + F_{s,Z}) \alpha_4 = 0 \quad (5.44)$$

where  $F$  is the external force, the alpha coefficients are given in **Table 5.9**. Moreover:

$$\Delta F_X = F_X - F_{X,r} = \frac{\pi^2 E (I_X - I_{X,r})}{(1 - \nu^2) L^2} \text{ and } F_{s,Z} = G A_{s,Z} \quad (5.45)$$

in which  $E$  and  $G$  are the modulus of elasticity and the shear modulus,  $\nu$  is the Poisson's ratio,  $L$  is the member length, while the applied cross-sectional properties are as follows:  $A$  is the cross-sectional area,  $I_X$  is the second moment of areas calculated with regard to global  $X$ -axis, with considering own plate inertias (i.e., the  $b_i t_i^3/12$  terms),  $I_{X,r}$  is the (reduced) second moment of area with regard to global  $X$ -axis with neglecting own plate inertias (i.e., the  $b_i t_i^3/12$  terms),  $A_{s,Z}$  is the shear area along the  $Z$  direction, defined as follows:

$$A_{s,Z} = \sum_{i=1}^n b_i t_i \cos \alpha_i \quad (5.46)$$

where  $b_i$  and  $t_i$  is the width and thickness of the  $i$ -th strip, respectively, while  $\alpha_i$  is the (signed) angle of the  $i$ -th strip with respect to the positive  $X$ -axis (i.e., the angle between the global and the  $i$ -th strip local coordinate system).

It is to observe that the value of alpha coefficients can be either 0 or 1, or at least close to 1.

It can also be observed that in case of  $n \times \times$  options the equation is first-order, therefore it leads to one single critical force. The single critical force value can be expressed as follows:

$$F_{cr,X}^{nnn} = F_{cr,X}^{nyn} = \frac{1}{1/F_{X,r} + 1/F_{s,Z}} \quad (5.47)$$

$$F_{cr,X}^{nny} = F_{cr,X}^{nyy} = \frac{1}{1/F_{X,r} + 1/F_{s,Z}} + \Delta F_X \quad (5.48)$$

In case of  $y \times \times$  options the equation is quadratic, therefore it leads to two critical force values. These critical values can be expressed as follows:

$$F_{cr,X}^{y \times \times} = \frac{F_a}{2\alpha_1 F_{X,r}} \left\{ F_{X,r} \alpha_2 + F_{s,Z} \alpha_3 \mp \sqrt{(F_{X,r} \alpha_2 + F_{s,Z} \alpha_3)^2 - \frac{4\alpha_1 F_{X,r}}{F_a} [F_{X,r} F_{s,Z} + \Delta F_X (F_{X,r} + F_{s,Z}) \alpha_4]} \right\} \quad (5.49)$$

**Table 5.9:** Coefficients in Eq. (5.44) and Eq. (5.49)

option	$\alpha_1$	$\alpha_2$	$\alpha_3$	$\alpha_4$
<i>nnn</i>	0	1	1	0
<i>nny</i>	0	1	1	1
<i>nyn</i>	0	1	1	0
<i>nyy</i>	0	1	1	1
<i>ynn</i>	1	1	$1 + \frac{F_{X,r}}{F_a}$	0
<i>yny</i>	1	$1 + \frac{\Delta F_X}{F_a}$	$1 + \frac{F_{X,r}}{F_a}$	1
<i>yy n</i>	$1 + \frac{\Delta F_X}{F_a}$	$1 + \frac{\Delta F_X}{F_a}$	$1 + \frac{F_{X,r}}{F_a} + \frac{\Delta F_X}{F_a}$	0
<i>yyy</i>	$1 + \frac{\Delta F_X}{F_a}$	$1 + 2 \frac{\Delta F_X}{F_a}$	$1 + \frac{F_{X,r}}{F_a} + \frac{\Delta F_X}{F_a}$	1

### 5.3.5 Demonstration of the buckling modes with shear

The critical force formulae derived above will be discussed and illustrated in this Section. The presented figures belong to the major-axis flexural buckling of an IPE400 steel column, but it is to emphasize that in this Section only the buckling behaviour and tendencies are presented and the formulae are discussed in general (therefore, the actual numerical values are not important at all). The length of the column is changing in an extremely wide range so that the differences between the various options would be more visible. Here, only the 4 consistent options are discussed.

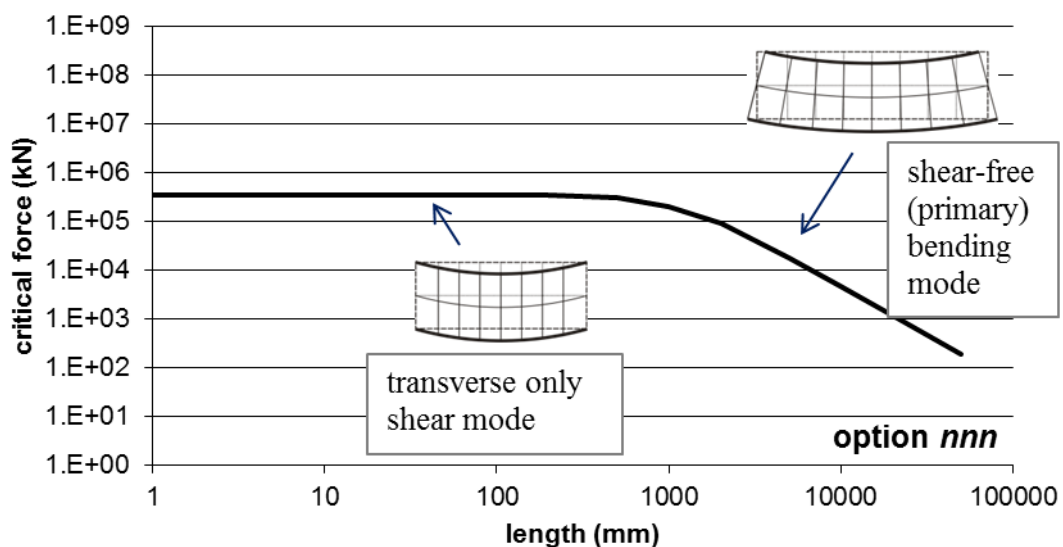
#### 5.3.5.1 Option *nnn*

In case of *nnn* option only one single critical force exists, as illustrated in **Figure 5.6**. The critical force and also the deformation is combined from two components: the classical shear-free flexural mode and the transverse-only shear mode. The formula, see Eq. (5.47) is a well-known interaction formula, known as Dunkerley-type summation formula. (More precisely, it is an example when the resulting buckling mode can exactly be calculated in accordance with the Föppl-Papkovich theorem, see [9/5].)

As it can clearly be seen from **Figure 5.6**, and can also be concluded from the critical force formula, for greater buckling lengths the shear-free mode is dominant, therefore, the critical force is practically identical to that calculated from Euler-formula. On the other hand, for small lengths the pure shear mode is dominant, that is why a (practically horizontal) shear plateau is found in the buckling force diagram. In **Figure 5.6** (as well in subsequent similar figures) these modes are illustrated, which are, therefore, not pure modes, but dominant modes for the given section of the buckling curve.

As far as the bending term is concerned, there is a clear difference between (5.47) and the Euler-formula, namely the  $(1-\nu^2)$  term in the denominator. This is clearly the consequence of the applied shell model and the global buckling definition which does not allow transverse extension/shortening of the strips ( $\varepsilon_x = 0$ ), as already discussed in Section 5.2.

It is also to mention that the derived solution for the *nnn* option is identical to the classical beam-model-based formula in [8/5], or also to the one (as a special case) in [11/5], if (but only if) the bending rigidity is calculated with neglecting the own plate inertias (i.e., the  $bt^3/12$  terms), and the Poisson's ratio is set to zero to avoid the artificial increase of rigidity.



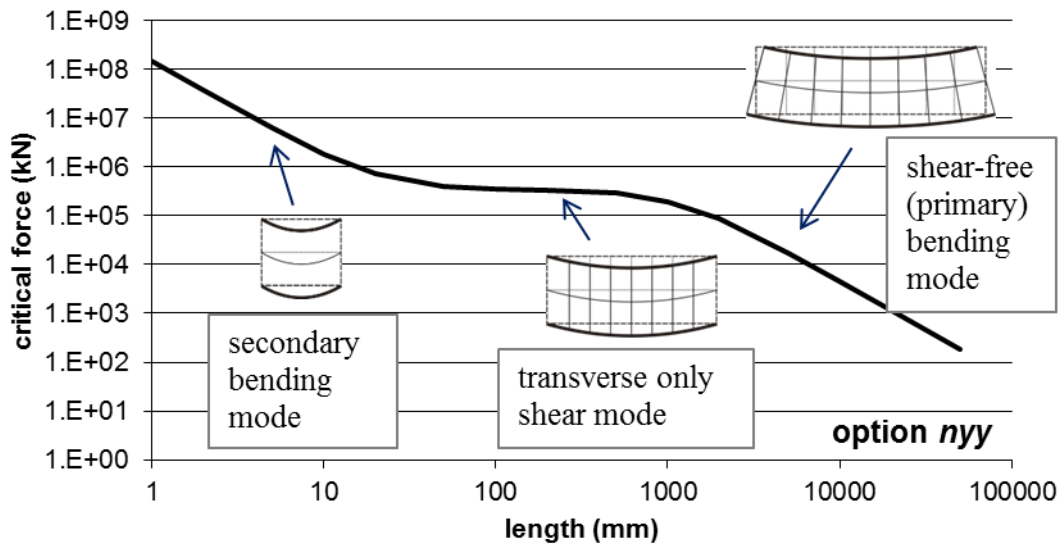
**Figure 5.6:** Illustration of critical forces and buckling modes in *nnn* option

### 5.3.5.2 Option *nyy*

In case of *nyy* option only one single critical force exists, as illustrated in **Figure 5.7**. The critical force and also the deformation is combined from three components: (i) the classical shear-free (primary) flexural mode, (ii) the transverse-only shear mode, and (iii) a secondary bending mode. The first two modes are identical to those found in option *nnn*. As far as primary and secondary bending modes are concerned, both are pure bending modes, however, in the primary mode the flexural rigidity is calculated with neglecting the own plate inertias (i.e., the  $bt^3/12$  terms), while in the secondary mode only the own plate inertias are considered in the rigidity. In most of practical thin-walled sections the secondary terms are small and are frequently neglected.

The formula of Eq (5.48) is a combination of two summation formulae: the primary bending mode and the pure shear mode is combined according to Dunkerley summation formula, while the secondary bending term is simply added to the combined effect of the two others, as it is the case in Southwell summation, see [9/5]. The secondary bending mode has little effect unless the column is extremely short (**Figure 5.7**), or the shear rigidity is very low.

It might be interesting to mention that if the shear rigidity is infinitely large, the formula tends to the classical Euler-formula. It is still slightly different from option *nnn*, however, since in option *nyy* the classical solution includes bending rigidity with considering the own plate inertias (i.e., includes the effect of secondary rigidity).



**Figure 5.7:** Illustration of critical forces and buckling modes in *nyy* option

### 5.3.5.3 Option *ynn*

In case of *ynn* option there are two or three critical forces. One is  $F_a$  which belongs to so-called axial mode. The other one or two critical values can be calculated by solving the equation from Eq. (5.49):

$$F^2 \frac{F_{X,r}}{F_a} - F \left( F_{X,r} + F_{s,Z} + \frac{F_{X,r} F_{s,Z}}{F_a} \right) + F_{X,r} F_{s,Z} = 0 \quad (5.50)$$

If none of  $F_{X,r}$  and  $F_{s,Z}$  is zero, the equation has two distinct real positive roots. However, if any of them zero (which might be a practical case), there is only one critical solution.

Let us explore the tendencies at extreme length values. If  $L \rightarrow 0$ , then  $1/F_{X,r} \cong 0$ , which leads to two critical forces as follows:

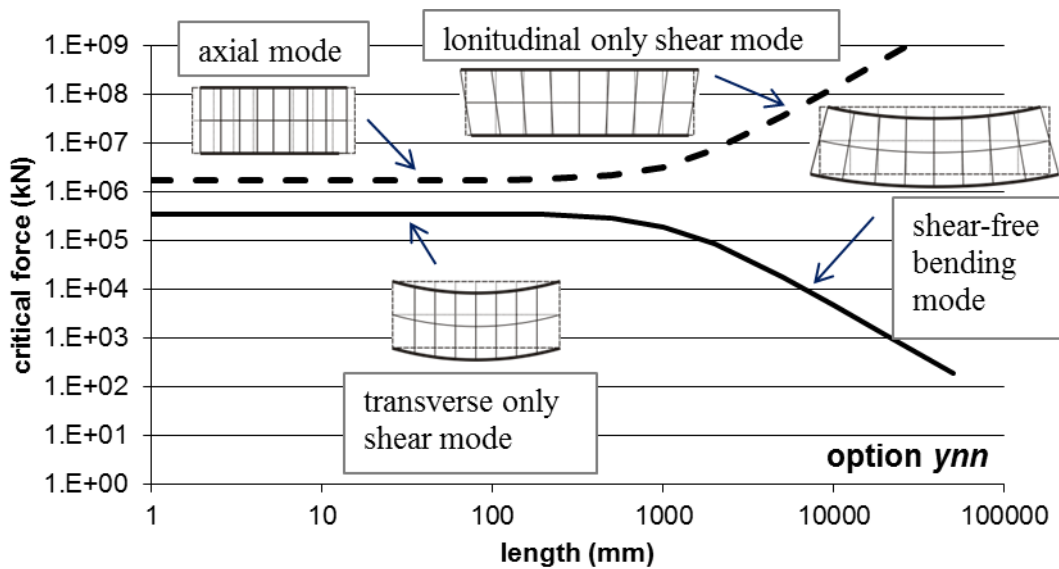
$$F_{cr,X}^{ynn} = F_a \text{ and } F_{cr,X}^{ynn} = F_{s,Z} \quad (5.51)$$

In case of any regular material  $F_{s,Z} < F_a$ , therefore the smaller critical force tends to  $F_{s,Z}$  as  $L$  approaches zero.

In case of large  $L$ -s it is fair to assume that  $1/F_a$  and  $1/F_{s,Z}$  are negligible small compared to  $1/F_{X,r}$ , from which two critical forces can be found:

$$F_{cr,X}^{ynn} \cong F_{X,r} \text{ and } F_{cr,X}^{ynn} \cong \frac{F_{s,Z} F_a}{F_{X,r}} \quad (5.52)$$

It means that in the *ynn* option four buckling modes are involved, though only two appear in the mode that belongs to the lowest eigen-value, as shown in **Figure 5.8**.

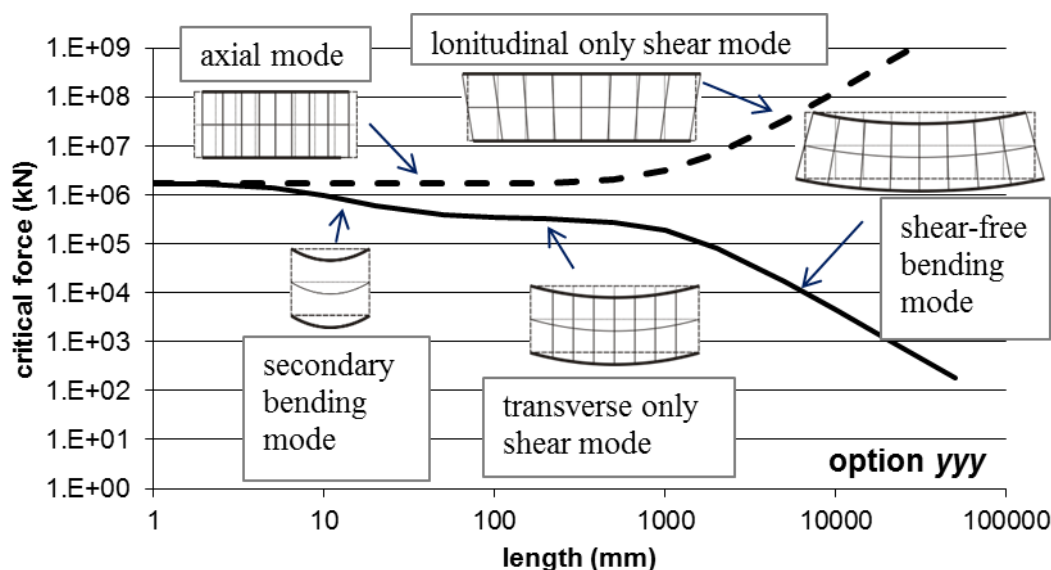


**Figure 5.8:** Illustration of critical forces and buckling modes in *ynn* option

#### 5.3.5.4 Option yyy

In case of *yyy* option, three critical forces can always be found. Altogether 5 buckling modes are involved, i.e., all the 5 modes that appear in other options. The modes and tendencies are demonstrated in **Figure 5.9**. As it can be seen from the figure (and can also be proved mathematically), all the three critical forces tend to  $F_a$  as  $L$  approaches zero. On the other hand, three distinct critical forces are found for large  $L$ -s, namely (in ascending order):

$$F_{cr,X}^{yyy} \cong F_{X,r}, \quad F_{cr,X}^{yyy} = F_a, \text{ and } F_{cr,X}^{yyy} \cong \frac{F_{s,Z} F_a}{F_{X,r}} \quad (5.53)$$



**Figure 5.9:** Illustration of critical forces and buckling modes in yyy option

### 5.3.6 Demonstrative numerical examples

In this Section some numerical examples are presented. First, the newly derived analytical formulae are verified by comparing the analytical results to other methods, namely: cFSM and shell FEM. In the second part of the numerical examples the effect of the various options of the analytical formulae are addressed and discussed.

Flexural buckling of simple two-hinged columns are considered, and critical force values are calculated and compared. The cross-sections are I-1 and I-2, as shown in **Figure 5.4**. Two materials are considered. ‘Mat1’ is basically a regular steel material, with  $E = 210\,000$  MPa. ‘Mat1’ is assumed to be isotropic, however, the Poisson’s ratio is set to zero in order to eliminate the (unrealistic) stiffness increasing caused by the  $1/(1-\nu^2)$  term in the critical force formulae. ‘Mat2’ is an orthotropic material, with  $E = 210\,000$  MPa, but with  $G = 2100$  MPa, which is  $1/50$  of the shear modulus of an equivalent isotropic material. Both major-axis and minor-axis buckling are considered. All the 8 options (according to Table 1) are briefly discussed here, though the focus is on the consistent options. The shell FEM results are obtained by carefully applied restraints, see [4/5].

**Table 5.10** and **5.11** summarize the results of comparison of various calculation methods. The effect of various options of the analytical formulae are also presented in Figures 5.10 and 5.11. It is to highlight that the yny option is used in the analytical results, since earlier studies proved that cFSM and the applied shell FEM follows assumptions identical to those of option yny. In all the cases primary shear deformation is assumed, i.e., the cross-sections planes remain planes during the deformations. As it can be seen the cFSM and analytical results are practically identical, the relative differences between them being less than  $10^{-6}$ . The differences between FEM and the analytical results are somewhat larger, but still very small, practically negligible, the maximal difference being less than 0.1%. It is also to highlight that the very good coincidence is obtained not only for usual steel sections, but for unusual sections with unusual material properties, too.

**Table 5.10** and **Figure 5.10** show results for a regular I section (I-1) with regular steel material. The main conclusion is that though differences exist between the various calculation



options, the differences are pronounced only for extremely short (theoretical) lengths, therefore the selection of option has negligible effect for typical length ranges.

In **Table 5.11** and **Figure 5.11** results for a (very) narrow I section (I-2) made of low shear rigidity material are shown. This section is characterized by relatively large secondary bending stiffness compared to the primary bending stiffness (especially in minor-axis bending). Therefore, there is a visible difference between  $\times \times n$  and  $\times \times y$  options even for regular steel material, which are enlarged if the material is orthotropic with low shear rigidity (**Figure 5.11**). It is to observe that non-negligible differences might exist in these cases even in the range of column lengths of practical interest.

**Table 5.10:** Comparison of various calculation methods for I-1

length	mm	20	200	2000	20000	buckl. mode
formula, yny	kN	731 282	340 161	83 600.3	1 150.65	I-1
cFSM	kN	731 282	340 161	83 600.3	1 150.65	Mat1
FEM	kN	731 028	340 109	83 602.5	1 150.67	major-axis
formula, yny	kN	610 579	270 921	6 694.64	68.0866	I-1
cFSM	kN	610 579	270 921	6 694.64	68.0866	Mat1
FEM	kN	610 138	270 963	6 694.98	68.1079	major-axis

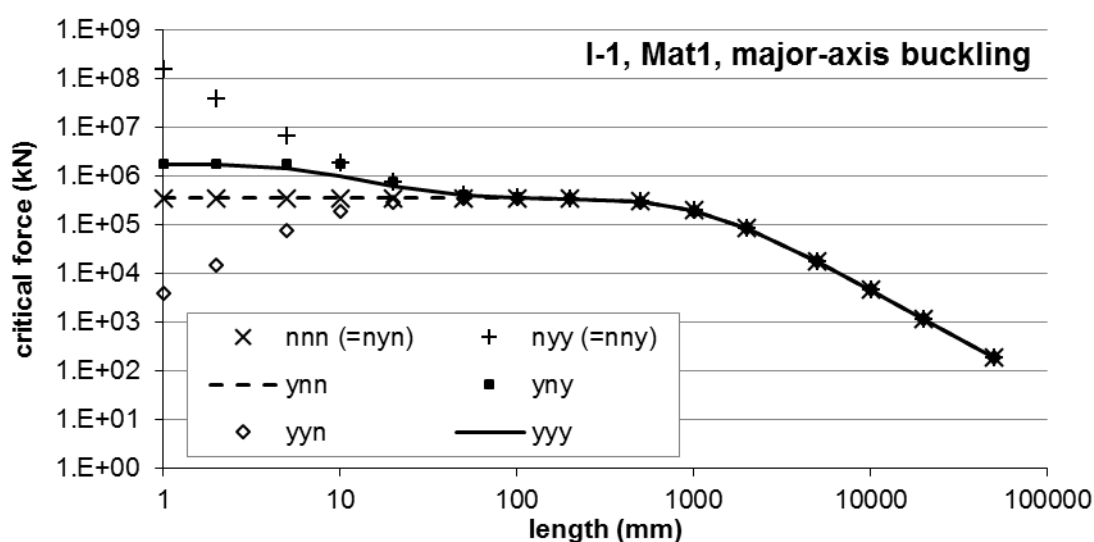
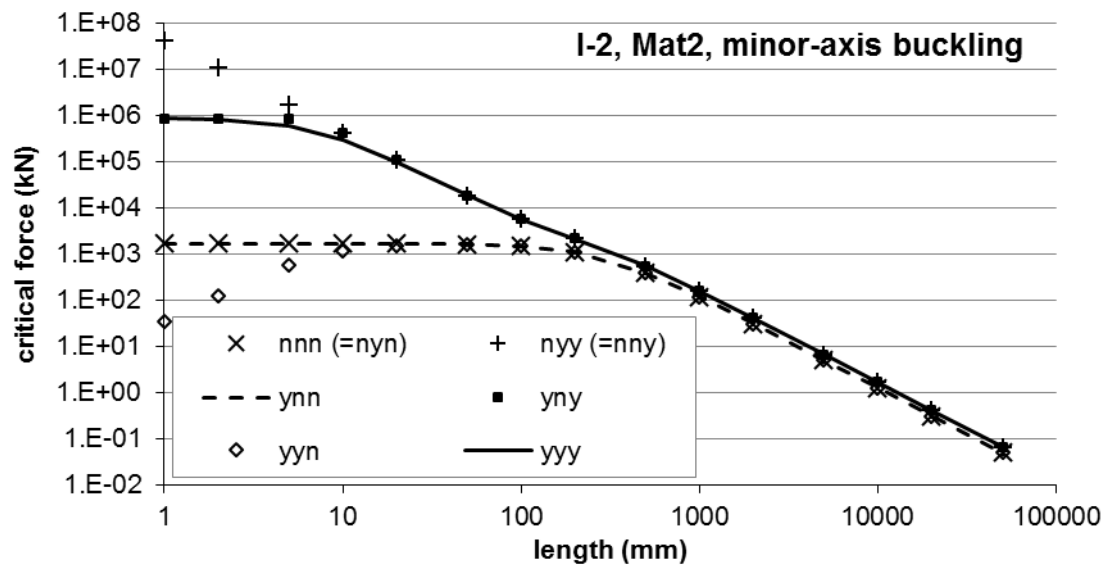


Figure 5.10: Major-axis buckling critical forces for the I-1 section in various options (Mat1)

**Table 5.11:** Comparison of various calculation methods for I-2

length	mm	10	100	1000	10000	buckl. mode
formula, yny	kN	261 951	9 526.58	6 689.90	1 223.03	I-2
cFSM	kN	261 951	9 526.58	6 689.90	1 223.03	Mat2
FEM	kN	262 274	9 526.48	6 689.88	1 223.04	major-axis
formula, yny	kN	426 299	5 743.39	159.674	1.68278	I-2
cFSM	kN	426 299	5 743.39	159.674	1.68278	Mat2
FEM	kN	425 959	5 742.84	159.678	1.68286	minor-axis



**Figure 5.11:** Minor-axis buckling critical forces for the I-2 section in various options (Mat2)

Thus, it can be concluded that the tendency of the critical force vs. buckling length curve is defined by the selected option, as well as the ratio of the participating stiffnesses. In case of regular cross-sections with isotropic material, there is little difference between the various options at least in the length range of practical interest. In these cases the effect of shear deformations is small, too. If the stiffness ratios are distinctly different from those of regular steel sections, (due to irregular cross-section shape and/or low shear rigidity material,) the tendencies might be different, as well as the differences between the various calculation options might be enlarged. In these cases the effect of shear deformations themselves might be more pronounced and non-negligible even for practical member lengths.

## 5.4 Summary and continuation of the work

In this Chapter new analytical formulae for the critical forces to column buckling are presented. The novelty of the analytical formulae is that they are based on shell model, i.e., the thin-walled member is modelled as a set of connected strips. As it was shown, the derivations can be completed in various options, depending on how the through-thickness variation of strains/stresses is considered and depending on how the second-order strain is defined. Formulae are derived with neglecting and also with considering in-plane shear deformations. The obtained formulae are discussed by theoretical considerations and validated by numerical studies. (See Thesis #4 in Chapter 6.)

Here, only buckling of shear-free columns, and flexural buckling of shear-deformable columns are presented, but some further results can be found in papers. In [12/5] formulae for the lateral-torsional buckling of doubly-symmetrical shear-free beams are presented. In [13/5] pure torsional buckling of shear-deformable columns are discussed and analytical formulae are derived for open and closed cross-sections. All these derivations are based on shell-model assumptions, unlike other solutions that are based on beam model (see, e.g. [14/5-15/5]). Obviously, further, practically interesting cases could be investigated (e.g., lateral-torsional buckling of mono-symmetrical cross-section beams, or, flexural-torsional buckling of shear-deformable columns, etc.). These cases are planned to analyse in the future.

## 6 Summary of the new scientific results

This dissertation summarizes the Author's scientific results from the period 2003-2014. The work started with the development of the constrained finite strip method, then continued in other closely related directions, partly by the Author, partly by other researchers. Naturally, this dissertation concentrates on those results which have been achieved with the primary contribution from the Author, while other results are just tangentially mentioned. Based on the achieved results, theses are formed as follows.

**Thesis #1:** I, together with Benjamin W. Schafer, have worked out the constrained finite strip method (cFSM) for the linear buckling analysis of thin-walled members with open, flat-walled cross-sections and pinned-pinned end restraints. [1/2-8/2]

The results in which my contribution is dominant are as follows:

- a) I have defined the mechanical criteria for the global, distortional and local buckling mode spaces.
- b) I have derived the constraint matrices for the global, distortional, local and other mode spaces, by implementing the mechanical criteria into the semi-analytical finite strip base functions.

**Thesis #2:** I have extended the constrained finite strip method for the linear buckling analysis of members with arbitrary flat-walled cross-sections, with considering various end restraints. [1/3-5/3]

The new results are detailed as follows:

- a) I have proposed decomposition within the local, shear and transverse extension mode spaces. I have given the mechanical description for the proposed sub-spaces.
- b) I have proposed base vectors for the shear mode spaces.
- c) I have derived the constraint matrices for all the sub-spaces.
- d) I have proposed a way for the orthogonalization and ordering of the base vectors within any sub-space, which leads to a practically meaningful set of base vectors that are independent of the longitudinal shape functions of the FSM.

**Thesis #3:** I have worked out a method for the modal identification of the displacement field of flat-walled members, if the displacements are calculated by shell finite element analysis. [1/4-2/4]

The new results are detailed as follows:

- a) I have derived the formulae necessary for the modal identification.
- b) I have proposed a measure for the accuracy of the modal identification.
- c) I have proposed a way for the reduction of the equation system to be solved, which makes the modal identification procedure computationally more efficient.

**Thesis #4:** I have derived shell-model-based analytical formulae for the calculation of the critical force of columns. [1/5-5/5]

The new results are detailed as follows:

- a) I have derived the formulae for flexural buckling, torsional buckling, and flexural torsional buckling of shear-undeformable thin-walled two-hinged columns.
- b) I have derived the formulae for flexural buckling of shear-deformable thin-walled two-hinged columns, considering in-plane shear deformations of the plate elements.
- c) I have shown how some assumptions of the derivation influence the critical load results.

## Acknowledgements

The work presented in this dissertation has been conducted at the Budapest University of Technology and Economics and also at the Johns Hopkins University (Baltimore, Maryland, USA) where the Author has spent two academic years during the period covered by this dissertation.

The work has been financially supported by various funds, namely:

- the Korányi Imre Scholarship of the Thomas Cholnoky Foundation,
- the János Bolyai Research Scholarship of the Hungarian Academy of Sciences.
- Tét Port-5/2005 project of the Hungarian-Portuguese Intergovernmental Science and Technology Cooperation Program,
- OTKA K049305 project of the Hungarian Scientific Research Fund,
- OTKA K062970 project of the Hungarian Scientific Research Fund,
- Senior Leaders and Scholars Fellowship program of The Hungarian American Enterprise Scholarship Fund.

The financial support of all these programs is gratefully acknowledged.

The presented work has been completed with supports from other persons, out of which three are named here:

- prof. Ben Schafer, a great colleague and friend, and an excellent host during my two longer (and multiple shorter) stays at Johns Hopkins University, who provided helps in many ways, and collaborated in developing the constrained finite strip method,
- Dávid Visy, my former PhD student, who had major role in performing shell finite element analyses the results of which are used also in this dissertation,
- Attila L. Joó, who – among multiple common projects – collaborated in verifying and extending the mode identification method and who had valuable contribution in solving various shell finite element analysis problems.

The help of all these named and other unnamed persons is gratefully acknowledged.

## References

The referenced publications are listed, as follows. They are grouped in accordance with the Chapter in which they appear first. This list includes the relevant publications from the Author, too. Those publications on the basis of which new scientific results are declared (see Chapter 6) are **highlighted**.

### Chapter 1

- [1/1] CEN, EN 1993-1-1:2005 - Eurocode 3: Design of steel structures - Part 1-1: General rules and rules for buildings, European Committee for Standardization, Brussels, Belgium, 2005.
- [2/1] CEN, EN 1993-1-3:2006 - Eurocode 3: Design of steel structures - Part 1-3: General rules, Supplementary rules for cold-formed members and sheeting, European Committee for Standardization, Brussels, Belgium, 2006.
- [3/1] CEN, EN 1993-1-5:2006 - Eurocode 3: Design of steel structures - Part 1-5: Plated structural elements, European Committee for Standardization, Brussels, Belgium, 2006.
- [4/1] CEN, EN 1993-1-6:2007 - Eurocode 3: Design of steel structures - Part 1-6: General rules - Strength and stability of shell structures, European Committee for Standardization, Brussels, Belgium, 2007.
- [5/1] NAS, North American specification for the design of cold-formed steel structural members. 2007 ed. Washington DC, USA, American Iron and Steel Institute, 2007.
- [6/1] Standards Australia, AS/NZS 4600 Cold-Formed Steel Structures (2005).
- [7/1] DSM (2006), American Iron and Steel Institute. Direct strength method design guide. Washington, DC, USA, 2006.
- [8/1] ANSYS Inc., ANSYS Mechanical, Release 17.1.
- [9/1] Cheung Y.K. (1968), "Finite strip method in the analysis of elastic plates with two opposite ends simply supported", *Proc Inst Civ Eng*, 40, 1-7, 1968.
- [10/1] Cheung Y.K. (1977), "Finite strip method in structural analysis", Pergamon Press, 1976.
- [11/1] Cheung Y.K., Tham L.G., (1997), *The Finite Strip Method*. CRC.
- [12/1] Hancock, G.J. (1978), "Local, Distortional, and lateral buckling of I-beams", *ASCE Journal of structural engineering*, 104(11), pp. 1787-1798.
- [13/1] Papangelis, J.P., Hancock, G.J. (1995). "Computer analysis of thin-walled structural members." *Computers & Structures*, 56(1)157-176.
- [14/1] THIN-WALL (1995), School of Civil Engineering, University of Sydney, Sydney, Australia, 1995.
- [15/1] THIN-WALL (2006): A computer program for cross-section analysis and finite strip buckling analysis and direct strength design of thin-walled structures, Version 2.1, School of Civil Engineering, University of Sydney, Sydney, Australia, 2006.
- [16/1] Schafer, B.W. (1997), "Cold-Formed Steel Behavior and Design: Analytical and Numerical Modeling of Elements and Members with Longitudinal Stiffeners", *Ph.D. Dissertation*, Cornell University, Ithaca, NY, USA.
- [17/1] CUFSM (2006): Elastic Buckling Analysis of Thin-Walled Members by Finite Strip Analysis. CUFSM v3.12, <http://www.ce.jhu.edu/bschafer/cufsm>
- [18/1] CUFSM (2012): Elastic Buckling Analysis of Thin-Walled Members by Finite Strip Analysis. CUFSM v4.05, <http://www.ce.jhu.edu/bschafer/cufsm>

- [19/1] Schardt, R. (1989), „Verallgemeinerte Technische Biegetheorie“, Springer Verlag, Berlin, Heidelberg, 1989.
- [20/1] Davies, J.M., Leach, P. (1994). “First-order generalised beam theory.” *J. of Constructional Steel Research*, 31(2-3), pp. 187-220.
- [21/1] Davies, J.M., Leach, P., Heinz, D. (1994). “Second-order generalised beam theory.” *J. of Constructional Steel Research*, 31(2-3), pp. 221-241.
- [22/1] Silvestre, N., Camotim, D. (2002a). “First-order generalised beam theory for arbitrary orthotropic materials.” *Thin-Walled Structures*, 40(9), pp. 755-789.
- [23/1] Silvestre, N., Camotim, D. (2002b). “Second-order generalised beam theory for arbitrary orthotropic materials.” *Thin-Walled Structures*, 40(9), pp. 791-820.
- [24/1] Silvestre, N., Camotim, D. (2003). “Nonlinear Generalized Beam Theory for Cold-formed Steel Members.” *International Journal of Structural Stability and Dynamics*. 3(4) pp. 461-490.
- [25/1] Dinis P. B., Camotim D., Silvestre N. (2006), „GBT formulation to analyse the buckling behaviour of thin-walled members with arbitrarily ‘branched’ open cross-sections”, *Thin-Walled Structures*, vol 44(1), January 2006, pp. 20-38.
- [26/1] Gonçalves R., Ritto-Corrêa M., Camotim D. (2010), “A new approach to the calculation of cross-section deformation modes in the framework of generalized beam theory”, *Computational Mechanics*, 46(5), 2010, pp. 759-781.
- [27/1] Silvestre N., Camotim D., Silva N.F. (2011), „Generalized Beam Theory revisited: from the kinematical assumptions to the deformation mode determination”, *Int. Journal of Structural Stability and Dynamics*, 11(5), Oct 2011, pp. 969-997.
- [28/1] Bebiano R., Gonçalves R., Camotim D. (2015), „A cross-section analysis procedure to rationalise and automate the performance of GBT-based structural analyses”, *Thin-Walled Structures*, vol 92, July 2015, pp. 29-47.
- [29/1] GBTUL (2008): Buckling and Vibration Analysis of Thin-Walled Members. GBTUL 1.0β. DECivil/IST, 2008. Technical University of Lisbon (<http://www.civil.ist.utl.pt/gbt>)
- [30/1] GBTUL 2.0 (2013): Buckling and Vibration Analysis of Thin-Walled Members. DECivil/IST, 2013. Technical University of Lisbon (<http://www.civil.ist.utl.pt/gbt>)

## Chapter 2

- [1/2] Ádány, S. (2004), „Buckling mode classification of members with open thin-walled cross-sections by using the Finite Strip Method”, *Research Report*, Johns Hopkins University, 2004. (at <http://www.ce.jhu.edu/bschafer>)
- [2/2] Ádány, S., Schafer, B.W. (2004), „Buckling Mode Classification of Members with open Thin-Walled Cross-Sections”, *Proceedings of the Fourth International Conference on Coupled Instabilities in Metal Structures (CIMS '04)*, Rome, Italy, Sept 27-29, 2004, pp. 467-476.
- [3/2] Schafer, B.W., Ádány, S. (2006), „Understanding and classifying local, distortional and global buckling in open thin-walled members”, *Proceedings of the Annual Technical Session and Meeting, Structural Stability Research Council*, Montreal, Quebec, Canada, May 2005, pp 27-46.
- [4/2] Ádány, S., Schafer, B.W. (2006), „Buckling mode decomposition of unbranched open cross-section members via Finite Strip Method: derivation”, *Thin-Walled Structures* 44(5), pp. 563-584.
- [5/2] Ádány, S., Schafer, B.W. (2006), „Buckling mode decomposition of unbranched open cross-section members via Finite Strip Method: application and examples”, *Thin-Walled Structures*, 44(5), pp. 585-600.

- [6/2] Schafer, B.W., Ádány, S. (2006), „Modal decomposition for thin-walled member stability using the finite strip method”, *Proceedings of the Conference on Advances in Engineering Structures, Mechanics and Construction*, May 14-17, 2006, Waterloo, Canada.
- [7/2] Schafer B.W., Ádány S. (2006), “Buckling analysis of cold-formed steel members using CUFSM: conventional and constrained finite strip methods”, *Proceedings of 18th International Specialty Conference on Cold-Formed Steel Structures*, October 26-28, 2006, Orlando, USA, pp. 39-54.
- [8/2] Ádány, S., Schafer, B.W. (2008), “A full modal decomposition of thin-walled, unbranched open cross-section members via the constrained finite strip method”, *Journal of Constructional Steel Research*, 64 (1), pp. 12-29.
- [9/2] Mathworks: Matlab, <http://www.mathworks.com>
- [10/2] Li, Z., Hanna, M.T., Ádány, S., Schafer, B.W. (2011), "Impact of basis, orthogonalization, and normalization on the constrained Finite Strip Method for stability solutions of open thin-walled members", *Thin-Walled Structures*, vol. 49, no. 9, pp. 1108-1122.
- [11/2] Ádány, S., Silvestre, N., Schafer, B.W., Camotim, D. (2006), “Buckling Analysis of Unbranched Thin-Walled Columns: Generalised Beam Theory vs. Constrained Finite Strip Method”, *Proceedings of the III European Conference on Computational Mechanics (ECCM 2006)*, June 5-8, 2006, Lisbon, Portugal. (available on CD-ROM)
- [12/2] Ádány S., Silvestre N., Schafer B.W. and Camotim D. (2006), “Buckling analysis of unbranched thin-walled members using cFSM and GBT: a comparative study”, *Proceedings of International Colloquium on Stability and Ductility of Steel Structures* (eds: D. Camotim, N. Silvestre, P.B. Dinis), September 6-8, 2006, Lisbon, Portugal, pp. 205-212.
- [13/2] Ádány, S., Silvestre, N., Schafer, B.W., Camotim, D. (2007), “On the Identification and Characterisation of Local, Distortional and Global Buckling Modes in Thin-Walled Members Using the cFSM and GBT Approaches”, *Proceedings of the 6th International Conference on Steel and Aluminium Structures (ICSAS 2007)*, July 24-27, 2007, Oxford, UK, pp. 760-767.
- [14/2] Ádány, S., Silvestre, N., Schafer, B.W., Camotim, D. (2009), “GBT and cFSM: two modal approaches to the buckling analysis of unbranched thin-walled members”, *Int. Journal Advanced Steel Construction*, Vol. 5, No. 2, pp. 195-223.
- [15/2] Li, Z., Schafer B.W. (2009), „Finite Strip Stability Solutions for General Boundary Conditions and the Extension of the Constrained Finite Strip Method”, in *Trends in Civil and Structural Engineering Computing*. 2009. Stirlingshire, UK: Saxe-Coburg Publications.
- [16/2] Li, Z., Schafer, B.W. (2010), "The constrained finite strip method for general end boundary conditions", *SSRC 2010 - Proceedings*, Structural Stability Research Council - Annual Stability Conference, pp. 573.
- [17/2] Li, Z., Schafer, B.W. (2010), "Buckling analysis of cold-formed steel members with general boundary conditions using CUFSM: Conventional and constrained finite strip methods", *Proceedings of the 20th International Specialty Conference on Cold-Formed Steel Structures - Recent Research and Developments in Cold-Formed Steel Design and Construction*, pp. 17.
- [18/2] Li, Z. (2011), „Finite strip modeling of thin-walled members”, *Phd Dissertation*, Johns Hopkins University, Baltimore, MD, USA, p. 240.
- [19/2] Djafour M., Djafour N., Megnounif A., Kerdal D.E. (2010), „A constrained finite strip method for open and closed cross-section members”, *Thin-Walled Structures*, 48(12), Dec 2010, pp. 955-965.

- [20/2] Djafour N., Djafour M., Megnounif A., Matallah M., Zendagui D. (2011), „A constrained finite strip method for prismatic members with branches and/or closed parts”, *Proceedings of the 6th International Conference on Thin-Walled Structures*, 5-7 Sept, 2011, Timisoara, Romania (eds: D Dubina, V Ungueranu), pp. 173-180.
- [21/2] Djafour N., Djafour M., Megnounif A., Matallah M., Zendagui D.: „A constrained finite strip method for prismatic members with branches and/or closed parts”, *Thin-Walled Structures*, Vol 61, Dec 2012, pp 42-48.
- [22/2] Djafour M., Dib H., Djelli M., Djafour N., Matallah M., Zendagui D. (2012), „Buckling Mode Decomposition of Thin-Walled Members using a Constrained Spline Finite Strip Method”, *Proceeding of the 6<sup>th</sup> International Conference on Coupled Instabilities in Metal Structures*, Glasgow, Scotland, Dec 3-5, 2012. (Eds: J Loughlan, D H Nash, J Rhodes), pp 467-474.
- [23/2] Casafont M., Marimon F., Pastor M.M.: „Combined GBT-FEM procedure for the determination of pure distortional buckling loads”, *Proceedings of the Fifth International Conference on Coupled Instabilities in Metal Structures (CIMS 2008)*, June 23-25, 2008, Sydney, Australia, pp. 273-280. (in Vol 1
- [24/2] Casafont M., Marimon F., Pastor M.M.: „Calculation of pure distortional elastic buckling loads of members subjected to compression via the finite element method”, *Thin-Walled Structures*, 47(6-7), June-July 2009, pp. 701-729.
- [25/2] Casafont M., Marimon F., Pastor M.M., Ferrer M.: „Linear buckling analysis of thin-walled members combining the Generalised Beam Theory and the Finite Element Method”, *Computers and Structures*, 89(21-22), Nov 2011, pp. 1982-2000.
- [26/2] Ádány, S., Beregszászi, Z. (2008), “Local and Distortional Buckling of Thin-Walled Members: Numerical Study to Compare Conventional and Constrained Finite Strip Method”, *Proceedings of the Fifth International Conference on Thin-Walled Structures (ICTWS 2008)*, June 18-20, 2008, Brisbane, Australia, pp. 1121-1128. (in Vol 2)
- [27/2] Ádány, S., Beregszászi, Z. (2008), “The Effect of Mode Coupling on the Design Buckling Resistance of Cold-Formed Members Calculated via the Direct Strength Method”, *Proceedings of the Eurosteel 2008 Conference (Eurosteel 2008)*, Sept 3-5, 2008, Graz, Austria, pp. 117-122. (in Vol A)
- [28/2] Beregszászi Z., Ádány S. (2009), “The effect of rounded corners of cold-formed steel members in the buckling analysis via the direct strength method“, *The Twelfth International Conference on Civil, Structural and Environmental Engineering Computing*, Funchal, Madeira, Portugal, 1-4 Sept, 2009. (paper #36 on CD-ROM, p. 14)
- [29/2] Beregszászi Z., Ádány S. (2011), „Application of the constrained finite strip method for the buckling design of cold-formed steel members via the direct strength method” *Computers and Structures*, 89 (2011), pp. 2020-2027.
- [30/2] Ádány S, Beregszászi Z. (2014), “Constrained finite strip method for thin-walled members with rounded corners”, *Proceedings of the 7th European Conference on Steel and Composite Structures, Eurosteel 2014*, (eds: R. Landolfo, F. Mazzolani) Sept 10-12, 2014. Napoli, Italy, #405, p. 6.
- [31/2] Ádány S, Beregszászi Z. (2015), “Modal Decomposition for Thin-walled Members with Rounded Corners: an Extension to cFSM by using Elastic Corner Elements”, *Proceedings of the Eighth International Conference on Advances in Steel Structures*, July 22-24, 2015, Lisbon, Portugal, p. 13.
- [32/2] Zeinoddini, V., Schafer, B.W. (2010), "Impact of corner radius on cold-formed steel member strength", *Proceeding of the 20th International Specialty Conference on Cold-*



- Formed Steel Structures - Recent Research and Developments in Cold-Formed Steel Design and Construction, pp. 1.
- [33/2] Li, Z., Schafer, B.W. (2010), "Application of the finite strip method in cold-formed steel member design", *Journal of Constructional Steel Research*, vol. 66, no. 8-9, pp. 971-980.
- [34/2] Gilbert, B.P., Savoyat, T.J.-M., Teh, L.H. (2012). "Self-shape optimisation of cold-formed steel columns", *Proceedings of the 21st International Specialty Conference on Cold-Formed Steel Structures - Recent Research and Developments in Cold-Formed Steel Design and Construction*, Saint Louis, Missouri, USA, Oct 24-25, 2012, (Eds: R A LaBoube, W W Yu), pp. 75-89.
- [35/2] Gilbert, B.P., Teh, L.H., Guan, H. (2012), "Self-shape optimisation principles: Optimisation of section capacity for thin-walled profiles". *Thin-Walled Structures*, vol 60, pp. 194-204.
- [36/2] Gilbert, B.P., Savoyat, T.J.-M., Teh, L.H. (2012). "Self-shape optimisation application: Optimisation of cold-formed steel columns". *Thin-Walled Structures*, vol 60, pp. 173-184.
- [37/2] Wang, B., Bosco G.L., Gilbert, B.P., Guan, H., Teh, L.H. (2016), "Unconstrained shape optimisation of singly-symmetric and open cold-formed steel beams and beam-columns". *Thin-Walled Structures*, vol 104, pp. 54-61.
- [38/2] Wang, B., Gilbert, B.P., Guan, H., Teh, L.H. (2016), "Unconstrained shape optimisation of singly-symmetric and open cold-formed steel beams and beam-columns". *Thin-Walled Structures*, vol 109, pp. 271-284.
- [39/2] Moharrami, M., Louhghalam, A., Tootkaboni M. (2014), "Optimal folding of cold formed steel cross sections under compression". *Thin-Walled Structures*, vol 76, pp. 145-156.
- [40/2] Zeinoddini, V.M., Schafer, B.W. (2012), "Simulation of geometric imperfections in cold-formed steel members", *Structural Stability Research Council Annual Stability Conference 2012*, pp. 567.
- [41/2] Zeinoddini, V.M., Schafer, B.W. (2012), "Simulation of geometric imperfections in cold-formed steel members using spectral representation approach", *Thin-Walled Structures*, vol. 60, pp. 105-117.

### Chapter 3

- [1/3] Ádány S. (2012), "Decomposition of Shear Modes in Constrained Finite Strip Method", *Proceeding of the 6<sup>th</sup> International Conference on Coupled Instabilities in Metal Structures*, Glasgow, Scotland, Dec 3-5, 2012. (Eds: J Loughlan, D H Nash, J Rhodes), pp 483-490.
- [2/3] Ádány S. (2013), "Decomposition of in-plane shear in thin-walled members", *Thin-Walled Structures*, vol. 73, pp. 27-38.
- [3/3] Li Z., Batista Abreu J. C., Leng J., Ádány S., Schafer B. W. (2013), "Review: Constrained Finite Strip Method Developments and Applications in Cold-formed Steel Design", *Thin-Walled Structures*, vol 81, pp. 2-18.
- [4/3] Ádány S., Schafer B. W. (2014), "Generalized constrained Finite Strip Method for thin-walled members with arbitrary cross-section: primary modes", *Thin-Walled Structures*, vol. 84, pp. 150-169.
- [5/3] Ádány S, Schafer B W (2014), "Generalized constrained finite strip method for thin-walled members with arbitrary cross-section: Secondary modes, orthogonality, examples", *Thin-Walled Structures*, vol. 84: pp. 123-133.

- [6/3] Visy D., **Ádány S.** (2014), “Local stiffness matrices for the semi-analytical Finite Strip Method in case of various boundary conditions”, *Periodica Polytechnica ser. Civil Engineering* Vol 58(3), pp. 187-201.
- [7/3] **Ádány S.**, Schafer B. (2014), “Constrained Finite Strip Method Stability Analysis of Thin-walled Members with Arbitrary Cross-section”, *Proceedings of the Annual Stability Conference of the Structural Stability Research Council*, March 25-28, 2014, St. Louis, USA, pp. 346-365.
- [8/3] **Ádány S.**, Schafer B. W. (2014), “Modal decomposition for thin-walled column and beam members with arbitrary cross-sections”, *Proceedings of the 7th European Conference on Steel and Composite Structures*, Eurosteel 2014, (eds: R. Landolfo, F. Mazzolani) Sept 10-12, 2014. Napoli, Italy, #407, p. 6.
- [9/3] **Ádány S.** (2014), “Constrained finite element method: demonstrative examples on the global modes of thin-walled members”, *Proceedings of the 22nd International Speciality Conference on Cold-Formed Steel Structures: Recent research and developments in cold-formed steel design and construction* (eds: R. LaBoube, W.W. Yu), Nov 5-6, 2014, St. Louis, USA, pp. 67-82.
- [10/3] **Ádány S.** (2016), “Shell element for constrained finite element analysis of thin-walled structural members”, *Thin-Walled Structures*, vol. 105, pp. 135-146.
- [11/3] **Ádány S.** (2016), “Constrained finite element method for the modal analysis of thin-walled members with holes”, *Proceedings of the Annual Stability Conference of the Structural Stability Research Council*, April 12-15, 2016, Orlando, USA, pp. 618-637.
- [12/3] **Ádány S.**, Visy D., Nagy R. (2016), “Buckling solutions for thin-walled members by using the constrained finite element method: demonstrative examples”, *Proceedings of the International Colloquium on Stability and Ductility of Steel Structures*, May 30-June 1, 2016, Temesvár, Románia, pp. 51-58.
- [13/3] **Ádány S.** (2016), „Understanding the buckling behavior of thin-walled members by using the constrained finite element methods”, *Proceedings of the 7th International Conference on Coupled Instabilities in Metal Structures*, Baltimore, USA, Nov 7-8, 2016, p. 20.
- [14/3] **Ádány S.** (2016), “Constrained finite element method for the analysis of shear buckling of thin-walled members”, *Proceedings of the 8th International Conference on Steel and Aluminium Structures* (eds: B. Young, Y. Cai), Dec 7-9, 2016, Hong Kong, p. 18.
- [15/3] Visy D., **Ádány S.**, “Local elastic and geometric stiffness matrices for the shell element applied in cFEM”, *Periodica Polytechnica ser. Civil Engineering*, In Press
- [16/3] **Ádány S.** (2017), “Constrained shell Finite Element Method for thin-walled members, Part 1: constraints for a single band of finite elements”, *Thin-Walled Structures*, In Press
- [17/3] **Ádány S.**, Visy D., Nagy R. (2017), “Constrained shell Finite Element Method for thin-walled members, Part 2: application to linear buckling analysis of thin-walled members”, *Thin-Walled Structures*, In Press
- [18/3] Rendall M.A., Hancock G.J., Rasmussen K.J.R. (2016), “Extension of the generalised constrained finite strip method to members under general loading including shear”, *Proceedings of the 7th International Conference on Coupled Instabilities in Metal Structures*, Baltimore, USA, Nov 7-8, 2016, p. 18.
- [19/3] Rendall M.A., Hancock G.J., Rasmussen K.J.R. (2016), “Modal participation for elastic buckling of polygonal tubes in torsion using the generalised cFSM”, *Proceedings of the 7th International Conference on Coupled Instabilities in Metal Structures*, Baltimore, USA, Nov 7-8, 2016, p. 14.

- [20/3] Rendall M.A., Hancock G.J., Rasmussen K.J.R. (2016), "Identifying shear buckling coefficients for channels with rectangular web stiffeners using the generalized cFSM", *Proceedings of the 22nd International Speciality Conference on Cold-Formed Steel Structures: Recent research and developments in cold-formed steel design and construction* (eds: R. LaBoube, W.W. Yu), Nov 5-6, 2014, St. Louis, USA, pp. 339-354.
- [21/3] Rendall M.A., Hancock G.J., Rasmussen K.J.R. (2016), "Modal analysis of lipped channel sections with rectangular web-stiffener in shear", *Proceedings of the 8th International Conference on Steel and Aluminium Structures* (eds: B. Young, Y. Cai), Dec 7-9, 2016, Hong Kong, p. 15.

## Chapter 4

- [1/4] Ádány S., Joó A. L., Schafer B.W. (2006), "Approximate identification of the buckling modes of thin-walled columns by using the cFSM modal base functions", *Proceedings of International Colloquium on Stability and Ductility of Steel Structures* (eds: D. Camotim, N. Silvestre, P.B. Dinis), September 6-8, 2006, Lisbon, Portugal, pp. 197-204.
- [2/4] Ádány S., Joó A. L., Schafer B.W. (2008), "Identification of FEM buckling modes of thin-walled columns by using cFSM base functions", *Proceedings of the Fifth International Conference on Coupled Instabilities in Metal Structures (CIMS 2008)*, June 23-25, 2008, Sydney, Australia, pp. 265-272.
- [3/4] Ádány S., Joó A. L., Schafer B. W. (2010), „Buckling Mode Identification of Thin-Walled Members by using cFSM Base Functions”, *Thin-Walled Structures*, 48(10-11), pp. 806-817.
- [4/4] Li Z., Joó A. L., Ádány S., Schafer B. W. (2011): "Modal identification for finite element models of thin-walled members", *Proceedings of the Sixth International Conference on Thin-Walled Structures (ICTWS 2011)*, Sept 5-7, 2011, Timisoara, Romania, (Eds. Dubina D & Ungureanu V., ISBN 978-92-9147-102-7, published by ECCS in Portugal), pp.189-196.
- [5/4] Joó A L, Ádány S. (2009), "FEM-based approach for the stability design of thin-walled members by using cFSM base functions", *Periodica Polytechnica ser. Civil Engineering*, Vol. 53, No. 2, pp. 61-74.
- [6/4] Li, Z., Joó, A.L., Ádány, S., Schafer, B.W. (2011), "Modal identification in nonlinear collapse analysis of thin-walled members", *Proceedings of the Structural Stability Research Council Annual Stability Conference 2011, ASC*, pp. 168.
- [7/4] Li Z., Ádány S., Schafer B. W. (2012), "Modal identification of cold-formed steel members in shell finite element models", *Proceedings of the 21st International Specialty Conference on Cold-Formed Steel Structures*, Saint Louis, Missouri, USA, Oct 24-25, 2012, (Eds: R A LaBoube, W W Yu) pp 1-16.
- [8/4] Li, Z., Ádány S., Schafer B.W. (2013), „Modal identification for shell finite element models of thin-walled members in nonlinear collapse analysis to thin-walled structures”, *Thin-Walled Structures*, vol 67, pp. 15-24.
- [9/4] Li, Z. (2016), „ Stochastic mode interaction of thin-walled cold-formed steel members using modal identification”, *Proceedings of the 7th International Conference on Coupled Instabilities in Metal Structures*, Baltimore, USA, Nov 7-8, 2016, p. 16.
- [10/4] Nedelcu, M. (2012), "GBT-based buckling mode decomposition from finite element analysis of thin-walled members", *Thin-Walled Structures*, vol. 54, pp. 156-163.
- [11/4] Nedelcu, M., Chira, N., Popa, A.G., Cucu, H.L. (2012), "GBT-based buckling mode identification from finite element analysis of thin-wal-led members", *ECCOMAS 2012*

- *European Congress on Computational Methods in Applied Sciences and Engineering, e-Book Full Papers*, pp. 1291.

- [12/4] Nedelcu, M., Cucu, H.L. (2012), „Buckling modes identification from FEA of thin-walled members using only GBT cross-sectional deformation modes”, *Proceeding of the 6<sup>th</sup> International Conference on Coupled Instabilities in Metal Structures*, Glasgow, Scotland, Dec 3-5, 2012. (Eds: J Loughlan, D H Nash, J Rhodes), pp 475-482.

## Chapter 5

- [1/5] Ádány S. (2006), “Flexural buckling of thin-walled columns: discussion on the definition and calculation”, *Proceedings of International Colloquium on Stability and Ductility of Steel Structures* (eds: D. Camotim, N. Silvestre, P.B. Dinis), September 6-8, 2006, Lisbon, Portugal, pp. 249-258.
- [2/5] Ádány, S. (2008), “Torsional Buckling of Thin-Walled Columns: Analytical Solution Based on Shell Model”, *Proceedings of the Fifth International Conference on Thin-Walled Structures (ICTWS 2008)*, June 18-20, 2008, Brisbane, Australia, pp. 1113-1120. (in Vol 2)
- [3/5] Ádány S. (2012), “Global Buckling of Thin-Walled Columns: Analytical Solutions based on Shell Model”, *Thin-Walled Structures*, vol 55, pp 64-75.
- [4/5] Ádány S., Visy D. (2012), “Global Buckling of Thin-Walled Columns: Numerical Studies”, *Thin-Walled Structures*, vol 54, pp 82-93.
- [5/5] Ádány S. (2014), “Flexural buckling of simply-supported thin-walled columns with consideration of membrane shear deformations: analytical solutions based on shell model”, *Thin-Walled Structures*, vol 74, pp. 36-48.
- [6/5] Oden, J.T. (1967), “Mechanics of Elastic Structures”, McGraw-Hill, 1967.
- [7/5] McGuire W., Gallagher R.H., Ziemian R.D. (2000), “Matrix Structural Analysis”, John Wiley and Sons, New York, 2000.
- [8/5] Timoshenko, S., Gere, J. (1961), “Theory of elastic stability”, McGraw-Hill, 1961.
- [9/5] Tarnai, T. (1995), “The Southwell and the Dunkerley Theorems”, in *Summation Theorems in Structural Stability*, CISM Courses and Lectures No. 354, Springer Verlag, 1995.
- [10/5] Halász O., Iványi M. (2001), “Stabilitáselemélet”, Akadémiai Kiadó, Budapest, 2001.
- [11/5] Kollár P. L. (2001), “Flexural–torsional buckling of open section composite columns with shear deformation”, *International Journal of Solids and Structures* 2001, 38, pp. 7525–7541.
- [12/5] Ádány S., Visy D. (2011), “Lateral-torsional buckling of thin-walled beams: an analytical solution based on shell model”, *Proceedings of the Sixth International Conference on Thin-Walled Structures (ICTWS 2011)*, Sept 5-7, 2011, Timisoara, Romania, (Eds. Dubina D & Ungureanu V., ISBN 978-92-9147-102-7, published by ECCS in Portugal), pp.125-132.
- [13/5] Ádány S. (2012), “Analytical Solution for the Pure Torsional Buckling of Thin-Walled Column with considering Shear Deformations”, *Proceeding of the 6<sup>th</sup> International Conference on Coupled Instabilities in Metal Structures*, Glasgow, Scotland, Dec 3-5, 2012. (Eds: J Loughlan, D H Nash, J Rhodes), pp 95-102.
- [14/5] Kollár P.L., Sapkás Á. (2002), “Lateral-torsional buckling of composite beams”, *International Journal of Solids and Structures*, 2002, 39, pp. 2939–2963.
- [15/5] Kollár P.L., Pluzsik A. (2002), “Torsion of closed section, orthotropic, thin-walled beams”, *International Journal of Solids and Structures*, 2006, 43, pp. 5307–5336.

## Appendix A: Orthogonality criteria

### A1. Orthogonality of $\mathbf{v}$

The orthogonality of  $v$  displacements is interpreted as follows:

$$\int v_r v_s ds = 0 \text{ if } r \neq s \quad (\text{A1})$$

where  $v_r$  and  $v_s$  are two warping distributions for the whole ‘cross-section’, and ‘cross-section’ is interpreted here as the line formed by the middle lines of the strips. Therefore:

$$\sum_{(k)=1}^p \int_0^{b^{(k)}} v_r^{(k)} v_s^{(k)} dx = 0 \text{ if } r \neq s \quad (\text{A2})$$

where  $b^{(k)}$  is the width of the  $k$ -th strip, and the summation is done for all the  $p$  strips. By substituting the FSM shape functions from Eq. (3.2), the orthogonality for one strip:

$$\int_0^{b^{(k)}} v_r^{(k)} v_s^{(k)} dx = \begin{bmatrix} v_{r1}^{(k)} & v_{r2}^{(k)} \end{bmatrix} \int_0^{b^{(k)}} \begin{bmatrix} 1 - \frac{x}{b^{(k)}} \\ \frac{x}{b^{(k)}} \end{bmatrix} \begin{bmatrix} 1 - \frac{x}{b^{(k)}} & \frac{x}{b^{(k)}} \end{bmatrix} dx \begin{bmatrix} v_{s1}^{(k)} \\ v_{s2}^{(k)} \end{bmatrix} \left( Y'_{[m]} \frac{a}{m\pi} \right)^2 \quad (\text{A3})$$

The integral expression can analytically be calculated which leads to the following formula:

$$\int_0^{b^{(k)}} v_r^{(k)} v_s^{(k)} dx = \begin{bmatrix} v_{r1}^{(k)} & v_{r2}^{(k)} \end{bmatrix} \begin{bmatrix} \frac{b^{(k)}}{3} & \frac{b^{(k)}}{6} \\ \frac{b^{(k)}}{6} & \frac{b^{(k)}}{3} \end{bmatrix} \begin{bmatrix} v_{s1}^{(k)} \\ v_{s2}^{(k)} \end{bmatrix} \left( Y'_{[m]} \frac{a}{m\pi} \right)^2 \quad (\text{A4})$$

The summation for all the strips is equivalent with the compilation of the above matrices strip by strip (utilizing also the simple relationship of local and global longitudinal displacements). The  $(Y'_{[m]} a / m\pi)^2$  term is constant for all the strips, and certainly non-zero, therefore it can be eliminated from the final expression. Eq. (A2) finally can be written as:

$$\mathbf{d}_r^T \mathbf{O}_v \mathbf{d}_s = 0 \text{ if } r \neq s \quad (\text{A5})$$

where  $\mathbf{d}_r$  and  $\mathbf{d}_s$  are two non-identical displacement vectors, and the  $\mathbf{O}_v$  matrix is compiled according to the following scheme:

$$\mathbf{O}_v = \sum_{(k)=1}^p \mathbf{O}_{v,(k-1)} + \begin{bmatrix} \vdots & \vdots \\ \vdots & \vdots \\ \dots & \dots & b^{(k)} / 3 & \dots & b^{(k)} / 6 & \dots & \dots \\ \vdots & \vdots \\ \dots & \dots & b^{(k)} / 6 & \dots & b^{(k)} / 3 & \dots & \dots \\ \vdots & \vdots \\ \vdots & \vdots \end{bmatrix} \quad (\text{A6})$$

$\mathbf{O}_v$  is a square matrix with as many rows and columns as many degrees of freedom the member has. It is to observe that  $\mathbf{O}_v$  is constructed very similarly to the elastic stiffness matrix, or more precisely, to those elements of the elastic stiffness matrix that belong to the longitudinal displacements. Indeed, the non-zero elements of  $\mathbf{O}_v$  can be distilled from  $\mathbf{K}_e$ .

## A2. Orthogonality of $u$

The orthogonality of  $u$  displacements is interpreted as follows:

$$\int u_r u_s ds = 0 \text{ and } r \neq s \quad (\text{A7})$$

where  $u_r$  and  $u_s$  are two transverse translation functions for the whole ‘cross-section’, and ‘cross-section’ is interpreted here as the middle line of the strips. Therefore, the expression can be re-formulated as follows:

$$\sum_{(k)=1}^p \int_0^{b^{(k)}} u_r^{(k)} u_s^{(k)} dx = 0 \text{ and } r \neq s \quad (\text{A8})$$

where  $b^{(k)}$  is the width of the  $k$ -th strip, and the summation is done for all the  $p$  strips. Since the shape functions for  $u$  and  $v$  are identical see Eqs. (3.1) and (3.2), the integration for a strip leads to an expression very similar to Eq. (A4), as follows:

$$\int_0^{b^{(k)}} u_r^{(k)} u_s^{(k)} dx = \begin{bmatrix} u_{r1}^{(k)} & u_{r2}^{(k)} \end{bmatrix} \begin{bmatrix} \frac{b^{(k)}}{3} & \frac{b^{(k)}}{6} \\ \frac{b^{(k)}}{6} & \frac{b^{(k)}}{3} \end{bmatrix} \begin{bmatrix} u_{s1}^{(k)} \\ u_{s2}^{(k)} \end{bmatrix} \left( Y'_{[m]} \frac{a}{m\pi} \right)^2 \quad (\text{A9})$$

After summation Eq. (A7) leads to:

$$\mathbf{d}_r^T \mathbf{O}_u \mathbf{d}_s = 0 \text{ if } r \neq s \quad (\text{A10})$$

where  $\mathbf{d}_r$  and  $\mathbf{d}_s$  are two non-identical displacement vectors, and the  $\mathbf{O}_u$  matrix is compiled from the  $b^{(k)}/3$  and  $b^{(k)}/6$  terms with considering the  $\sin\alpha^{(k)}$  and  $\cos\alpha^{(k)}$  terms due to local-to-global coordinate transformation.

$\mathbf{O}_u$  is a square matrix with as many rows and columns as many degrees of freedom the member has. It is to observe that  $\mathbf{O}_u$  is constructed very similarly to those elements of the elastic stiffness matrix that belong to the transverse displacements. Indeed, the non-zero elements of  $\mathbf{O}_u$  can be distilled from  $\mathbf{K}_e$ .

## A3. Orthogonality of $\partial v / \partial x$

The orthogonality of  $\partial v / \partial x$  is interpreted as follows:

$$\int \frac{\partial v_r}{\partial x} \frac{\partial v_s}{\partial x} ds = 0 \text{ and } r \neq s \quad (\text{A11})$$

where  $v_r$  and  $v_s$  are warping functions for the whole ‘cross-section’, and ‘cross-section’ is interpreted here as the middle line of the strips. The integration for one single strip:

$$\int_0^{b^{(k)}} \frac{\partial v_r}{\partial x} \frac{\partial v_s}{\partial x} dx = \begin{bmatrix} v_{r1}^{(k)} & v_{r2}^{(k)} \end{bmatrix} \int_0^{b^{(k)}} \begin{bmatrix} -\frac{1}{b^{(k)}} \\ \frac{1}{b^{(k)}} \end{bmatrix} \begin{bmatrix} -\frac{1}{b^{(k)}} & \frac{1}{b^{(k)}} \end{bmatrix} dx \begin{bmatrix} v_{s1}^{(k)} \\ v_{s2}^{(k)} \end{bmatrix} \left( Y'_{[m]} \frac{a}{m\pi} \right)^2 \quad (\text{A12})$$

The integral expression can analytically be calculated by using the FSM shape functions. For one single strip:

$$\int_0^{b^{(k)}} \frac{\partial v_r^{(k)}}{\partial x} \frac{\partial v_s^{(k)}}{\partial x} dx = \begin{bmatrix} v_{r1}^{(k)} & v_{r2}^{(k)} \end{bmatrix} \begin{bmatrix} \frac{1}{b^{(k)}} & -\frac{1}{b^{(k)}} \\ -\frac{1}{b^{(k)}} & \frac{1}{b^{(k)}} \end{bmatrix} \begin{bmatrix} v_{s1}^{(k)} \\ v_{s2}^{(k)} \end{bmatrix} \left( Y'_{[m]} \frac{a}{m\pi} \right)^2 \quad (\text{A13})$$

After compilation Eq. (A11) becomes:

$$\mathbf{d}_r^T \mathbf{O}_{\mathbf{d}\mathbf{v}\mathbf{x}} \mathbf{d}_s = 0 \text{ if } r \neq s \quad (\text{A14})$$

where  $\mathbf{d}_r$  and  $\mathbf{d}_s$  are two non-identical displacement vectors, and the  $\mathbf{O}_{\mathbf{d}\mathbf{v}\mathbf{x}}$  matrix is compiled from the  $1/b^{(k)}$  terms, similarly as illustrated by Eq. (A6).

$\mathbf{O}_{\mathbf{d}\mathbf{v}\mathbf{x}}$  is a square matrix with as many rows and columns as many degrees of freedom the member has.

#### A4. Orthogonality of $\epsilon_x$

The orthogonality of  $\epsilon_x$  is interpreted as follows:

$$\int \epsilon_{x,r} \epsilon_{x,s} ds = \int \frac{\partial u_r}{\partial x} \frac{\partial u_s}{\partial x} ds = 0 \text{ and } r \neq s \quad (\text{A15})$$

where  $u_r$  and  $u_s$  are local displacement functions for the whole ‘cross-section’, and ‘cross-section’ is interpreted here as the middle line of the strips. The expression is essentially similar to Eq. (A11), therefore, leads to equations similar to Eqs. (A13) and (A14). For one single strip:

$$\int_0^{b^{(k)}} \frac{\partial u_r^{(k)}}{\partial x} \frac{\partial u_s^{(k)}}{\partial x} dx = \begin{bmatrix} u_{r1}^{(k)} & u_{r2}^{(k)} \end{bmatrix} \begin{bmatrix} \frac{1}{b^{(k)}} & -\frac{1}{b^{(k)}} \\ -\frac{1}{b^{(k)}} & \frac{1}{b^{(k)}} \end{bmatrix} \begin{bmatrix} u_{s1}^{(k)} \\ u_{s2}^{(k)} \end{bmatrix} \left( Y'_{[m]} \frac{a}{m\pi} \right)^2 \quad (\text{A16})$$

After compilation Eq. (A15) becomes:

$$\mathbf{d}_r^T \mathbf{O}_{\mathbf{e}\mathbf{x}} \mathbf{d}_s = 0 \text{ if } r \neq s \quad (\text{A17})$$

where  $\mathbf{d}_r$  and  $\mathbf{d}_s$  are two non-identical displacement vectors, and the  $\mathbf{O}_{\mathbf{e}\mathbf{x}}$  matrix is compiled from the  $1/b^{(k)}$  terms.

#### A5. Orthogonality of $\kappa_x$

The orthogonality of the transverse curvature is interpreted as follows:

$$\int \kappa_{x,r} \kappa_{x,s} ds = 0 \text{ and } r \neq s \quad (\text{A18})$$

where  $\kappa_{x,r}$  and  $\kappa_{x,s}$  are two transverse curvature functions for the whole ‘cross-section’. Therefore, the expression can be re-formulated as follows:

$$\sum_{(k)=1}^p \int_0^{b^{(k)}} \kappa_{x,r}^{(k)} \kappa_{x,s}^{(k)} dx = 0 \text{ and } r \neq s \quad (\text{A19})$$

where  $b^{(k)}$  is the width of the  $k$ -th strip, and the summation is done for all the  $p$  strips. The transverse curvature is the second derivative of the  $w$  displacement function with respect to  $x$ , see e.g. Eq. (B25). For one single strip the integration can be done as follows:

$$\int_0^{b^{(k)}} \kappa_{x,r}^{(k)} \kappa_{x,s}^{(k)} dx = \begin{bmatrix} w_{r1}^{(k)} \\ \vartheta_{r1}^{(k)} \\ w_{r2}^{(k)} \\ \vartheta_{r2}^{(k)} \end{bmatrix}^T \int_0^{b^{(k)}} \begin{bmatrix} \left( -\frac{6}{(b^{(k)})^2} + \frac{12x}{(b^{(k)})^3} \right) & \left( -\frac{6}{(b^{(k)})^2} + \frac{12x}{(b^{(k)})^3} \right) \\ \left( \frac{4}{b^{(k)}} - \frac{6x}{(b^{(k)})^2} \right) & \left( \frac{4}{b^{(k)}} - \frac{6x}{(b^{(k)})^2} \right) \\ \left( \frac{6}{(b^{(k)})^2} - \frac{12x}{(b^{(k)})^3} \right) & \left( \frac{6}{(b^{(k)})^2} - \frac{12x}{(b^{(k)})^3} \right) \\ \left( \frac{2}{b^{(k)}} - \frac{6x}{(b^{(k)})^2} \right) & \left( \frac{2}{b^{(k)}} - \frac{6x}{(b^{(k)})^2} \right) \end{bmatrix} dx \begin{bmatrix} w_{s1}^{(k)} \\ \vartheta_{s1}^{(k)} \\ w_{s2}^{(k)} \\ \vartheta_{s2}^{(k)} \end{bmatrix} (Y_{[m]})^2 \quad (\text{A20})$$

which leads to:

$$\int_0^{b^{(k)}} \kappa_{x,r}^{(k)} \kappa_{x,s}^{(k)} dx = \begin{bmatrix} w_{r1}^{(k)} \\ \vartheta_{r1}^{(k)} \\ w_{r2}^{(k)} \\ \vartheta_{r2}^{(k)} \end{bmatrix}^T \begin{bmatrix} \frac{12}{(b^{(k)})^3} & -\frac{6}{(b^{(k)})^2} & -\frac{12}{(b^{(k)})^3} & -\frac{6}{(b^{(k)})^2} \\ -\frac{6}{(b^{(k)})^2} & \frac{4}{b^{(k)}} & \frac{6}{(b^{(k)})^2} & \frac{2}{b^{(k)}} \\ -\frac{12}{(b^{(k)})^3} & \frac{6}{(b^{(k)})^2} & \frac{12}{(b^{(k)})^3} & \frac{6}{(b^{(k)})^2} \\ -\frac{6}{(b^{(k)})^2} & \frac{2}{b^{(k)}} & \frac{6}{(b^{(k)})^2} & \frac{4}{b^{(k)}} \end{bmatrix} \begin{bmatrix} w_{s1}^{(k)} \\ \vartheta_{s1}^{(k)} \\ w_{s2}^{(k)} \\ \vartheta_{s2}^{(k)} \end{bmatrix} (Y_{[m]})^2 \quad (\text{A21})$$

Eq. (A18) can finally be written as:

$$\mathbf{d}_r^T \mathbf{O}_{\mathbf{kx}} \mathbf{d}_s = 0 \text{ if } r \neq s \quad (\text{A22})$$

where  $\mathbf{d}_r$  and  $\mathbf{d}_s$  are two non-identical displacement vectors, and the  $\mathbf{O}_{\mathbf{kx}}$  matrix is compiled similarly as e.g.,  $\mathbf{O}_u$ , considering also the local-to-global coordinate transformation.

$\mathbf{O}_{\mathbf{kx}}$  is a square matrix with as many rows and columns as many degrees of freedom the member has. It is to observe that  $\mathbf{O}_{\mathbf{kx}}$  is constructed very similarly to those elements of the elastic stiffness matrix that belong to the transverse displacements. Indeed, the non-zero elements of  $\mathbf{O}_{\mathbf{kx}}$  can be distilled from  $\mathbf{K}_e$ . More precisely,  $\mathbf{O}_{\mathbf{kx}}$  itself can be interpreted as a stiffness matrix, which belongs to a 2D frame, the geometry of which is the cross-section mid-line, and the frame is modelled by beam elements with 2 DOF per node (namely: one rotation and one translation perpendicular to the beam) and all the beam elements have identical stiffness properties.



## Appendix B: Null criteria

### B1. Null transverse strain

The null transverse normal strain criterion is as follows:

$$\varepsilon_x = \frac{\partial u}{\partial x} = 0 \quad (\text{B1})$$

which is interpreted for the middle surface.

In FSM the  $u$  displacement of the middle surface is expressed as a product of the shape function and the nodal displacements.

$$u(x, y) = \left[ \left( 1 - \frac{x}{b} \right) \left( \frac{x}{b} \right) \right] \begin{bmatrix} u_1 \\ u_2 \end{bmatrix} Y_{[m]} \quad (\text{B2})$$

where  $Y_{[m]}$  is the longitudinal shape function, which depends on the assumed end restraints, see Eqs. (3.4)-(3.8). For example, in case of S-S, it is a simple sine function.

Substituting Eq. (B2) into Eq. (B1) we get:

$$\varepsilon_x = \frac{\partial u}{\partial x} = \frac{-u_1 + u_2}{b} Y_{[m]} = 0, \quad (\text{B3})$$

and since  $Y_{[m]}$  function is generally not equal to zero, the two nodal displacements have to be equal. In a member there are multiple strips, therefore, for the  $(k)$ -th strip:

$$u_1^{(k)} = u_2^{(k)} \quad (\text{B4})$$

This criterion means constraint for the global  $U$  and  $W$  translational displacements of the two nodes (nodal lines) of the strip. It is well-known that the relationship between the local  $x, y$  and the global  $X, Y$  co-ordinates can generally be expressed as:

$$\begin{bmatrix} x \\ z \end{bmatrix} = \begin{bmatrix} \cos \alpha & -\sin \alpha \\ \sin \alpha & \cos \alpha \end{bmatrix} \begin{bmatrix} X \\ Z \end{bmatrix} \quad (\text{B5})$$

Therefore, assuming that the start and end node of the  $(k)$ -th strip is  $i$  and  $j$ , respectively:

$$U_i \cos \alpha^{(k)} - W_i \sin \alpha^{(k)} = U_j \cos \alpha^{(k)} - W_j \sin \alpha^{(k)} \quad (\text{B6})$$

from which:

$$U_i \cos \alpha^{(k)} - W_i \sin \alpha^{(k)} - U_j \cos \alpha^{(k)} + W_j \sin \alpha^{(k)} = 0 \quad (\text{B7})$$

where  $\alpha^{(k)}$  is the (signed) angle of the  $(k)$ -th strip with regard to the positive  $X$  axis.

The same equation can be written to each strip. In matrix form we may write these equations as follows:

$$\mathbf{R}_{\mathbf{e}\mathbf{v}}\mathbf{d}=\mathbf{0} \tag{B9}$$

## B2. Null longitudinal strain

$$\varepsilon_y = \frac{\partial v}{\partial y} = 0 \quad (\text{B10})$$
$$v(x, y) = \left[ \begin{pmatrix} 1 - \frac{x}{b} \\ \frac{x}{b} \end{pmatrix} \begin{pmatrix} x \\ b \end{pmatrix} \right] \begin{bmatrix} v_1 \\ v_2 \end{bmatrix} Y'_{[m]} \frac{a}{m\pi} \quad (\text{B11})$$
$$\frac{\partial v}{\partial y} = \left[ \left( 1 - \frac{x}{b} \right) \begin{pmatrix} x \\ b \end{pmatrix} \right] \begin{bmatrix} v_1 \\ v_2 \end{bmatrix} Y''_{[m]} \frac{a}{m\pi} = 0 \quad (\text{B12})$$
$$V_i = 0 \quad \text{for all the nodes} \quad (\text{B13})$$
$$\gamma_{xy} = \frac{\partial u}{\partial y} + \frac{\partial v}{\partial x} = 0 \quad (\text{B14})$$

114



## B4. Null transverse curvature

The null transverse curvature criterion is as follows:

$$\kappa_x = \frac{\partial^2 w}{\partial x^2} = 0 \quad (\text{B23})$$

which is interpreted for the middle surface.

The  $w$  function in FSM is expressed as follows:

$$w(x, y) = \left[ \left( 1 - \frac{3x^2}{b^2} + \frac{2x^3}{b^3} \right) \left( -x + \frac{2x^2}{b} - \frac{x^3}{b^2} \right) \left( \frac{3x^2}{b^2} - \frac{2x^3}{b^3} \right) \left( \frac{x^2}{b} - \frac{x^3}{b^2} \right) \right] \begin{bmatrix} w_1 \\ \vartheta_1 \\ w_2 \\ \vartheta_2 \end{bmatrix} Y_{[m]} \quad (\text{B24})$$

Taking the second derivative with regard to  $x$ , applying it for the  $(k)$ -th strip (and taking advantage that  $Y_{[m]}$  is non-zero), the criterion can be written as follows:

$$\left[ \left( -\frac{6}{(b^{(k)})^2} + \frac{12x}{(b^{(k)})^3} \right) \left( \frac{4}{b^{(k)}} - \frac{6x}{(b^{(k)})^2} \right) \left( \frac{6}{(b^{(k)})^2} - \frac{12x}{(b^{(k)})^3} \right) \left( \frac{2}{b^{(k)}} - \frac{6x}{(b^{(k)})^2} \right) \right] \begin{bmatrix} w_1 \\ \vartheta_1 \\ w_2 \\ \vartheta_2 \end{bmatrix} = 0 \quad (\text{B25})$$

After rearranging:

$$x \frac{1}{(b^{(k)})^3} (12w_1 - 6b^{(k)}\vartheta_1 - 12w_2 - 6b^{(k)}\vartheta_2) + \frac{1}{(b^{(k)})^2} (-6w_1 + 4b^{(k)}\vartheta_1 + 6w_2 + 2b^{(k)}\vartheta_2) = 0 \quad (\text{B26})$$

The equation is satisfied for any  $x$  if (and only if) both terms in brackets are equal to zero:

$$12w_1 - 6b^{(k)}\vartheta_1 - 12w_2 - 6b^{(k)}\vartheta_2 = 0 \quad \text{and} \quad -6w_1 + 4b^{(k)}\vartheta_1 + 6w_2 + 2b^{(k)}\vartheta_2 = 0 \quad (\text{B27})$$

These equations are satisfied if:

$$\vartheta_1 - \vartheta_2 = 0 \quad \text{and} \quad w_1 - w_2 - b^{(k)}\vartheta = 0 \quad (\text{B28})$$

These equations define rigid-body motion of the strip cross-section. We have similar two equations for each strip. From the  $\vartheta_1 - \vartheta_2 = 0$  equations it can be concluded that the rotational displacement must be equal at all the nodes (which will simply be denoted here as  $\Theta$ ). Plus, the relationship between rotational and translational DOF can be expressed as follows:

$$U_i \sin \alpha^{(k)} + W_i \cos \alpha^{(k)} - U_j \sin \alpha^{(k)} - W_j \cos \alpha^{(k)} - b^{(k)}\Theta = 0 \quad (\text{B29})$$



The equation is satisfied if all the terms in brackets are equal to zero:

$$\begin{cases} 2w_1 - b^{(k)}\vartheta_1 - 2w_2 - b^{(k)}\vartheta_2 = 0 \\ -3w_1 + 2b^{(k)}\vartheta_1 + 3w_2 + b^{(k)}\vartheta_2 = 0 \\ \vartheta_1 = 0 \\ w_1 = 0 \end{cases} \quad (\text{B35})$$

These equations are satisfied if:

$$w_1 = 0 \quad \text{and} \quad \vartheta_1 = 0 \quad \text{and} \quad w_2 = 0 \quad \text{and} \quad \vartheta_2 = 0 \quad (\text{B36})$$

We have similar equations for each strip. From the rotational equations it can be concluded that the rotational displacement must be equal to zero at all the nodes. Moreover, the translational equations can be expressed as follows:

$$U_i \sin \alpha^{(k)} + W_i \cos \alpha^{(k)} = 0 \quad \text{and} \quad U_j \sin \alpha^{(k)} + W_j \cos \alpha^{(k)} = 0 \quad (\text{B37})$$

In matrix form:

$$\begin{bmatrix} 0 \\ 0 \\ 0 \\ \vdots \\ \vdots \\ \vdots \end{bmatrix} = \begin{bmatrix} \cdot & \cdot & \cdot & \cdot & \cdot & \cdot & \cdot & \cdot & \cdot & \cdot & \cdot & \cdot & \cdot & \cdot & \cdot & \cdot \\ \cdot & \cdot & \cdot & \cdot & \cdot & \cdot & \cdot & \cdot & \cdot & \cdot & \cdot & \cdot & \cdot & \cdot & \cdot & \cdot \\ 0 & 0 & \sin \alpha^{(k)} & 0 & 0 & \cdot & 0 & \cos \alpha^{(k)} & 0 & 0 & \cdot & 0 & 0 & 0 & 0 & 0 \\ 0 & 0 & 0 & \sin \alpha^{(k)} & 0 & \cdot & 0 & 0 & \cos \alpha^{(k)} & 0 & \cdot & 0 & 0 & 0 & 0 & 0 \\ \cdot & \cdot & \cdot & \cdot & \cdot & \cdot & \cdot & \cdot & \cdot & \cdot & \cdot & \cdot & \cdot & \cdot & \cdot & \cdot \\ \cdot & \cdot & \cdot & \cdot & \cdot & \cdot & \cdot & \cdot & \cdot & \cdot & \cdot & \cdot & \cdot & \cdot & \cdot & \cdot \end{bmatrix} \begin{bmatrix} \cdot \\ \cdot \\ U_i \\ U_j \\ \cdot \\ \cdot \\ W_i \\ W_j \\ \cdot \\ \cdot \\ \cdot \\ \cdot \\ \cdot \\ \cdot \\ \cdot \end{bmatrix} \quad (\text{B38})$$

or:

$$\mathbf{R}_{\mathbf{ky}} \mathbf{d} = \mathbf{0} \quad \text{and} \quad \Theta_i = 0 \quad \text{for all the nodes} \quad (\text{B39})$$

It means that the null longitudinal curvature criterion is satisfied (i) if all the rotational DOF are zero, and (ii) if the displacement vector satisfies the above equation. The number of columns of  $\mathbf{R}_{\mathbf{ky}}$  is equal to the number of DOF, the number of rows is *twice* the number of strips.

## B6. Null mixed curvature

The null longitudinal curvature criterion is as follows:

$$\kappa_{xy} = \frac{\partial^2 w}{\partial x \partial y} = 0 \quad (\text{B40})$$

which is interpreted for the middle surface. The  $w$  function in FSM is expressed above. Thus, the criterion is:

$$\frac{\partial^2 w}{\partial x \partial y} = \left[ \left( -\frac{6x}{b^2} + \frac{6x^2}{b^3} \right) \left( -1 + \frac{4x}{b} - \frac{3x^2}{b^2} \right) \left( \frac{6x}{b^2} - \frac{6x^2}{b^3} \right) \left( \frac{2x}{b} - \frac{3x^2}{b^2} \right) \right] \begin{bmatrix} w_1 \\ \vartheta_1 \\ w_2 \\ \vartheta_2 \end{bmatrix} Y'_{[m]} = 0 \quad (\text{B41})$$

Since  $Y'_{[m]}$  is non-zero, it can be eliminated. After rearranging and applying to the  $(k)$ -th strip:

$$x^2 \frac{1}{(b^{(k)})^3} (6w_1 - 3b^{(k)}\vartheta_1 - 6w_2 - 3b^{(k)}\vartheta_2) + x \frac{1}{(b^{(k)})^2} (-6w_1 + 4b^{(k)}\vartheta_1 + 6w_2 + 2b^{(k)}\vartheta_2) - (\vartheta_1) = 0 \quad (\text{B42})$$

The equation is satisfied if all the terms in brackets are equal to zero:

$$\begin{cases} 6w_1 - 3b^{(k)}\vartheta_1 - 6w_2 - 3b^{(k)}\vartheta_2 = 0 \\ -6w_1 + 4b^{(k)}\vartheta_1 + 6w_2 + 2b^{(k)}\vartheta_2 = 0 \\ \vartheta_1 = 0 \end{cases} \quad (\text{B43})$$

These equations are satisfied if:

$$w_1 - w_2 = 0 \quad \text{and} \quad \vartheta_1 = \vartheta_2 = 0 \quad (\text{B44})$$

We have similar equations for each strip. From the rotational equations it can be concluded that the rotational displacement must be equal to zero at all the nodes. Moreover, the translational equations can be expressed as follows:

$$U_i \sin \alpha^{(k)} + W_i \cos \alpha^{(k)} - U_j \sin \alpha^{(k)} - W_j \cos \alpha^{(k)} = 0 \quad (\text{B45})$$

In matrix form:

$$\begin{bmatrix} 0 \\ 0 \\ 0 \\ \vdots \\ \vdots \\ \vdots \end{bmatrix} = \begin{bmatrix} \cdot & \cdot & \cdot & \cdot & \cdot & \cdot & \cdot & \cdot & \cdot & \cdot & \cdot & \cdot & \cdot \\ \cdot & \cdot & \cdot & \cdot & \cdot & \cdot & \cdot & \cdot & \cdot & \cdot & \cdot & \cdot & \cdot \\ 0 & 0 & \sin \alpha^{(k)} & -\sin \alpha^{(k)} & 0 & \cdot & 0 & \cos \alpha^{(k)} & -\cos \alpha^{(k)} & 0 & \cdot & 0 & 0 \\ \cdot & \cdot & \cdot & \cdot & \cdot & \cdot & \cdot & \cdot & \cdot & \cdot & \cdot & \cdot & \cdot \\ \cdot & \cdot & \cdot & \cdot & \cdot & \cdot & \cdot & \cdot & \cdot & \cdot & \cdot & \cdot & \cdot \\ \cdot & \cdot & \cdot & \cdot & \cdot & \cdot & \cdot & \cdot & \cdot & \cdot & \cdot & \cdot & \cdot \end{bmatrix} \begin{bmatrix} \cdot \\ \cdot \\ \dot{U}_i \\ U_j \\ \cdot \\ \cdot \\ \cdot \\ W_i \\ W_j \\ \cdot \\ \cdot \\ \cdot \\ \cdot \\ \cdot \end{bmatrix} \quad (\text{B46})$$

or:

$$\mathbf{R}_{\text{kxy}} \mathbf{d} = \mathbf{0} \quad \text{and} \quad \Theta_i = 0 \quad \text{for all the nodes} \quad (\text{B47})$$

It means that the null mixed curvature criterion is satisfied (i) if all the rotational DOF are zero, and (ii) if the displacement vector satisfies the above equation. The number of columns of  $\mathbf{R}_{\text{kxy}}$  is equal to the number of DOF, the number of rows is equal to the number of strips.

## B7. Transverse equilibrium of the cross-section

Transverse equilibrium of the cross-section is interpreted as follows.

- a) The 2D frame is assumed, the geometry of which is identical to the line defined by the cross-section mid-line.
- b) Some stiffness properties are assigned to the beams. The most convenient (and simplest) idea is to assume uniform stiffness for all the beams (e.g.,  $EI = 1$ ).
- c) The 2D frame is modelled by beam elements with 2 DOF per node (namely: one rotation and one translation perpendicular to the beam).
- d) The beam is loaded by prescribed displacements at the corner nodes (i.e., at the junction of beams).
- e) The free DOF of this frame model are determined so that the whole frame would be in equilibrium.

In (d) the prescribed displacements are the  $U$  and  $V$  translations of the corner nodes, while the unknown displacements are the  $\theta$  rotations of the corner nodes and the  $U$ ,  $V$  and  $\theta$  of all the other nodes. Since there are no supports and force-type loading on the 2D frame, equilibrium means that reaction forces may develop at the prescribed DOF, but reaction forces are zero at the free DOF. Thus, this equilibrium criterion can be formulated similarly to the null-strain criteria, as follows:

$$\mathbf{R}_{eq} \mathbf{d} = \mathbf{0} \quad (\text{B48})$$

where  $\mathbf{R}_{eq}$  can readily be constructed from the transverse (elastic) stiffness matrix of the cross-section. However, the transverse (elastic) stiffness matrix is nothing else then the  $\mathbf{O}_{kx}$  matrix as discussed above. Basically,  $\mathbf{R}_{eq}$  is consisted of those rows of  $\mathbf{O}_{kx}$  which belong to the un-prescribed DOF. Thus, the number of column of  $\mathbf{R}_{eq}$  is equal to the number of DOF, while the number of rows of  $\mathbf{R}_{eq}$  is equal to the number of un-prescribed DOF.



## Appendix C: Derivation of the coefficient matrix for column buckling with neglecting in-plane shear

### C1. Global displacements of the member

Global displacements are defined for the reference line of the member. The reference line for the translational components is the (straight) line that goes through the centroid of the cross-sections, while the reference line for the rotation is the (straight) line that goes through the shear centres of the cross-sections. For the coordinate systems, see **Figure 5.1**.

The transverse displacement functions:

$$U = U_0 \sin \frac{m\pi y}{L} = U_0 \sin(k_m y) \quad (\text{C1})$$

$$W = W_0 \sin \frac{m\pi y}{L} = W_0 \sin(k_m y) \quad (\text{C2})$$

$$\Theta = \Theta_0 \sin \frac{m\pi y}{L} = \Theta_0 \sin(k_m y) \quad (\text{C3})$$

The longitudinal displacement function:

$$V = V_0 \cos \frac{m\pi y}{L} = V_0 \cos(k_m y) \quad (\text{C4})$$

In the above expressions:

$$k_m = m\pi/L \quad (\text{C5})$$

where  $L$  is the member length.

### C2. Local displacements of a strip

#### Displacements in the mid-point

For the rotations it is evident that the rotation of any strip must be equal to the rotation of the cross-section itself, which is a direct consequence of the rigid cross-sections. Thus, for the  $i$ -th strip (i.e., for each strip):

$$\theta_{m,i} = \Theta \quad (\text{C6})$$

where ‘ $m$ ’ in the subscript denotes that the local displacement is interpreted at the *midpoint* of the strip (i.e.,  $x = z = 0$ ). Knowing that the global rotation function has sinusoidal longitudinal distribution, similar longitudinal distribution of the local rotation functions is obtained, that can be expressed as:

$$\theta_{m,i} = \theta_{m0,i} \sin \frac{m\pi y}{L} = \theta_{m0,i} \sin(k_m y) \quad (\text{C7})$$

where  $\theta_{m0,i}$  thus the amplitude of the local rotation functions of the  $i$ -th strip, interpreted in the middle point of the strip, and obviously:

$$\theta_{m0,i} = \Theta_0 \quad (\text{C8})$$

The transverse translations (i.e.,  $u$  and  $w$ ) can be expressed by using the well-known geometric transformations, namely, for the  $i$ -th strip, assuming small rotations, it can be written that:

$$u_{m,i} = U \cos \alpha_i + W \sin \alpha_i + \Theta \left( -(X_{m,i} - X_S) \cos \alpha_i + (Z_{m,i} - Z_S) \sin \alpha_i \right) \quad (\text{C9})$$

$$w_{m,i} = -U \sin \alpha_i + W \cos \alpha_i + \Theta \left( -(X_{m,i} - X_S) \sin \alpha_i - (Z_{m,i} - Z_S) \cos \alpha_i \right) \quad (\text{C10})$$

where  $X_{m,i}$  and  $Z_{m,i}$  are the global coordinates of the strips' mid-points,  $X_S$  and  $Z_S$  are the global coordinates of the shear centre of the cross-section, while  $\alpha_i$  is the (signed) angle of the  $i$ -th strip with respect to the positive  $X$ -axis (i.e., the angle between the global and the  $i$ -th strip local coordinate system).

Obviously, the local transverse translation functions have sinusoidal longitudinal distributions, therefore they can be expressed as:

$$u_{m,i} = u_{m0,i} \sin \frac{m\pi y}{L} = u_{m0,i} \sin(k_m y) \quad (\text{C11})$$

$$w_{m,i} = w_{m0,i} \sin \frac{m\pi y}{L} = w_{m0,i} \sin(k_m y) \quad (\text{C12})$$

The amplitudes  $u_{m0,i}$  and  $w_{m0,i}$  therefore can be expressed by the global displacement amplitudes as follows:

$$u_{m0,i} = U_0 \cos \alpha_i + W_0 \sin \alpha_i + \Theta_0 \left( -(X_{m,i} - X_S) \cos \alpha_i + (Z_{m,i} - Z_S) \sin \alpha_i \right) \quad (\text{C13})$$

$$w_{m0,i} = -U_0 \sin \alpha_i + W_0 \cos \alpha_i + \Theta_0 \left( -(X_{m,i} - X_S) \sin \alpha_i - (Z_{m,i} - Z_S) \cos \alpha_i \right) \quad (\text{C14})$$

For the longitudinal displacements (i.e., warping) the following equation is valid for any value of  $y = Y$ :

$$v_{m,i} = V - \Phi_z (X_{m,i} - X_C) - \Phi_x (Z_{m,i} - Z_C) + \Theta' \omega_{m,i} \quad (\text{C15})$$

where  $X_{m,i}$  and  $Z_{m,i}$  are the global coordinates of the strips' mid-points,  $X_C$  and  $Z_C$  are the global coordinates of the mass centre of the cross-section,  $\Phi_x$  and  $\Phi_z$  are the rotations of the given cross-section about its global  $x$  and  $z$ -axis, respectively,  $\omega_{m,i}$  is the sectoral coordinate (with respect to shear centre) at the location of the  $i$ -th strip mid-point, while  $\Theta'$  is the rate of change of the twist of the cross-section. Note that formulae for the calculation of shear centre and sectoral coordinates can be found in textbooks, as well as a good summary is given in the Eurocode for cold-formed steel, see Annex C of [2/1].

$\Phi_x$ ,  $\Phi_z$  and  $\Theta'$  can be expressed by as the first derivative of the corresponding displacement function, as follows:

$$\Phi_x = \frac{\partial W}{\partial y} = W_0 k_m \cos(k_m y) = \Phi_{x0} \cos(k_m y) \quad (\text{C16})$$

$$\Phi_z = \frac{\partial U}{\partial y} = U_0 k_m \cos(k_m y) = \Phi_{z0} \cos(k_m y) \quad (\text{C17})$$

$$\Theta' = \frac{\partial \Theta}{\partial y} = \Theta_0 k_m \cos(k_m y) = \Theta'_0 \cos(k_m y) \quad (\text{C18})$$

Obviously, the local warping function has cosine distribution along the length, therefore can also be expressed as:

$$v_{m,i} = v_{m0,i} \cos \frac{m\pi y}{L} = v_{m0,i} \cos(k_m y) \quad (\text{C19})$$

The  $v_{m0,i}$  amplitude can be get by combining Eqs. (C15) and (C18):

$$v_{m0,i} = V_0 - \Phi_{z0}(X_{m,i} - X_C) - \Phi_{x0}(Z_{m,i} - Z_C) + \Theta' \omega_{m0,i} \quad (\text{C20})$$

Then, by considering Eqs. (C16), (C17) and (C18):

$$v_{m0,i} = V_0 - U_0 k_m (X_{m,i} - X_C) - W_0 k_m (Z_{m,i} - Z_C) + \Theta_0 k_m \omega_{m0,i} \quad (\text{C21})$$

### Adding displacement distribution over the strip cross-section

When constructing the distribution in an arbitrary  $x, z$  position, the following criteria must be satisfied.

- Since the cross-section is rigid, transverse extension must be zero for each strip, thus  $\varepsilon_x = 0$ , which means that  $u$  is constant in  $x$ .
- The  $v$  longitudinal (warping) displacements linearly vary in  $x$ , since in-plane shear is assumed to be zero. This assumption also implies that rotation about local  $z$ -axis can be expressed by the first derivative of the  $v$  warping displacement (at the middle of the strip).
- Since cross-section distortion is excluded, the transverse curvature is zero,  $\kappa_x = 0$ , which means that  $w$  must be linear in  $x$ , while the  $\theta$  rotation is constant (in  $x$ ).
- Kirchhoff plate theory assumes that normals to the undeformed middle plane remain straight, normal and inextensional during the deformations, thus, the  $u$  and  $v$  displacements vary linearly in  $z$ , while  $w$  displacement is constant along the thickness. Moreover, the rotation about  $x$  and  $y$  can be calculated as the first derivative of  $w$  (at the middle-plane).

Considering all the above criteria, the local displacement functions for any strip in any cross-section (i.e., any value of  $y$ ) may be written as follows:

$$\theta_i = \theta_{m,i} \quad (\text{C22})$$

$$u_i = u_{m,i} + \theta_{m,i} z \quad (\text{C23})$$

$$w_i = w_{m,i} - \theta_{m,i} x \quad (\text{C24})$$

$$v_i = v_{m,i} - \phi_{z,i} x - \phi_{x,i} z \quad (\text{C25})$$

where  $u_i$ ,  $v_i$ ,  $w_i$  and  $\theta_i$  are the local displacement functions,  $u_{m,i}$ ,  $v_{m,i}$  and  $w_{m,i}$  are the local translation functions of the given strip mid-line in the  $x$ ,  $y$  and  $z$  direction, respectively,  $\theta_{m,i}$  is the twisting rotation of the strip middle point, while  $\phi_{x,i}$  and  $\phi_{z,i}$  are the rotations of the given strip about its local  $x$  and  $z$ -axis. (Note, all of these quantities should belong to the same  $y$  value.)

Since the strips' rotations are dependent on the displacements of the strips' (longitudinal) mid-lines, the following equations may be written:

$$\phi_{x,i} = \frac{\partial w_{m,i}}{\partial y} = w_{m0,i} k_m \cos(k_m y) = \phi_{x0,i} \cos(k_m y) \quad (\text{C26})$$

$$\phi_{z,i} = \frac{\partial u_{m,i}}{\partial y} = u_{m0,i} k_m \cos(k_m y) = \phi_{z0,i} \cos(k_m y) \quad (\text{C27})$$

Combining Eqs (C26), (C27) and Eq (C25), the local displacement functions of the  $i$ -th strip can be written as follows:

$$u_i = (u_{m0,i} + \theta_{m0,i} z) \sin(k_m y) \quad (\text{C28})$$

$$v_i = (v_{m0,i} - \phi_{z0,i} x - \phi_{x0,i} z) \cos(k_m y) = (v_{m0,i} - u_{m0,i} k_m x - w_{m0,i} k_m z) \cos(k_m y) \quad (\text{C29})$$

$$w_i = (w_{m0,i} - \theta_{m0,i} x) \sin(k_m y) \quad (\text{C30})$$

$$\theta_i = \theta_{m0,i} \sin(k_m y) \quad (\text{C31})$$

It is to observe, thus, that the local displacement functions for any strip are expressed by the maximum local displacements of the strips' (longitudinal) mid-lines, namely:  $u_{m0,i}$ ,  $v_{m0,i}$ ,  $w_{m0,i}$  and  $\theta_{m0,i}$ . Since the local displacement amplitudes are expressed by the global displacement amplitudes, see Eqs. (C8), (C13), (C14) and (C21), ultimately the local displacement functions are expressed by 4 parameters, thus, the whole displacement field of the beam is expressed by the parameters  $U_0$ ,  $V_0$ ,  $W_0$  and  $\Theta_0$ .

### C3. Strains

For the out-of-plane deformations the classical Kirchhoff thin plate theory is applied. The geometric equations are usually expressed as follows:

$$\kappa_{x,i} = -\frac{\partial^2 w_{m,i}}{\partial x^2} \quad (\text{C32})$$

$$\kappa_{y,i} = -\frac{\partial^2 w_{m,i}}{\partial y^2} \quad (\text{C33})$$

$$\kappa_{xy,i} = -2\frac{\partial^2 w_{m,i}}{\partial x \partial y} \quad (\text{C34})$$

For the in-plane behaviour, the following geometric equations must be satisfied:

$$\epsilon_{x,i} = \frac{\partial u_{m,i}}{\partial x} \quad (\text{C35})$$

$$\epsilon_{y,i} = \frac{\partial v_{m,i}}{\partial y} \quad (\text{C36})$$

$$\gamma_{xy,i} = \frac{\partial u_{m,i}}{\partial y} + \frac{\partial v_{m,i}}{\partial x} \quad (\text{C37})$$

## C4. Stresses

Linear elastic material is assumed, thus, the constitutive equation is the generalized Hooke's law. The applied strip model is consisted of a plane stress membrane and a Kirchhoff plate, the constitutive equation is necessary to define for both in-plane and out-of-plane behaviour.

For the in-plane behaviour the 2D Hooke's law is used, which can be simplified because of  $\varepsilon_{x,i} = \gamma_{xy,i} = 0$ :

$$\begin{bmatrix} \sigma_{x,i} \\ \sigma_{y,i} \\ \tau_{xy,i} \end{bmatrix} = \begin{bmatrix} \frac{E}{1-\nu^2} & \frac{\nu E}{1-\nu^2} & 0 \\ \frac{\nu E}{1-\nu^2} & \frac{E}{1-\nu^2} & 0 \\ 0 & 0 & G \end{bmatrix} \begin{bmatrix} \varepsilon_{x,i} \\ \varepsilon_{y,i} \\ \gamma_{xy,i} \end{bmatrix} = \begin{bmatrix} \frac{\nu E}{1-\nu^2} \varepsilon_{y,i} \\ \frac{E}{1-\nu^2} \varepsilon_{y,i} \\ 0 \end{bmatrix} \quad (\text{C38})$$

where  $E$  and  $G$  are the modulus of elasticity and the shear modulus, while  $\nu$  is the Poisson's ratio.

For the out-of-plane behaviour the constitutive equation is most frequently expressed by stress resultants rather than by stresses. The relationship can again be simplified due to  $\kappa_{x,i} = 0$ .

$$\begin{bmatrix} m_{x,i} \\ m_{y,i} \\ m_{xy,i} \end{bmatrix} = \frac{Et_i^3}{12(1-\nu^2)} \begin{bmatrix} 1 & \nu & 0 \\ \nu & 1 & 0 \\ 0 & 0 & \frac{1-\nu}{2} \end{bmatrix} \begin{bmatrix} \kappa_{x,i} \\ \kappa_{y,i} \\ \kappa_{xy,i} \end{bmatrix} = \frac{t_i^3}{12} \begin{bmatrix} \frac{E}{1-\nu^2} \nu \kappa_{y,i} \\ \frac{E}{1-\nu^2} \kappa_{y,i} \\ G \kappa_{xy,i} \end{bmatrix} \quad (\text{C39})$$

where  $t$  is the thickness of the considered strip,  $m_{x,i}$ ,  $m_{y,i}$  and  $m_{xy,i}$  are moments for a unit-width strip portion.

## C5. External potential

The external potential is expressed as discussed by Section 5.2.3. The work done by the external (uniformly distributed)  $p_y$  loading is:

$$W = p_y \sum_{i=1}^n \left[ \int_{-\frac{t_i}{2}}^{+\frac{t_i}{2}} \int_0^L \int_{-\frac{b_i}{2}}^{+\frac{b_i}{2}} (\varepsilon_{y,i}^{II}) dx dy dz \right] \text{ or } W = p_y \sum_{i=1}^n \left[ t_i \int_0^L \int_{-\frac{b_i}{2}}^{+\frac{b_i}{2}} (\varepsilon_{y,i}^{II}) dx dy \right] \quad (\text{C40})$$

where  $L$  is the member length,  $b_i$  and  $t_i$  is the width and thickness of the  $i$ -th strip, respectively,  $n$  is the number of strips, and the second-order strain term is expressed as:

$$\varepsilon_{y,i}^{II} = \frac{1}{2} \left[ \left( \frac{\partial u_i}{\partial y} \right)^2 + \left( \frac{\partial w_i}{\partial y} \right)^2 \right] \text{ or } \varepsilon_{y,i}^{II} = \frac{1}{2} \left[ \left( \frac{\partial u_i}{\partial y} \right)^2 + \left( \frac{\partial v_i}{\partial y} \right)^2 + \left( \frac{\partial w_i}{\partial y} \right)^2 \right] \quad (\text{C41})$$

It is to observe that the external potential energy can be expressed by the 4 displacement parameters.

## C6. Internal potential

The accumulated elastic strain energy as the member is deformed can be expressed by well-known integral formulae, as discussed in Section 5.2.3. For the investigated problem, utilizing that  $\varepsilon_{x,i} = \kappa_{x,i} = \gamma_{xy,i} = 0$ , the expression is:

$$\Pi_{int} = \frac{1}{2} \sum_{i=1}^n \left[ \int_0^L \int_{-\frac{b_i}{2}}^{\frac{b_i}{2}} (\sigma_{y,i} \varepsilon_{y,i}) dx dy \right] + \frac{1}{2} \sum_{i=1}^n \left[ \int_0^L \int_{-\frac{b_i}{2}}^{\frac{b_i}{2}} (m_{y,i} \kappa_{y,i}) dx dy \right] + \frac{1}{2} \sum_{i=1}^n \left[ \int_0^L \int_{-\frac{b_i}{2}}^{\frac{b_i}{2}} (m_{xy,i} \kappa_{xy,i}) dx dy \right]$$

or, with neglecting the bending energy terms: (C42)

$$\Pi_{int} = \frac{1}{2} \sum_{i=1}^n \left[ \int_0^L \int_{-\frac{b_i}{2}}^{\frac{b_i}{2}} (\sigma_{y,i} \varepsilon_{y,i}) dx dy \right] \quad (C43)$$

where  $L$  is the member length,  $b_i$  and  $t_i$  is the width and thickness of the  $i$ -th strip, respectively, while  $n$  is the number of strips.

It is to observe that the internal potential energy can be expressed by the 4 displacement parameters.

## C7. Total potential

The total potential is the sum of the internal potential (i.e., strain energy) and of the external potential (i.e., negative of the work done by the external loading). Since the external potential can be calculated by 4 different ways, while internal potential by 2 different ways, the total potential energy can be expressed by 8 different ways. The applied options are summarized in **Table 5.1**.

## C8. Coefficient matrix

Utilizing that in equilibrium the total potential energy is stationary, a set of 4 (linear) equations can be established for the 4 displacement parameters of the problem:

$$\begin{aligned} \frac{\partial \Pi}{\partial V_0} &= 0 \\ \frac{\partial \Pi}{\partial U_0} &= 0 \\ \frac{\partial \Pi}{\partial W_0} &= 0 \\ \frac{\partial \Pi}{\partial \Theta_0} &= 0 \end{aligned} \quad \rightarrow \quad \begin{bmatrix} C_{11} & 0 & 0 & 0 \\ 0 & C_{22} & C_{23} & C_{24} \\ 0 & C_{32} & C_{33} & C_{34} \\ 0 & C_{42} & C_{43} & C_{44} \end{bmatrix} \begin{bmatrix} V_0 \\ U_0 \\ W_0 \\ \Theta_0 \end{bmatrix} = \begin{bmatrix} 0 \\ 0 \\ 0 \\ 0 \end{bmatrix} \quad (C44)$$

Note, the coefficient matrix is symmetric. The non-zero elements of the coefficient matrix are given in **Table C1** and **Table C2**.

**Table C1:** Elements of coefficient matrix for  $n \times \times$  options

option	$nnn$	$nny$	$nyn$	$nyy$
$C_{11}$	$-F_a$	$-F_a$	$-F_a$	$-F_a$
$C_{22}$	$F - F_{Z,r}$	$F - F_Z$	$F - F_{Z,r}$	$F - F_Z$
$C_{33}$	$F - F_{X,r}$	$F - F_X$	$F - F_{X,r}$	$F - F_X$
$C_{44}$	$r_{0S,r}^2 F - F_{w,r}$	$r_{0S,r}^2 F - (F_w + F_t)$	$r_{0S}^2 F - F_{w,r}$	$r_{0S}^2 F - (F_w + F_t)$
$C_{23}$	$-F_{XZ,r}$	$-F_{XZ}$	$-F_{XZ,r}$	$-F_{XZ}$
$C_{24}$	$-Z_{SC}F$	$-Z_{SC}(F - F_{\omega Z})$	$-Z_{SC}F$	$-Z_{SC}(F - F_{\omega Z})$
$C_{34}$	$X_{SC}F$	$X_{SC}(F - F_{\omega X})$	$X_{SC}F$	$X_{SC}(F - F_{\omega X})$

**Table C2:** Elements of coefficient matrix for  $y \times \times$  options

option	$ynn$	$yny$	$yyn$	$yyy$
$C_{11}$	$C_{11}^{nnn} + F$	$C_{11}^{nny} + F$	$C_{11}^{nyn} + F$	$C_{11}^{nyy} + F$
$C_{22}$	$C_{22}^{nnn} + F \frac{F_{Z,r}}{F_a}$	$C_{22}^{nny} + F \frac{F_{Z,r}}{F_a}$	$C_{22}^{nyn} + F \frac{F_Z}{F_a}$	$C_{22}^{nyy} + F \frac{F_Z}{F_a}$
$C_{33}$	$C_{33}^{nnn} + F \frac{F_{X,r}}{F_a}$	$C_{33}^{nny} + F \frac{F_{X,r}}{F_a}$	$C_{33}^{nyn} + F \frac{F_X}{F_a}$	$C_{33}^{nyy} + F \frac{F_X}{F_a}$
$C_{44}$	$C_{44}^{nnn} + F \frac{F_{w,r}}{F_a}$	$C_{44}^{nny} + F \frac{F_{w,r}}{F_a}$	$C_{44}^{nyn} + F \frac{F_w}{F_a}$	$C_{44}^{nyy} + F \frac{F_w}{F_a}$
$C_{23}$	$C_{23}^{nnn} + F \frac{F_{XZ,r}}{F_a}$	$C_{23}^{nny} + F \frac{F_{XZ,r}}{F_a}$	$C_{23}^{nyn} + F \frac{F_{XZ}}{F_a}$	$C_{23}^{nyy} + F \frac{F_{XZ}}{F_a}$
$C_{24}$	$C_{24}^{nnn}$	$C_{24}^{nny}$	$C_{24}^{nyn} - Z_{SC}F \frac{F_{\omega Z}}{F_a}$	$C_{24}^{nyy} - Z_{SC}F \frac{F_{\omega Z}}{F_a}$
$C_{34}$	$C_{34}^{nnn}$	$C_{34}^{nny}$	$C_{34}^{nyn} + X_{SC}F \frac{F_{\omega X}}{F_a}$	$C_{34}^{nyy} + X_{SC}F \frac{F_{\omega X}}{F_a}$

In **Table C1** and **Table C2**  $F$  is the applied axial force, and the other symbols are as follows.

$$F_X = \frac{\pi^2 EI_X}{(1-\nu^2)L^2} \text{ and } F_{X,r} = \frac{\pi^2 EI_{X,r}}{(1-\nu^2)L^2} \quad (\text{C45})$$

$$F_Z = \frac{\pi^2 EI_Z}{(1-\nu^2)L^2} \text{ and } F_{Z,r} = \frac{\pi^2 EI_{Z,r}}{(1-\nu^2)L^2} \quad (\text{C46})$$

$$F_{XZ} = \frac{\pi^2 EI_{XZ}}{(1-\nu^2)L^2} \text{ and } F_{XZ,r} = \frac{\pi^2 EI_{XZ,r}}{(1-\nu^2)L^2} \quad (\text{C47})$$

$$F_w = \frac{\pi^2 EI_w}{(1-\nu^2)L^2} \text{ and } F_{w,r} = \frac{\pi^2 EI_{w,r}}{(1-\nu^2)L^2} \quad (\text{C48})$$

$$F_{\omega X} = \frac{\pi^2 EI_{\omega X}}{(1-\nu^2)L^2} \text{ and } F_{\omega Z} = \frac{\pi^2 EI_{\omega Z}}{(1-\nu^2)L^2} \quad (\text{C49})$$

$$F_t = GI_t \quad (\text{C50})$$

$$F_a = \frac{EA}{1-\nu^2} \quad (\text{C51})$$

in which  $E$  and  $G$  are the modulus of elasticity and the shear modulus,  $\nu$  is the Poisson's ratio,  $L$  is the member length, while the applied cross-sectional properties are as follows:

- $A$  is the cross-sectional area,
- $I_X$  and  $I_Z$  are the second moment of areas calculated with regard to global  $X$  and  $Z$ -axis, respectively, with considering own plate inertias (i.e., the  $bit_i^3/12$  terms),
- $I_{X,r}$  and  $I_{Z,r}$  are (reduced) second moment of areas with regard to global  $X$  and  $Z$ -axis, respectively, with neglecting own plate inertias (i.e., the  $bit_i^3/12$  terms),
- $I_{XZ,r}$  and  $I_{XZ}$  are the product moment of area with regard to  $X$  and  $Z$ -axis with neglecting or considering the own plate inertias, respectively,
- $I_w$  and  $I_{w,r}$  are warping constant, with and without considering the through-thickness warping variation, respectively,
- $I_t$  is the torsion constant,
- $X_{SC}$  and  $Z_{SC}$  are the coordinates of shear centre with regard to mass centre, i.e.,  $X_{SC} = X_S - X_C$  and  $Z_{SC} = Z_S - Z_C$ , where  $X_C$  and  $Z_C$  are the global coordinates of the mass centre of the cross-section, while  $X_S$  and  $Z_S$  are the global coordinates of the shear centre of the cross-section, and
- $r_{0S}^2 = \frac{I_X + I_Z}{A} + X_{SC}^2 + Z_{SC}^2$  and  $r_{0S,r}^2 = \frac{I_{X,r} + I_{Z,r}}{A} + X_{SC}^2 + Z_{SC}^2$



- $I_{\omega X}$  and  $I_{\omega Z}$  are cross-section properties defined as follows:

$$I_{\omega X} = \begin{cases} \frac{1}{X_{SC}} \int_A \omega \cdot (Z - Z_C) dA & \text{if } X_{SC} \neq 0 \\ 0 & \text{if } X_{SC} = 0 \end{cases} \quad (\text{C52})$$

$$I_{\omega Z} = \begin{cases} -\frac{1}{Z_{SC}} \int_A \omega \cdot (X - X_C) dA & \text{if } Z_{SC} \neq 0 \\ 0 & \text{if } Z_{SC} = 0 \end{cases} \quad (\text{C53})$$

The critical forces can be calculated by utilizing that the coefficient matrix has to be singular, therefore, finally the following equation must be solved:

$$\det(\mathbf{C}) = 0 \quad (\text{C54})$$

The results, i.e., the critical forces are discussed in Chapter 5.

## Appendix D: Derivation of the coefficient matrix for flexural buckling with considering in-plane shear

### D1. Global displacements of the member

Global displacements are defined for the reference line of the member. The reference line for the translational components is the (straight) line that goes through the centroid of the cross-sections, while the reference line for the rotation is the (straight) line that goes through the shear centres of the cross-sections. For the coordinate systems, see **Figure 5.1**.

The transverse displacement function is assumed to be the sum of two components: a no-shear and a shear components, as follows:

$$W = W_0 \sin \frac{m\pi y}{L} = W_0 \sin(k_m y) = (W_0^n + W_0^s) \sin(k_m y) \quad (\text{D1})$$

The longitudinal displacement function:

$$V = V_0 \cos \frac{m\pi y}{L} = V_0 \cos(k_m y) \quad (\text{D2})$$

In the above expressions:

$$k_m = m\pi/L \quad (\text{D3})$$

where  $L$  is the member length.

### D2. Local displacements of a strip

#### Displacements in the mid-point

By utilizing that no cross-section distortion is allowed (by the global buckling definition), the transverse displacement and rotation of the reference point of any cross-section fully determines the displacements of the strips. First, let us express the displacements of the strips' (longitudinal) mid-lines in the local coordinate system:

$$u_{m,i} = W \sin \alpha_i \quad (\text{D4})$$

$$w_{m,i} = W \cos \alpha_i \quad (\text{D5})$$

where  $u_{m,i}$ , and  $w_{m,i}$  are the local displacement functions of the  $i$ -th strip mid-line in the  $x$  and  $z$  direction, respectively, while  $\alpha_i$  is the (signed) angle of the  $i$ -th strip with respect to the positive  $X$ -axis (i.e., the angle between the global and the  $i$ -th strip local coordinate system).

Obviously, the local transverse translation functions have sinusoidal longitudinal distributions, therefore they can be expressed as:

$$u_{m,i} = u_{m0,i} \sin \frac{m\pi y}{L} = u_{m0,i} \sin(k_m y) \quad (\text{D6})$$

$$w_{m,i} = w_{m0,i} \sin \frac{m\pi y}{L} = w_{m0,i} \sin(k_m y) \quad (\text{D7})$$

where the amplitudes  $u_{m0,i}$  and  $w_{m0,i}$  can be expressed by the global displacement amplitudes, by using the well-known geometric transformations. Namely, for the  $i$ -th strip, assuming small rotations, it can be written that:

$$u_{m0,i} = (W_0^n + W_0^s) \sin \alpha_i \quad (\text{D8})$$

$$w_{m0,i} = (W_0^n + W_0^s) \cos \alpha_i \quad (\text{D9})$$

For the longitudinal displacements (i.e., warping) the following equation is valid for any value of  $y = Y$ :

$$v_{m,i} = V + \Phi_x (Z_{m,i} - Z_C) \quad (\text{D10})$$

where  $Z_{m,i}$  is the global coordinate of the strips' mid-points,  $Z_C$  is the global coordinates of the mass centre of the cross-section, and  $\Phi_x$  is the rotation of the given cross-section about its global  $x$ -axis.

$\Phi_x$ , can be expressed by as the first derivative of the corresponding displacement function, as follows:

$$\Phi_x = \frac{\partial W^n}{\partial y} = W_0^n k_m \cos(k_m y) = \Phi_{x0} \cos(k_m y) \quad (\text{D11})$$

Obviously, the local warping function has cosine distribution along the length, therefore can also be expressed as:

$$v_{m,i} = v_{m0,i} \cos \frac{m\pi y}{L} = v_{m0,i} \cos(k_m y) \quad (\text{D12})$$

The  $v_{m0,i}$  amplitude can be get by combining Eqs. (D10) and (D12):

$$v_{m0,i} = V_0 - \Phi_{x0} (Z_{m,i} - Z_C) \quad (\text{D13})$$

Then, by considering Eq. (D11):

$$v_{m0,i} = V_0 - W_0^n k_m (Z_{m,i} - Z_C) \quad (\text{D14})$$

Note, there is no twisting rotation of any strip.

#### Adding displacement distribution over the strip cross-section

The next step is to construct the local displacement functions for each strip, from the local displacements of the strip's mid-line. To do this, the following considerations are necessary:

- Since the cross-section is rigid, transverse extension must be zero for each strip, thus  $\varepsilon_x = 0$ , which means that  $u$  is constant in  $x$ .
- The  $v$  longitudinal (warping) displacements linearly vary in  $x$ . Moreover, rotation about local  $z$ -axis can be expressed by the first derivative of the  $v$  warping displacement (at the middle of the strip).

- Since cross-section distortion is excluded, the transverse curvature is zero,  $\kappa_x = 0$ , which means that  $w$  must be linear in  $x$ , while the  $\theta$  rotation is constant (in  $x$ ). However, if the twisting rotation of the cross-section is excluded, as in the case of flexural buckling, the constant  $\theta$  twisting rotation will be zero for any strip.
- Kirchhoff plate theory assumes that normals to the undeformed middle plane remain straight, normal and inextensional during the deformations, thus, the  $u$  and  $v$  displacements vary linearly in  $z$ , while  $w$  displacement is constant along the thickness. Moreover, the rotation about  $x$  and  $y$  can be calculated as the first derivative of  $w$  (at the middle-plane).

By utilizing the above assumptions, the  $\phi_x$  and  $\phi_z$  rotations of the  $i$ -th strip about its local  $x$  and  $z$ -axis can be written:

$$\phi_{x,i} = \frac{\partial w_{m,i}}{\partial y} = k_m (w_{m0,i}^n + w_{m0,i}^s) \cos(k_m y) = \phi_{x0,i} \cos(k_m y) \quad (\text{D15})$$

$$\phi_{z,i} = \frac{\partial u_{m,i}}{\partial y} = k_m (u_{m0,i}^n) \cos(k_m y) = \phi_{z0,i} \cos(k_m y) \quad (\text{D16})$$

By considering Eqs (D8), (D9) and (D14) plus Eqs (D15) and (D16), the local displacement functions of the  $i$ -th strip can be written as follows:

$$u_i = (u_{m0,i}^n + u_{m0,i}^s) \sin(k_m y) \quad (\text{D17})$$

$$w_i = (w_{m0,i}^n + w_{m0,i}^s) \sin(k_m y) \quad (\text{D18})$$

$$v_i = (v_{m0,i} - \phi_{z0,i} x - \phi_{x0,i} z) \cos(k_m y) \quad (\text{D19})$$

$$= [v_{m0,i} - k_m u_{m0,i}^n x - k_m (w_{m0,i}^n + w_{m0,i}^s) z] \cos(k_m y)$$

It is to observe, thus, that the local displacement functions for any strip are expressed by the maximum local displacements of the strips' (longitudinal) mid-lines, which, however, are expressed by the three global displacement parameters,  $V_0$ ,  $W_0^n$  and  $W_0^s$ , thus, the whole displacement field of the member is expressed by the three global parameters.

### D3. Strains

For the out-of-plane deformations the classical Kirchhoff thin plate theory is applied. The geometric equations are usually expressed as follows:

$$\kappa_{x,i} = -\frac{\partial^2 w_{m,i}}{\partial x^2} \quad (\text{D20})$$

$$\kappa_{y,i} = -\frac{\partial^2 w_{m,i}}{\partial y^2} \quad (\text{D21})$$

$$\kappa_{xy,i} = -2 \frac{\partial^2 w_{m,i}}{\partial x \partial y} \quad (\text{D22})$$

For the in-plane behaviour the following geometric equations must be satisfied:

$$\varepsilon_{x,i} = \frac{\partial u_{m,i}}{\partial x} \quad (\text{D23})$$

$$\varepsilon_{y,i} = \frac{\partial v_{m,i}}{\partial y} \quad (\text{D24})$$

$$\gamma_{xy,i} = \frac{\partial u_{m,i}}{\partial y} + \frac{\partial v_{m,i}}{\partial x} \quad (\text{D25})$$

## D4. Stresses

Linear elastic material is assumed, thus, the constitutive equation is the generalized Hooke's law. The applied strip model is consisted of a plane stress membrane and a Kirchhoff plate, the constitutive equation is necessary to define for both in-plane and out-of-plane behaviour.

For the in-plane behaviour the 2D Hooke's law is used, which can be simplified because of  $\varepsilon_{x,i} = 0$ :

$$\begin{bmatrix} \sigma_{x,i} \\ \sigma_{y,i} \\ \tau_{xy,i} \end{bmatrix} = \begin{bmatrix} \frac{E}{1-\nu^2} & \frac{\nu E}{1-\nu^2} & 0 \\ \frac{\nu E}{1-\nu^2} & \frac{E}{1-\nu^2} & 0 \\ 0 & 0 & G \end{bmatrix} \begin{bmatrix} \varepsilon_{x,i} \\ \varepsilon_{y,i} \\ \gamma_{xy,i} \end{bmatrix} = \begin{bmatrix} \frac{\nu E}{1-\nu^2} \varepsilon_{y,i} \\ \frac{E}{1-\nu^2} \varepsilon_{y,i} \\ G \gamma_{xy,i} \end{bmatrix} \quad (\text{D26})$$

where  $E$  and  $G$  are the modulus of elasticity and the shear modulus, while  $\nu$  is the Poisson's ratio.

For the out-of-plane behaviour the constitutive equation is most frequently expressed by stress resultants rather than by stresses. The relationship can again be simplified due to  $\kappa_{x,i} = \kappa_{xy,i} = 0$ .

$$\begin{bmatrix} m_{x,i} \\ m_{y,i} \\ m_{xy,i} \end{bmatrix} = \frac{Et_i^3}{12(1-\nu^2)} \begin{bmatrix} 1 & \nu & 0 \\ \nu & 1 & 0 \\ 0 & 0 & \frac{1-\nu}{2} \end{bmatrix} \begin{bmatrix} \kappa_{x,i} \\ \kappa_{y,i} \\ \kappa_{xy,i} \end{bmatrix} = \frac{t_i^3}{12} \begin{bmatrix} \frac{E}{1-\nu^2} \nu \kappa_{y,i} \\ \frac{E}{1-\nu^2} \kappa_{y,i} \\ 0 \end{bmatrix} \quad (\text{D27})$$

where  $t$  is the thickness of the considered strip,  $m_{x,i}$ ,  $m_{y,i}$  and  $m_{xy,i}$  are moments for a unit-width strip portion.

## D5. External potential

The external potential is expressed as discussed by Section 5.3.3. The work done by the external (uniformly distributed)  $p_y$  loading is:

$$(\text{D28})$$

$$W = p_y \sum_{i=1}^n \left[ \int_{-\frac{t_i}{2}}^{+\frac{t_i}{2}} \int_0^L \int_{-\frac{b_i}{2}}^{+\frac{b_i}{2}} (\varepsilon_{y,i}^{II}) dx dy dz \right] \text{ or } W = p_y \sum_{i=1}^n \left[ t_i \int_0^L \int_{-\frac{b_i}{2}}^{+\frac{b_i}{2}} (\varepsilon_{y,i}^{II}) dx dy \right]$$

where  $L$  is the member length,  $b_i$  and  $t_i$  is the width and thickness of the  $i$ -th strip, respectively,  $n$  is the number of strips, and the second-order strain term is expressed as:

$$\varepsilon_{y,i}^{II} = \frac{1}{2} \left[ \left( \frac{\partial u_i}{\partial y} \right)^2 + \left( \frac{\partial w_i}{\partial y} \right)^2 \right] \text{ or } \varepsilon_{y,i}^{II} = \frac{1}{2} \left[ \left( \frac{\partial u_i}{\partial y} \right)^2 + \left( \frac{\partial v_i}{\partial y} \right)^2 + \left( \frac{\partial w_i}{\partial y} \right)^2 \right] \quad (\text{D29})$$

It is to observe that the external potential energy can be expressed by the 3 displacement parameters.

## D6. Internal potential

The accumulated elastic strain energy as the member is deformed can be expressed by well-known integral formulae, as discussed in Section 5.2.3. For the investigated problem, utilizing that  $\varepsilon_{x,i} = \kappa_{x,i} = \kappa_{xy,i} = 0$ , the expression is:

$$\Pi_{int} = \frac{1}{2} \sum_{i=1}^n \left[ t_i \int_0^L \int_{-\frac{b_i}{2}}^{+\frac{b_i}{2}} (\sigma_{y,i} \varepsilon_{y,i}) dx dy \right] + \frac{1}{2} \sum_{i=1}^n \left[ t_i \int_0^L \int_{-\frac{b_i}{2}}^{+\frac{b_i}{2}} (\tau_{xy,i} \gamma_{xy,i}) dx dy \right] + \frac{1}{2} \sum_{i=1}^n \left[ t_i \int_0^L \int_{-\frac{b_i}{2}}^{+\frac{b_i}{2}} (m_{y,i} \kappa_{y,i}) dx dy \right] \quad (\text{D30})$$

or, with neglecting the bending energy term:

$$\Pi_{int} = \frac{1}{2} \sum_{i=1}^n \left[ t_i \int_0^L \int_{-\frac{b_i}{2}}^{+\frac{b_i}{2}} (\sigma_{y,i} \varepsilon_{y,i}) dx dy \right] + \frac{1}{2} \sum_{i=1}^n \left[ t_i \int_0^L \int_{-\frac{b_i}{2}}^{+\frac{b_i}{2}} (\tau_{xy,i} \gamma_{xy,i}) dx dy \right] \quad (\text{D31})$$

where  $L$  is the member length,  $b_i$  and  $t_i$  is the width and thickness of the  $i$ -th strip, respectively, while  $n$  is the number of strips.

It is to observe that the internal potential energy can be expressed by the 3 displacement parameters.

## D7. Total potential

The total potential is the sum of the internal potential (i.e., strain energy) and of the external potential (i.e., negative of the work done by the external loading). Since the external potential can be calculated by 4 different ways, while internal potential by 2 different ways, the total potential energy can be expressed by 8 different ways. The applied options are summarized in **Table 5.1**.

## D8. Coefficient matrix

Utilizing that in equilibrium the total potential energy is stationary, a set of 4 (linear) equations can be established for the 4 displacement parameters of the problem:

$$\begin{aligned}
\frac{\partial \Pi}{\partial V_0} &= 0 \\
\frac{\partial \Pi}{\partial W_0^n} &= 0 \\
\frac{\partial \Pi}{\partial W_0^s} &= 0
\end{aligned}
\rightarrow \begin{bmatrix} C_{11} & 0 & 0 \\ 0 & C_{22} & C_{23} \\ 0 & C_{32} & C_{33} \end{bmatrix} \begin{bmatrix} V_0 \\ W_0^n \\ W_0^s \end{bmatrix} = \begin{bmatrix} 0 \\ 0 \\ 0 \end{bmatrix} \quad (\text{D32})$$

Note, the coefficient matrix is symmetric. The coefficient matrices for the various options are given by the following equations.

$$\mathbf{C}^{\text{nnn}} = \mathbf{C}^{\text{nyy}} = \begin{bmatrix} -F_a & 0 & 0 \\ 0 & F - F_{X,r} & F \\ 0 & F & F - F_{s,Z} \end{bmatrix} \quad (\text{D33})$$

$$\mathbf{C}^{\text{nyy}} = \mathbf{C}^{\text{nyy}} = \begin{bmatrix} -F_a & 0 & 0 \\ 0 & F - F_X & F - \Delta F_X \\ 0 & F - \Delta F_X & F - F_{s,Z} - \Delta F_X \end{bmatrix} \quad (\text{D34})$$

$$\mathbf{C}^{\text{yyn}} = \mathbf{C}^{\text{nnn}} + \begin{bmatrix} F & 0 & 0 \\ 0 & F \frac{F_{X,r}}{F_a} & 0 \\ 0 & 0 & 0 \end{bmatrix} = \begin{bmatrix} F - F_a & 0 & 0 \\ 0 & F - F_{X,r} + F \frac{F_{X,r}}{F_a} & F \\ 0 & F & F - F_{s,Z} \end{bmatrix} \quad (\text{D35})$$

$$\mathbf{C}^{\text{yny}} = \mathbf{C}^{\text{nyy}} + \begin{bmatrix} F & 0 & 0 \\ 0 & F \frac{F_{X,r}}{F_a} & 0 \\ 0 & 0 & 0 \end{bmatrix} = \begin{bmatrix} F - F_a & 0 & 0 \\ 0 & F - F_X + F \frac{F_{X,r}}{F_a} & F - \Delta F_X \\ 0 & F - \Delta F_X & F - F_{s,Z} - \Delta F_X \end{bmatrix} \quad (\text{D36})$$

$$\mathbf{C}^{\text{yyn}} = \mathbf{C}^{\text{nyy}} + \begin{bmatrix} F & 0 & 0 \\ 0 & F \frac{F_X}{F_a} & F \frac{\Delta F_X}{F_a} \\ 0 & F \frac{\Delta F_X}{F_a} & F \frac{\Delta F_X}{F_a} \end{bmatrix} = \begin{bmatrix} F - F_a & 0 & 0 \\ 0 & F - F_{X,r} + F \frac{F_X}{F_a} & F + F \frac{\Delta F_X}{F_a} \\ 0 & F + F \frac{\Delta F_X}{F_a} & F - F_{s,Z} + F \frac{\Delta F_X}{F_a} \end{bmatrix} \quad (\text{D37})$$

$$\mathbf{C}^{\text{yyy}} = \mathbf{C}^{\text{nyy}} + \begin{bmatrix} F & 0 & 0 \\ 0 & F \frac{F_X}{F_a} & F \frac{\Delta F_X}{F_a} \\ 0 & F \frac{\Delta F_X}{F_a} & F \frac{\Delta F_X}{F_a} \end{bmatrix} = \begin{bmatrix} F - F_a & 0 & 0 \\ 0 & F - F_X + F \frac{F_X}{F_a} & F - \Delta F_X + F \frac{F_X}{F_a} \\ 0 & F - \Delta F_X + F \frac{F_X}{F_a} & F - F_{s,Z} - \Delta F_X + F \frac{F_X}{F_a} \end{bmatrix} \quad (\text{D38})$$

with the following symbols:

$$F_X = \frac{\pi^2 EI_X}{(1-\nu^2)L^2} \text{ and } F_{X,r} = \frac{\pi^2 EI_{X,r}}{(1-\nu^2)L^2} \quad (\text{D39})$$

$$\Delta F_X = F_X - F_{X,r} = \frac{\pi^2 E(I_X - I_{X,r})}{(1-\nu^2)L^2} \quad (\text{D40})$$

$$F_a = \frac{EA}{1-\nu^2} \quad (\text{D41})$$

$$F_{s,Z} = GA_{s,Z} \quad (\text{D42})$$

in which  $E$  and  $G$  are the modulus of elasticity and the shear modulus,  $\nu$  is the Poisson's ratio,  $L$  is the member length, while the applied cross-sectional properties are as follows:

- $A$  is the cross-sectional area,
- $I_X$  is the second moment of areas calculated with regard to global  $X$ -axis, with considering own plate inertias (i.e., the  $b_i t_i^3/12$  terms),
- $I_{X,r}$  is the (reduced) second moment of areas with regard to global  $X$ -axis, with neglecting own plate inertias (i.e., the  $b_i t_i^3/12$  terms),
- $A_{s,Z}$  is the shear area along the  $Z$  direction, defined as follows:

$$A_{s,Z} = \sum_{i=1}^n b_i t_i \cos \alpha_i \quad (\text{D43})$$

where  $b_i$  and  $t_i$  is the width and thickness of the  $i$ -th strip, respectively, while  $\alpha_i$  is the (signed) angle of the  $i$ -th strip with respect to the positive  $X$ -axis (i.e., the angle between the global and the  $i$ -th strip local coordinate system).

The critical forces can be calculated by utilizing that the coefficient matrix has to be singular. The results, i.e., the critical forces are discussed in Chapter 5.